People`s Democratic Republic of Algeria

Ministry of Higher Education and Scientific Research

University of Echahid Hamma Lakhdar - El Oued

Faculty of Technology

Department of Process Engineering and Petrochemical

Dissertation

ACADEMIC MASTER

Domain: Technology

Division: Process Engineering

Specialty: Chemical Engineering

Presented by:

1. BAHI Ferdous
2. HEMICI Mohammed Intisar

Entitled:

A Comprehensive Review of Nanoparticle Synthesis Methods and Characterization Techniques with Emphasis on Recent Applications in Wastewater Remediation and Biomedical Fields

Publicly defended in: 13/06/2026

Board of Examiners:

Dr. BENAMARA Hacen	**Chairman**
Dr. BOUAFIA Abderrhmane	**Supervisor**
Mr. NESRAT Hocine Sadam	**Assistant Supervisor**
Dr. GUEMARI Fathi	**Examiner**

Academic Year: 2025/2026

Dedication

Dedication

We dedicate this humble work to our dear parents, whom God has made the foundation of righteousness and the source of generosity, in appreciation of their kindness and unwavering support. We pray that God preserves them and grants them abundant health and well-being. We also express our deep gratitude to our brothers and sisters who have always been a source of support and assistance, with whom we share life's moments and challenges. We faithfully remember our departed companions on this journey, whose impact remains vivid in our hearts. We extend our sincere thanks and appreciation to our esteemed professors, who contributed to our intellectual and academic development, guiding us with their knowledge and wisdom throughout our studies. We also dedicate this work to students, researchers, and all those seeking knowledge, hoping that they will find something in this work that enriches their pursuits and contributes to achieving their academic goals. In conclusion, we ask God Almighty to accept this effort from us, and to make it purely for His noble countenance, beneficial to those who read it, and included in the balance of our good deeds.

Acknowledgements

Acknowledgements

All praise is due to Allah, who granted us success and aided us in completing this work through His grace and generosity. At the outset of this achievement, we extend our deepest gratitude and appreciation to our supervisor, ***Professor Bouafia Abderrhmane****, in recognition of his invaluable efforts and continuous guidance, which were instrumental in the completion of this work.*

We also express our sincere thanks and gratitude to all the professors of Process Engineering who contributed to our academic development throughout our university studies.

Furthermore, we would like to thank the esteemed members of the judging panel for their time in reviewing and evaluating this work. We also thank all the professors, the second-year Master's students in Chemical Engineering, our friends, and everyone who offered their assistance and contributed, directly or indirectly, to the completion of this research.

Abstract

ملخص

Résumé

Abstract

The past three decades have witnessed a genuine scientific revolution with the rise of nanotechnology, a discipline that enables the design and manipulation of matter at the 1-100 nanometer scale, unlocking optical, magnetic, electronic, and catalytic properties with no equivalent in conventional bulk materials. This work provides an in-depth review of four principal nanoparticle synthesis routes, physical, chemical, green, and microfluidic methods, evaluated against rigorous criteria of cost, environmental footprint, scalability, and control over particle properties. A comprehensive portfolio of physicochemical characterization techniques is then surveyed, encompassing structural and morphological analysis through XRD, TEM, SEM, and AFM, colloidal analysis via DLS and zeta potential, as well as spectroscopic tools and surface chemistry methods. On the application side, nanoparticles demonstrate outstanding efficiency in wastewater treatment through adsorption and photocatalysis, leveraging iron oxides, titanium dioxide, and carbon-based nanomaterials. In the biomedical field, they open promising avenues for targeted drug delivery, diagnostic imaging, and antimicrobial platforms. However, real challenges remain, including environmental toxicity, particle recovery difficulties, and regulatory uncertainty. The work ultimately concludes that reproducibility, rigorous multi-modal characterization, and sustainability are the defining pillars for responsibly translating these promising technologies from laboratory research into meaningful and safe real-world deployment.

Keywords: *Nanoparticles; synthesis strategies; physicochemical characterization; wastewater remediation; drug delivery; biomedical applications; green nanotechnology; structure–property relationships*

Résumé

Ces trois dernières décennies ont marqué un tournant scientifique majeur avec l'émergence des nanotechnologies, discipline qui permet de concevoir et de manipuler la matière à l'échelle de 1 à 100 nanomètres, révélant des propriétés optiques, magnétiques, électroniques et catalytiques sans équivalent dans les matériaux conventionnels. Ce travail examine de manière approfondie quatre voies de synthèse des nanoparticules, méthodes physiques, chimiques, vertes et microfluidiques, en les évaluant selon des critères rigoureux de coût, d'empreinte environnementale, de mise à l'échelle et de contrôle des propriétés particulaires. Un panorama complet des techniques de caractérisation physicochimique est ensuite présenté, couvrant l'analyse structurale et morphologique par XRD, TEM, SEM et AFM, l'analyse colloïdale par DLS et potentiel zêta, ainsi que les outils spectroscopiques et l'analyse de chimie de surface. Sur le plan des applications, les nanoparticules démontrent une efficacité remarquable dans le traitement des eaux usées, notamment par adsorption et photocatalyse grâce aux oxydes de fer, au dioxyde de titane et aux matériaux carbonés. En biomédecine, elles ouvrent des perspectives prometteuses pour l'administration ciblée de médicaments, l'imagerie diagnostique et la lutte antimicrobienne. Toutefois, des défis persistent, notamment la toxicité environnementale, la récupération des particules et l'incertitude réglementaire. Le travail conclut que la reproductibilité, la caractérisation multimodale rigoureuse et la durabilité constituent les piliers essentiels pour une transition responsable de ces technologies vers un déploiement réel et bénéfique.

Mots-clés : *Nanoparticules ; stratégies de synthèse ; caractérisation physicochimique ; dépollution des eaux usées ; administration de médicaments ; applications biomédicales ; nanotechnologie verte ; relations structure–propriété*

ملخص

شهدت العقود الثلاثة الأخيرة تحولاً علمياً حقيقياً مع ظهور تقنيات النانو، التي أتاحت التحكم في المادة عند مقياس يتراوح بين 1 و100 نانومتر، والكشف عن خصائص بصرية ومغناطيسية وإلكترونية وحفازية فريدة لا نظير لها في المواد التقليدية. يتناول هذا العمل أربع مسارات رئيسية لتصنيع الجسيمات النانوية، هي الطرق الفيزيائية والكيميائية والخضراء وتقنيات التدفق المستمر، مع تقييم كل منها وفق معايير التكلفة والأثر البيئي وقابلية التوسع ودرجة التحكم في خصائص الجسيمات. يستعرض العمل كذلك منظومة متكاملة من تقنيات التوصيف الفيزيوكيميائي، تشمل تحليل البنية والمورفولوجيا باستخدام XRD وTEM وSEM وAFM، وتحليل الغرويات عبر DLS وجهد زيتا، فضلاً عن الأدوات الطيفية وتحليل كيمياء السطح. وعلى صعيد التطبيقات، تُظهر الجسيمات النانوية كفاءة استثنائية في معالجة مياه الصرف من خلال الامتزاز والتحفيز الضوئي باستخدام أكاسيد الحديد وثاني أكسيد التيتانيوم والمواد الكربونية. كما تفتح في المجال الطبي الحيوي آفاقاً واعدة في الإيصال الدوائي الموجّه والتصوير التشخيصي ومكافحة الميكروبات. غير أن تحديات حقيقية لا تزال قائمة، في مقدمتها السُّمية البيئية وصعوبة استرداد الجسيمات والغموض التنظيمي. ويخلص العمل إلى أن قابلية الاستنساخ والتوصيف الدقيق متعدد الأساليب والاستدامة هي المحاور الجوهرية لتحويل هذه التقنيات الواعدة من نطاق المختبر إلى التطبيق الفعلي والمسؤول.

الكلمات المفتاحية: الجسيمات النانوية؛ استراتيجيات التصنيع؛ التوصيف الفيزيوكيميائي؛ معالجة مياه الصرف؛ الإيصال الدوائي؛ التطبيقات الطبية الحيوية؛ النانو التقنية الخضراء؛ علاقات البنية بالخاصية

TABLE OF CONTENTS

Table of Contents

Chapter II: Synthesis Strategies and Methods of Nanomaterials

Chapter III: Characterization Techniques for Nanoparticles

List of Figures

Chapter III : Characterization Techniques for Nanoparticles

Chapter IV : Nanoparticles in Wastewater Remediation

Chapter V : Nanoparticles in Biomedical Applications

List of Tables

List of Abbreviations

ABBREVIATION	FULL TERM
NPs	Nanoparticles
AgNPs	Silver Nanoparticles
AuNPs	Gold Nanoparticles
IONPs	Iron Oxide Nanoparticles
SPIONs	Superparamagnetic Iron Oxide Nanoparticles
USPIONs	Ultrasmall Superparamagnetic Iron Oxide Nanoparticles
ZnO NPs	Zinc Oxide Nanoparticles
TiO_2	Titanium Dioxide
MSNs	Mesoporous Silica Nanoparticles
QDs	Quantum Dots
LSPR	Localized Surface Plasmon Resonance
SERS	Surface-Enhanced Raman Spectroscopy
XRD	X-ray Diffraction
TEM	Transmission Electron Microscopy
HR-TEM	High-Resolution Transmission Electron Microscopy
SEM	Scanning Electron Microscopy
FE-SEM	Field-Emission Scanning Electron Microscopy
AFM	Atomic Force Microscopy
DLS	Dynamic Light Scattering
NTA	Nanoparticle Tracking Analysis
XPS	X-ray Photoelectron Spectroscopy
EDX / EDS	Energy-Dispersive X-ray Spectroscopy
ICP-MS	Inductively Coupled Plasma Mass Spectrometry
FTIR	Fourier Transform Infrared Spectroscopy
UV-Vis	Ultraviolet-Visible Spectroscopy
PDI	Polydispersity Index

VSM	Vibrating Sample Magnetometer
SQUID	Superconducting Quantum Interference Device
LAL	Laser Ablation in Liquid
PVD	Physical Vapor Deposition
CVD	Chemical Vapor Deposition
ALD	Atomic Layer Deposition
MM	Mechanical Milling
HiPIMS	High-Power Impulse Magnetron Sputtering
SDGs	Sustainable Development Goals
MtNPs	Metallic Nanoparticles (microbially synthesized)
ROS	Reactive Oxygen Species
AOPs	Advanced Oxidation Processes
GO	Graphene Oxide
rGO	Reduced Graphene Oxide
CNTs	Carbon Nanotubes
SWCNTs	Single-Walled Carbon Nanotubes
MWCNTs	Multi-Walled Carbon Nanotubes
nZVI	Nanoscale Zero-Valent Iron
AC	Activated Carbon
MOFs	Metal-Organic Frameworks
EDCs	Endocrine Disrupting Chemicals
EPS	Extracellular Polymeric Substance
BPA	Bisphenol A
NF	Nanofiltration
UF	Ultrafiltration
TFN	Thin-Film Nanocomposite
MMMs	Mixed-Matrix Membranes
PPCPs	Pharmaceuticals and Personal Care Products
EPR	Enhanced Permeability and Retention
PLGA	Poly(lactic-co-glycolic acid)
PEG	Polyethylene Glycol

LNPs	Lipid Nanoparticles
SLNs	Solid Lipid Nanoparticles
MRI	Magnetic Resonance Imaging
CT	Computed Tomography
PET	Positron Emission Tomography
SPECT	Single-Photon Emission Computed Tomography
GBCAs	Gadolinium-Based Contrast Agents
NIR	Near-Infrared
PLQY	Photoluminescence Quantum Yield
AMR	Antimicrobial Resistance
MDR	Multidrug-Resistant
MRSA	Methicillin-Resistant Staphylococcus aureus
MIC	Minimum Inhibitory Concentration
QS	Quorum Sensing
AHL	N-acyl Homoserine Lactone
GRAS	Generally Recognized as Safe
ELISA	Enzyme-Linked Immunosorbent Assay
PCR	Polymerase Chain Reaction
LOC	Lab-on-a-Chip
GFET	Graphene Field-Effect Transistor
EIS	Electrochemical Impedance Spectroscopy
FDA	U.S. Food and Drug Administration
EMA	European Medicines Agency
EPA	U.S. Environmental Protection Agency
TSCA	Toxic Substances Control Act
TOC	Total Organic Carbon
BET	Brunauer–Emmett–Teller (surface area analysis)
FWHM	Full-Width at Half-Maximum

General Introduction

General Introduction

Over the past three decades, nanoscience and nanotechnology have evolved from a largely theoretical pursuit into one of the most dynamic and consequential fields in modern science and engineering. The ability to design, synthesize, and manipulate matter at the scale of 1 to 100 nanometers has unlocked a remarkable set of size-dependent properties, optical, magnetic, electronic, mechanical, and catalytic, that have no counterpart in conventional bulk materials. These properties emerge not from a change in chemical composition, but from the dramatic increase in surface-to-volume ratio and the onset of quantum mechanical effects that accompany the reduction in particle dimensions. It is this fundamental distinction that has made nanoparticles so scientifically compelling and technologically promising across an extraordinarily wide range of disciplines.

The motivation behind undertaking this graduation study stems from the observation that two of the most pressing challenges facing modern chemical engineering, the remediation of contaminated water resources and the development of more effective biomedical therapies, are increasingly being addressed through nanoparticle-based solutions. On the environmental side, the contamination of water by heavy metals, synthetic dyes, pharmaceutical residues, and emerging micropollutants represents one of the most serious public health and ecological threats of the twenty-first century. Conventional treatment technologies such as coagulation, activated carbon adsorption, and biological degradation are frequently insufficient to meet increasingly stringent regulatory thresholds, particularly for trace-level contaminants present in complex matrices. Nanoparticles offer a compelling alternative, combining exceptionally high specific surface areas, tunable surface chemistry, and in many cases intrinsic photocatalytic or magnetic functionality that enables both efficient contaminant removal and straightforward post-treatment recovery [1].

On the biomedical side, the limitations of conventional therapeutics, poor aqueous solubility, non-specific biodistribution, rapid systemic clearance, and the growing global threat of antimicrobial resistance, have created a powerful incentive to develop smarter and more targeted therapeutic platforms. Engineered nanoparticles, by virtue of their tunable size, adaptable surface

chemistry, and stimuli-responsive behavior, have emerged as uniquely versatile candidates for encapsulating and delivering therapeutic agents to specific tissue compartments, for generating contrast in magnetic resonance and optical imaging, and for disrupting microbial biofilms that remain impervious to conventional antibiotics [2].

Underpinning both of these application domains is a challenge that is sometimes underappreciated: the reliable and reproducible synthesis of nanoparticles with well-defined and controllable properties, followed by their rigorous physicochemical characterization. The performance of a nanoparticle in any application is ultimately determined by a set of structural and colloidal parameters, particle size and size distribution, crystalline phase, surface chemistry, surface charge, and colloidal stability, which are themselves dictated by the synthesis route and conditions employed. The relationship between synthesis, structure, and function therefore represents the central design equation of applied nanotechnology, and a solid understanding of this relationship is an indispensable competency for any chemical engineer working in this field [3].

Scope and Objectives of the Study

This graduation study was conceived with the explicit aim of providing a comprehensive and integrated review of nanoparticle synthesis methods and characterization techniques, with a focused emphasis on their recent applications in wastewater remediation and biomedical fields. Rather than treating synthesis, characterization, and application as separate topics, this work adopts a unified perspective that traces the logical progression from particle fabrication through physicochemical characterization and ultimately to real-world functional performance. In doing so, it seeks to equip the reader with a coherent, technically grounded framework that reflects the interdisciplinary nature of modern nanotechnology research as it relates to chemical engineering practice.

The specific objectives of this study are as follows:

- To present a systematic and comparative overview of the principal nanoparticle synthesis strategies, physical, chemical, green and biogenic, and emerging advanced methods, with

attention to the practical trade-offs between scalability, cost, environmental impact, and the degree of control they afford over particle properties.

- To survey the full portfolio of characterization techniques applied to nanoparticle systems, spanning structural and morphological methods, solution-phase colloidal analysis, spectroscopic and optical tools, surface chemistry and elemental analysis, and, where functionally relevant, magnetic, electrical, and nanomechanical measurements, with emphasis on the complementarity of these techniques and the limitations of each.
- To review the state of the art in two high-impact application domains, wastewater remediation and biomedical science, with a focus on establishing clear, evidence-based connections between the physicochemical properties of nanoparticles and their observed functional performance.
- To identify the key challenges that currently hinder the broader translation of nanoparticle technologies from laboratory-scale research to real-world deployment, including issues related to toxicity, regulatory compliance, reproducibility, and environmental fate.

Structure of the Study

This study is organized into five chapters, each building logically upon the preceding one. **Chapter I** lays the conceptual groundwork by defining nanoparticles, delineating the classification schemes in common use, and explaining the physicochemical origins of the size-dependent properties that distinguish nanomaterials from their bulk counterparts. The major classes of nanomaterials, metallic, metal oxide, carbon-based, polymeric, and hybrid, are introduced alongside the structure–property–application relationships that run as a common thread throughout the study [4].

Chapter II surveys the landscape of nanoparticle synthesis strategies, from top-down physical and mechanical methods to bottom-up chemical routes, green and biogenic approaches, and emerging microfluidic and continuous-flow technologies. The chapter concludes with a comparative analysis that evaluates each strategy against criteria of direct relevance to chemical engineering practice: cost, scalability, degree of control over particle properties, and environmental footprint [5].

Chapter III is devoted to characterization techniques and represents the most technically detailed portion of the thesis. It addresses structural and morphological methods including XRD, TEM, SEM, and AFM; solution-phase methods including DLS, zeta potential measurements, and NTA; spectroscopic tools including UV–Vis, FTIR, Raman and SERS, and photoluminescence spectroscopy; surface chemistry and compositional analysis by XPS, EDX, ICP-MS, and NMR; and, where applicable, magnetic, electrical, and nanomechanical characterization. The chapter concludes by examining how the combined characterization dataset can be systematically correlated with functional performance [3].

Chapter IV addresses wastewater remediation applications, covering the use of metal and metal oxide nanoparticles as adsorbents for heavy metal removal, carbon-based nanomaterials for organic pollutant capture, photocatalytic systems based on TiO_2 and ZnO, and magnetically recoverable nanocatalysts for Fenton-like oxidation. Green-synthesized nanoparticles and their integration into treatment systems are also discussed, followed by an assessment of the practical challenges, fouling, particle recovery, ecotoxicity, and regulatory uncertainty, that must be addressed before widespread deployment becomes feasible [6].

Chapter V examines biomedical applications, covering nanocarriers for drug delivery, inorganic nanoparticles for imaging and diagnostics, antimicrobial nanoparticles, and biosensing platforms. Particular attention is given to the relationship between nanoparticle physicochemical properties and biological outcomes such as biodistribution, cellular uptake, and cytotoxicity, concluding with a discussion of the biocompatibility and regulatory considerations that govern clinical translation [7].

Taken as a whole, this study aspires to serve as an integrated reference that provides second-year Master's students in Chemical Engineering with the conceptual and technical foundation needed to approach nanoparticle research critically and systematically, from the selection of a synthesis route and characterization protocol to the rational design of a nanoparticle system for a specific engineering application.

References

1. Pervaiz S, Javed M, Shah A, et al (2025) Environmental applications of magnetic nanohybrid materials. RSC Adv 15:19899–19936. https://doi.org/10.1039/d5ra03470a

2. Peer D, Karp JM, Hong S, et al (2007) Nanocarriers as an emerging platform for cancer therapy. Nat Nanotechnol 2:751–760. https://doi.org/10.1038/nnano.2007.387

3. Mourdikoudis S, Pallares RM, Thanh NTK (2018) Characterization techniques for nanoparticles: Comparison and complementarity upon studying nanoparticle properties. Nanoscale 10:12871–12934. https://doi.org/10.1039/c8nr02278j

4. Buzea C, Pacheco II, Robbie K (2007) Nanomaterials and nanoparticles: Sources and toxicity. Biointerphases 2:MR17–MR71. https://doi.org/10.1116/1.2815690

5. Iravani S (2011) Green synthesis of metal nanoparticles using plants. Green Chem 13:2638–2650. https://doi.org/10.1039/c1gc15386b

6. Zheng X, Li X, Deng J, et al (2026) Green-Synthesized Nanoparticles for Efficient Dye Degradation: Mechanisms, Applications, and Future Perspectives. Catalysts 16:125. https://doi.org/10.3390/catal16020125

7. Anselmo AC, Mitragotri S (2019) Nanoparticles in the clinic: An update. Bioeng Transl Med 4:. https://doi.org/10.1002/btm2.10143

CHAPTER I

Fundamentals of Nanoparticles

I.1. Definition of Nanoparticles:

Nanoparticle chemistry is a dynamic and profoundly influential field that bridges the gap between classical material science and quantum physics. Although the term "nanotechnology" is a modern construct, these materials have been part of our natural world for eons, present in everything from atmospheric dust to volcanic ash and forest fire smoke. Long before the scientific community could visualize these entities, they were instinctively utilized by ancient artisans to create vibrant pigments and the iconic optical effects seen in medieval stained glass. However, it was only in the late 20th century, with the development of high-resolution imaging techniques like Electron Microscopy, that the field transitioned from empirical craft to a rigorous academic discipline [1].

From a structural perspective, a nanoparticle is fundamentally defined by its dimensions, typically falling within the range of 1 to 100 nm. As illustrated in **Figure (I.1)**, nanoparticles occupy a unique "mesoscopic" position in the physical hierarchy. They are significantly smaller than the bulk objects governed by Newtonian laws of motion, yet larger than the individual atoms or simple molecules that operate under the laws of quantum mechanics [2]. This intermediate sizing is what grants nanoparticles their extraordinary physicochemical properties such as an immense surface-to-volume ratio, which differ drastically from those of their macro-scale counterparts [3].

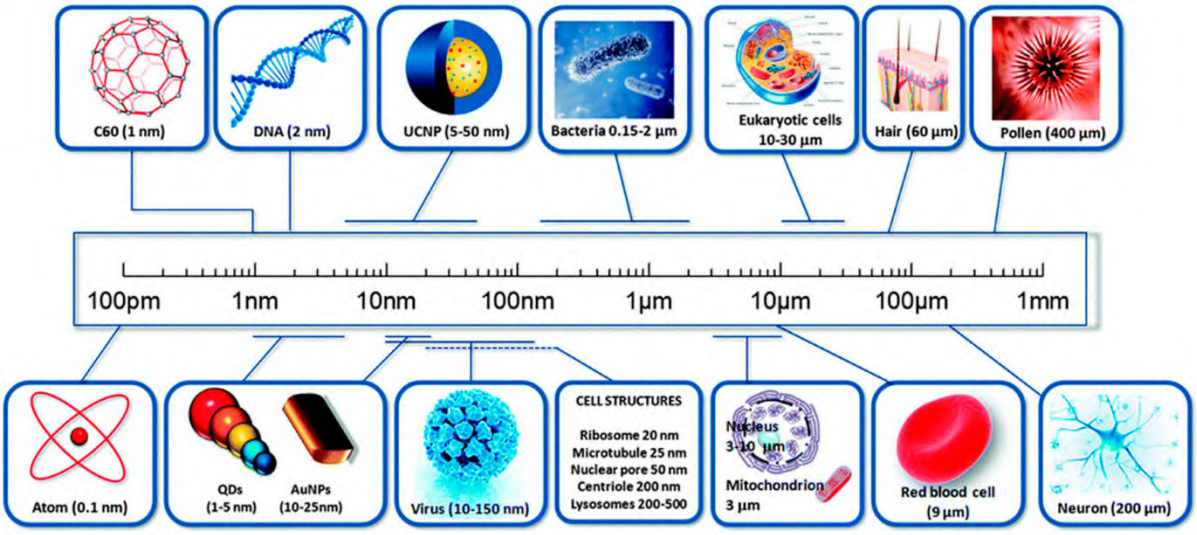

Figure (I.1): A comprehensive scale of biological and physical entities, illustrating the transition from atomic dimensions to the macroscopic world [4].

I.1.1. Size Regime and Classification of Nanoparticles:

Understanding nanoparticles requires looking beyond their mere physical dimensions; they represent a "third state" of matter that bridges the gap between individual atoms and bulk materials. At this scale, the laws of classical physics begin to give way to quantum mechanical effects. According to the foundational frameworks established in the field [5], nanoparticles are systematically categorized through three primary analytical lenses:

- **A) By Origin: Natural vs. Engineered:** A fundamental distinction is drawn between natural nanoparticles and synthetic (engineered) nanoparticles. Natural varieties have been ubiquitous in the Earth's ecosystem for eons, resulting from geophysical processes such as volcanic eruptions, forest fires, and sea spray. In contrast, engineered nanoparticles are the hallmark of modern nanotechnology; they are fabricated with "geometric intentionality" to control their size, shape, and surface chemistry. This precision allows scientists to tailor their physicochemical properties for highly specific applications, such as targeted drug delivery or enhanced catalytic performance [6].
- **B) By Dimensionality: The Spatial Confinement:**

  This is the most critical classification for material scientists, as it describes how the movement of electrons is restricted within the material. As illustrated in **Figure (I.2)**, nanomaterials are not classified simply because they are "small," but based on the number of dimensions that remain confined below the 100 nm threshold [7]:

  1. **Zero-Dimensional (0D):** All dimensions are within the nanoscale, confining electrons in a single point (e.g., Quantum Dots or spherical nanoparticles).
  2. **One-Dimensional (1D):** One dimension is outside the nanoscale, allowing electrons to move freely along a single axis, forming needle-like structures (e.g., Nanotubes or Nanowires).
  3. **Two-Dimensional (2D):** Two dimensions are outside the nanoscale, resulting in plate-like structures with immense surface area but negligible thickness (e.g., Nanosheets or Graphene).

4. **Three-Dimensional (3D):** These are bulk materials that do not have any dimension confined to the nanoscale externally, yet they are composed of an internal network of individual nanocrystals or dispersed nanoparticles.

- **C) By Chemical Composition:**

The classification also extends to the chemical nature of the core. This distinguishes between **organic** nanomaterials (such as liposomes and dendrimers), inorganic materials (including noble metals and metal oxides like ZnO or MgO), and carbon-based structures. Each category follows distinct stabilization protocols based on its surface reactivity [5].

The Stability Paradox

The definition of a nanoparticle is inseparable from its physicochemical stability, a term describing the particle's ability to preserve its size, crystalline structure, and surface chemistry over time [6].

This leads to the **"Stability Paradox"**: because nanoparticles possess an exceptionally high surface-to-volume ratio, the majority of their atoms reside on the surface rather than in the bulk. This configuration results in immense surface energy, rendering the particles thermodynamically unstable. According to the laws of thermodynamics [8], these particles naturally seek to minimize this energy by adhering to one another, a process known as "aggregation" or "agglomeration," effectively returning to a stable bulk state.

Consequently, nanoparticle stability is a relative, meta-stable state. For instance, in metallic nanoparticles, maintaining stability is vital for preserving unique optical phenomena like Localized Surface Plasmon Resonance (LSPR). To prevent spontaneous aggregation, researchers employ "stabilizing agents" or "capping agents." These molecules act as protective shields, ensuring the particles retain their nano-identity and technological functionality long enough to be utilized in practical applications [6, 8].

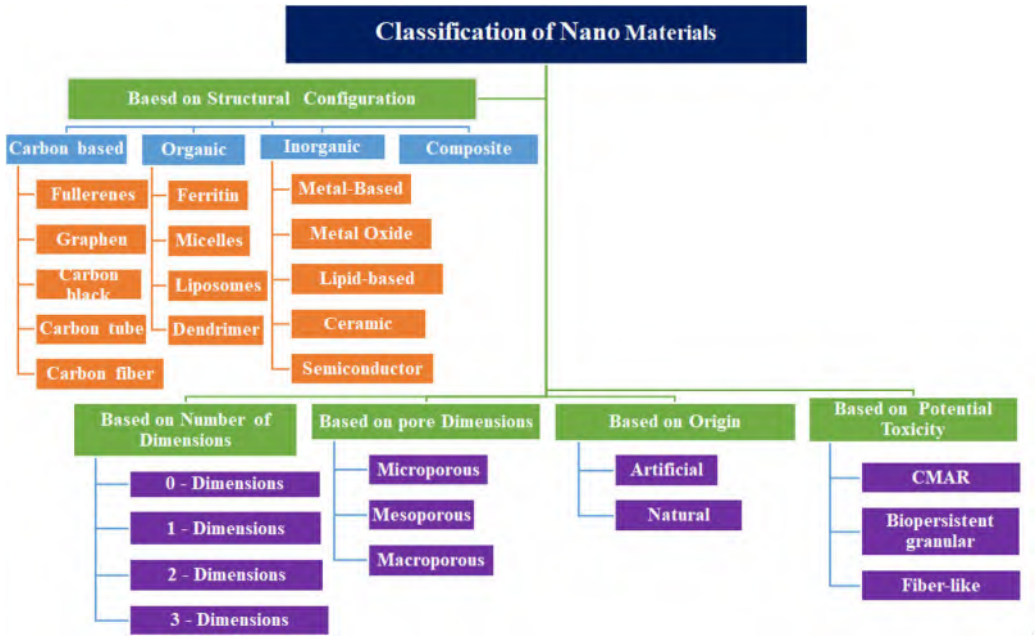

Figure (I.2) : Classification of nanomaterials based on geometric dimensions, illustrating the transition from 0D quantum dots to 3D bulk structures [9].

I.2. physicochemical properties at the nanoscale:

The transition from bulk materials to the nanometric regime induces a fundamental shift in material behavior. This metamorphosis is not merely a change in scale but a profound alteration of the material's identity, driven by the exponential increase in relative surface area and the emergence of quantum confinement effects.

I.2.1. Physical Properties

Physical characteristics at the nanoscale are no longer constant; they become "size-dependent," governed by the structural arrangement of atoms and geometric constraints.

- **Size and Surface Area:** The most definitive physical trait of a nanoparticle is its high surface-area-to-volume ratio. As dimensions shrink to the 1–100 nm range, the proportion of atoms located on the surface increases dramatically, a phenomenon visualized in **Figure (I.3)**. These surface atoms possess "dangling bonds" and fewer neighbors than atoms in the bulk, which significantly enhances the material's reactivity and alters its basic physical presence [10].

- **Morphology (Shape):** The physical geometry, whether spherical, rod-like, or fibrous, dictates the particle's mobility and how it interacts with biological and chemical environments. For example, morphology is a critical factor in the mechanical reinforcement of composites; fibrous nanocellulose exhibits different structural capabilities compared to spherical metallic oxides due to its high aspect ratio [5, 11].
- **Crystallinity:** The arrangement of the crystal lattice at the nanoscale directly affects mechanical strength and rigidity. Modifications during synthesis, such as acid hydrolysis, can alter the crystallinity index, a physical change that impacts the material's hardness and resistance to degradation [11].
- **Thermal Stability and Melting Point:** Nanomaterials exhibit unique thermal signatures compared to their bulk counterparts. Due to high surface energy and the increased mobility of surface atoms, nanoparticles often exhibit a "melting point depression," where they begin to melt at temperatures significantly lower than the standard melting point of the bulk material [10, 12].
- **Optical Properties (LSPR):** Many nanoparticles, particularly noble metals like Gold and Silver, display vibrant colors that are absent in the macroscale. This is caused by **Localized Surface Plasmon Resonance (LSPR)**, a physical phenomenon where the collective oscillation of surface electrons resonates with incident light. This property is highly sensitive to the particle's specific size and shape [12].

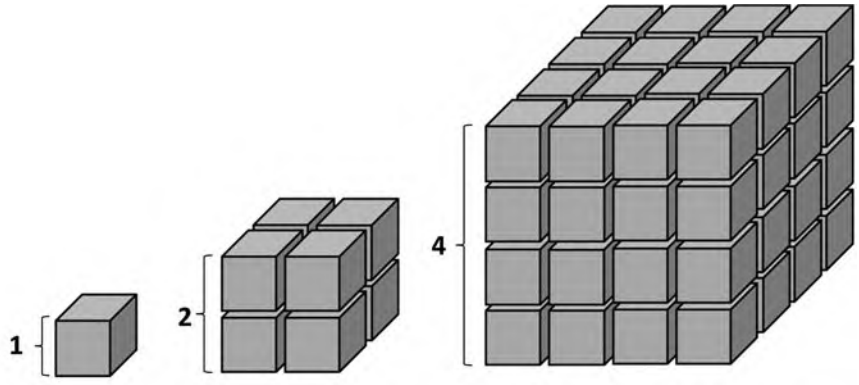

Side of Cube	Area of side	Area of cube surface	Volume	Ration of surface area to volume
1 cm	1 cm^2	6 * 1 cm^2	1 cm^3	6/1
2 cm	4 cm^2	6 * 4 cm^2	8 cm^3	24/8 =3/1
4 cm	16 cm^2	6 * 16 cm^2	64 cm^3	96/64 = 3/2

Figure (I.3): Schematic representation showing the exponential increase in the fraction of surface atoms and surface-area-to-volume ratio as particle size decreases toward the nanoscale [13].

I.2.2. Chemical Properties

Chemical properties are defined by how the nanoparticle interacts with its environment and its molecular tailoring.

- **Zeta Potential and Stability:** The surface charge, or *Zeta potential*, is vital for chemical stability. A high Zeta potential creates electrostatic repulsion, preventing the particles from chemically bonding or "clumping" together (agglomeration) [3].
- **Surface Functionalization:** A hallmark of nanochemistry is the ability to modify the surface by attaching ligands or functional groups. As shown in **Figure (I.4)**, this molecular tailoring (using organic or inorganic ligands) allows for targeted chemical interactions, which is essential for selective environmental remediation or drug delivery [2, 4].
- **The Stability Paradox:** Because nanoparticles possess exceptionally high surface energy, they are inherently *thermodynamically unstable*. This drives them toward spontaneous aggregation to reach a lower energy state. Consequently, maintaining a "meta-stable" state via capping agents is a cornerstone of modern synthesis [1, 4].

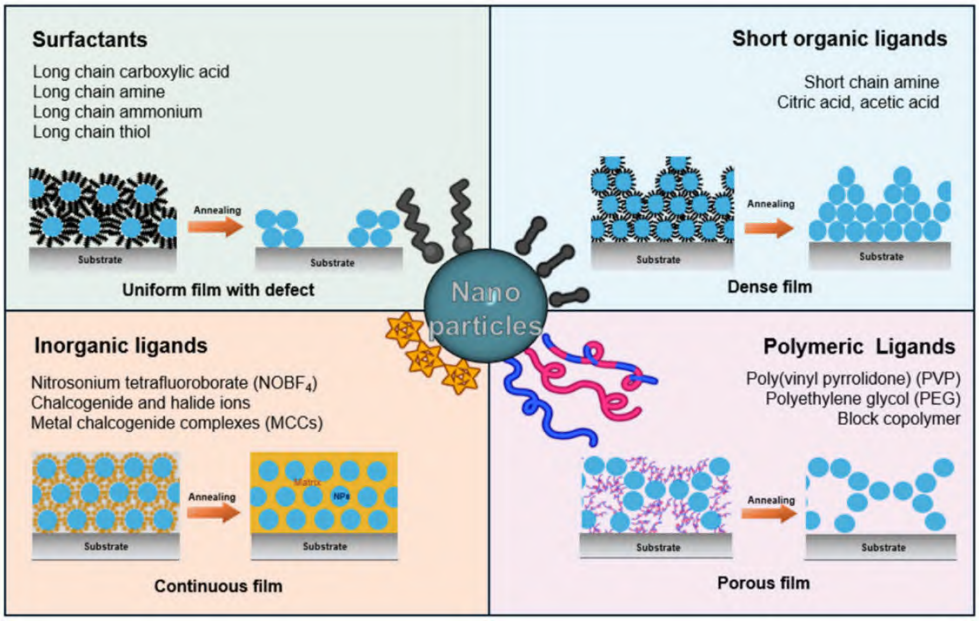

Figure (I.4): Schematic classification of nanoparticle surface functionalization strategies, illustrating the use of organic, inorganic, and polymeric ligands to control film morphology and chemical reactivity [14].

I.3. Types of Nanomaterials: From Elemental Metals to Advanced Hybrids

The landscape of nanotechnology is characterized by a diverse array of architectures, each engineered for specific functional outcomes. Nanomaterials are systematically categorized based on their chemical composition, structural geometry, and intrinsic physical properties. The following sections detail the primary classes of nanomaterials currently driving innovation in research and industry [15, 16].

As illustrated in **Figure (I.5)**, the classification of nanomaterials is fundamentally rooted in their spatial confinement. This hierarchy organizes materials into zero-dimensional (0D) spheres, one-dimensional (1D) tubes, two-dimensional (2D) layers, and three-dimensional (3D) polycrystalline assemblies, each offering unique paths for electron transport and mechanical stability [5, 17].

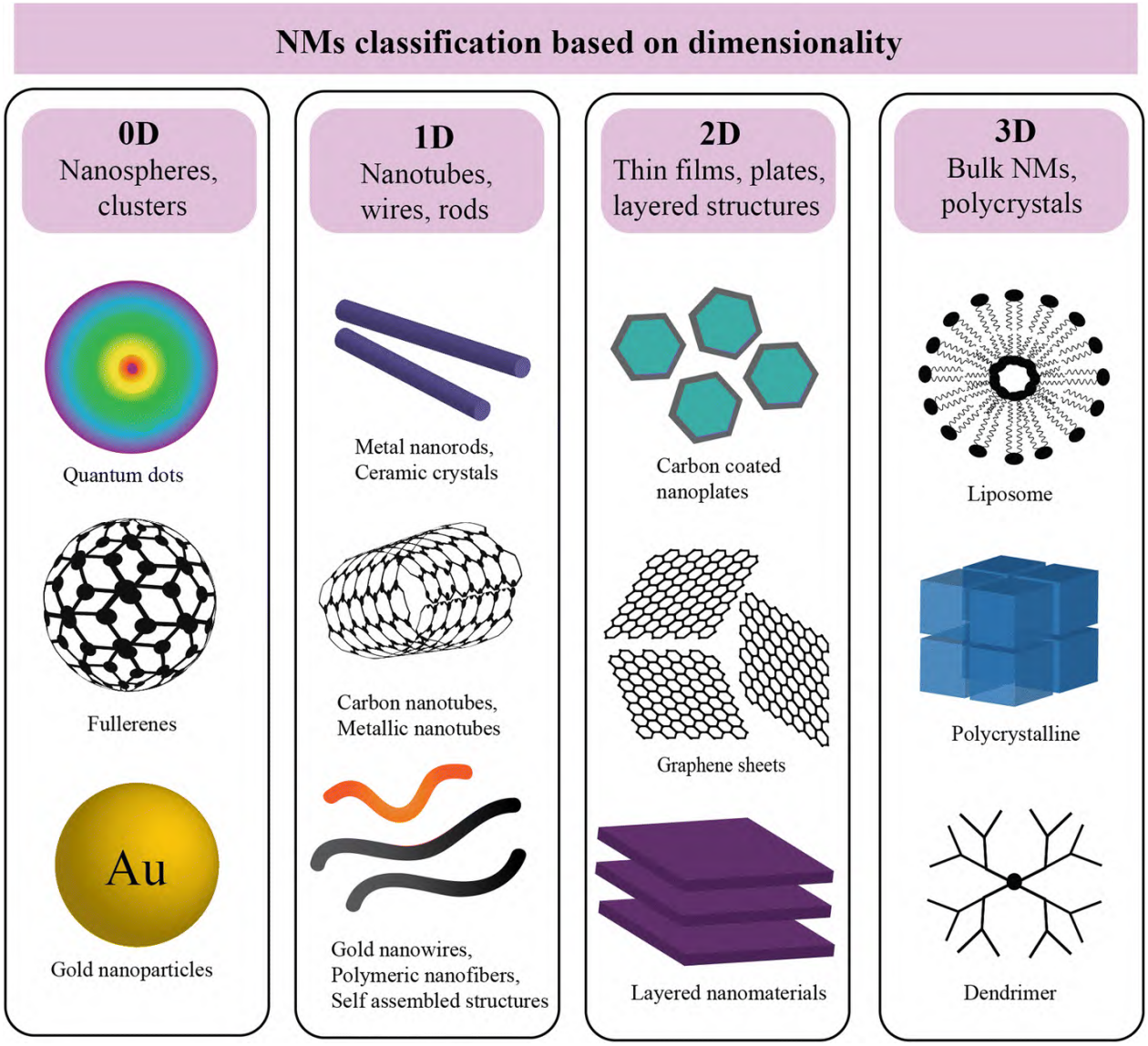

Figure (I.5): Dimensional Classification of Nanostructured Materials [17].

I.3.1. Metal Nanoparticles (MNPs)

Metal nanoparticles, predominantly Gold (Au) and Silver (Ag), exhibit distinct physicochemical properties governed by the Localized Surface Plasmon Resonance (LSPR) effect. Recent advancements focus on sustainable fabrication, where biogenic or "green" synthesis methods, utilizing plant extracts or microbial strains, are employed to produce stable metal clusters with reduced environmental toxicity. [10].

I.3.2. Metal Oxide Nanoparticles (MONPs)

Metal oxides (e.g., TiO_2, ZnO, MgO) are critical in catalysis and biomedical engineering. For instance, ZnO and Sb_2O_3 nanoparticles synthesized via low-cost biogenic routes have shown significant potential in wastewater treatment. In clinical applications, such as restorative dentistry, metal oxide and hydroxyapatite-based nanoparticles are utilized as bioactive coatings to provide long-term antibacterial protection to dentine surfaces [18].

The transition from bulk precursors to refined nanoparticles is achieved through two primary strategic directions, as shown in **Figure (I.6)**. The **"Top-Down"** approach involves the physical breakdown of bulk materials, while the **"Bottom-Up"** approach involves the controlled assembly of molecular sulfates and precursors into nano-sized clusters [16, 18].

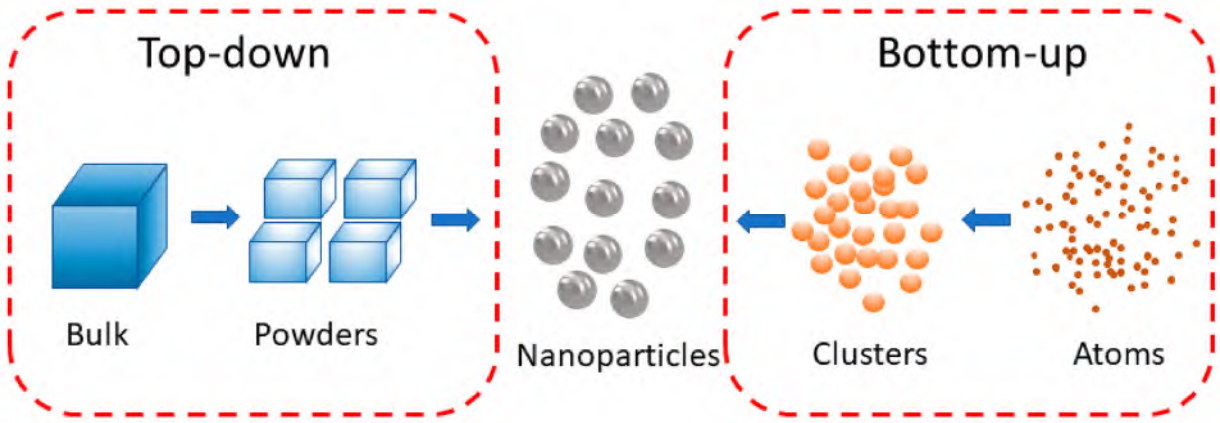

Figure (I.6): A schematic representation of the "Top-Down" and "Bottom-Up" fabrication pathways for engineered nanoparticles (NPs) [19].

I.3.3. Carbon-Based Nanomaterials

This group encompasses high-strength structures including Carbon Nanotubes (CNTs), Fullerenes (C_{60}), Graphene, and Diamond. As depicted in **Figure (I.7)**, these materials are defined by their dimensionality and the unique hybridization of carbon atoms. For instance, Fullerenes (B) represent 0D spheres, while Graphene (A) consists of a single-atom-thick 2D sheet. Carbon nanotubes, shown in both lateral and frontal views (C, D, E), are 1D cylinders that exhibit exceptional electrical conductivity and mechanical toughness, making them ideal

candidates for reinforcing dental polymers and developing high-performance electronic sensors [20, 21].

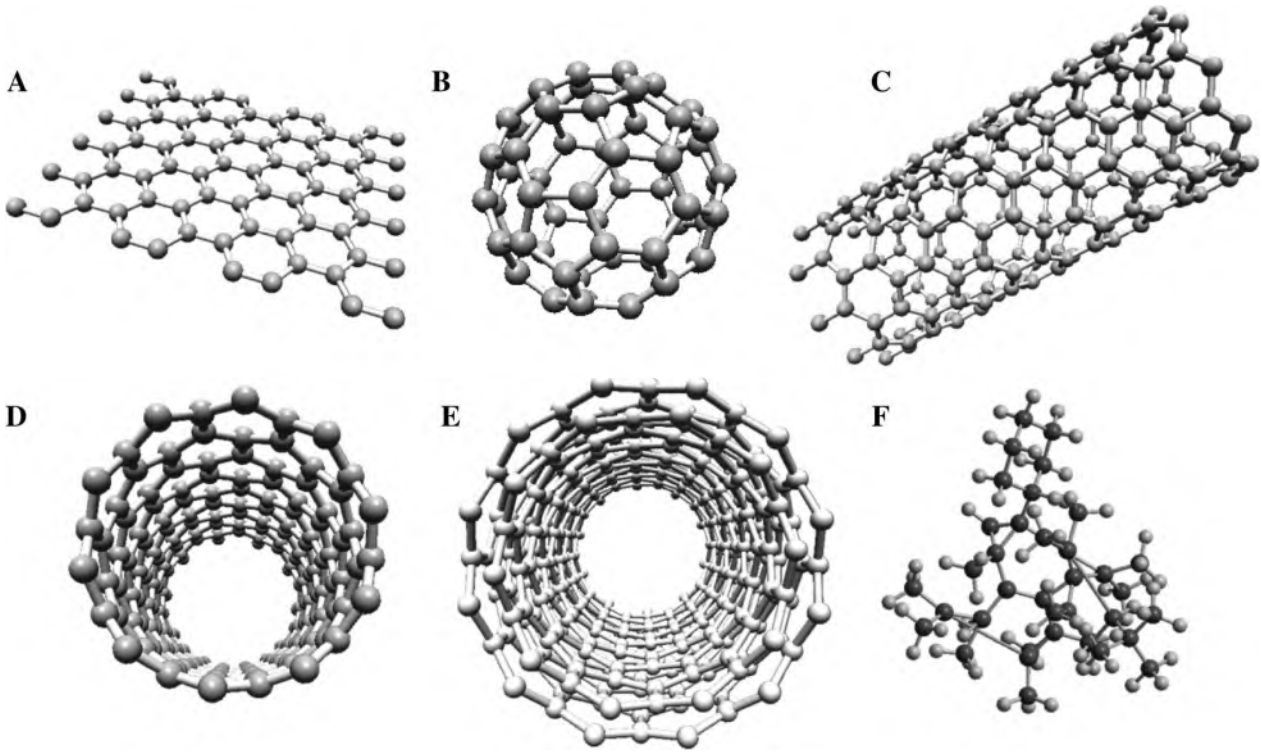

Figure (I.7): Carbon-based nanomaterials: (A) graphene; (B) fullerene; (C) SWCNT; (D) SWCNT chiral vector; (E) MWCNT; (F) diamond [22].

I.3.4. Polymeric Nanomaterials

Polymeric nanoparticles, including Chitosan and PMMA-based systems, are extensively utilized for targeted drug delivery and protective antimicrobial coatings. In dentistry, Chitosan nanoparticles are highly valued for their biocompatibility and antimicrobial efficacy; however, rigorous cytotoxicity assessments are required to ensure the safety of dental pulp cells during treatment [18, 23].

I.3.5. Hybrid Nanomaterials

Hybrid nanomaterials represent the "state-of-the-art" in nanomedicine, consisting of synergistic combinations of organic and inorganic constituents. These include Metal-Organic Frameworks (MOFs) and polymer-lipid hybrids. They are specifically engineered to integrate

multiple functionalities, such as the simultaneous delivery of chemotherapy and photothermal therapy for synergistic cancer immunotherapy [15, 24].

I.4. Structure, property, application relationships

The transition from bulk matter to the nanoscale represents a fundamental shift in how materials interact with the physical world. At this regime, typically defined between 1 and 100 nm, traditional Newtonian physics gives way to surface-dominated effects and quantum confinement phenomena [25]. This intricate relationship, where the physical architecture dictates the resulting characteristics and subsequent utility, forms the cornerstone of modern nanotechnology [26].

I.4.1. The Structural Foundation: Dimensionality and Surface Energy

The evolution of a nanomaterial begins with its physical dimensionality. Materials are systematically classified into categories ranging from zero-dimensional (0-D) clusters to three-dimensional (3-D) bulk nanostructures. This structural variety is the primary determinant of the "surface-to-volume ratio," which increases exponentially as particle size decreases [25, 27].

Because a high percentage of atoms reside on the surface, they possess fewer nearest neighbors than atoms in the bulk interior. This lack of coordination leads to "unsatisfied" or *dangling bonds*, resulting in significantly higher surface energy and heightened chemical reactivity [27, 28]. For instance, in mineralogical systems, specific phases like ferrihydrite remain stable only at these minute scales, where surface energy dominates the thermodynamic bonding considerations [29].

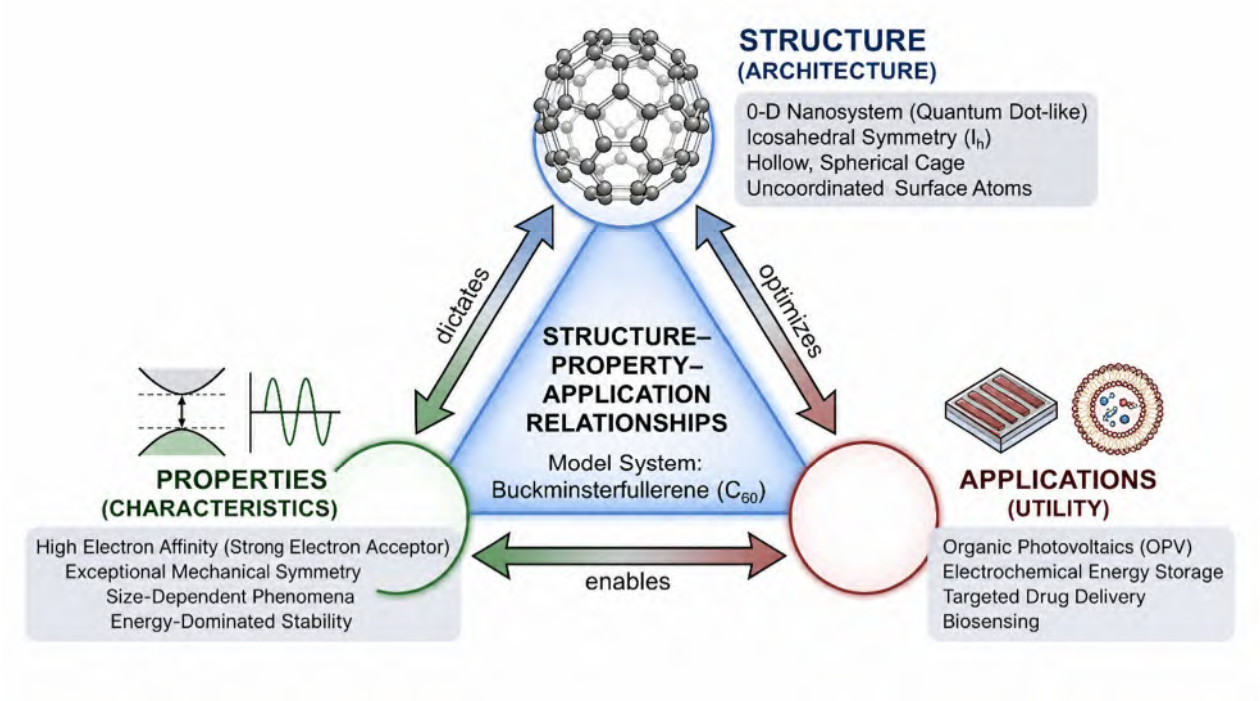

Figure (I.8): The Nanoscale Triad: Correlating Atomic Architecture with Physicochemical Performance and Industrial Application

As illustrated in **Figure (I.8)**, the functionality of a system like Buckminsterfullerene (C_{60}) is directly derived from its 0-D symmetry. Its hollow, spherical structure (Architecture) provides exceptional electron-accepting capabilities (Property), which is why it is utilized as a primary model for high-efficiency organic photovoltaics (Application) [26, 29].

I.4.2. From Structure to Unique Properties

The distinct structural characteristics of nanomaterials at the nanoscale give rise to a set of extraordinary physicochemical properties that are fundamentally absent in their bulk counterparts. These emergent properties span optical behavior, mechanical and thermal responses, and quantum electronic phenomena, and collectively define the scientific rationale for the intensive study of nanostructured systems [30, 31].

- **Optical Properties:**

In metallic nanoparticles, particularly silver nanoparticles (Ag NPs), the physical morphology whether spherical, rod-shaped, or triangular governs the spectral position of the localized surface plasmon resonance (LSPR). The LSPR arises from the coherent oscillation of conduction electrons upon interaction with incident electromagnetic radiation, and its wavelength

is exquisitely sensitive to particle geometry and size [30]. As demonstrated in recent studies, precise control over the shape and size of Ag NPs enables researchers to tune the LSPR absorption peak across the visible spectrum, from violet to green wavelengths, simply by modifying the nanoparticle's dimensions or symmetry [31, 32]. This high degree of spectral tunability renders Ag NPs especially valuable for applications in biosensing, surface-enhanced Raman spectroscopy (SERS), and plasmonic photovoltaics (**Figure (I.9)**).

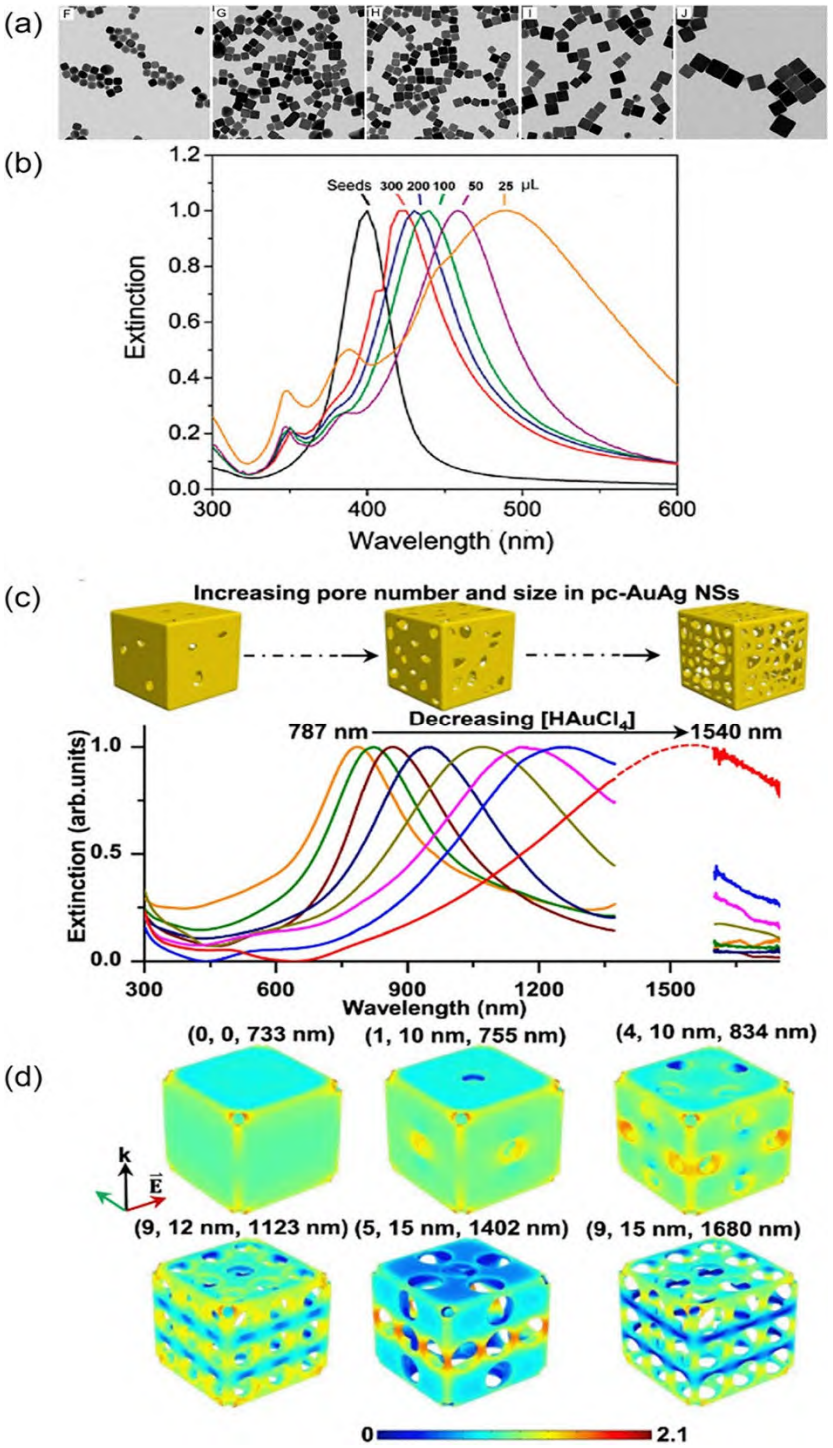

Figure (I.9): Size and porosity effects on the LSPR of nanocubes. (a, b) TEM images and UV-Vis spectra of Ag nanocubes showing a size-dependent redshift (~400 to ~500 nm). (c, d) Effect of increasing porosity on AuAg nanocubes with simulated near-field enhancement maps. *(Adapted from Hang et al., Chem. Soc. Rev., 2024)*[33].

- **Mechanical and Thermal Shifts:**

The relationship between grain size and mechanical strength in nanocrystalline materials is well described by the Hall–Petch effect, which states that a reduction in grain size increases yield strength by impeding dislocation motion at grain boundaries [30, 31]. As grain sizes approach the nanoscale (below ~30 nm), the density of grain boundaries rises sharply, trapping dislocations and rendering the material markedly stiffer. However, for grain sizes below approximately 10–15 nm, an inverse Hall–Petch relationship may emerge, whereby grain boundary sliding and diffusional mechanisms supersede dislocation-based plasticity, leading to softening [34].

Concurrently, the melting point of nanoscale materials is dramatically reduced relative to their bulk equivalents. For gold nanoparticles (Au NPs), this size-dependent melting point depression is attributed to the elevated surface-to-volume ratio: surface atoms have fewer neighboring bonds and thus lower cohesive energy, facilitating phase transition at significantly lower temperatures. Theoretical models and experimental studies consistently show that Au NPs can melt at temperatures hundreds of Kelvin below the bulk melting point of gold (1337 K), with the depression becoming most pronounced for particles smaller than 5 nm [35, 36].

- **Quantum Confinement:**

As nanoparticle dimensions approach the de Broglie wavelength of electrons, the electronic wavefunctions become spatially confined, causing energy levels to transition from a quasi-continuous band structure into discrete, quantized states [32]. This quantum confinement effect fundamentally alters the electronic and optical behavior of materials. One of its most striking manifestations is the emergence of unconventional magnetic behavior in inherently diamagnetic metals. Bulk gold, for instance, is well known to be diamagnetic; however, nanostructured gold films and nanoclusters have been shown to exhibit ferromagnetic-like or spin-glass behavior, arising from the geometric confinement of electrons, the disproportionately large fraction of surface atoms, and the redistribution of surface charge carriers [37, 38]. These findings underscore how quantum-scale confinement can activate physical properties entirely absent at the macroscopic level.

I.4.3. Translating Properties into Innovative Applications

The ultimate goal of engineering nanomaterial properties is to translate them into practical, real-world solutions that address pressing challenges across medicine, electronics, and environmental sustainability. As the following applications demonstrate, nanomaterials have already begun to reshape entire industrial and scientific sectors [39–41].

A) Medicine:

The broad-spectrum antimicrobial activity of Ag NPs arises from their capacity to generate reactive oxygen species (ROS), disrupt bacterial cell membranes, and impair nucleic acid replication. Their high surface-area-to-volume ratio ensures maximized contact with bacterial membranes, making smaller particles inherently more reactive and lethal to pathogens such as Escherichia coli and Staphylococcus aureus [39, 42]. Recent in vitro studies confirm that Ag NPs at concentrations as low as 5.5 µg/mL display antibacterial efficacy against E. coli, with even enhanced performance when conjugated with antibiotic agents [43]. Beyond direct antimicrobial action, Ag NPs have been incorporated into injectable hydrogels and polymer nanocomposites that promote fibroblast migration, reduce infection rates, and release drugs in a controlled, pH responsive manner, enabling advanced wound healing and targeted drug delivery systems [44, 45].

B) Electronics:

The intrinsically high electrical conductivity of silver, combined with the extraordinary aspect ratios achievable in silver nanowires (Ag NWs), has opened a transformative chapter in flexible printed electronics. Ag NW networks deposited as thin films exhibit simultaneously high optical transmittance (>85%) and ultralow sheet resistance (~21 Ω/sq), making them ideal candidates to replace the brittle and indium-scarce indium tin oxide (ITO) in next-generation devices [40]. Screen-printable and inkjet-printable Ag NW inks have been formulated with conductivities reaching 1.9×10^5 S/m while sustaining over 1000 bending cycles without significant resistance increase, a critical benchmark for wearable and foldable devices [46]. As shown in **Figure (I.10)**, Au nanorods exemplify how tuning the aspect ratio (AR) of metallic nanostructures yields discrete, well-separated absorption peaks spanning the visible to near-infrared spectrum, a principle directly exploited in the design of plasmonic sensors, photodetectors, and transparent film heaters for touch panels [33].

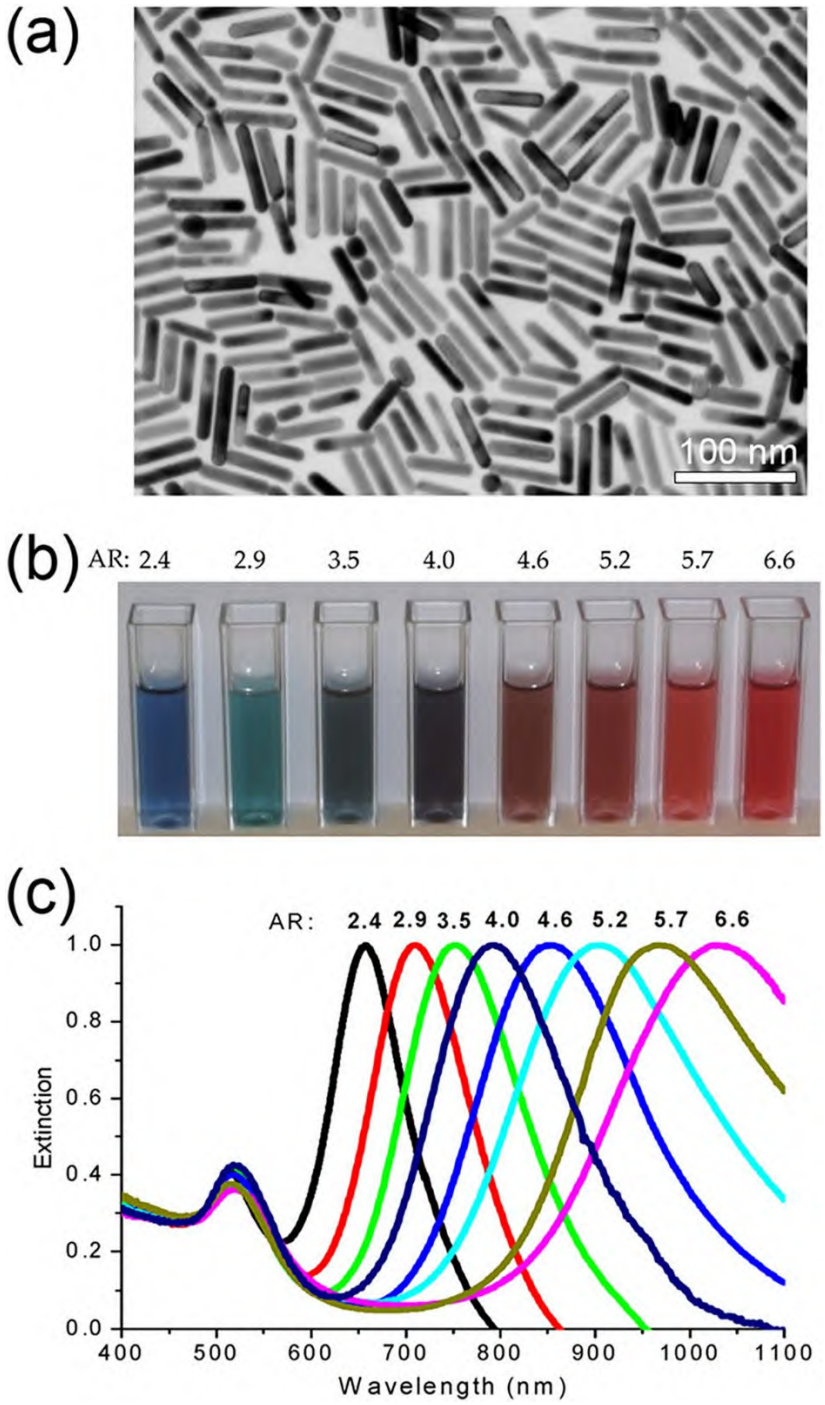

Figure (I.10): *Effect of aspect ratio (AR) on Au nanorods. (a) TEM image of Au nanorods with varying AR (2.4–6.6). (b) Optical photographs showing AR-dependent color tuning from blue to red. (c) UV-Vis spectra showing a systematic redshift of the longitudinal LSPR peak from ~640 nm to >1000 nm for plasmonic sensing and photodetection applications. (Adapted from Hang et al., Chem. Soc. Rev., 2024)*[33].

C) Environment and Agriculture:

Nanomaterials have emerged as powerful catalytic platforms for environmental remediation. Photocatalytic nanoparticles such as TiO_2 and ZnO generate reactive oxygen species (ROS) upon light irradiation, enabling the degradation of persistent organic pollutants, pharmaceutical residues, and textile dyes in wastewater with high efficiency and without secondary chemical additives [47, 48]. Silver nanoparticles further contribute to water disinfection by inactivating waterborne pathogens through membrane disruption and oxidative stress mechanisms [47]. In agriculture, engineered nanomaterials function as precision "nanofertilizers" that regulate the release of macro- and micronutrients in synchrony with plant demand, thereby minimizing leaching losses, reducing chemical input, and improving crop yields under both optimal and stress conditions [41]. Nanotechnology-based systems for targeted delivery of nutrients and pesticides represent a paradigm shift toward sustainable, resource-efficient farming.

In conclusion, the structure, property, application triad underscores that the transformative power of nanotechnology lies in our ability to engineer materials atom by atom and layer by layer. By mastering both "top-down" and "bottom-up" synthesis strategies, researchers can precisely tailor structural features (size, shape, surface chemistry, and dimensionality) that unlock the unique physicochemical properties demanded by the next generation of biomedical, electronic, and environmental breakthroughs [33, 39, 41].

References

References

1. Hulla J, Sahu S, Hayes A (2015) Nanotechnology. Hum Exp Toxicol 34:1318–1321. https://doi.org/10.1177/0960327115603588

2. ISO ISO (2015) TS 80004-2: 2015 nanotechnologies—vocabulary—part 2: nano-objects. Int Organ Stand Geneva 80004:

3. Roduner E (2006) Size matters: Why nanomaterials are different. Chem Soc Rev 35:583–592. https://doi.org/10.1039/b502142c

4. Gnach A, Lipinski T, Bednarkiewicz A, et al (2015) Upconverting nanoparticles: assessing the toxicity. Chem Soc Rev 44:1561–1584. https://doi.org/10.1039/C4CS00177J

5. Tiwari JN, Tiwari RN, Kim KS (2012) Zero-dimensional, one-dimensional, two-dimensional and three-dimensional nanostructured materials for advanced electrochemical energy devices. Prog Mater Sci 57:724–803. https://doi.org/10.1016/j.pmatsci.2011.08.003

6. Joudeh N, Linke D (2022) Nanoparticle classification, physicochemical properties, characterization, and applications: a comprehensive review for biologists. J Nanobiotechnology 20:262. https://doi.org/10.1186/s12951-022-01477-8

7. Pokropivny V V., Skorokhod V V. (2007) Classification of nanostructures by dimensionality and concept of surface forms engineering in nanomaterial science. Mater Sci Eng C 27:990–993. https://doi.org/10.1016/j.msec.2006.09.023

8. Heiligtag FJ, Niederberger M (2013) The fascinating world of nanoparticle research. Mater Today 16:262–271. https://doi.org/10.1016/j.mattod.2013.07.004

9. Mekuye B, Abera B (2023) Nanomaterials: An overview of synthesis, classification, characterization, and applications. Nano Sel 4:486–501. https://doi.org/10.1002/nano.202300038

10. Mekuye B, Abera B (2023) Nanomaterials: An overview of synthesis, classification, characterization, and applications. Nano Sel 4:486–501. https://doi.org/10.1002/nano.202300038

11. Kumari S, Sarkar L (2021) A review on nanoparticles: structure, classification, synthesis &

applications. J Sci Res 65:42–46

12. Eker F, Duman H, Akdaşçi E, et al (2024) A Comprehensive Review of Nanoparticles: From Classification to Application and Toxicity. Molecules 29:3482. https://doi.org/10.3390/molecules29153482

13. Pouran HM (2019) Engineered Nanomaterials in the Environment, their Potential Fate and Behaviour and Emerging Techniques to Measure Them. In: Handbook of Environmental Materials Management. Springer International Publishing, Cham, pp 1–15

14. Choi J, Kim BH (2024) Ligands of Nanoparticles and Their Influence on the Morphologies of Nanoparticle-Based Films. Nanomaterials 14:1685. https://doi.org/10.3390/nano14201685

15. Saleh TA (2020) Nanomaterials: Classification, properties, and environmental toxicities. Environ Technol Innov 20:101067. https://doi.org/10.1016/j.eti.2020.101067

16. Baig N, Kammakakam I, Falath W, Kammakakam I (2021) Nanomaterials: A review of synthesis methods, properties, recent progress, and challenges. Mater Adv 2:1821–1871. https://doi.org/10.1039/d0ma00807a

17. Poh TY, Ali NABM, Mac Aogáin M, et al (2018) Inhaled nanomaterials and the respiratory microbiome: clinical, immunological and toxicological perspectives. Part Fibre Toxicol 15:46. https://doi.org/10.1186/s12989-018-0282-0

18. Eker F, Duman H, Akdaşçi E, et al (2024) A Comprehensive Review of Nanoparticles: From Classification to Application and Toxicity. Molecules 29:3482. https://doi.org/10.3390/molecules29153482

19. Lu H, Tang SY, Yun G, et al (2020) Modular and Integrated Systems for Nanoparticle and Microparticle Synthesis—A Review. Biosensors 10:165. https://doi.org/10.3390/BIOS10110165

20. Shete MB, Patil TS, Deshpande AS, et al (2022) Current trends in theranostic nanomedicines. J Drug Deliv Sci Technol 71:103280. https://doi.org/10.1016/j.jddst.2022.103280

21. Díez-Pascual AM (2021) Carbon-based nanomaterials. Int J Mol Sci 22:7726. https://doi.org/10.3390/ijms22147726

22. Bhong SY, More N, Choppadandi M, Kapusetti G (2019) Review on carbon nanomaterials as typical candidates for orthopaedic coatings. SN Appl Sci 1:76. https://doi.org/10.1007/s42452-018-0082-z

23. Beach MA, Nayanathara U, Gao Y, et al (2024) Polymeric Nanoparticles for Drug Delivery. Chem Rev 124:5505–5616. https://doi.org/10.1021/acs.chemrev.3c00705

24. Gomez-Romero P, Pokhriyal A, Rueda-García D, et al (2024) Hybrid Materials: A Metareview. Chem Mater 36:8–27. https://doi.org/10.1021/acs.chemmater.3c01878

25. Hulla JE, Sahu SC, Hayes AW (2015) Nanotechnology: History and future. Hum Exp Toxicol 34:1318–1321. https://doi.org/10.1177/0960327115603588

26. Logothetidis S (2012) Nanotechnology: Principles and applications. In: NanoScience and Technology. pp 1–22

27. Pokropivny V, Lohmus R, Hussainova I, et al (2007) Introduction to nanomaterials and nanotechnology. Est Univ Tartu

28. Rahman M, Rimon MIH, Hasan Z, et al (2025) Nanotechnology and thermodynamics: a comprehensive review. Nanomater Energy 14:109–134. https://doi.org/10.1680/jnaen.24.00093

29. Gandhi M, Ramki S (2023) Role of Nanosystems for Electrochemical Mapping Using Diverse Carbon-Based Nanomaterials. In: Advanced Energy Materials. pp 1035–1065

30. Huang Q, Yang W, Zhou H (2024) Migration of grain boundary triple junctions in nanocrystalline metals initiated by accumulated dislocations. Int J Plast 173:103872. https://doi.org/10.1016/j.ijplas.2023.103872

31. Dangwal S, Edalati K, Valiev RZ, Langdon TG (2023) Breaks in the Hall–Petch Relationship after Severe Plastic Deformation of Magnesium, Aluminum, Copper, and Iron. Crystals 13:413. https://doi.org/10.3390/cryst13030413

32. Buerkle M, Lozac'h M, Mariotti D, Švrček V (2023) Quasi-band structure of quantum-

confined nanocrystals. Sci Rep 13:4684. https://doi.org/10.1038/s41598-023-31989-8

33. Hang Y, Wang A, Wu N (2024) Plasmonic silver and gold nanoparticles: shape- and structure-modulated plasmonic functionality for point-of-caring sensing, bio-imaging and medical therapy. Chem Soc Rev 53:2932–2971. https://doi.org/10.1039/d3cs00793f

34. Zhang X, Yan W, Lou X, et al (2024) Multi-field Coupled Inverse Hall–Petch Relations for Ferroelectric Nanocrystals. Acta Mech Solida Sin 37:139–147. https://doi.org/10.1007/s10338-023-00449-1

35. Guenther G, Guillon O (2014) Models of size-dependent nanoparticle melting tested on gold. J Mater Sci 49:7915–7932. https://doi.org/10.1007/s10853-014-8544-1

36. Hu S, Hu KJ, Zhao Z, et al (2024) In situ heating characterization of structural evolution and size-dependent melting point depression in gold nanoclusters: a comprehensive thermodynamic investigation. Nanoscale 16:18399–18409. https://doi.org/10.1039/d4nr02111h

37. Harke S, Habibpourmoghadam A, Evlyukhin AB, et al (2023) Low-frequency magnetic response of gold nanoparticles. Sci Rep 13:21588. https://doi.org/10.1038/s41598-023-48813-y

38. Das SK, Sahoo UP, Das B, et al (2023) Defect Induced Unconventional Ferromagnetism in Au Intercalated Bi2Se3 Nanocrystals for Spintronic Applications. Adv Quantum Technol 6:. https://doi.org/10.1002/qute.202300169

39. Jangid H, Singh S, Kashyap P, et al (2024) Advancing biomedical applications: an in-depth analysis of silver nanoparticles in antimicrobial, anticancer, and wound healing roles. Front Pharmacol 15:1438227. https://doi.org/10.3389/fphar.2024.1438227

40. Kayaharman M, Argasinski H, Atkinson J, et al (2023) Enhancing and Understanding the High Stretchability of Printable, Conductive Silver Nanowire Ink. J Electron Mater 52:4634–4643. https://doi.org/10.1007/s11664-023-10417-7

41. Karnwal A, Dohroo A, Malik T (2023) Unveiling the Potential of Bioinoculants and Nanoparticles in Sustainable Agriculture for Enhanced Plant Growth and Food Security. Biomed Res Int 2023:6911851. https://doi.org/10.1155/2023/6911851

42. Crisan MC, Pandrea SL, Matros L, et al (2024) In vitro antimicrobial activity of silver nanoparticles against selected Gram-negative and Gram-positive pathogens. Med Pharm Reports 97:280–297. https://doi.org/10.15386/mpr-2750

43. Ivanova N, Ermenlieva N, Simeonova L, et al (2023) Chlorhexidine–Silver Nanoparticle Conjugation Leading to Antimicrobial Synergism but Enhanced Cytotoxicity. Pharmaceutics 15:2298. https://doi.org/10.3390/pharmaceutics15092298

44. Harun-Ur-Rashid M, Foyez T, Krishna SBN, et al (2025) Recent advances of silver nanoparticle-based polymer nanocomposites for biomedical applications. RSC Adv 15:8480–8505. https://doi.org/10.1039/d4ra08220f

45. Zhang M, Gu G, Xu Y, et al (2024) Injectable Self-Healing Antibacterial Hydrogels with Tailored Functions by Loading Peptide Nanofiber-Biomimetic Silver Nanoparticles. Macromol Rapid Commun 45:2400173. https://doi.org/10.1002/marc.202400173

46. Li W, Yang S, Shamim A (2019) Screen printing of silver nanowires: balancing conductivity with transparency while maintaining flexibility and stretchability. npj Flex Electron 3:13. https://doi.org/10.1038/s41528-019-0057-1

47. Sanni SE, Oni BA, Okoro EE, Pandya S (2024) Recent advances in the use of biogenic nanomaterials and photocatalysts for wastewater treatment: challenges and future prospects. Front Nanotechnol 6:. https://doi.org/10.3389/fnano.2024.1469309

48. Elhenawy S, Khraisheh M, AlMomani F, et al (2024) Emerging Nanomaterials for Drinking Water Purification: A New Era of Water Treatment Technology. Nanomaterials 14:1707. https://doi.org/10.3390/nano14211707

CHAPTER II

Synthesis Strategies and Methods of Nanomaterials

II.1. Overview of Synthesis Strategies: Top-Down vs. Bottom-Up

Nanotechnology is fundamentally defined by the ability to engineer and manipulate matter within the precise range of 1 to 100 nm [1]. At this scale, traditional macroscopic laws of physics yield to surface-area-driven effects and quantum phenomena, resulting in materials whose chemical and physical properties differ drastically from their bulk counterparts. To harness these unique behaviors, researchers utilize two primary architectural philosophies: the Top-Down and Bottom-Up approaches. These strategies represent two divergent paths through which nanoscale complexity is achieved, each offering distinct advantages in terms of chemical purity, scalability, and structural control [1].

II.1.1. The Top-Down Philosophy: Precision Through Reduction

The top-down strategy is essentially a physical process of subtraction or fragmentation. It begins with a bulk material that is systematically broken down into successively smaller entities until the desired nanoscale dimensions are reached [1–3].

A) Core Mechanisms: This approach relies on powerful physical forces. Key techniques include **mechanical milling**, where high-energy impacts in planetary or shaker mills produce nanostructures from bulk powders [4]. Additional methods encompass **lithography** (using light or electron beams to pattern surfaces), **sputtering**, and **electrospinning** for nanofiber production [5].

B) The Power of Laser Ablation: A prominent green method within this category is **Laser Ablation in Liquid (LAL)** [6, 7]. An intense laser pulse strikes a solid target submerged in a liquid (typically deionized water), generating a plasma plume [8]. This plume produces expansive cavitation bubbles in which crystalline nanoparticles nucleate and coalesce. Upon bubble collapse, the particles diffuse into the surrounding liquid, forming a stable, ligand-free colloidal suspension [1].

C) Strategic Outlook: Top-down methods are valued for producing large quantities of high-purity nanoparticles that are often free from chemical contaminants [3]. However, they are energy-intensive, require substantial capital investment, and frequently yield broad particle-size distributions due to uncontrolled fracture events [2].

II.1.2. The Bottom-Up Philosophy: Complexity Through Assembly

The bottom-up approach mimics biological growth by assembling structures atom-by-atom or molecule-by-molecule [9]. It involves the controlled aggregation of molecular constituents through carefully managed nucleation and growth phases [2] , as illustrated in **Figure (II.1)**.

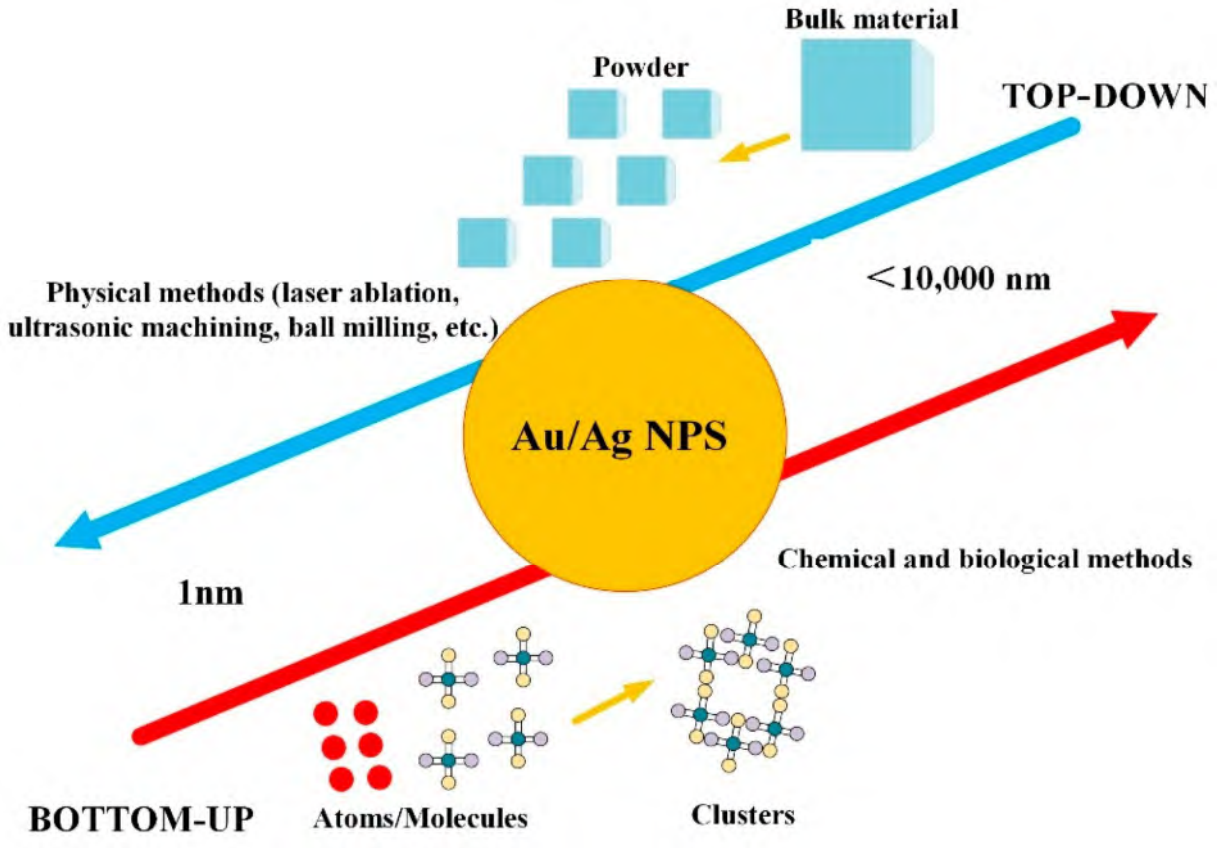

Figure (II.1): Schematic comparison of top-down and bottom-up approaches for the synthesis of Au/Ag nanoparticles, illustrating mass-reduction mechanisms (physical/mechanical routes) versus molecular-construction pathways (biological and chemical routes) [2].

A) Chemical and Wet-Lab Methods: The most common path owing to its low cost and high scalability [1]. Techniques such as **sol-gel processing**, **co-precipitation**, and **chemical vapor deposition (CVD)** enable the creation of highly uniform nanoparticles [10]. In the sol-gel method, metal alkoxide precursors are hydrolyzed and condensed to form a stable gel network, allowing researchers to fine-tune particle size by adjusting pH, temperature, and precursor concentration [1].

B) Biological and Green Synthesis: To circumvent hazardous chemicals, "green" synthesis has emerged as a vital bottom-up sub-category [5]. This approach employs **plant extracts** (rich in flavonoids and phenols), **microorganisms** (bacteria and fungi), or **algae** as natural reducing and capping agents [1]. Algae, for example, hyper-accumulate heavy-metal ions and transform them into malleable nanoparticle forms using proteins and polysaccharides as catalysts [11]. The resulting biogenic nanoparticles are highly valued in medicine for their superior biocompatibility [3].

C) Polymer-Based Assembly: Advanced methods such as Polymerization Induced Self Assembly (PISA) enable the creation of intricate morphologies, worms, spheres, and vesicles, at high solid concentrations (up to 50%) [12].

D) Strategic Outlook: Bottom-up methods offer unparalleled control over internal structure and chemical functionality [13]. While generally more cost-effective than top-down routes, they are sensitive to processing conditions (pH, temperature, and solvent choice), and chemical variants often require additional purification steps to remove unreacted precursors [14].

II.1.3. Morphology Control and Biological Efficacy

The choice between these strategies is rarely arbitrary; it is driven by the intended application. The size and shape of a nanomaterial are primary determinants of its biological efficacy [15]. For example, high aspect-ratio particles (rods and tubes) often exhibit prolonged circulation times in vivo and distinct cellular uptake kinetics compared to spherical counterparts [13].

Top down methods such as 3D printing and flow lithography are increasingly employed to fabricate complex, non-spherical shapes, including helical micro swimmers for targeted drug delivery, that are difficult to achieve through simple self-assembly [13, 16]. Conversely, bottom-up self-assembly of peptide amphiphiles (PAs) can generate long nanoribbons with exceptional mechanical strength, mimicking the porosity of natural tissue scaffolds [13].

II.1.4. The Synergistic Frontier

While top-down and bottom-up methods are traditionally viewed as opposing strategies, the future of materials science lies in their integration [13]. Synergistic approaches combine the

scalability of bottom-up assembly with the spatial precision of top-down fabrication [13], as illustrated in **Figure (II.2)**. A notable example is the 3D printing of shape-defined droplets or fibers, where top-down patterning provides architectural scaffolding for bottom-up self-assembled networks [13]. By mastering nanoparticle nucleation through these combined strategies, scientists can engineer the next generation of biocompatible sensors, catalysts, and targeted drug-delivery systems [2].

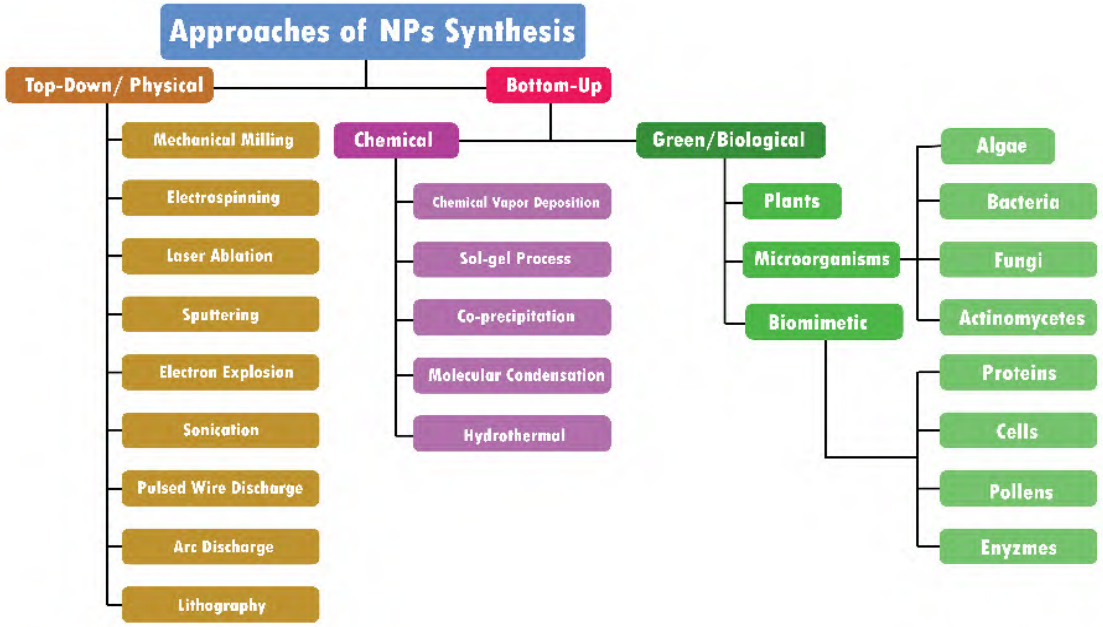

Figure (II.2): Classification of nanoparticle synthesis methodologies: a comprehensive overview of top-down (physical) and bottom-up (chemical and biological) paradigms, their principal techniques, and the resulting nanomaterial properties [1].

II.2. Physical Synthesis Methods

Engineering the Nanoscale through Direct Forces. Physical synthesis methodologies represent a robust architectural philosophy within nanotechnology, operating primarily under the top-down approach. This strategy begins with macroscopic bulk materials that are subsequently reduced to the nanoscale through a sequence of energetic operations [17]. Unlike chemical routes, physical methods rely on mechanical, thermal, optical, or electrical energies to dismantle matter, offering a pathway to high-purity materials with distinctive surface properties [18].

II.2.1. Mechanical Fragmentation: The Power of Attrition

Mechanical (ball) milling is one of the most established physical techniques for producing solid-state nanoparticles. The process involves loading bulk material into a rotating container filled with hard milling balls (hardened steel or tungsten carbide) under an inert atmosphere [19, 20].

A) Mechanism: Kinetic energy transferred from moving balls to the powder causes fracture, disrupts chemical bonds, and creates highly reactive new surfaces bearing dangling bonds [20].

B) Variables: The resulting particle morphology and size, typically 10–100 nm, are governed by milling duration, rotational speed, and the atmospheric medium used [21]. Although cost effective and capable of producing complex alloys, the method is energy intensive and prone to particle agglomeration in the absence of chemical stabilizers [18].

II.2.2. Laser-Based Synthesis: Precision through Light

Pulsed Laser Ablation in Liquid (LAL) has emerged as a green physical alternative to conventional synthesis. An intense pulsed laser beam, typically Nd:YAG, is focused onto a solid target submerged in a solvent such as deionized water or ethanol [22], as illustrated in **Figure (II.3)**.

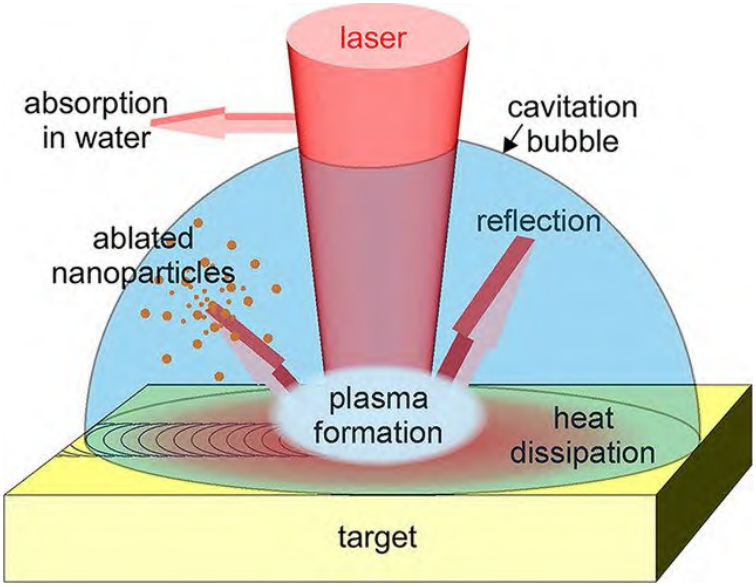

Figure (II.3): Mechanistic overview of laser ablation in liquid (LAL): plasma plume formation, cavitation bubble dynamics, and the nucleation/release of ligand-free nanoparticles into the surrounding colloidal medium. Reproduced with permission [23].

a) The Plasma Plume: The laser rapidly heats the target beyond its boiling point, generating a plasma plume , as illustrated in **Figure (II.4)**. As the plume cools and expands into the surrounding liquid, metal atoms condense and coalesce into nanoscale clusters [7].

b) Key Advantages: Nanoparticles produced via LAL are prized for being ligand-free and exceptionally pure [24], making them highly suitable for sensitive biomedical and food-industry applications. However, high equipment costs and relatively low production yields presently limit large-scale industrial adoption.

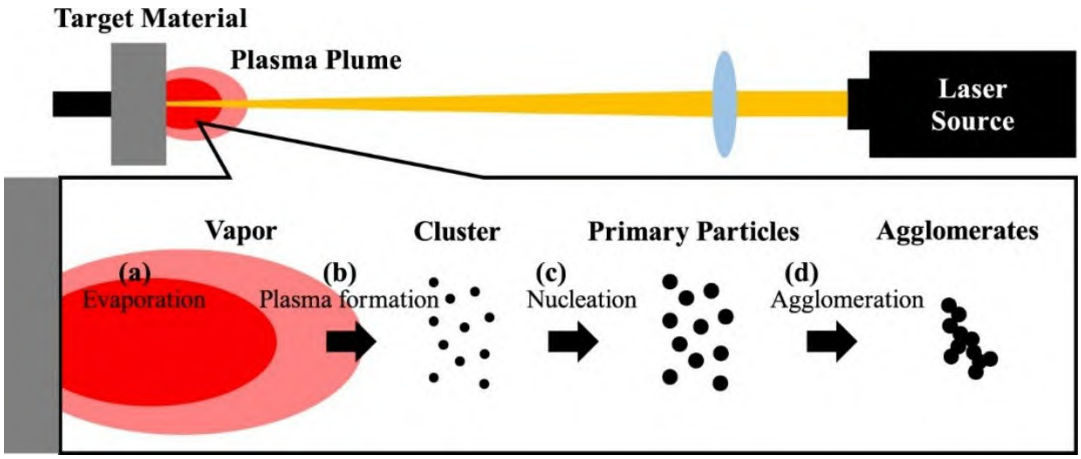

Figure (II.4): Detailed mechanistic diagram of nanoparticle formation via laser ablation in liquid: illustrating multiphoton ionization, plasma expansion, cavitation bubble collapse, and the release of stable, surfactant-free colloidal nanoparticles [25].

II.2.3. Vapor and Condensation Strategies

Vapor-based methods involve the phase transition of matter from condensed to gaseous, followed by controlled condensation.

a) Physical Vapor Deposition (PVD) and Sputtering: These techniques involve bombarding a target with high-energy ions (arc sputtering) or using thermal energy (evaporation) to eject atoms that deposit onto a substrate [26]. Sputtering is particularly effective for thin films, with particle size governed by substrate temperature and annealing duration [27].

b) Inert Gas Condensation: Metals are vaporized in a chamber containing inert gases (argon or helium). The vaporized atoms lose kinetic energy through collisions with the gas and are cooled by liquid nitrogen to yield fine particles in the 2–100 nm range [28, 29].

II.2.4. High-Energy Discharge and Pyrolysis

Additional high-energy physical routes focus on rapid vaporization via electrical discharge or intense heat:

a) Electrical Arc-Discharge: A high-current DC circuit is passed through electrodes (typically silver or titanium) submerged in a solvent, reducing metal ions or melting electrode tips to produce nanoparticle condensates [30].

b) Pulsed Wire Discharge: A pulsed high current vaporizes a metal wire, which then cools in an ambient gas atmosphere, yielding nanoparticles with high fabrication speed and energy productivity [19].

c) Laser Pyrolysis: Unlike solid-target ablation, this technique focuses an intense laser on a gaseous reactant mixture. The prevailing gas pressure critically determines the final particle-size distribution [28].

II.2.5. Strategic Outlook

The primary advantage of physical synthesis lies in its simplicity and chemical purity [17]. By avoiding hazardous chemical precursors, these methods eliminate complex purification steps. However, the top down nature of the processes typically demands substantial capital installations and sophisticated vacuum or high energy systems. Although they excel in producing high quality single crystalline films, e.g., via Ionized Cluster Beam Deposition [31], the challenge remains in scaling these energy intensive operations for global industrial demand without compromising nanoparticle uniformity.

II.2.6. Mechanical Milling and Attrition

Mechanical milling (MM) has proven to be a premier top-down approach for low-cost, high-yield production of nanomaterials. Unlike chemical assembly methods, MM relies on raw physical forces to dismantle macroscopic materials into nanostructured powders, alloys, and composites, as illustrated in **Figure (II.5).** The process occurs within a cylindrical milling chamber in which the kinetic energy of moving media is directly transferred to the powder charge [32].

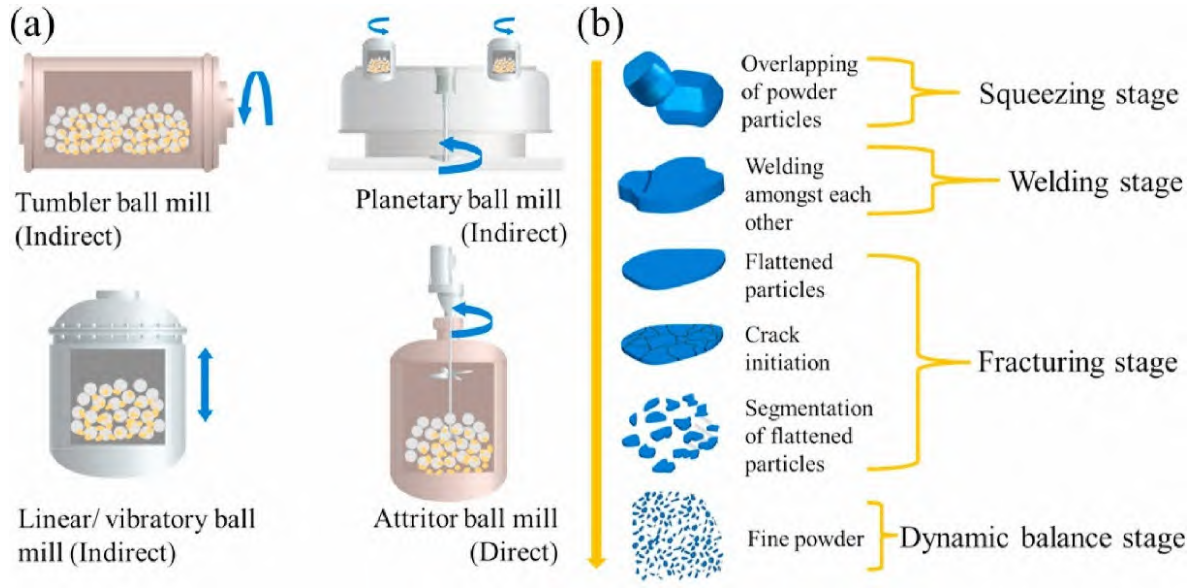

Figure (II.5): Schematic illustration of ball-milling configurations (tumbler, attritor, and SPEX shaker mills) and the mechanistic cycle of plastic deformation, cold-welding, and fracture in mechanical alloying, showing progressive nanocrystalline grain refinement [33] .

II.2.6.1. The Core Mechanics: A Cycle of Destruction and Rebuilding

At the heart of every milling operation is the ball–powder–ball collision [32]. When material is trapped between colliding balls of steel or tungsten carbide, it undergoes plastic deformation, cold-welding, and fracture. Fracture reduces particle size and creates chemically reactive surfaces. Cold-welding coalesces particles, temporarily increasing size. Through repetitive cycles of fragmentation and welding, the material reaches a steady-state nanocrystalline size distribution [32]. Mechanochemical energy at impact sites can induce local temperatures >1000 °C and pressures of several GPa, enabling the synthesis of metastable phases inaccessible by conventional thermal routes [34].

II.2.6.2. Technological Evolution: From Tumblers to Attritors

a) Tumbler Ball Mills: The most economical choice for large-scale production; the rotating cylinder causes balls to cascade, impacting the powder charge [32].

b) Attritor (Attrition) Mills: Invented by Szegvari (1922), these operate via a rotating vertical shaft with horizontal impellers, generating higher surface contact and differential movement than tumbler mills [32].

c) High-Energy Shaker Mills (e.g., SPEX): Used primarily in research, they agitate the charge in three mutually perpendicular directions at ~1200 rpm and are an order of magnitude faster than attrition mills [35].

II.2.6.3. Critical Process Variables and Kinetics

The kinetics of mechanical alloying are governed by energy-transfer efficiency [32]. Key parameters include:

a) Milling Media: Dense materials such as tungsten carbide are preferred because kinetic energy scales with ball mass and velocity [36].

b) Ball-to-Powder Ratio (BPR): Mass ratios of 5:1–10:1 are typically employed to maintain high collision frequency without reducing the mean free path of the balls [37].

c) Atmosphere and Contamination Control: Reactive metals such as aluminum or titanium require inert-gas atmospheres or process control agents (PCAs, e.g., polyethylene glycol) to suppress agglomeration and prevent contamination from mill media and ambient gases [18, 32].

II.2.6.4. Historical Context and Modern Applications

The technique was revolutionized in the late 1960s by **John Benjamin** at the International Nickel Company, who used mechanical alloying to produce Oxide Dispersion-Strengthened (ODS) superalloys [37, 38]. Today, MM is exploited to fabricate nanocrystalline phases with grain sizes as small as 10–20 nm [18], supporting applications ranging from wear-resistant coatings to hydrogen-storage materials [32].

II.2.7. Physical Vapor Deposition and Sputtering

Physical Vapor Deposition (PVD) represents a sophisticated class of vacuum coating technologies in which material is transformed from a condensed phase to vapor and then re-deposited as a thin film on a substrate, growing atom by atom [38]. PVD has become essential for extending the service life of machining tools, improving the tribological behavior of mechanical components, and enabling functional coatings in microelectronics [39]. High-purity coatings with thicknesses from a few atomic layers to several microns are routinely produced [40].

II.2.7.1. The PVD Landscape: Segmentation of Techniques

PVD technologies are categorized based on the mechanism used to eject material from the target: **Sputtering**, **Evaporation**, and **Arc Deposition** [41]. These methods differ significantly in atomic energy, deposition rates, and resulting coating microstructure [42].

II.2.7.2. Evaporation: The Thermal Route

a) Mechanism: The target is heated, typically by a high power electron beam, until its vapor pressure is sufficient to release particles that then condense on the cooler substrate [43].

b) Industrial Advantage: Exceptionally high deposition rates (up to 750,000 Å/min). Materials such as Cr and SiO are commonly deposited via sublimation [44].

c) Limitations: Compared with sputtering, evaporation yields larger grain sizes, lower adatom energy (~0.1–0.5 eV), and inferior film adhesion to the substrate [43].

II.2.7.3. Sputtering: The Kinetic Masterpiece

Sputtering (cathodic spraying) has emerged as a superior alternative for applications requiring precise stoichiometry and high surface quality. Unlike heat-driven evaporation, sputtering is powered entirely by kinetic energy [45].

a) The Process: Argon ions, accelerated by high voltage, bombard the target, ejecting atomic-sized particles that deposit on the substrate [43].

b) Power Sources: DC sputtering is used for conductive targets; **RF sputtering** for electrical insulators such as SiO_2 [44].

c) Magnetron Enhancement: Permanent magnets beneath the target concentrate argon plasma near the surface, increasing sputtering rate. **Magnetron Sputtering (MS)** improves film densification and enables deposition at substrate temperatures from 50 °C, reducing residual stresses [43].

II.2.7.4. Advanced Frontiers: HiPIMS and Reactive Sputtering

High-Power Impulse Magnetron Sputtering (HiPIMS) offers ionization rates up to 30%, delivering excellent film adhesion and conformal coverage of complex geometries [46]. Reactive sputtering introduces O_2 or N_2 into the process to deposit functional compound films, oxides

(Al_2O_3, TiO_2) or nitrides (TiN, ZrN), essential for hard, wear resistant applications [47], as illustrated in **Figure (II.6).**

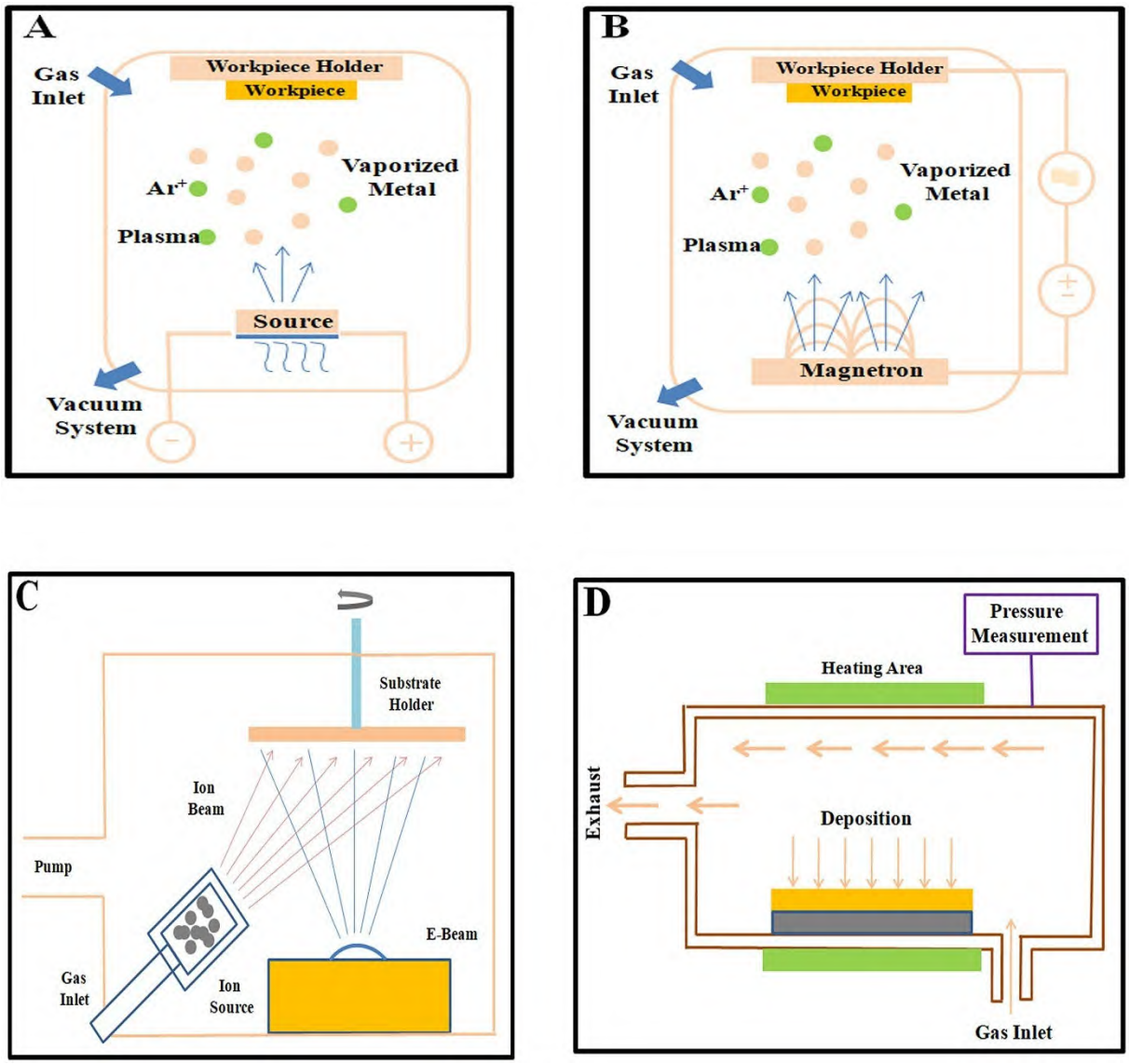

Figure (II.6): Schematic of PVD process variants (thermal evaporation, DC/RF sputtering, and magnetron sputtering), showing plasma generation, target-erosion mechanisms, and thin-film growth on substrate surfaces [48].

II.2.7.5. Strategic Outlook and Sustainability

A critical factor favoring PVD over traditional CVD is energy efficiency. Comparative studies show PVD consumes significantly less energy (e.g., 112 kWh for TiN) than CVD equivalents (974 kWh for $TiCN/Al_2O_3$), because PVD operates at lower temperatures (350–600 °C vs. 750–1150 °C) [49]. The integration of Computational Fluid Dynamics (CFD) and Finite Element Method (FEM) simulations is increasingly guiding reactor design and coating optimization [39].

II.2.8. Laser Ablation and Pulsed Laser Techniques

Operating as a robust physical top-down strategy [50], laser ablation employs high-power pulsed beams to rapidly vaporize solid targets submerged in liquid media [18], generating a plasma plume that condenses into exceptionally pure, ligand-free nanoparticles [51].

II.2.8.1. Fundamental Ablation Mechanisms: Nd:YAG or similar laser sources heat the target faster than thermal diffusion can dissipate energy, triggering multiphoton absorption and plasma formation. Metal atoms coalesce into nanoscale clusters as the plume cools [52].

II.2.8.2. Surface Purity and Biocompatibility: "Naked" nanoparticles devoid of chemical stabilizers are produced, making LAL a premier green substitute for conventional chemical-reduction methods and offering high biocompatibility for medical and food-industry applications [53].

II.3. Chemical Synthesis Methods

Chemical synthesis represents the most widespread bottom-up philosophy, in which atoms and molecules are assembled into nanoscale aggregates through controlled nucleation and growth [53]. These routes are prized for their simplicity, high production rates, and cost-effectiveness [54].

II.3.1. Principles of Molecular Assembly:

Nanoparticles emerge through electron transfer from precursor salts (e.g., $AgNO_3$ or metal chlorides) dissolved in a solvent [54]. By adjusting reactant concentrations and reaction conditions, specific morphologies, spheres, rods, and nanowires, can be engineered [55].

II.3.2. Functional Capping and Reduction:

The process relies on a balance between **reducing agents** (e.g., sodium borohydride, which donates electrons to reduce metal ions) and **stabilizers (capping agents)**, which coat particle surfaces to prevent aggregation and environmental degradation [56, 57].

II.3.3. Co-precipitation and Wet Chemical Routes

Co-precipitation involves mixing precursor salts with a base to trigger rapid solid formation in the liquid phase [58], as illustrated in **Figure (II.7)**. This energy-efficient process is particularly valued for large-scale production of metal oxides such as magnetite (Fe_3O_4) [59].

II.3.3.1. Kinetics of Rapid Precipitation: Phase formation completes within seconds [58]. Simultaneous precipitation of Fe^{2+} and Fe^{3+} ions by NaOH or NH_4OH immediately yields crystalline magnetite [58].

II.3.3.2. Challenges in Agglomeration and Stabilization: Precipitation and agglomeration occur simultaneously [58]. Colloidal stability is achieved by de-agglomeration using organic acids (e.g., citric acid) to ensure uniform aqueous dispersion [60].

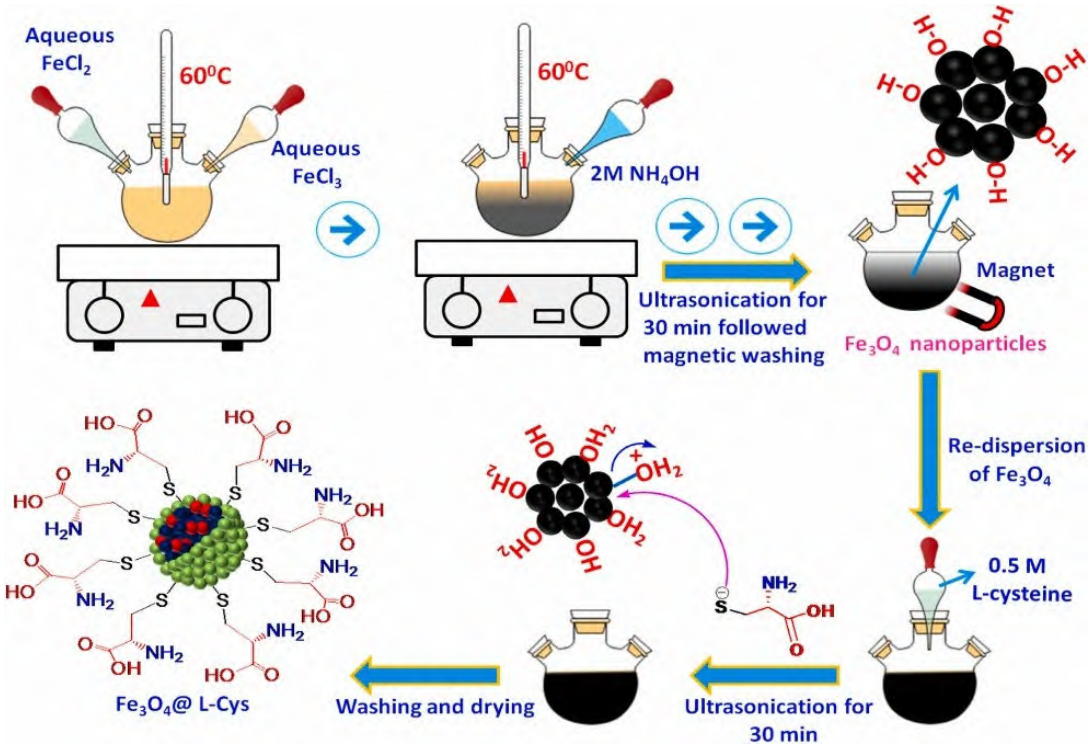

Figure (II.7): Coprecipitation approach for the synthesis of magnetically recyclable L-cysteine capped Fe_3O_4 nanoadsorbent. *(Adapted with permission from Bashir et al., 2021)*[61].

II.3.4. Sol–Gel and Hydrothermal/Solvothermal Methods

II.3.4.1. The Sol–Gel Network Evolution

The sol–gel process involves the sequential hydrolysis and condensation of metal alkoxide precursors, progressively transforming a colloidal "sol" into a three-dimensional rigid "gel" network [62]. As mechanistically depicted in **Figure (II.8)** , the process proceeds through distinct stages, precursor hydrolysis, polycondensation, gelation, drying (yielding xerogel or aerogel), and final calcination, ultimately producing crystalline metal oxide or perovskite nanostructures [62]. This route yields high-purity materials with large surface areas in a simple, cost-effective, and low-energy manner, while achieving molecular-level compositional homogeneity [62, 63].

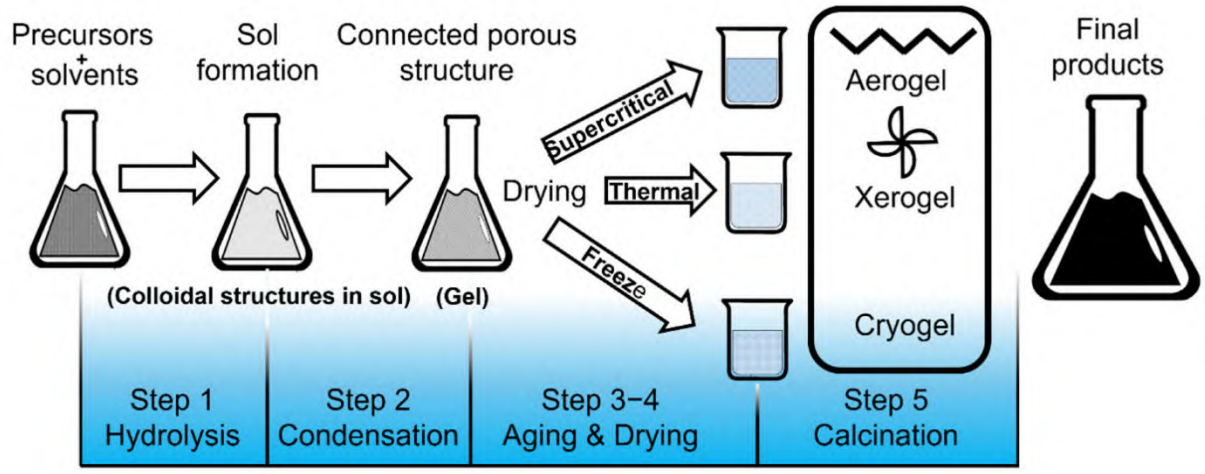

Figure (II.8): Schematic of the sol–gel synthesis process for metal oxide and perovskite nanomaterials: precursor hydrolysis and condensation steps, gelation, drying (xerogel/aerogel formation), and final calcination to produce crystalline nanostructures. [*Adapted from: Navas D. et al., Gels 2021, 7(4), 275.* [62]. Open Access, CC BY 4.0]

II.3.4.2. High-Pressure Hydrothermal/Solvothermal Routes

Hydrothermal and solvothermal methods employ aqueous or non-aqueous solvent media, respectively, under elevated temperatures and autogenous pressures within sealed reactors to direct crystal nucleation and growth [64]. The complete synthesis sequence is illustrated in **Figure (II.9)** metal ion sources and organic linkers are first mixed under stirring to form a

homogeneous reaction mixture, which is then transferred into a PTFE inner chamber housed within a sealed Teflon reactor, subjected to controlled temperature and pressure, and finally washed and dried to recover the crystalline product, in this case, Metal–Organic Framework (MOF) crystals [65]. This approach enables single-step fabrication of shaped, size-controlled crystalline materials, including MOFs, ceramics, and complex oxides, without requiring high-temperature sintering [64].

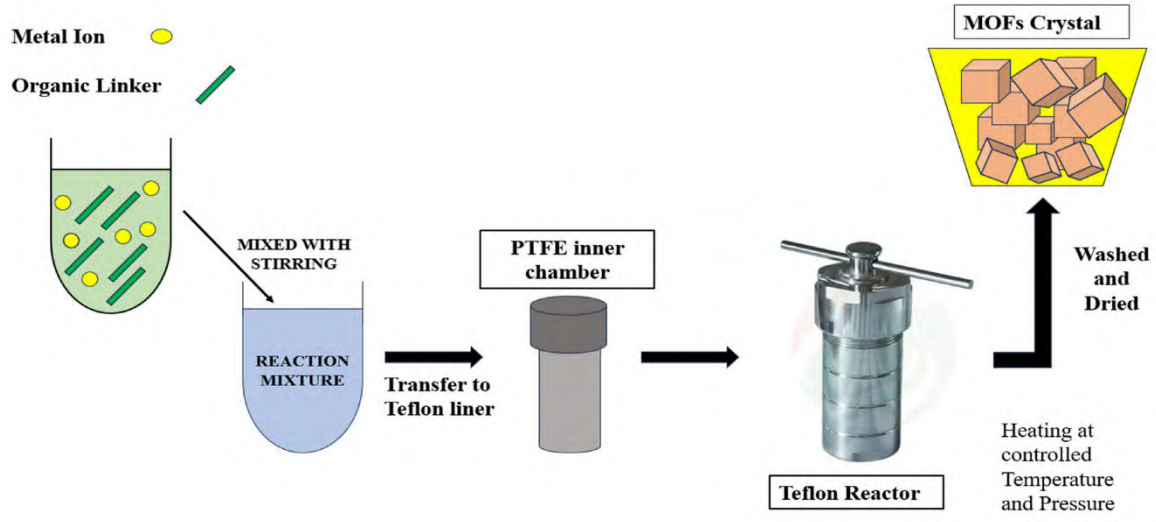

Figure (II.9): Schematic workflow of the hydrothermal/solvothermal synthesis of MOFs, from reaction mixture preparation to the recovery of dried MOF crystals. [*Adapted from: Lalawmpuia R. et al., Preprints 2023, 2023090192.* [66]. *Open Access, CC BY 4.0*]

Together, these soft solution processing routes, sol gel, hydrothermal, and solvothermal, provide a powerful and complementary toolkit for engineering advanced inorganic and hybrid materials with low energy consumption, precise morphological control, and molecular level compositional homogeneity [62, 64].

II.3.5. Microemulsion and Reverse Micelle Techniques

Microemulsions are isotropic, as schematically shown in **Figure (II.10)**, thermodynamically stable systems of oil, water, and amphiphilic surfactants that serve as precision nanoreactor templates for synthesizing monodisperse nanoparticles [67].

II.3.5.1. Reverse Micelles as Nanoreactors: In water-in-oil reverse micelle systems, hydrophilic surfactant heads sequester nanoscale "water pools," confining the reaction and preventing spontaneous aggregation of noble-metal colloids [67, 68].

II.3.5.2. Kinetic Regulation and Morphology Control: Final particle size is governed by the water-to-surfactant molar ratio (W): smaller W values yield tighter water pools and more stabilized nanoparticles [69]. Surfactant and reductant concentrations can direct growth into 1D nanowires [70].

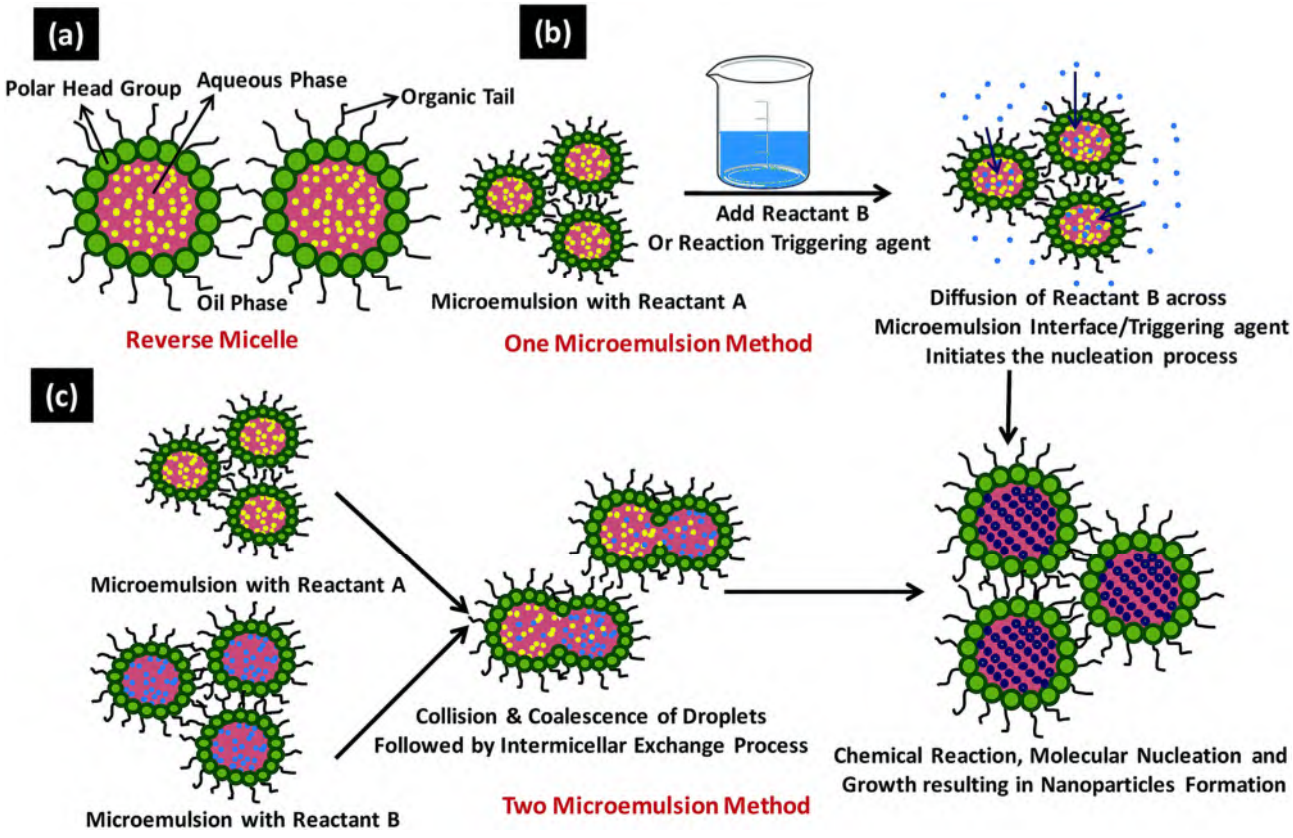

Figure (II.10): Schematic illustration of microemulsion-based synthesis of nanoparticles: (a) typical reverse micelle system, (b) steps in the one-microemulsion process, and (c) reaction sequence in the two-microemulsion process. *(Adapted with permission from Dhand et al., RSC Adv., 2015,* [71]*)*

II.3.6. Chemical Vapor Deposition (CVD) and Atomic Layer Deposition (ALD)

Vapor-phase technologies have revolutionized thin-film and 3D nanostructure fabrication by transcending liquid-phase limitations [72].

II.3.6.1. CVD – Rapid Source-Controlled Deposition: Vapor-phase precursors react to form solid thin films on a heated substrate [73]. High deposition rates and excellent scalability make CVD ideal for carbon-based nanomaterials and high-surface-area current collectors in energy-storage devices [74].

II.3.6.2. ALD – Surface-Controlled Atomic Precision: ALD uses sequential, self-limiting surface reactions to achieve angstrom-level control over film thickness and composition. Its "non-line-of-sight" capability ensures conformal coatings on complex 3D architectures, critical for pinhole-free protective shells in lithium-ion batteries [75], as illustrated in **Figure (II.11)**.

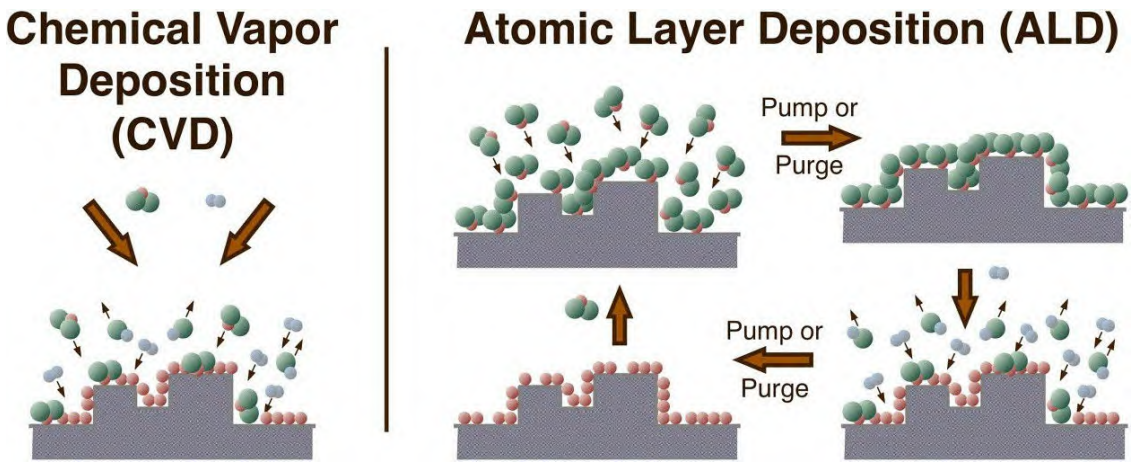

Figure (II.11): Schematic comparison of CVD and ALD processes: precursor delivery, surface reaction mechanisms, self-limiting growth characteristics, and the resulting thin-film morphologies for battery and supercapacitor electrode applications [76].

II.4. Green and Biogenic Synthesis

Biosynthesis is a component of green nanotechnology, relying on a bottom up strategy. This method utilizes natural sources, plants and microorganisms, as reducing and stabilizing agents to convert metal ions into nanoparticles, entirely replacing toxic chemical reagents.

Strategic Advantages: Biogenic synthesis surpasses traditional physical and chemical approaches by being low-cost, environmentally benign, non-toxic, and often performable in a single step under mild conditions (room temperature, neutral pH).

Biogenic synthesis directly contributes to several United Nations Sustainable Development Goals (SDGs) [77]:

* **SDG 3 – Good Health and Well-being:** Reduces mortality and disease caused by hazardous chemicals by replacing them with safe, bio-based alternatives [77].

* **SDG 6 – Clean Water and Sanitation:** Improves water quality by eliminating chemical waste and hazardous substance discharge [77].

* **SDG 9 – Industry, Innovation, and Infrastructure:** Promotes cleaner, resource-efficient industrial processes with reduced carbon footprints [77].

* **SDG 12 – Responsible Consumption and Production:** Achieves environmentally sound management of chemicals and wastes throughout their lifecycle, minimizing release into air, water, and soil [77].

* **SDG 12 (Waste Reduction):** Reduces waste generation through prevention, reduction, recycling, and reuse [77].

Biosynthetic methods contribute to these goals by employing green solvents (primarily water), maximizing atomic economy to minimize waste, and operating under mild conditions to conserve energy.

II.4.1. Plant-Extract-Mediated Synthesis

Plant-mediated synthesis has emerged as the most favored green strategy owing to its rapid kinetics and ease of industrial implementation. This method bypasses hazardous chemical reagents by exploiting renewable biological resources [78]. It is categorized within the bottom-up framework, consistent with the overall synthesis paradigm described in **Figure (II.2)**.

II.4.1.1. Phytochemicals as Dual Reducing and Capping Agents: Plant extracts are complex cocktails of bioactive molecules, flavonoids, phenols, terpenoids, alkaloids, and proteins [78]. These dual-function agents reduce metal ions (e.g., $Ag^{+} \rightarrow Ag^{0}$) and then cap

the resulting particles, forming a stable protective layer that prevents oxidation and agglomeration without external stabilizers [79], as illustrated in **Figure (II.12)**.

II.4.1.2. The Tri-Phase Mechanism of Nanoparticle Formation: (1) **Reduction/Nucleation Phase**: phyto-actives reduce metal ions to zero-valent atoms; (2) **Growth Phase**: atoms aggregate into larger nanostructures; (3) **Termination Phase**: biomolecules enrich the nanoparticle surface, defining the final morphology (spheres, triangles, or rods) [80].

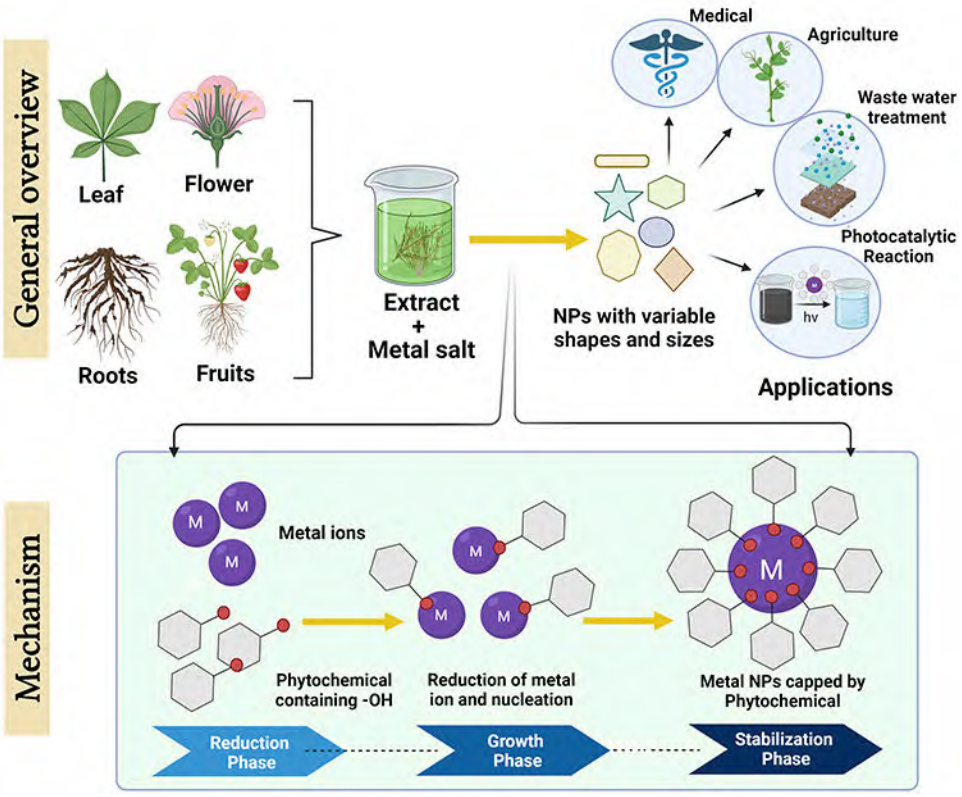

Figure (II.12): Schematic of plant-extract-mediated green synthesis of metallic nanoparticles, illustrating the dual role of phytochemicals (flavonoids, phenols, terpenoids) as reducing and capping agents and the three-phase formation mechanism: nucleation, growth, and termination [81].

II.4.2. Microbial and Enzyme-Assisted Routes: Living Nanofactories

Beyond plants, microorganisms and specific enzymes serve as highly precise biological platforms for nanoparticle fabrication, offering unique advantages in structural control and synthesis selectivity.

Microorganisms represent highly efficient living nano-factories for metallic nanoparticle (MtNP) biosynthesis. Microbial resources, including bacteria, fungi, yeast, algae, and viruses, synthesize nanoparticles through intracellular and extracellular routes, relying on bio-reducing agents such as enzymes, peptides, proteins, electron shuttle quinones, and exopolysaccharides [82]. As schematically illustrated in **Figure (II.13)**, these two routes are mechanistically distinct: in the intracellular pathway, metal ions are transported inside the cell and reduced by intracellular enzymes to form nanoparticles within the cell wall, while in the extracellular pathway, ions are reduced by secreted enzymes and released directly into the culture broth [82, 83].

The extracellular pathway is strongly preferred for industrial scale-up, as it entirely bypasses complex cell-disruption and downstream processing steps [82]. Extracellular microbial enzymes play a significant role as reducing agents in MtNP production; cofactors such as NADH and NADPH dependent enzymes act as electron carriers, transferring electrons from NADH to metal ions, thereby initiating reduction, for example, reducing Au^{3+} to Au^{0} to form gold nanoparticles [83]. Several fungi produce extracellular enzymes, including acetyl xylan esterase, cellobiohydrolase D, glucosidase, and β glucosidase, which play a significant role in MtNP biosynthesis, with nitrate reductase being a key enzyme secreted by fungi to facilitate bioreduction and nanoparticle formation [83]. This enzymatic capacity significantly enhances particle stability, yield, and monodispersity [83, 84].

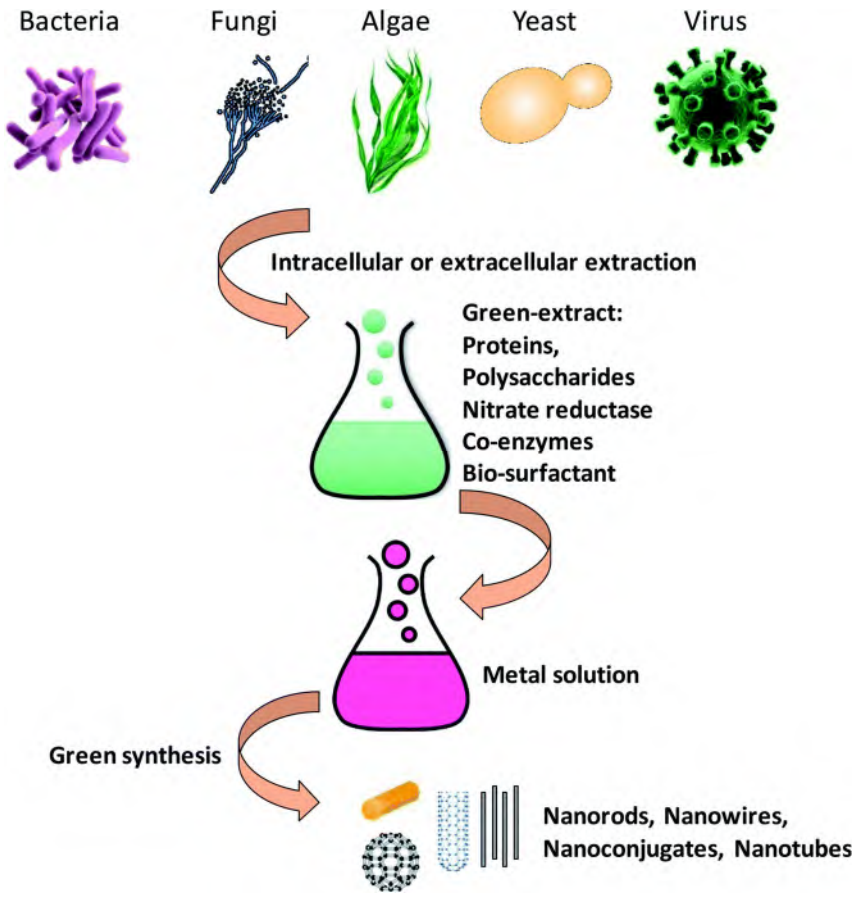

Figure (II.13): Schematic comparison between the extracellular (reductase-mediated secretion) and intracellular (inside the cell) enzymatic pathways for microbial metal nanoparticle biosynthesis. [*Adapted from: Ovais M. et al., Int. J. Mol. Sci. 2018, 19, 4100.* [83]. *Open Access, CC BY 4.0*]

Modern enzyme-assisted extraction (EAE) employs specific hydrolytic enzymes to disrupt the lignocellulosic matrix of plant cell walls, as mechanistically depicted in **Figure (II.14)**. Three principal enzyme classes operate synergistically: cellulases cleave glycosidic bonds in the cellulose backbone; hemicellulases hydrolyze hemicellulose backbones; and pectinases degrade the pectin matrix, collectively releasing phenolic compounds, reducing sugars, and polysaccharides that serve as both reducing and capping agents for nanoparticle synthesis [84, 85]. The released bioactive compounds can substantially increase NP synthesis yield compared to conventional solvent extraction, while the mild processing conditions (30–60°C, pH 4–6, without hazardous organic solvents) ensure exceptional biocompatibility of the resulting nanoparticles [85, 86]. Furthermore, enzymes can be immobilized on magnetic nanoparticles for

multi-cycle reuse, rendering the process economically attractive for industrial implementation [85].

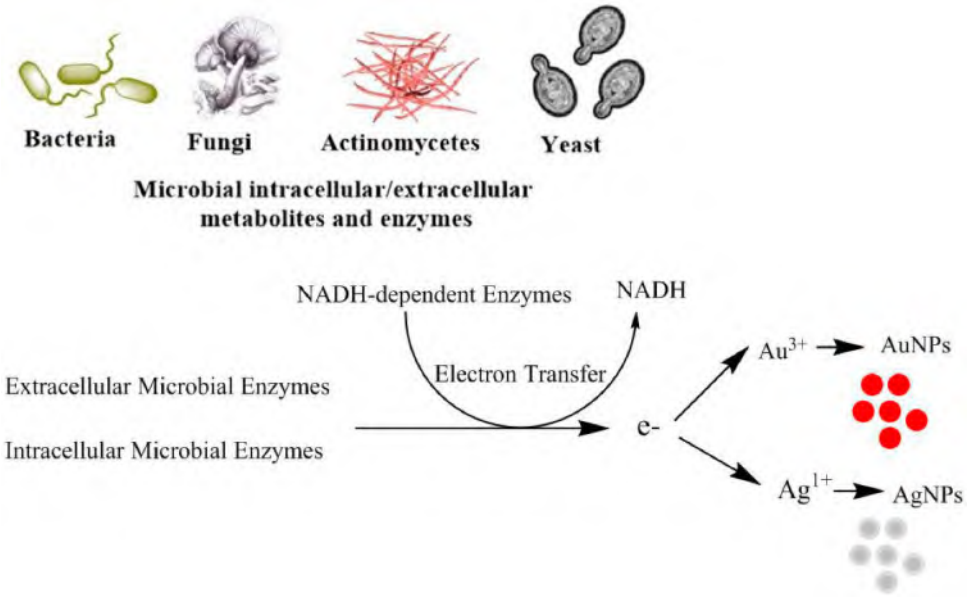

Figure (II.14): Overview of NADH-dependent microbial enzymes in MtNP biosynthesis, detailing the extracellular reduction mechanism, involved fungal enzymes, synthesized nanoparticles (Ag, Au, metal oxides), and its advantages. [*Adapted from: Gahlawat G. & Choudhury A.R., RSC Adv. 2019, 9, 12944–12967.* [82]. *Open Access, CC BY-NC 3.0*]

II.4.3. Advantages, Limitations, and Scalability of Green Synthesis

II.4.3.1. Strategic Superiority and Clinical Safety: Green synthesis aligns with Sustainable Development Goals [77]. It is cost-effective, non-toxic, and energy-efficient at room temperature and neutral pH [78]. Eliminating toxic residues (e.g., sodium borohydride) yields nanoparticles with superior **biocompatibility**, making them safer for clinical drug delivery and antimicrobial coating applications [77].

II.4.3.2. Technical Hurdles – Reproducibility and Industrial Expansion: The complexity of biological extracts poses major **reproducibility** challenges. Metabolite concentrations vary with plant geography and season, hindering the atom-level uniformity required for precision electronics. Microbial processes can take 24–120 hours and require strict culture maintenance, escalating industrial costs. Consistent large-scale production

while managing heat transfer and mass limitations in bioreactors remains an active research focus [2].

II.5. Emerging and Advanced Synthesis Approaches

Modern nanotechnology is transitioning away from traditional "trial-and-error" batch processes toward high-precision, automated, and hybrid methodologies. These emerging approaches prioritize spatiotemporal control of reactions, enabling the creation of materials that are often unattainable in standard glassware [87]. They bridge the gap between top-down physical forces and bottom-up chemical assembly, opening a new operational window for engineering non-equilibrium states and complex architectures [88].

II.5.1. Microwave-Assisted and Ultrasonic Methods

These techniques exploit specific energy forms, electromagnetic radiation and acoustic waves, to overcome the kinetic barriers of conventional thermal heating, as illustrated in **Figure (II.15)**.

II.5.1.1. Microwave-Assisted Synthesis (MAS): Microwaves interact directly with polar components of the reaction mixture via magnetic and dielectric loss mechanisms, producing rapid, uniform "volumetric heating" that significantly reduces reaction times and suppresses side reactions, as exemplified in green synthesis of fluorescent N-CQDs from natural precursors like lemon/onion juices or xylan under domestic or commercial microwave conditions [89].

II.5.1.2. Ultrasonic-Assisted Extraction and Synthesis (UAE): This method relies on acoustic cavitation, the formation, growth, and violent collapse of microbubbles. The implosion creates localized hot spots (~5000 °C, ~2000 atm) that intensify mass transport and rupture chemical bonds [2].

II.5.1.3. Synergistic Hybridization (UMAE): Combining ultrasonic and microwave energies delivers far higher yields and shorter processing times than either technique alone [90].

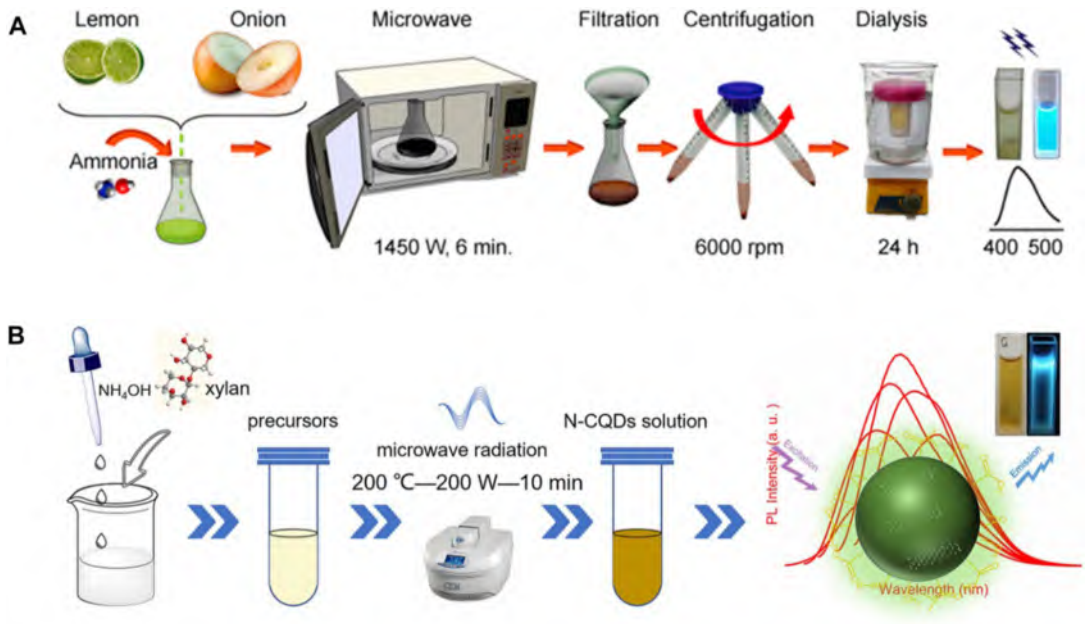

Figure (II.15): Microwave-assisted synthesis of N-doped carbon quantum dots (N-CQDs) from bio-based precursors using domestic (A) and commercial (B) microwave methods. *[Monte-Filho et al., J. Pharm. Analysis 2019, 9, 209.* [91] *& Yang et al., Opt. Mater. 2018, 85, 329.* [92]*– Open Access sources].*

II.5.2. Electrochemical and Sonochemical Routes

II.5.2.1. Precision Electrochemical Synthesis

Electrochemical synthesis enables the formation of high-entropy metal hydroxide nanoparticles (and oxides after subsequent calcination) at the cathode, boosted by the hydrogen evolution reaction (HER), without the need for stoichiometric oxidants or metal catalysts. This method simplifies purification, reduces toxic residues in the final product, and leverages local alkalinity generation for controlled precipitation [93]. As shown in **Figure (II.16)**, a high current density drives the cathodic HER ($2H_2O + 2e^- \rightarrow H_2 + 2OH^-$), producing OH^- ions and hydrogen bubbles that create a turbulent environment. These OH^- ions then react with multiple metal cations (e.g., Fe^{3+}, Mn^{2+}, Ni^{2+}, Ca^{2+}, Mg^{2+}) in the electrolyte to form high-entropy hydroxide nanoparticles ($M^{n+} + xOH^- \rightarrow M(OH)_x$). Adjusting the current density alone controls nucleation kinetics, particle size, morphology, elemental homogeneity, and prevents agglomeration, offering significant advantages over conventional sol-gel or multi-step chemical routes [93, 94].

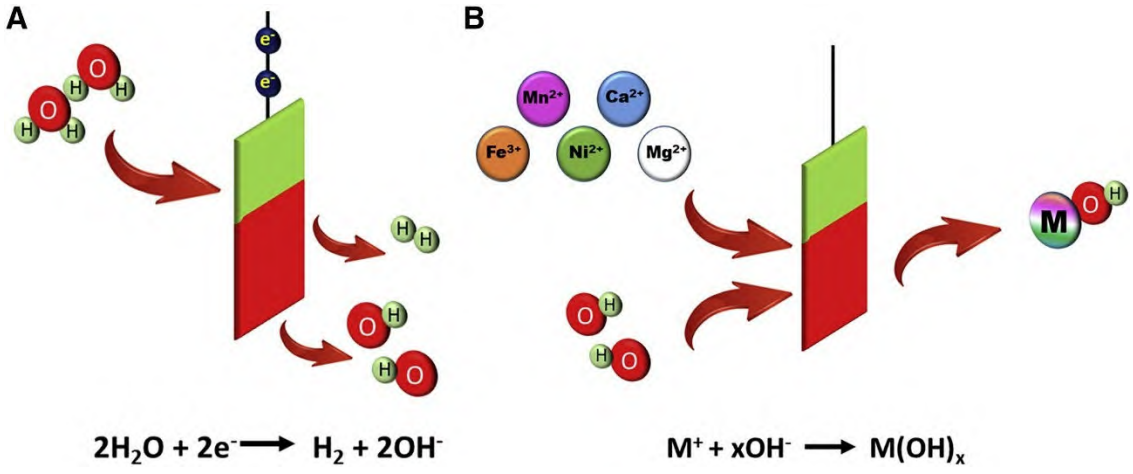

Figure (II.16): Schematic illustration of the mechanism in high current density electrochemical synthesis of high-entropy hydroxides boosted by hydrogen evolution reaction (HER). *(Adapted from Ritter et al.* [93]*)*

II.5.2.2. Sonochemical Catalysis

Acoustic cavitation drives sonochemical synthesis: ultrasonic irradiation nucleates microbubbles that accumulate energy over successive oscillation cycles and then collapse implosively, generating local hotspot temperatures exceeding 5000 K and pressures above 1000 atm [95]. These extreme transient conditions produce primary OH• and H• radicals via homolytic water sonolysis, which initiate reductive reactions to yield amorphous metal nanoparticles or crystalline composites in aqueous or non-aqueous media [95, 96]. As depicted in **Figure (II.17)**, reactivity unfolds across three zones: the bubble interior (Zone 1, primary radical generation), the bubble-liquid interface (Zone 2, seed nucleation), and the bulk solution (Zone 3, nanoparticle growth and stabilization) [95]. The approach is inherently green, operating at ambient bulk temperature and pressure with no metal catalysts required [95].

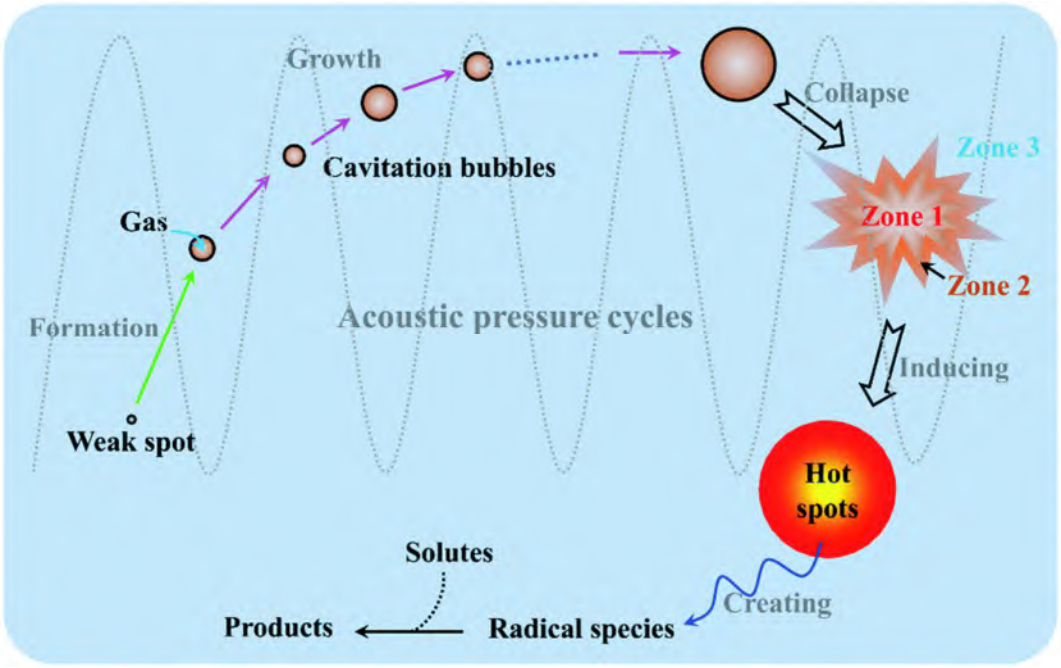

Figure (II.17): Schematic of the three reaction zones in acoustic cavitation for sonochemical synthesis: Zone 1 (bubble interior/hotspot, primary radicals OH•/H•), Zone 2 (interface, seed nucleation), Zone 3 (bulk liquid, nanoparticle growth). *(Adapted from Li et al. [95])*

II.5.2.3. Sonoelectrochemistry

Sonoelectrochemistry couples ultrasonic irradiation with electrochemical deposition to deliver synergistic improvements unavailable to either technique alone [97]. Acoustic streaming enhances mass transport of reactant ions to the electrode surface; cavitation collapse continuously removes passivating oxide layers and electrogenerated gas bubbles, maintaining a pristine reactive interface; and acoustic perturbation during nucleation promotes finer grain size and higher nucleation density. The combined approach yields exceptionally pure nanostructures with superior electrochemical activity, making it particularly valuable for fuel cell electrocatalysts and voltammetric sensors [97].

II.5.3. Microfluidic and Continuous-Flow Synthesis

Microfluidic technology enables the meticulous management of the particle-forming environment, handling fluid volumes ranging from 10^{-9} to 10^{-18} L through channels of tens to hundreds of micrometers, offering precise spatiotemporal control over nucleation and growth [87].

II.5.3.1. Continuous-Flow Paradigms

In continuous-flow microfluidic devices, the laminar flow regime (low Reynolds number) enables the controlled formation of tunable and self-engineered Reaction–Diffusion (RD) environments. Mixing occurs solely by molecular diffusion, establishing conditions that mimic processes found in nature and allowing the capture of metastable kinetic states unattainable by conventional bulk mixing [87, 98].

II.5.3.2. Segmented (Droplet) Microfluidics

Segmented-flow microfluidic systems compartmentalize reagents into micro-droplet arrays separated by an immiscible phase, providing very fast homogenization methods and well-defined supersaturation regimes that can be manipulated and controlled at the millisecond scale [87]. Each droplet acts as an independent nanoreactor confined to picoliter-sized volumes, enabling high-throughput synthesis of nanoparticles with narrow size distributions [98].

II.5.3.3. Scalability via "Numbering Up"

Rather than the complex sequential scale-up approach of batch reactors, microfluidic systems are scaled through parallelization, replicating identical, optimized micro-units operating simultaneously. This strategy maintains reactor geometry stability while enabling high throughput through linear scaling by increasing the number of channels, thus preserving laboratory scale precision during mass production [98].

II.5.3.4. Hyphenated In-Situ Monitoring

Integration of microfluidic synthesis with real time characterization tools, including SAXS and XANES, allows scientists to observe nanoparticle nucleation and growth as they occur. This provides experimental evidence to refine mechanistic models such as the LaMer and Brust Schiffrin models [98].

The key strategies governing microfluidic synthesis are illustrated in **Figure (II.18)**, which presents a comparative overview of continuous-flow laminar mixing for Reaction–Diffusion (RD) control alongside segmented droplet microfluidics functioning as isolated nanoreactors [87, 98]. The figure also depicts the "numbering up" scale-up strategy and the coupling with in-situ SAXS/XANES monitoring to track nanoparticle formation in real time [98, 99].

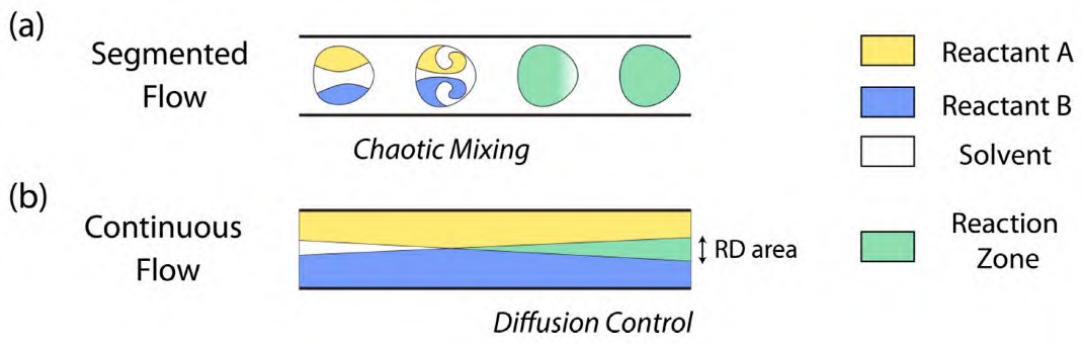

Figure (II.18): Comparison of segmented-flow and continuous-flow microfluidic systems for nanoparticle synthesis and characterization [87].

II.6. Comparative Analysis of Synthesis Methods

Choosing a synthesis pathway is a strategic decision that balances desired material properties with economic and environmental constraints. As shown in **Figure (II.19),** researchers must weigh high-energy top-down solid-matter fractionation against high-precision bottom-up molecular assembly [84]. While physical methods offer high purity, they are limited by capital costs, whereas chemical and biological methods offer scalability at the expense of environmental-toxicity risks or complex purification requirements [100].

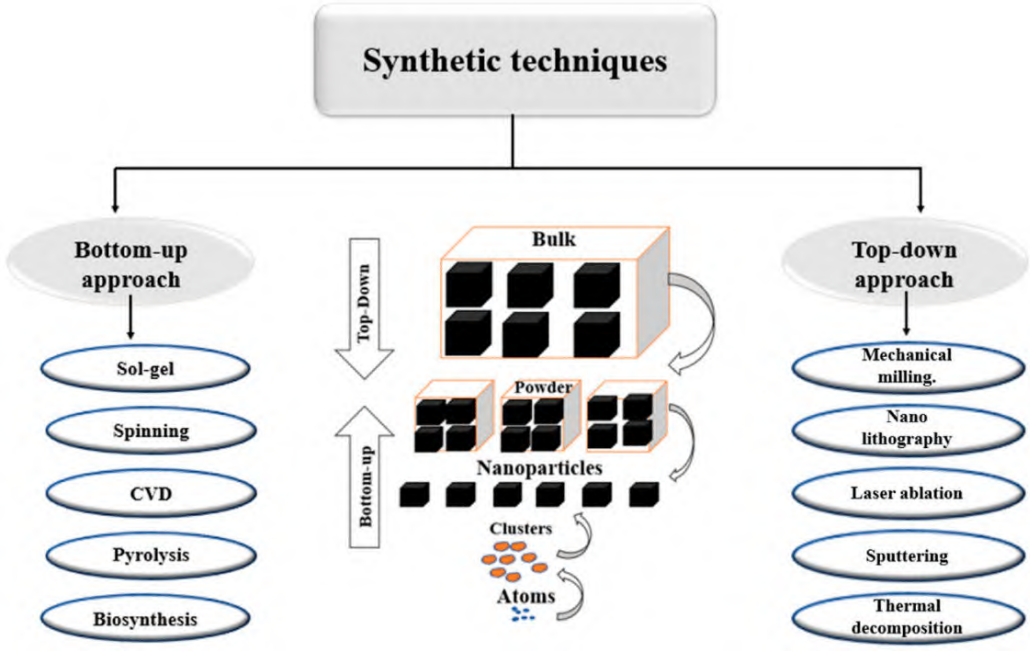

Figure (II.19): Comparison of top-down and bottom-up nanoparticle synthesis approaches.

[Khan, Y. et al. Catalysts 2022, 12 (11), 1386. [101]]

A multidimensional evaluation of these synthesis pathways is presented in **Table (II.1)**, which compares the methods across four critical criteria: environmental impact, morphological control, industrial scalability, and economic cost. This comparative framework enables researchers to select the most appropriate synthesis route based on their specific application requirements and resource constraints.

Table (II.1): Multidimensional comparative analysis of nanomaterial synthesis methods across environmental impact, morphological control, industrial scalability, and economic cost.

Synthesis Method	**Economic Cost**	**Industrial Scalability**	**Morphological Control**	**Environmental Impact**
Mechanical Milling (Top-down)	Very Low – most cost-effective for mass production	High – standard industrial process for powders and alloys	Poor – wide particle-size distribution; limited shape control	**High – noise pollution and risk of media contamination**
Laser Ablation (Top-down)	High – requires sophisticated pulsed-laser installations	Moderate – limited by low production yields in current configurations	Excellent – yields ultrapure, ligand-free colloidal nanoparticles	**Low – regarded as a "green" physical alternative to chemical reduction**
Sol-Gel Processing (Bottom-up)	Moderate/Low – cost-effective precursors	High – applicable to large-scale coatings and porous films	Very High – atomic-level compositional homogeneity and porosity control	**Moderate – lower energy use; involves some chemical precursors**
Biosynthesis (Bottom-up)	Low – leverages inexpensive, renewable biological feedstocks	Challenging – limited by long reaction times and complex purification	Moderate – size and shape vary with biological source and seasonality	**Minimal – non-toxic, aqueous-based; aligned with green chemistry**

				principles
CVD / ALD (Bottom-up)	High – specialized equipment and precursor gases	Very High – suited for continuous, high-volume thin-film production	Excellent – atomic and molecular-level structural precision	**High – involves toxic, explosive, or corrosive precursor gases**
Molten-Salt Synthesis (MSS) (Bottom-up)	Low – uses simple, reusable molten-salt reaction medium	High – intrinsically scalable for crystalline ceramic powders	High – size and shape readily tuned via salt identity and temperature	**Low – non-toxic media; short reaction times**

References

References

1. Altammar KA (2023) A review on nanoparticles: characteristics, synthesis, applications, and challenges. Front Microbiol 14:. https://doi.org/10.3389/fmicb.2023.1155622
2. Jiang Z, Li L, Huang H, et al (2022) Progress in Laser Ablation and Biological Synthesis Processes: "Top-Down" and "Bottom-Up" Approaches for the Green Synthesis of Au/Ag Nanoparticles. Int J Mol Sci 23:. https://doi.org/10.3390/ijms232314658
3. Shin WK, Cho J, Kannan AG, et al (2016) Cross-linked Composite Gel Polymer Electrolyte using Mesoporous Methacrylate-Functionalized SiO2 Nanoparticles for Lithium-Ion Polymer Batteries. Sci Rep 6:26332. https://doi.org/10.1038/srep26332
4. Rao NH, Lakshmidevi N, Pammi SVN, et al (2016) Green synthesis of silver nanoparticles using methanolic root extracts of Diospyros paniculata and their antimicrobial activities. Mater Sci Eng C 62:553–557. https://doi.org/10.1016/j.msec.2016.01.072
5. Baig N, Kammakakam I, Falath W, Kammakakam I (2021) Nanomaterials: A review of synthesis methods, properties, recent progress, and challenges. Mater Adv 2:1821–1871. https://doi.org/10.1039/d0ma00807a
6. Patil PP, Phase DM, Kulkarni SA, et al (1987) Pulsed-laser induced reactive quenching at liquid-solid interface: Aqueous oxidation of iron. Phys Rev Lett 58:238–241. https://doi.org/10.1103/PhysRevLett.58.238
7. Zhang D, Gökce B, Barcikowski S (2017) Laser Synthesis and Processing of Colloids: Fundamentals and Applications. Chem Rev 117:3990–4103. https://doi.org/10.1021/acs.chemrev.6b00468
8. Ogale SB (1988) Pulsed-laser-induced and ion-beam-induced surface synthesis and modification of oxides, nitrides and carbides. Thin Solid Films 163:215–227. https://doi.org/10.1016/0040-6090(88)90426-9
9. Wu W, Shevchenko E V. (2018) The surface science of nanoparticles for catalysis: electronic and steric effects of organic ligands. J Nanoparticle Res 20:255. https://doi.org/10.1007/s11051-018-4319-y
10. Das G, Shin HS, Patra JK (2020) Comparative assessment of antioxidant, anti-diabetic and cytotoxic effects of three peel/ shell food waste extract-mediated silver nanoparticles. Int J Nanomedicine 15:9075–9088. https://doi.org/10.2147/IJN.S277625
11. Negi S, Singh V (2018) Algae: A potential source for nanoparticle synthesis. J Appl Nat

Sci 10:1134–1140. https://doi.org/10.31018/jans.v10i4.1878

12. Larnaudie SC, Sanchis J, Nguyen TH, et al (2018) Cyclic peptide-poly(HPMA) nanotubes as drug delivery vectors: In vitro assessment, pharmacokinetics and biodistribution. Biomaterials 178:570–582. https://doi.org/10.1016/j.biomaterials.2018.03.047
13. Cook AB, Clemons TD (2022) Bottom-Up versus Top-Down Strategies for Morphology Control in Polymer-Based Biomedical Materials. Adv NanoBiomed Res 2:. https://doi.org/10.1002/anbr.202100087
14. Chen S, Yang L, Leung FKC, et al (2022) Photoactuating Artificial Muscles of Motor Amphiphiles as an Extracellular Matrix Mimetic Scaffold for Mesenchymal Stem Cells. J Am Chem Soc 144:3543–3553. https://doi.org/10.1021/jacs.1c12318
15. Li J, Mao H, Kawazoe N, Chen G (2017) Insight into the interactions between nanoparticles and cells. Biomater Sci 5:173–189. https://doi.org/10.1039/c6bm00714g
16. Doherty RP, Varkevisser T, Teunisse M, et al (2020) Catalytically propelled 3D printed colloidal microswimmers. Soft Matter 16:10463–10469. https://doi.org/10.1039/d0sm01320j
17. Iqbal P, Mendes PM, Preece JA (2012) Nanotechnology: The "Top-Down" and "Bottom-Up" Approaches. In: Supramolecular Chemistry. Wiley, pp 1–14
18. Duman H, Eker F, Akdaşçi E, et al (2024) Silver Nanoparticles: A Comprehensive Review of Synthesis Methods and Chemical and Physical Properties. Nanomaterials 14:1527. https://doi.org/10.3390/nano14181527
19. Krishnappa K, Pandiyan J, Paramanandham J, Elumalai K (2018) International Journal of Zoology Studies Antibacterial and mosquitocidal potentials of selected Indian medicinal plants extracts and synthesized silver nanoparticles. Int J Zool Stud 3:15–25
20. Winterer M, Hahn H (2003) Nanoceramics by chemical vapour synthesis. Zeitschrift fuer Met Res Adv Tech 94:1084–1090. https://doi.org/10.3139/146.031084
21. Abid N, Khan AM, Shujait S, et al (2022) Synthesis of nanomaterials using various top-down and bottom-up approaches, influencing factors, advantages, and disadvantages: A review. Adv Colloid Interface Sci 300:102597. https://doi.org/10.1016/j.cis.2021.102597
22. Dahoumane SA, Mechouet M, Wijesekera K, et al (2017) Algae-mediated biosynthesis of inorganic nanomaterials as a promising route in nanobiotechnology-a review. Green Chem 19:552–587. https://doi.org/10.1039/c6gc02346k

23. Reich S, Letzel A, Gökce B, et al (2019) Incubation Effect of Pre-Irradiation on Bubble Formation and Ablation in Laser Ablation in Liquids. ChemPhysChem 20:1036–1043. https://doi.org/10.1002/cphc.201900075
24. Guilger-Casagrande M, Lima R de (2019) Synthesis of Silver Nanoparticles Mediated by Fungi: A Review. Front Bioeng Biotechnol 7:287. https://doi.org/10.3389/fbioe.2019.00287
25. Kim M, Osone S, Kim T, et al (2017) Synthesis of nanoparticles by laser ablation: A review. KONA Powder Part J 2017:80–90. https://doi.org/10.14356/kona.2017009
26. V S, MK D (2016) Green Synthesis of Silver Nanoparticles from Glycyrrhiza glabra Root Extract for the Treatment of Gastric Ulcer. J Dev Drugs 05:152. https://doi.org/10.4172/2329-6631.1000152
27. Arroyo CR, Debut A, Vaca A V., et al (2016) Reliable tools for quantifying the morphogical properties at the nanoscale. Biol Med 8:1. https://doi.org/10.4172/0974-8369.1000281
28. Shenashen MA, El-Safty SA, Elshehy EA (2014) Synthesis, morphological control, and properties of silver nanoparticles in potential applications. Part Part Syst Charact 31:293–316. https://doi.org/10.1002/ppsc.201300181
29. Das S, Srivasatava VC (2016) Synthesis and characterization of Zno-Mgo nanocomposite by co-precipitation method. Smart Sci 4:190–195. https://doi.org/10.1080/23080477.2016.1260425
30. Xing T, Sunarso J, Yang W, et al (2013) Ball milling: A green mechanochemical approach for synthesis of nitrogen doped carbon nanoparticles. Nanoscale 5:7970–7976. https://doi.org/10.1039/c3nr02328a
31. Behera S, Nayak PL (2013) In vitro Antibacterial Activity of Green Synthesized Silver Nanoparticles Using Jamun Extract Against Multiple Drug Resistant Bacteria. World J Nano Sci Technol 2:62–65
32. Prasad Yadav T, Manohar Yadav R, Pratap Singh D (2012) Mechanical Milling: a Top Down Approach for the Synthesis of Nanomaterials and Nanocomposites. Nanosci Nanotechnol 2:22–48. https://doi.org/10.5923/j.nn.20120203.01
33. Dhiman S, Joshi RS, Singh S, et al (2021) A framework for effective and clean conversion of machining waste into metal powder feedstock for additive manufacturing. Clean Eng

Technol 4:100151. https://doi.org/10.1016/j.clet.2021.100151

34. Khayati GR, Janghorban K (2012) The nanostructure evolution of Ag powder synthesized by high energy ball milling. Adv Powder Technol 23:393–397. https://doi.org/10.1016/j.apt.2011.05.005
35. Calka A (1991) Formation of titanium and zirconium nitrides by mechanical alloying. Appl Phys Lett 59:1568–1569. https://doi.org/10.1063/1.106285
36. Ward TS, Chen W, Schoenitz M, et al (2005) A study of mechanical alloying processes using reactive milling and discrete element modeling. Acta Mater 53:2909–2918. https://doi.org/10.1016/j.actamat.2005.03.006
37. Benjamin JS, Bomford MJ (1977) Dispersion Strengthened Aluminum Made By Mechanical Alloying. Met Trans A 8 A:1302–1305. https://doi.org/10.1007/bf02643845
38. Bakker H, Zhou GF, Yang H (1995) Mechanically driven disorder and phase transformations in alloys. Prog Mater Sci 39:159–241. https://doi.org/10.1016/0079-6425(95)00001-1
39. Baptista A, Silva F, Porteiro J, et al (2018) Sputtering physical vapour deposition (PVD) coatings: A critical review on process improvement andmarket trend demands. Coatings 8:. https://doi.org/10.3390/COATINGS8110402
40. Schuster A, Larsen L, Fischer F, et al (2018) Smart Manufacturing of Thermoplastic CFRP Skins. Procedia Manuf 17:935–943. https://doi.org/10.1016/j.promfg.2018.10.147
41. Tiwari A, Natarajan S (2017) Applied Nanoindentation in Advanced Materials. John Wiley & Sons
42. Baptista A, Silva FJG, Campilho RDSG, et al (2020) Applying DMADV on the industrialization of updated components in the automotive sector: A case study. Procedia Manuf 51:1332–1339. https://doi.org/10.1016/j.promfg.2020.10.186
43. Baptista A, Silva FJG, Porteiro J, et al (2018) On the Physical Vapour Deposition (PVD): Evolution of Magnetron Sputtering Processes for Industrial Applications. Procedia Manuf 17:746–757. https://doi.org/10.1016/j.promfg.2018.10.125
44. Pauleau Y (1992) Physical Vapor Deposition Techniques I: Evaporation and Sputtering. Microelectron Eng 135–179. https://doi.org/10.1007/978-94-017-0631-5_7
45. Mattox DM (2007) Handbook of Physical Vapor Deposition (PVD) Processing. William Andrew

46. Lin J, Wei R (2018) A comparative study of thick TiSiCN nanocomposite coatings deposited by dcMS and HiPIMS with and without PEMS assistance. Surf Coatings Technol 338:84–95. https://doi.org/10.1016/j.surfcoat.2018.01.082
47. Barshilia HC, Ananth A, Khan J, Srinivas G (2012) Ar + H 2 plasma etching for improved adhesion of PVD coatings on steel substrates. Vacuum 86:1165–1173. https://doi.org/10.1016/j.vacuum.2011.10.028
48. Kumar S, Roy DN, Dey V (2021) A comprehensive review on techniques to create the anti-microbial surface of biomaterials to intervene in biofouling. Colloid Interface Sci Commun 43:100464. https://doi.org/10.1016/j.colcom.2021.100464
49. Bras P, Frisk C, Tempez A, et al (2017) Ga-grading and Solar Cell Capacitance Simulation of an industrial Cu(In,Ga)Se2 solar cell produced by an in-line vacuum, all-sputtering process. Thin Solid Films 636:367–374. https://doi.org/10.1016/j.tsf.2017.06.031
50. Craciunescu O, Seciu AM, Zarnescu O (2021) In vitro and in vivo evaluation of a biomimetic scaffold embedding silver nanoparticles for improved treatment of oral lesions. Mater Sci Eng C 123:112015. https://doi.org/10.1016/j.msec.2021.112015
51. Amendola V, Meneghetti M (2009) Laser ablation synthesis in solution and size manipulation of noble metal nanoparticles. Phys Chem Chem Phys 11:3805–3821. https://doi.org/10.1039/b900654k
52. Reza Sadrolhosseini A, Adzir Mahdi M, Alizadeh F, Abdul Rashid S (2019) Laser Ablation Technique for Synthesis of Metal Nanoparticle in Liquid. In: Laser Technology and its Applications. IntechOpen
53. Sportelli MC, Izzi M, Volpe A, et al (2018) The pros and cons of the use of laser ablation synthesis for the production of silver nano-antimicrobials. Antibiotics 7:67. https://doi.org/10.3390/antibiotics7030067
54. Li Z, Dong H, Wu Z, et al (2020) Novel p-n type porous Ag2O/Bi5O7I heterojunction for Uv–Vis-NIR activated high efficient photocatalytic degradation of bisphenol A: Photoelectric properties and degradation mechanism. Appl Surf Sci 529:147162. https://doi.org/10.1016/j.apsusc.2020.147162
55. Dreaden EC, Alkilany AM, Huang X, et al (2012) The golden age: Gold nanoparticles for biomedicine. Chem Soc Rev 41:2740–2779. https://doi.org/10.1039/c1cs15237h
56. Ijaz I, Gilani E, Nazir A, Bukhari A (2020) Detail review on chemical, physical and green

synthesis, classification, characterizations and applications of nanoparticles. Green Chem Lett Rev 13:59–81. https://doi.org/10.1080/17518253.2020.1802517

57. Vishwanath R, Negi B (2021) Conventional and green methods of synthesis of silver nanoparticles and their antimicrobial properties. Curr Res Green Sustain Chem 4:100205. https://doi.org/10.1016/j.crgsc.2021.100205
58. Besenhard MO, LaGrow AP, Hodzic A, et al (2020) Co-precipitation synthesis of stable iron oxide nanoparticles with NaOH: New insights and continuous production via flow chemistry. Chem Eng J 399:125740. https://doi.org/10.1016/j.cej.2020.125740
59. Chen L, Xie J, Wu H, et al (2018) Precise study on size-dependent properties of magnetic iron oxide nanoparticles for in vivo magnetic resonance imaging. J Nanomater 2018:1–9. https://doi.org/10.1155/2018/3743164
60. Ahn T, Kim JH, Yang HM, et al (2012) Formation pathways of magnetite nanoparticles by coprecipitation method. J Phys Chem C 116:6069–6076. https://doi.org/10.1021/jp211843g
61. Bashir A, Pandith AH, Malik LA, et al (2021) Magnetically recyclable L-cysteine capped Fe3O4 nanoadsorbent: A promising pH guided removal of Pb(II), Zn(II) and HCrO4- contaminants. J Environ Chem Eng 9:105880. https://doi.org/10.1016/j.jece.2021.105880
62. Navas D, Fuentes S, Castro-Alvarez A, Chavez-Angel E (2021) Review on Sol-Gel Synthesis of Perovskite and Oxide Nanomaterials. Gels 7:275. https://doi.org/10.3390/gels7040275
63. Sahil K, Akanksha M, Premjeet S, et al (2011) Microsphere: A review. Int J Res Pharm Chem 1:1184–1198
64. Yu SH (2001) Hydrothermal/solvothermal processing of advanced ceramic materials. J Ceram Soc Japan 109:. https://doi.org/10.2109/jcersj.109.1269_s65
65. Srinivasan L V., Rana SS (2024) A critical review of various synthesis methods of nanoparticles and their applications in biomedical, regenerative medicine, food packaging, and environment. Discov Appl Sci 6:371. https://doi.org/10.1007/s42452-024-06040-8
66. Lalawmpuia R, Lalhruaitluangi M, Lalhmunsiama, Tiwari D (2024) Metal organic framework (MOF): Synthesis and fabrication for the application of electrochemical sensing. Environ Eng Res 29:. https://doi.org/10.4491/eer.2023.636
67. Shiri MSZ, Henderson W, Mucalo MR (2019) A review of the lesser-studied

microemulsion-based synthesis methodologies used for preparing nanoparticle systems of the noble metals, Os, Re, Ir and Rh. Materials (Basel) 12:1–8. https://doi.org/10.3390/ma12121896

68. Zhou S, Zhao M, Yang TH, Xia Y (2019) Decahedral nanocrystals of noble metals: Synthesis, characterization, and applications. Mater Today 22:108–131. https://doi.org/10.1016/j.mattod.2018.04.003
69. Sanchez-Dominguez M, Pemartin K, Boutonnet M (2012) Preparation of inorganic nanoparticles in oil-in-water microemulsions: A soft and versatile approach. Curr Opin Colloid Interface Sci 17:297–305. https://doi.org/10.1016/j.cocis.2012.06.007
70. Kolb MA, Maier WF, Stöwe K (2011) High-throughput syntheses of nano-scaled mixed metal sulphides. Catal Today 159:64–73. https://doi.org/10.1016/j.cattod.2010.07.010
71. Dhand C, Dwivedi N, Loh XJ, et al (2015) Methods and strategies for the synthesis of diverse nanoparticles and their applications: A comprehensive overview. RSC Adv 5:105003–105037. https://doi.org/10.1039/c5ra19388e
72. Meng X (2020) Atomic layer deposition of solid-state electrolytes for next-generation lithium-ion batteries and beyond: Opportunities and challenges. Energy Storage Mater 30:296–328. https://doi.org/10.1016/j.ensm.2020.05.001
73. Hamrayev H, Korpayev S, Shameli K (2024) Advances in Synthesis Techniques and Environmental Applications of TiO2 Nanoparticles for Wastewater Treatment: A Review. J Res Nanosci Nanotechnol 12:1–24. https://doi.org/10.37934/jrnn.12.1.124
74. Wang X, Yushin G (2015) Chemical vapor deposition and atomic layer deposition for advanced lithium ion batteries and supercapacitors. Energy Environ Sci 8:1889–1904. https://doi.org/10.1039/c5ee01254f
75. Marichy C (2012) Atomic layer deposition of metal oxide by non-aqueous sol-gel chemistry
76. Zaera F (2024) The surface chemistry of the atomic layer deposition of metal thin films. Nanotechnology 35:362001. https://doi.org/10.1088/1361-6528/ad54cb
77. Nyandoro VO, Masioge HK, Malago ZL (2025) Biogenic synthesis of metal nanoparticles: promoting green nanotechnology and sustainable development goals. Clean Technol Environ Policy 27:517–530. https://doi.org/10.1007/s10098-024-02966-0
78. Bao Y, He J, Song K, et al (2021) Plant-Extract-Mediated Synthesis of Metal

Nanoparticles. J Chem 2021:. https://doi.org/10.1155/2021/6562687

79. Sriramulu M, Shanmugam S, Ponnusamy VK (2020) Agaricus bisporus mediated biosynthesis of copper nanoparticles and its biological effects: An in-vitro study. Colloids Interface Sci Commun 35:100254. https://doi.org/10.1016/j.colcom.2020.100254
80. Dinesh GK, Pramod M, Chakma S (2020) Sonochemical synthesis of amphoteric Cu0-Nanoparticles using Hibiscus rosa-sinensis extract and their applications for degradation of 5-fluorouracil and lovastatin drugs. J Hazard Mater 399:123035. https://doi.org/10.1016/j.jhazmat.2020.123035
81. Singh H, Desimone MF, Pandya S, et al (2023) Revisiting the Green Synthesis of Nanoparticles: Uncovering Influences of Plant Extracts as Reducing Agents for Enhanced Synthesis Efficiency and Its Biomedical Applications. Int J Nanomedicine Volume 18:4727–4750. https://doi.org/10.2147/IJN.S419369
82. Gahlawat G, Choudhury AR (2019) A review on the biosynthesis of metal and metal salt nanoparticles by microbes. RSC Adv 9:12944–12967. https://doi.org/10.1039/c8ra10483b
83. Ovais M, Khalil AT, Ayaz M, et al (2018) Biosynthesis of metal nanoparticles via microbial enzymes: A mechanistic approach. Int J Mol Sci 19:. https://doi.org/10.3390/ijms19124100
84. Dikshit PK, Kumar J, Das AK, et al (2021) Green synthesis of metallic nanoparticles: Applications and limitations. Catalysts 11:1–35. https://doi.org/10.3390/catal11080902
85. Streimikyte P, Viskelis P, Viskelis J (2022) Enzymes-Assisted Extraction of Plants for Sustainable and Functional Applications. Int J Mol Sci 23:. https://doi.org/10.3390/ijms23042359
86. Ahmed J, Gultekinoglu M, Edirisinghe M (2020) Bacterial cellulose micro-nano fibres for wound healing applications. Biotechnol Adv 41:107549. https://doi.org/10.1016/j.biotechadv.2020.107549
87. Gonidec M, Puigmartí-Luis J (2019) Continuous-versus segmented-flow microfluidic synthesis in materials science. Crystals 9:. https://doi.org/10.3390/cryst9010012
88. Song H, Ismagilov RF (2003) Millisecond Kinetics on a Microfluidic Chip Using Nanoliters of Reagents. J Am Chem Soc 125:14613–14619. https://doi.org/10.1021/ja0354566
89. López-Salazar H, Camacho-Díaz BH, Arenas Ocampo ML, Jiménez-Aparicio AR (2023)

Microwave-assisted Extraction of Functional Compounds from Plants: A Review. BioResources 18:6614–6638. https://doi.org/10.15376/biores.18.3.Lopez-Salazar

90. Chan CH, Yusoff R, Ngoh GC, Kung FWL (2011) Microwave-assisted extractions of active ingredients from plants. J Chromatogr A 1218:6213–6225. https://doi.org/10.1016/j.chroma.2011.07.040
91. Monte-Filho SS, Andrade SIE, Lima MB, Araujo MCU (2019) Synthesis of highly fluorescent carbon dots from lemon and onion juices for determination of riboflavin in multivitamin/mineral supplements. J Pharm Anal 9:209–216. https://doi.org/10.1016/j.jpha.2019.02.003
92. Yang P, Zhu Z, Chen M, et al (2018) Microwave-assisted synthesis of xylan-derived carbon quantum dots for tetracycline sensing. Opt Mater (Amst) 85:329–336. https://doi.org/10.1016/j.optmat.2018.06.034
93. Ritter TG, Phakatkar AH, Rasul MG, et al (2022) Electrochemical synthesis of high entropy hydroxides and oxides boosted by hydrogen evolution reaction. Cell Reports Phys. Sci. 3
94. Iravani S (2011) Green synthesis of metal nanoparticles using plants. Green Chem 13:2638–2650. https://doi.org/10.1039/c1gc15386b
95. Li Z, Dong J, Zhang H, et al (2021) Sonochemical catalysis as a unique strategy for the fabrication of nano-/micro-structured inorganics. Nanoscale Adv 3:41–72. https://doi.org/10.1039/d0na00753f
96. Głowniak S, Szczęśniak B, Choma J, Jaroniec M (2023) Recent Developments in Sonochemical Synthesis of Nanoporous Materials. Molecules 28
97. Sun X, Cheng H, Li M, et al (2022) Collision Electrochemical Synthesis of Metal Nanoparticles Using Electrons as Green Reducing Agent. ACS Appl. Mater. Interfaces 14:57189–57196
98. Makgwane PR, Ray SS (2014) Synthesis of nanomaterials by continuous-flow microfluidics: A review. J Nanosci Nanotechnol 14:1338–1363. https://doi.org/10.1166/jnn.2014.9129
99. Zhou Z (2010) Hybrid Materials of Block Copolymers and Magnetic Nanoparticles by
100. Pourzahedi L, Eckelman MJ (2015) Comparative life cycle assessment of silver nanoparticle synthesis routes. Environ Sci Nano 2:361–369.

https://doi.org/10.1039/c5en00075k

101. Khan Y, Sadia H, Ali Shah SZ, et al (2022) Classification, Synthetic, and Characterization Approaches to Nanoparticles, and Their Applications in Various Fields of Nanotechnology: A Review. Catalysts 12:1386. https://doi.org/10.3390/catal12111386

CHAPTER III
Characterization Techniques for Nanoparticles

III.1. Importance of Comprehensive Nanoparticle Characterization

What sets a nanoparticle apart from a miniaturized piece of bulk material is not merely its reduced dimensions, but rather the emergence of entirely new properties that only manifest at the nanoscale. When matter shrinks to nanometer level dimensions, its behavior becomes governed by factors that are virtually imperceptible at larger scales, geometric shape, degree of crystallinity, surface charge, and colloidal stability. Taken together, these factors dictate how a given nanoparticle will perform in its target environment, whether that environment is a wastewater remediation column, a tumor-targeted drug delivery vehicle, or an antimicrobial surface coating. Without a thorough and rigorous characterization of these parameters, meaningful comparisons between studies become unreliable, and any attempt at scale-up remains little more than informed guesswork [1].

Over the past two decades, a broad consensus has gradually taken shape within the nanotechnology community: no single analytical technique, however powerful, is capable of fully capturing the complexity of a nanoparticle system. A multi-modal characterization strategy, one that integrates structural, morphological, colloidal, spectroscopic, and compositional measurements, has consequently been elevated to the minimum acceptable standard for peer reviewed publications [2]. This position is not merely academic. Regulatory agencies including the European Food Safety Authority (EFSA) and the U.S. Food and Drug Administration (FDA) have both stipulated that nanomaterial dossiers submitted for approval must include at least two independent sizing methods, one of which must be electron microscopy [3]. These requirements stem from a straightforward practical reality: each technique interrogates a fundamentally different physical property of the material. X-ray diffraction probes long-range crystalline order across the bulk of the sample, electron microscopy captures the local morphology of individual particles with sub-nanometer spatial resolution, light-scattering methods report on the hydrodynamic behavior of particles moving freely in suspension, and spectroscopic tools reveal the chemical identity of surface functional groups and electronic transitions that purely physical measurements cannot access [1, 2].

The characterization techniques surveyed in this chapter are organized into five broad categories, each reflecting a distinct dimension of nanoparticle characterization. Section III.2 addresses structural and morphological methods, including X-ray diffraction (XRD), transmission

electron microscopy (TEM), scanning electron microscopy (SEM), and atomic force microscopy (AFM), that collectively reveal what a nanoparticle looks like and how its atoms are arranged internally. Section III.3 shifts to solution phase techniques, namely dynamic light scattering (DLS), zeta potential measurements, and nanoparticle tracking analysis (NTA), which characterize size distribution, surface charge, and colloidal stability under conditions that more closely approximate the particle's functional environment. Section III.4 introduces spectroscopic and optical techniques, UV Vis spectroscopy, FTIR, Raman and SERS, and fluorescence and photoluminescence spectroscopy, that probe the interaction of electromagnetic radiation with the nanoparticle to yield information about electronic transitions, molecular bonding environments, and optical properties. Section III.5 moves to surface chemistry and elemental composition analysis through XPS, EDX, ICP-MS, and NMR, providing quantitative insight into what elements are present at and near the nanoparticle surface and in what chemical states. Finally, Section III.6 addresses the magnetic, electrical, and nanomechanical characterization techniques that become indispensable for nanoparticles whose intended application depends specifically on those functional properties, while Section III.7 draws the chapter together by examining how the full set of characterization data can be systematically correlated with observed performance across drug delivery, catalysis, and environmental remediation applications.

Throughout all sections, attention is drawn not only to what each technique measures, but also to where it falls short, because it is precisely at those boundaries that the value of cross validating results using complementary approaches becomes most apparent, and where the risk of drawing incomplete or misleading conclusions is greatest [1, 2].

III.2. Structural and Morphological Characterization

III.2.1. X-ray Diffraction (XRD)

X ray diffraction is arguably the most information rich bulk technique available for nanoparticle characterization. By irradiating a powdered sample with monochromatic X rays, most commonly Cu Kα radiation at $\lambda = 1.54056$ Å, and recording the angular positions and intensities of the resulting Bragg reflections, one can simultaneously identify the crystalline phase, assess phase purity, estimate the mean crystallite size, and detect lattice strain [4]. The relationship between peak position and interplanar spacing follows Bragg's law ($n\lambda = 2d \sin\theta$), where each set of (hkl) planes produces a characteristic diffraction peak whose position is a

fingerprint of the crystal structure. Comparison with reference patterns from databases such as the International Centre for Diffraction Data (ICDD) enables unambiguous phase identification, a task that is particularly valuable when distinguishing between polymorphic forms, for example anatase versus rutile TiO_2, or magnetite (Fe_3O_4) versus maghemite (γ-Fe_2O_3), that share similar morphologies but exhibit markedly different functional properties [5].

Beyond phase identification, the Scherrer equation ($D = K\lambda / \beta \cos\theta$) relates the full width at half maximum (FWHM) of a diffraction peak, β, to the mean crystallite dimension D, where K is a dimensionless shape factor approximately equal to 0.9 for spherical particles. It is important to appreciate that the Scherrer size is a crystallographic quantity; it describes the coherent scattering domain and not necessarily the particle diameter measured by electron microscopy. Particles that are polycrystalline or that contain stacking faults and microstrain will yield Scherrer sizes smaller than the geometric particle size. When both broadening sources are present, the modified Williamson Hall plot, which deconvolutes size and strain contributions, provides a more accurate picture [4]. As illustrated in **Figure (III.1)**, which reproduces the seminal tutorial published by Mourdikoudis et al. in ACS Nano, the progressive broadening of diffraction peaks as particle size decreases from the micrometer to the nanometer regime is visually striking and quantitatively tractable using these approaches.

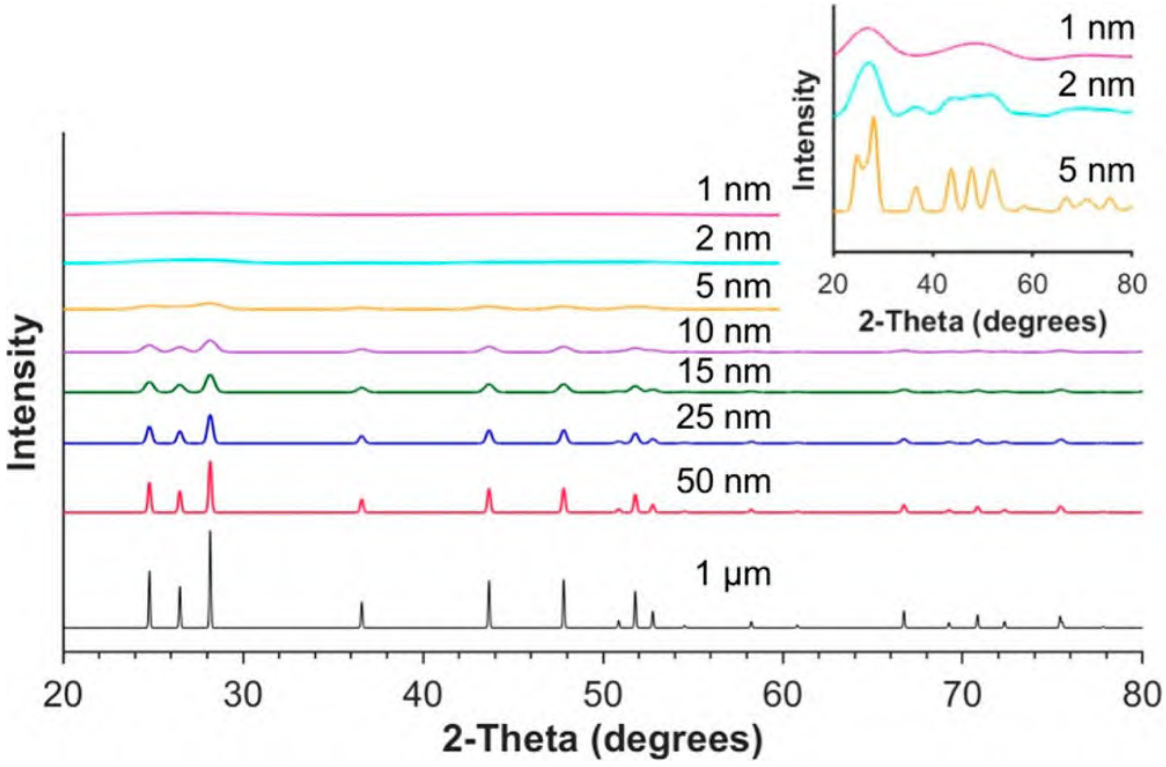

Figure (III.1): Simulated powder XRD patterns showing peak broadening as crystallite size decreases from bulk (1 μm) to 5 nm for wurtzite CdS nanoparticles, demonstrating the application of the Scherrer equation to nanoscale materials [4].

One practical consideration that is frequently overlooked is preferred orientation. When anisotropic nanoparticles, such as nanorods, nanoplates, or nanocubes, are drop cast onto a substrate for measurement, they tend to align with their largest face parallel to the surface. The result is a diffraction pattern whose relative peak intensities deviate from the database reference, potentially leading to misidentification or erroneous phase quantification. Preparing a thoroughly randomized powder and cross checking peak intensities against simulated patterns is therefore strongly recommended, particularly for shape engineered nanoparticle systems [4].

III.2.2. Transmission Electron Microscopy (TEM)

While XRD yields ensemble averaged structural information, transmission electron microscopy (TEM) provides direct, spatially resolved images of individual nanoparticles at atomic to nanometer resolution. In a TEM instrument, a high energy electron beam, typically operated at 80–300 kV, is transmitted through an ultra thin sample, and the resulting image records contrast arising from differences in electron scattering by the specimen. Heavy atoms scatter electrons more strongly than light ones, creating mass thickness contrast that delineates particle boundaries and allows size and shape to be measured with sub nanometer precision [6].

High-resolution TEM (HR-TEM) extends this capability to the atomic lattice level, making it possible to directly visualize the interplanar spacings and crystallographic orientations of individual nanoparticles. The measured d-spacings can be matched against tabulated values to confirm the phase assignment made by XRD, while selected-area electron diffraction (SAED) patterns provide complementary polycrystalline or single-crystal diffraction data from a chosen region of the sample. Energy-dispersive X-ray spectroscopy (EDS or EDX) attached to the TEM column further enables elemental mapping at near-atomic spatial resolution, which is indispensable for verifying the composition of core-shell or doped nanostructures [6]. TEM is widely regarded as the gold standard for nanoparticle sizing; the European Food Safety Authority, for instance, explicitly requires TEM as one of two mandatory sizing methods for nanomaterial characterization in regulatory submissions [3].

The principal limitation of conventional TEM is that sample preparation involves drying the colloidal dispersion onto a carbon-coated copper grid, which may induce aggregation artefacts that are absent in the native liquid environment. Cryo-TEM, in which the sample is vitrified by rapid plunge-freezing and imaged at cryogenic temperatures, largely eliminates this concern and has become the method of choice for soft-matter nanoparticles such as liposomes and polymer micelles, where the native hydrated morphology is critical to function [7].

III.2.3. Scanning Electron Microscopy (SEM) and Field-Emission SEM

In contrast to TEM, scanning electron microscopy (SEM) detects electrons that are scattered back from or emitted by the surface of the specimen following irradiation by a focused electron beam. The dominant signal channels are secondary electrons (SE), which are sensitive to surface topography, and backscattered electrons (BSE), which depend on the mean atomic number of the material and therefore provide compositional contrast. Because SEM interrogates the surface rather than the bulk of the particle, it is particularly well suited to characterizing surface morphology, roughness, porosity, and particle to particle aggregation behaviour [8].

Conventional SEM instruments operate in the 1–30 kV range and typically achieve spatial resolutions of 5–20 nm. For nanoparticles below approximately 50 nm in diameter, however, the spatial resolution of standard SEM is often insufficient, and field emission SEM (FE SEM), which uses a field emission gun (FEG) to produce a more coherent and brighter electron source, becomes necessary. FE-SEM instruments routinely achieve resolutions of 1–2 nm, bringing even small nanoparticles into the resolvable range. A practical requirement for non-conductive or weakly conductive samples, such as silica or polymer-based nanoparticles, is the deposition of a thin conductive coating (commonly gold, platinum, or carbon) to prevent charge accumulation on the surface; this coating introduces a dimensional offset of up to 5–14 nm that must be accounted for when making absolute size measurements [8]. When SEM is combined with energy-dispersive X-ray spectroscopy (SEM-EDX), elemental analysis at the micrometer scale becomes straightforward, providing a powerful complement to TEM-EDX for compositional verification.

III.2.4. Atomic Force Microscopy (AFM)

Atomic force microscopy occupies a distinct niche in nanoparticle characterization by measuring the forces between a nanoscale cantilever tip and the sample surface as the tip is

raster-scanned in close proximity. Unlike electron microscopies, AFM requires no vacuum environment, no conductive coating, and no staining of biological specimens; it can operate in ambient air, liquids, and even physiological buffers, which makes it an attractive tool for studying nanoparticles under conditions that approximate their functional environment [9]. The deflection of the cantilever, monitored by a laser reflected onto a position sensitive photodetector, is converted into a three dimensional topographic map of the surface with sub nanometer height resolution.

For nanoparticle characterization, AFM provides height, lateral size, and surface roughness measurements that complement the two-dimensional projected images yielded by electron microscopy. It is worth noting that AFM systematically overestimates lateral dimensions due to tip-broadening artefacts arising from the finite radius of curvature of the cantilever tip (typically 5–20 nm), while height measurements along the Z-axis are largely free of this artefact and often serve as the most reliable size estimate [9]. Beyond topography, tapping-mode phase imaging captures variations in viscoelastic properties across the sample surface, enabling the identification of soft versus hard domains within composite nanoparticles or at the particle-polymer interface. More recently, force volume AFM and peak force quantitative nanomechanical (QNM) mapping have extended AFM's repertoire to quantitative measurements of elastic modulus, adhesion, and deformation at the single particle level, information of direct relevance to drug delivery systems where nanoparticle stiffness governs cellular uptake and biodistribution [9].

III.3. Size Distribution, Surface Charge, and Colloidal Stability

III.3.1. Dynamic Light Scattering (DLS)

Dynamic light scattering (DLS), also referred to as photon correlation spectroscopy (PCS), is the most widely used technique for routine sizing of nanoparticles in colloidal suspension. Its appeal lies in speed, non-invasiveness, and the large statistical sampling inherent in an ensemble measurement: within minutes, DLS analyses the Brownian motion of billions of particles simultaneously, extracting a hydrodynamic size distribution through the Stokes Einstein equation [10]. The physical principle is straightforward: a monochromatic laser illuminates the suspension, and the time dependent fluctuations in scattered light intensity, caused by the random translational diffusion of particles, are recorded by an autocorrelation function. The translational

diffusion coefficient extracted from this function is then converted to the hydrodynamic diameter (Dh), which includes both the particle core and any solvation shell or surface coating.

The polydispersity index (PDI), which ranges from 0 (perfectly monodisperse) to 1 (highly polydisperse), is a key output that conveys the width of the size distribution and is routinely used as a quality metric for nanoparticle formulations intended for pharmaceutical applications. PDI values below 0.2 are generally considered acceptable for injectable nanocarriers [10]. A limitation that users must appreciate is that DLS weights its size distribution by scattered intensity, which scales with the sixth power of particle diameter ($I \propto d^6$). A small proportion of large aggregates or dust particles can therefore dominate the signal and produce an artifactually large apparent mean size. Proper sample preparation, including filtration through 0.22 µm membranes and appropriate dilution, is thus essential for reliable DLS measurements. As illustrated in **Figure (III.2)**, NTA and DLS produce comparable size distributions for monodisperse samples such as polystyrene beads, yet they differ in their sensitivity to particle populations due to their respective measurement principles [11].

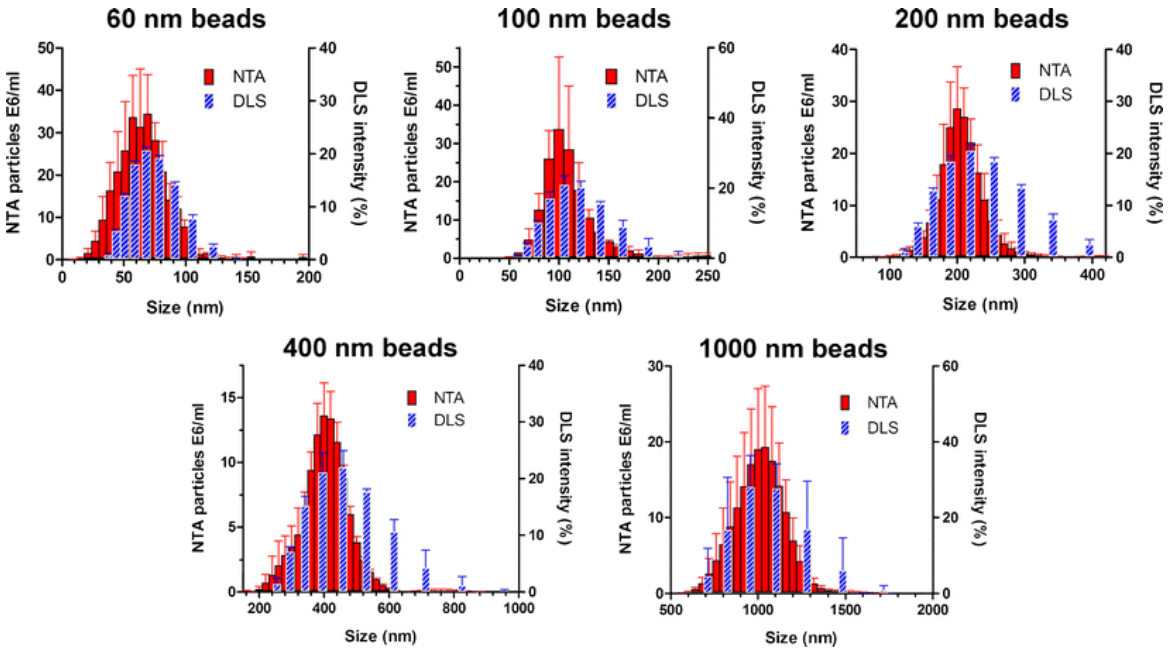

Figure (III.2): Size distribution from NTA and DLS measurements of monodisperse polystyrene beads. Error bars represent standard deviations obtained from three measurements of the same sample [11].

III.3.2. Zeta Potential Measurements

The zeta potential (ζ) is the electric potential at the so-called slip plane, the boundary between the layer of ions that move rigidly with the nanoparticle during electrophoretic migration and the surrounding bulk solvent. It is experimentally accessed through electrophoretic light scattering (ELS), in which an oscillating electric field drives particle migration and the resulting Doppler shift of the scattered laser light is used to determine the electrophoretic mobility μe. This mobility is then converted to zeta potential via Henry's equation, reduced to either the Hückel approximation (for small particles in low-ionic-strength media) or the Helmholtz-Smoluchowski approximation (for larger particles in high-salt conditions) depending on the ratio of particle radius to Debye screening length [12].

The zeta potential is not a direct measure of surface charge, but it is a practical surrogate for colloidal stability. The empirical threshold widely cited in the literature, $|\zeta| > 30$ mV for electrostatically stabilized dispersions, represents the point at which the repulsive electrostatic barrier is sufficiently large to prevent aggregation driven by van der Waals attraction [12]. Dispersions with $|\zeta| < 10$ mV are typically considered unstable. These thresholds should, however, be interpreted cautiously for sterically stabilized nanoparticles, such as those coated with polyethylene glycol (PEG), where the polymer brush provides an independent stabilization mechanism that is not captured by the zeta potential alone. pH and ionic strength profoundly influence the zeta potential: as pH increases, surface hydroxyl groups deprotonate and the potential becomes more negative, while increasing salt concentration compresses the electrical double layer and reduces the measured value. Reporting zeta potential without specifying the suspension medium, pH, and ionic strength is therefore of limited scientific value [12].

III.3.3. Nanoparticle Tracking Analysis (NTA)

Nanoparticle tracking analysis (NTA) was introduced as an orthogonal technique to DLS that tracks individual particles one by one rather than analysing the ensemble-averaged correlation function. In an NTA instrument, a thin laser beam illuminates the sample within a temperature-controlled flow cell, and a high-sensitivity sCMOS or EMCCD camera records videos of the light scattered by individual particles as they undergo Brownian motion. Dedicated software identifies each particle in every video frame, tracks its two-dimensional trajectory, calculates the mean-squared displacement, and applies the Stokes-Einstein equation to derive a

hydrodynamic diameter on a particle-by-particle basis. Because thousands of individual particles are tracked in a typical measurement, NTA yields a number weighted size distribution, a fundamentally different statistical quantity from the intensity weighted distribution produced by DLS [13].

This difference has practical consequences. Because NTA weights each particle equally regardless of its size, rare populations of large aggregates that would dominate a DLS measurement are represented proportionally, making NTA far more sensitive to the presence of distinct subpopulations in a polydisperse sample. *Filipe et al*. demonstrated that NTA accurately resolved co-existing particle populations separated by as little as 100 nm in mean diameter, a resolution impossible to achieve by DLS alone [13]. An additional capability of NTA is the direct enumeration of particle concentration, expressed as particles per millilitre, which is of considerable importance for pharmaceutical quality control and for calculating occupancy ratios in drug-loaded nanocarriers. Limitations include a narrower accessible size range (approximately 30–1000 nm, compared to 1 nm – 10 μm for DLS) and a lower statistical throughput, since each video captures only a few hundred to a few thousand particles. As a practical guideline, NTA and DLS are best employed together: DLS for rapid, reproducible mean size and PDI measurements on monodisperse or near-monodisperse samples, and NTA for detailed subpopulation analysis and particle concentration determination in heterogeneous formulations [11, 13].

III.4. Spectroscopic and Optical Techniques

Electron microscopy and scattering based methods reveal the physical dimensions and colloidal behaviour of nanoparticles, but they convey little about the chemical identity of surface functional groups, electronic transitions, or molecular bonding environments. Spectroscopic techniques fill this gap by probing the interaction of electromagnetic radiation, spanning the ultraviolet, visible, infrared, and near infrared regions, with the sample. Each spectral window interrogates a different set of material properties, and the combined picture they provide is often indispensable for confirming that a synthesis has proceeded as intended, that a surface functionalization is complete, and that the optical properties are consistent with the intended application [2].

III.4.1. UV–Visible Spectroscopy

Among the simplest and most routinely applied spectroscopic tools in nanomaterial laboratories, UV–Vis spectroscopy provides rapid, non-destructive information about the electronic absorption properties of nanoparticles in solution. The technique measures the attenuation of light transmitted through a sample across the 200–800 nm wavelength range, yielding an absorption spectrum that is sensitive to particle composition, size, shape, and local dielectric environment [2].

For semiconductor nanoparticles such as quantum dots and metal oxide nanostructures, the onset of absorption, commonly referred to as the optical bandgap, shifts to shorter wavelengths as particle size decreases, a direct consequence of quantum confinement that causes the valence and conduction bands to discretize into size dependent energy levels. This blue shift in the absorption edge can be quantified using the Tauc plot method to extract the optical bandgap energy, information that is directly relevant to photocatalytic and sensing applications [14].

Perhaps the most striking UV Vis signature in nanoscience is the localized surface plasmon resonance (LSPR) exhibited by noble metal nanoparticles. When the frequency of incident light matches the collective oscillation frequency of conduction electrons confined within the nanoparticle, strong absorption and scattering occur at a characteristic wavelength, approximately 520 nm for spherical gold nanoparticles of 20 nm diameter and around 400 nm for silver. The LSPR peak position, width, and intensity encode information about particle size, shape, aggregation state, and the refractive index of the surrounding medium, making UV Vis spectroscopy a convenient, real time monitor of colloidal stability: the appearance of a red shifted shoulder or a broadened plasmon band signals the onset of interparticle aggregation [15].

The Beer-Lambert law ($A = \varepsilon cl$) further allows precise molar concentration determination from the absorbance at the LSPR maximum when the molar extinction coefficient ε is known. As illustrated in **Figure (III.3)**, the progressive red-shift and broadening of the LSPR band as AuNPs grow from 20 to 100 nm captures in a single panel both the sizing sensitivity and the aggregation-reporting capability of the technique.

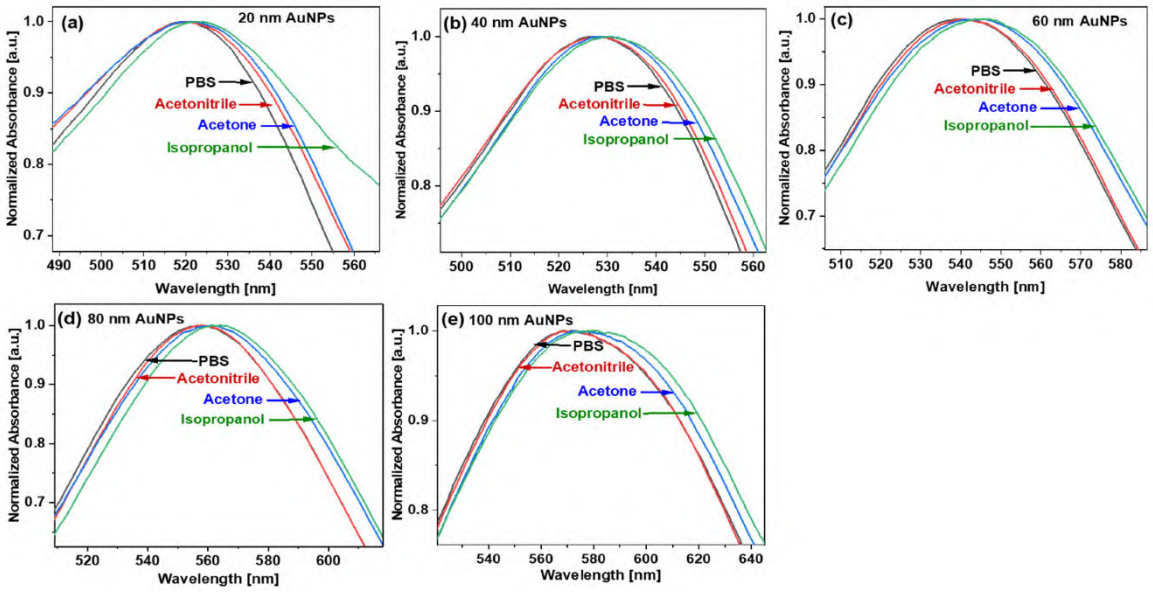

Figure (III.3): Experimental UV–Vis absorption spectra of spherical gold nanoparticles with average diameters of 20 nm, 40 nm, 60 nm, 80 nm, and 100 nm, showing the progressive red-shift and broadening of the localized surface plasmon resonance (LSPR) band with increasing particle size [16].

III.4.2. Fourier Transform Infrared Spectroscopy (FTIR)

Fourier transform infrared spectroscopy is the primary technique used to identify and characterize the molecular functional groups present on a nanoparticle surface. The physical basis is the absorption of mid infrared photons (400–4000 cm^{-1}) by molecular vibrations, stretching, bending, and rocking, that are infrared active when the motion involves a change in electric dipole moment. Each chemical bond and functional group absorb at characteristic wavenumbers: the carbonyl stretch of carboxylic acids near 1710 cm^{-1}, the broad O–H stretch of surface hydroxyls between 3200 and 3500 cm^{-1}, the asymmetric and symmetric C–H stretches of alkyl chains near 2920 and 2850 cm^{-1}, and the Si–O–Si stretching vibration near 1050 cm^{-1} for silica-coated nanoparticles [4]. By comparing the spectrum of a functionalized nanoparticle with those of the bare particle and the free ligand, one can confirm the presence of surface-bound molecules, identify whether the binding mode has altered the functional group chemistry (for instance, a shift in carboxylate vas and vs indicates bidentate coordination to a metal surface), and monitor the completeness of ligand exchange reactions [17].

For practical measurements on nanoparticle suspensions and powders, attenuated total reflectance (ATR-FTIR) has largely replaced conventional transmission-mode FTIR because it requires no sample preparation beyond placing a small amount of material directly on the ATR crystal. In the ATR geometry, an evanescent field penetrates only 1–3 μm into the sample, which largely eliminates the saturated background absorption that would complicate transmission measurements of highly scattering powders [17]. Diffuse reflectance infrared Fourier transform spectroscopy (DRIFTS) offers an alternative for dry powders and is especially useful for in-situ measurements at elevated temperatures. An important limitation of FTIR for nanoparticle surface analysis is that the technique detects all molecules in the sampling volume, not exclusively surface species, so bulk impurities or physisorbed solvents can generate overlapping signals. Careful control experiments with blank substrates and free ligands are therefore essential for unambiguous spectral assignment.

III.4.3. Raman and Surface-Enhanced Raman Spectroscopy (SERS)

Raman spectroscopy is the inelastic counterpart to FTIR: rather than measuring the absorption of infrared photons, it records the shift in frequency of visible photons scattered by molecular vibrations. The Raman shift is identical to the vibrational frequency detected by FTIR for the same bond, but the selection rules differ; vibrations that involve changes in molecular polarizability are Raman active, while those involving a change in dipole moment are infrared active. This complementarity means that Raman and FTIR often reveal different sets of vibrations in the same sample; water, for instance, is a weak Raman scatterer but a strong infrared absorber, making Raman uniquely suited to measurements in aqueous suspension without solvent interference [2]. Carbon based nanomaterials such as graphene, reduced graphene oxide, and carbon nanotubes are particularly well characterized by Raman spectroscopy: the D band near 1350 cm^{-1} reports on defect density, the G band near 1580 cm^{-1} arises from the in plane E_2g phonon mode of sp^2 carbon, and the 2D (or G′) overtone around 2700 cm^{-1} is sensitive to the The inherently weak nature of spontaneous Raman scattering, with cross sections approximately 14 orders of magnitude smaller than fluorescence, is dramatically overcome by surface enhanced Raman spectroscopy (SERS). When a molecule adsorbs on the surface of a plasmonic nanoparticle, particularly at a nanoscale gap or junction between two nanoparticles, referred to as a hotspot, the local electromagnetic field enhancement ($|E|^4$) amplifies the Raman signal by

factors of 10^6 to 10^{14}, routinely enabling detection at nanomolar concentrations and, in optimized geometries, even single molecule sensitivity [19]. SERS is therefore not merely an analytical tool for detecting target molecules but also a powerful probe of the molecular environment at the nanoparticle surface: shifts in band position and changes in relative intensity compared to the free-molecule spectrum reveal surface binding geometry, molecular orientation, and metal–molecule charge transfer interactions. The technique is increasingly deployed in biomedical sensing, where gold or silver nanoparticle SERS substrates labelled with reporter molecules serve as highly multiplexed, spectrally barcoded probes for in vitro diagnostics and immunoassays [19].

III.4.4. Fluorescence and Photoluminescence Spectroscopy

Fluorescence and photoluminescence (PL) spectroscopy probe the emission of light following optical excitation and are indispensable for characterizing nanoparticles whose intended function is optical, quantum dots, carbon nanodots, lanthanide doped upconversion nanoparticles, and fluorescent silica shells among them. In a fluorescence measurement, the sample is excited at a fixed wavelength and the resulting emission spectrum is recorded; the Stokes shift, the difference between excitation and emission maxima, reflects energy losses to lattice vibrations and molecular reorganization. For quantum dots, the PL emission wavelength is determined primarily by particle size through the quantum confinement relationship, and the narrow, symmetric emission peak (full-width at half-maximum of 20–30 nm for high-quality CdSe QDs, compared to 100–150 nm for organic fluorophores) is a hallmark of their monodisperse size distribution [20]. Photoluminescence quantum yield (PLQY), defined as the ratio of photons emitted to photons absorbed, is a critical performance metric for fluorescent nanoparticles used in imaging or display applications; values exceeding 90% are now achievable for core-shell QD architectures such as CdSe/ZnS and InP/ZnS [20].

Beyond sizing and quantum yield determination, PL spectroscopy is sensitive to the surface chemistry of nanoparticles. Surface trap states, arising from dangling bonds, adsorbed oxygen, or ligand vacancies, act as non-radiative recombination centres that quench fluorescence, producing broad, red shifted trap emission bands that can be distinguished from the sharp excitonic peak. Monitoring the ratio of excitonic to trap emission before and after surface passivation treatments, or during ligand exchange, provides a quantitative handle on surface

defect density [20]. Time resolved photoluminescence (TRPL), in which the emission decay kinetics are measured following pulsed excitation, further distinguishes radiative from non-radiative decay channels and reveals multi exponential dynamics indicative of heterogeneous surface environments, information that static emission spectra cannot provide.

III.5. Surface Chemistry and Composition Analysis

The preceding spectroscopic techniques characterize molecular vibrations, electronic transitions, and optical emission, but a complete surface chemistry analysis requires techniques capable of identifying the elements present at a nanoparticle surface, their oxidation states, and the spatial distribution of composition, from the outermost monolayer down through the particle interior. The four techniques discussed in this section, XPS, EDX, ICP MS, and NMR, address complementary aspects of this challenge, spanning depth of analysis from the topmost 5–10 nm of the surface to the bulk elemental composition of dissolved nanoparticle suspensions [10].

III.5.1. X-ray Photoelectron Spectroscopy (XPS)

X ray photoelectron spectroscopy (XPS) has become one of the key tools for nanoparticle characterization. It provides quantitative information on elemental composition and chemical bonding, but is inherently surface sensitive, probing only the outermost ~5–10 nm of a particle [21].

Here's how it works in practice: you place the sample in an ultra-high vacuum (usually better than 10^{-9} mbar) and hit it with a monochromatic X-ray beam, most often the Al Kα line at 1486.6 eV. The photoelectrons that fly out from the core levels are collected by a hemispherical analyser, and their kinetic energy is measured. From there you calculate the binding energy with the simple relation:

$$\mathbf{BE = h\nu - KE - \varphi}$$

where hν is the X ray energy, KE is the measured kinetic energy of the emitted electrons, and φ is the spectrometer work function. This binding energy acts as a chemical fingerprint, enabling identification of elements and, more importantly, their oxidation states [21].

This is clearly illustrated in iron oxide systems. In magnetite nanoparticles, the Fe 2p region exhibits small but distinct chemical shifts (typically 1–4 eV) between Fe^{2+} and Fe^{3+}, often

accompanied by characteristic satellite features. The same principle applies to other metals; for example, in gold nanoparticles, metallic Au^0 (Au $4f_{7/2}$ around 83.8 eV) can be distinguished from Au(III) (around 86.5 eV). By combining careful peak deconvolution with reference databases such as NIST, reliable assignment of surface chemical states can be achieved [21].

For nanoparticles, though, the extreme surface sensitivity is both a blessing and a bit of a headache. Because the particles are so small and curved, photoelectrons coming from deeper inside have to travel through different amounts of material depending on the emission angle. That geometry tends to make the outer shell (or ligand layer) look more prominent than it really is. That's exactly why Shard and co-workers developed curvature-corrected models that adjust the raw intensities and give you a much more accurate picture of the true composition, especially for particles under about 10 nm [22].

As shown in **Figure (III.4)**, high-resolution XPS spectra provide excellent detail on oxidation states. The Fe 2p spectrum clearly reveals the satellite structures and the specific binding energy positions that distinguish Fe^{2+} from Fe^{3+} through careful curve fitting.

If you want depth information without destroying the sample, angle resolved XPS (ARXPS) is the way to go. Simply tilting the sample changes the effective probing depth, so you can reconstruct composition gradients across a core shell interface at sub nanometre resolution, without sputtering [21].

One last practical point that people sometimes forget: non-conductive samples like silica, polymer-coated particles or most oxide nanoparticles charge up under the X-ray beam. All the peaks shift unless you use a flood gun or calibrate everything against the adventitious carbon C 1s line at 284.8 eV. Getting this right makes the difference between clean, trustworthy data and a messy spectrum [21].

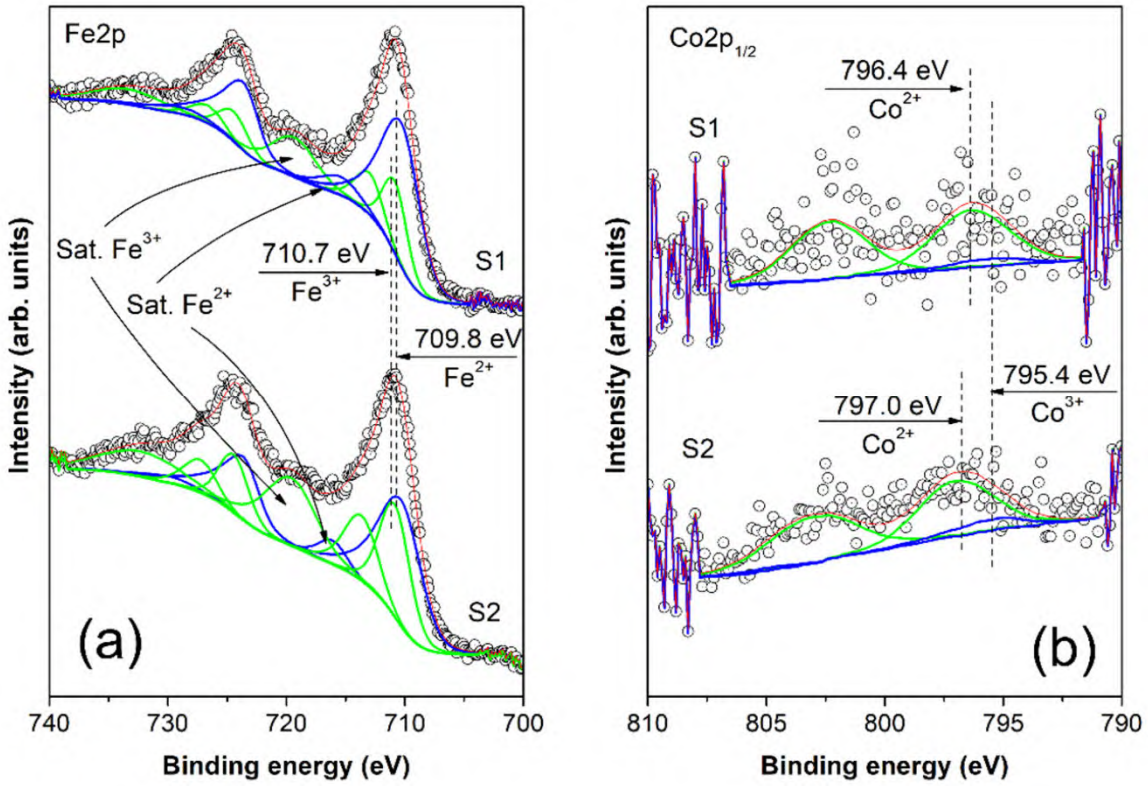

Figure (III.4): High-resolution XPS spectra of Fe 2p (a) and Co 2p (b) for Co-doped ferrite nanoparticles (S1 and S2) [23].

III.5.2. Energy-Dispersive X-ray Spectroscopy (EDX/EDS)

Energy dispersive X ray spectroscopy is most commonly encountered as an attachment to electron microscopes, both TEM and SEM, where the same electron beam used for imaging is also used to generate characteristic X ray fluorescence from the sample. When a high energy electron ejects an inner shell electron from an atom, an outer shell electron fills the vacancy, releasing an X ray photon whose energy is exactly the difference between the two electronic levels and is therefore characteristic of the element. An EDX detector placed near the sample collects these X ray photons and produces an energy resolved spectrum in which the position of each peak identifies the element and the peak area, after appropriate sensitivity corrections using atomic number, absorption, and fluorescence (ZAF) factors, quantifies its concentration [24].

In the context of nanoparticle characterization, EDX combined with STEM (scanning transmission electron microscopy) enables elemental mapping at the atomic scale. STEM EDX maps overlay elemental distribution images on the structural image, revealing whether the

intended core shell architecture has been achieved, where dopant atoms are segregated, and whether surface contamination is present. The spatial resolution of STEM EDX is determined primarily by the probe size of the electron beam; aberration corrected instruments achieve below 0.1 nm probe diameters, and is therefore orders of magnitude better than the several micron lateral resolution of conventional SEM EDX [24]. A fundamental limitation of EDX is its inability to detect light elements reliably: beryllium, lithium, and hydrogen are below the detection threshold of most detectors, and carbon, nitrogen, and oxygen quantification is imprecise owing to absorption of their low energy characteristic X rays by the sample itself and by the detector window. For nanoparticle systems where the organic ligand shell, composed predominantly of C, N, H, and O, is of primary interest, XPS or FTIR therefore provides complementary information that EDX cannot supply.

III.5.3. Inductively Coupled Plasma Mass Spectrometry (ICP-MS)

Inductively coupled plasma mass spectrometry is the gold standard for absolute elemental quantification of nanoparticle dispersions, offering detection limits in the nanogram-per-litre (ppt) range for most transition metals and a dynamic range spanning 8–10 orders of magnitude within a single analytical run [25]. In a conventional ICP MS measurement, the sample is nebulized into an argon plasma operating at approximately 6000–8000 K, which completely atomizes and ionizes all elements present. The resulting ions are extracted through a series of sampling and skimmer cones into a high vacuum mass spectrometer, most commonly a quadrupole, although time of flight (ToF) and sector field instruments are used for simultaneous multi element acquisition and ultra-low detection limits, respectively, where they are separated by their mass to charge ratio (m/z) and quantified against isotopically labelled internal standards and external calibration curves [25].

For nanoparticle characterization, ICP MS serves two distinct but complementary roles. In its conventional, solution mode configuration, nanoparticles are first digested in concentrated acid or dissolved in an appropriate solvent, converting them to ionic species that are then quantified to yield total elemental loading, the metal content per particle, ligand to metal molar ratios, or dopant concentrations. This is particularly valuable for confirming drug loading efficiencies in inorganic-core nanocarriers and for establishing mass balances in stability studies where partial dissolution is expected. In its single-particle mode (sp-ICP-MS), however, the

instrument is configured with a dwell time of 50–100 µs per measurement, allowing individual nanoparticles arriving at the detector to produce discrete ion pulses that can be resolved in time. The mass of metal per pulse is proportional to particle size, enabling direct measurement of the particle size distribution without any prior digestion, alongside simultaneous determination of particle number concentration [26]. *Montaño et al*. demonstrated that sp ICP MS can distinguish and quantify co existing populations of nanoparticles differing in size by as little as 15 nm in environmental water matrices, a selectivity that is essentially impossible to achieve by DLS or NTA in complex real world samples [26].

III.5.4. Nuclear Magnetic Resonance (NMR) for Surface Ligands

Solution-state nuclear magnetic resonance spectroscopy provides uniquely rich molecular-level information about the ligands bound to nanoparticle surfaces, complementing the bulk-ensemble data of FTIR and the surface-sensitive but element-limited information of XPS. In an NMR experiment, nuclei with non-zero spin quantum numbers, most commonly ^{1}H, ^{13}C, ^{31}P, and ^{19}F in nanoparticle research, are polarized by a static magnetic field and then perturbed by a radiofrequency pulse. The characteristic resonance frequency (chemical shift) of each nucleus is sensitive to its electronic environment, and the coupling between adjacent nuclei encodes connectivity information, allowing complete assignment of molecular structure [27]. For nanoparticle surface ligands, three NMR phenomena are of particular diagnostic value: (i) broadening of ligand resonances upon surface binding relative to the free ligand in solution, arising from restricted tumbling and proximity to the paramagnetic or diamagnetic nanoparticle core; (ii) changes in chemical shift that report on the binding mode, for thiolate ligands on gold, for instance, the alpha-CH_2 protons shift by 0.1–0.3 ppm upon surface coordination; and (iii) the complete disappearance of exchangeable ligands from the spectrum as they adsorb irreversibly to the surface [27].

Diffusion-ordered spectroscopy (DOSY) extends standard NMR by incorporating pulsed field gradients to resolve signals by molecular diffusion coefficient, providing a hydrodynamic size estimate for each species in solution. DOSY thus allows free ligands and surface-bound ligands to be distinguished in the same spectrum without physical separation, since nanoparticles diffuse orders of magnitude more slowly than free small molecules [27]. The technique has been applied to determine ligand shell thickness in PEG-coated AuNPs and to monitor real-time ligand

exchange kinetics in situ, information of direct relevance to the design of stimuli-responsive drug delivery systems where surface chemistry must switch predictably in response to pH or redox conditions. A limitation that constrains the broad adoption of NMR for nanoparticle surface analysis is the relatively large sample quantity required, typically 1–10 mg of nanoparticles, and the long acquisition times needed for ^{13}C and ^{31}P measurements. The presence of paramagnetic nanoparticle cores, such as iron oxide, further broadens all ^{1}H resonances, making chemical shift assignment challenging without careful selection of ligand nuclei and pulse sequences [27].

III.6. Magnetic, Electrical, and Mechanical Characterization (Where Applicable)

Not every nanoparticle system requires the same characterization portfolio. While techniques such as XRD, TEM, and DLS represent a near-universal minimum for any colloidal nanomaterial, a meaningful subset of nanoparticles possesses additional functional properties, magnetism, electrical conductivity, or mechanical stiffness, that are central to their intended application and that demand dedicated measurement approaches. Iron oxide nanoparticles synthesized for MRI contrast enhancement or magnetic hyperthermia therapy must be characterized magnetically before any biological evaluation can be meaningfully interpreted; conductive nanoparticles destined for printed electronics or electrochemical sensors require resistivity measurements; and polymer-based or lipid-core nanocarriers intended for drug delivery benefit from nanomechanical characterization because their deformability governs cellular uptake and blood circulation lifetime [1, 2]. This section reviews the principal techniques applied in each of these three domains, with particular attention to the concepts and measurable parameters that carry the greatest predictive relevance for downstream application performance.

III.6.1. Magnetic Characterization: VSM and SQUID Magnetometry

The magnetic response of iron oxide and ferrite nanoparticles to an applied field is the foundation on which essentially all of their biomedical and environmental applications rest, from MRI contrast enhancement and targeted drug delivery to magnetic separation of contaminants from wastewater. Two instruments dominate routine magnetic characterization: the vibrating sample magnetometer (VSM) and the superconducting quantum interference device (SQUID) magnetometer. Both measure magnetization as a function of applied field, but they differ significantly in sensitivity and operational scope. A VSM operates by oscillating the sample

within the gap of an electromagnet and detecting the voltage induced in a set of pickup coils; it is robust, cost-effective, and suitable for samples in the range of 10^{-6} emu, which covers most powder and suspension measurements encountered in nanoparticle research [28]. A SQUID magnetometer, by contrast, detects flux changes with a sensitivity approaching 10^{-10} emu, four orders of magnitude better than VSM, making it indispensable when dealing with weakly magnetic materials, thin films, or dilute suspensions in which the magnetic signal would be swamped by instrumental noise in a conventional VSM [29].

The central output of both instruments is the magnetization versus applied field (M–H) loop, from which several physically meaningful parameters are extracted. Saturation magnetization (Ms), reached when all magnetic domains are aligned with the applied field, reflects the intrinsic magnetic moment per unit mass and is sensitive to crystalline quality, cation distribution within the spinel lattice, and the presence of a non-magnetic surface layer (the so-called magnetically dead layer), whose relative contribution grows disproportionately as particle size decreases [28]. Coercivity (Hc), the field required to reduce the net magnetization to zero after saturation, and remanence (Mr), the magnetization that persists at zero applied field, together determine the shape of the hysteresis loop and encode information about the magnetic anisotropy and domain structure of the particles.

For biomedical applications, the most desirable magnetic state is superparamagnetism, in which the particle contains only a single magnetic domain and the thermal energy at room temperature is sufficient to randomize the magnetization direction when no field is applied. As illustrated in **Figure (III.5)**, superparamagnetic iron oxide nanoparticles yield a closed, non-hysteretic S-shaped M–H curve that passes through the origin (vanishing Hc and Mr) at room temperature, in contrast to the open hysteresis loop characteristic of multi-domain or blocked ferromagnetic particles. This distinction is operationally critical: residual magnetization in the absence of a field would cause particles to aggregate irreversibly in biological media, negating their utility as injectable agents [29].

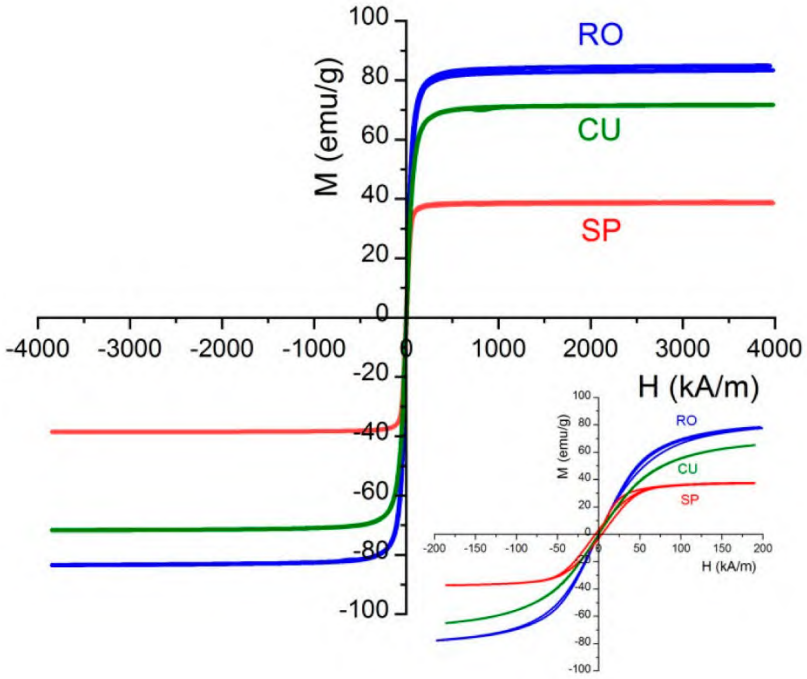

Figure (III.5): Representative magnetization (M–H) curves showing the characteristic non-hysteretic S-shaped loop of superparamagnetic iron oxide nanoparticles (right or bottom) in contrast to the open hysteresis loop of blocked ferromagnetic nanoparticles (left or top) [29].

Temperature-dependent measurements further enrich the magnetic characterization picture. In a zero-field-cooled / field-cooled (ZFC/FC) protocol, the sample is first cooled to cryogenic temperatures in the absence of a field and then a small DC field is applied while the temperature is ramped upward; the peak in the ZFC magnetization curve identifies the blocking temperature (TB), below which the magnetic moments are thermally frozen and the material transitions from superparamagnetic to blocked behaviour. The blocking temperature scales with particle volume and anisotropy constant, which means that TB measurements provide an independent, magnetic-domain-based estimate of particle size that can be compared with the geometric size from TEM, discrepancies between the two are diagnostic of polydispersity, surface spin disorder, or interparticle interactions [29]. Dynamic AC susceptometry, in which the in-phase (χ') and out-of-phase (χ'') components of the susceptibility are measured across a range of frequencies, additionally allows the dominant relaxation mechanism, Néel relaxation (internal spin reorientation within the particle) versus Brownian relaxation (physical rotation of the whole particle in the carrier fluid), to be distinguished. This distinction has direct implications for

hyperthermia applications, since the specific absorption rate (SAR) depends strongly on which relaxation pathway dominates under the applied oscillating field [30].

III.6.2. Electrical Characterization: Conductivity and Impedance Measurements

For nanoparticle systems intended for electronic, sensing, or electrochemical applications, such as conductive carbon nanotubes, graphene quantum dots, metallic nanoparticle inks, or semiconductor nanocrystal films, electrical characterization is as fundamental as size and morphology. The most direct measurement is four-probe (or four-point probe) conductivity, in which two outer probes inject a known current into the sample while two inner probes measure the resulting voltage drop; the geometric separation of the probes allows sheet resistance or bulk conductivity to be extracted without contact resistance artefacts that would corrupt a two-probe measurement [31]. For nanoparticle films deposited on insulating substrates, this approach is straightforward and routinely applied during the development of printed electronics and transparent conductive coatings.

Electrochemical impedance spectroscopy (EIS) provides a complementary perspective by applying a small sinusoidal voltage perturbation across a frequency range (typically 0.01 Hz to 10 MHz) and measuring the amplitude and phase of the current response. The resulting impedance spectrum, displayed as a Nyquist or Bode plot, can be modelled with equivalent circuits to deconvolute bulk resistive, interfacial capacitive, and charge-transfer contributions, information critical for optimizing nanoparticle-modified electrodes in biosensing and electrocatalysis [31]. EIS has been particularly widely used to characterize the passivating oxide layers on iron nanoparticles and the Helmholtz double-layer capacitance of nanoparticle suspensions, since the interfacial electrical properties directly govern corrosion resistance and colloidal charging behaviour. It is worth noting that the electrical conductivity of nanoparticle assemblies is generally significantly lower than that of the corresponding bulk material, due to the large number of grain boundaries and interparticle tunnelling junctions that scatter charge carriers; characterizing this size-dependent conductivity reduction is therefore an important step in evaluating the suitability of any conductive nanomaterial for device integration [31].

III.6.3. Nanomechanical Characterization: Nanoindentation and AFM Force Spectroscopy

The mechanical properties of nanoparticles, stiffness, hardness, adhesion, and viscoelastic response, are not merely academic curiosities; they govern behaviour in applications ranging from drug delivery (where nanoparticle deformability controls blood circulation time and cellular uptake) to nanocomposite reinforcement (where interfacial load transfer depends on particle modulus) and nanoscale tribology (where particle hardness determines wear resistance) [32]. Two techniques provide quantitative access to these properties at the nanoscale: instrumented nanoindentation using a sharp Berkovich or cube-corner tip, and AFM-based force spectroscopy using a calibrated cantilever.

In instrumented nanoindentation, a diamond tip is driven into the sample surface under a prescribed load function, and the load-displacement (P–h) curve is recorded continuously during both loading and unloading. The Oliver–Pharr method extracts the reduced elastic modulus Er and hardness H from the initial slope of the unloading curve and the projected contact area at maximum load, respectively [32]. For nanoparticles individually deposited on a flat substrate, the technique requires careful control of the maximum indentation depth to avoid substrate interference, a general rule of thumb is to limit penetration to less than 10% of the particle diameter. Zhang et al. demonstrated that AFM nanoindentation on submicron ZIF-8 MOF crystals revealed a 40% reduction in Young's modulus compared to bulk single-crystal values, attributable to size-dependent defect density and surface energy effects [33]. AFM force spectroscopy accesses an overlapping but distinct parameter space: in a force-distance curve measurement, the deflection of a calibrated cantilever is recorded as the tip approaches and retracts from the particle surface, yielding adhesion forces, pull-off energies, and stiffness values from the contact regime that are analysed using Hertz or DMT contact mechanics models [9]. Peak-force quantitative nanomechanical (QNM) mapping extends this to produce spatially resolved elastic modulus maps at rates of tens of kilohertz per pixel, enabling the simultaneous acquisition of topography and mechanical contrast across heterogeneous nanoparticle surfaces, for instance, distinguishing a rigid inorganic core from a compliant polymer shell in a core-shell drug carrier [9].

III.7. Correlating Characterization Data with Performance in Applications

The preceding sections have surveyed characterization techniques largely as independent methods, each probing a specific physical or chemical property of the nanoparticle system. In

practice, however, the real value of comprehensive characterization lies not in the isolated measurements themselves but in the relationships that can be established between physicochemical parameters and observed functional performance. This structure–property–function paradigm, borrowed from classical materials science, is now being applied with increasing rigour to nanoparticle research, driven by the recognition that empirical screening of formulation variables, without a mechanistic understanding of how they connect to outcomes, is both resource-intensive and poor at predicting behaviour across different biological or environmental contexts [34]. The following paragraphs discuss how characterization data from the techniques described earlier in this chapter can be systematically correlated with performance in three representative application domains: drug delivery, heterogeneous catalysis, and environmental adsorption.

In drug delivery, the primary performance metrics are encapsulation efficiency, drug release kinetics, cellular uptake, blood circulation time, and tumour accumulation. Each of these is sensitive to a specific set of physicochemical parameters. Hydrodynamic diameter, measured by DLS, is perhaps the most consequential single parameter: nanoparticles below approximately 8 nm are rapidly cleared by renal filtration, those above 200 nm are efficiently sequestered by the mononuclear phagocyte system in the liver and spleen, and those in the 10–100 nm window benefit most from the enhanced permeability and retention (EPR) effect in solid tumours [35]. The polydispersity index (PDI) complements the mean size: formulations with PDI > 0.3 exhibit batch-to-batch variability in biodistribution that is difficult to control and that has been cited as a contributing factor to the poor translation of many preclinical nanomedicine findings into clinical settings [34]. Zeta potential, measured by ELS, predicts colloidal stability in physiological media and, for cationic nanoparticles, correlates with haemolytic toxicity and non-specific cellular uptake, a relationship first systematically documented by Leroueil et al. and subsequently confirmed across multiple nanoparticle chemistries [36]. Surface chemistry, probed by FTIR and XPS, determines protein corona formation: the identities and affinities of the serum proteins that adsorb onto the nanoparticle surface within seconds of entry into the bloodstream largely reset the biological identity of the particle, and the relationship between surface hydrophilicity, PEG chain density, and corona composition has become one of the most actively studied structure–function correlations in nanomedicine [35].

As illustrated in **Figure (III.6)**, the physicochemical properties of nanoparticles, particularly size, surface charge, shape and surface coating, exert a profound influence on in vivo biodistribution through the interplay of EPR-mediated tumour accumulation, size-dependent renal clearance, and MPS sequestration.

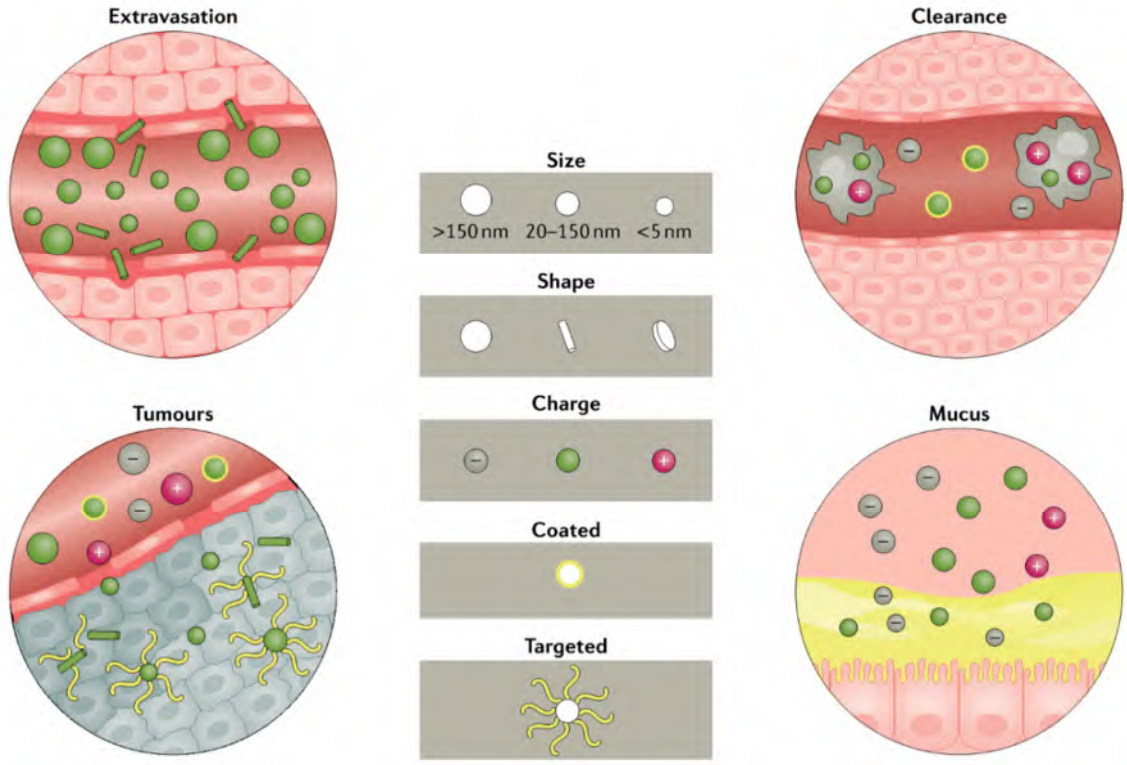

Figure (III.6): Influence of nanoparticle physicochemical properties on in vivo biodistribution and biological fate [34].

In heterogeneous catalysis, the key performance indicators are specific activity (reaction rate per unit mass of catalyst), turnover frequency (TOF, molecules converted per active site per second), and selectivity toward the desired product. Crystal phase, identified by XRD and confirmed by HR-TEM, is frequently determinative: in photocatalytic water splitting with TiO_2, for instance, the anatase phase outperforms rutile under UV irradiation by roughly one order of magnitude in hydrogen evolution rate, a difference traced to the superior electron mobility and more favourable band alignment of anatase despite the two phases being identical in elemental composition [37]. Specific surface area, measured by the Brunauer–Emmett–Teller (BET) nitrogen adsorption method, a technique deliberately excluded from this chapter's main coverage

because it addresses porosity rather than particle-level properties, is routinely correlated with catalytic activity across a wide range of systems: rate constants for dye degradation by TiO_2 and ZnO nanoparticles scale approximately linearly with BET surface area when particle size is varied systematically, confirming that the reaction is surface-limited [37]. The relationship between crystallite size from Scherrer analysis and catalytic activity is more nuanced: while a smaller crystallite exposes more surface atoms, it also contains a higher defect density that can simultaneously serve as active sites and as recombination centres for photogenerated electron-hole pairs, illustrating why a single characterization metric rarely provides a complete mechanistic picture.

In environmental adsorption applications, the removal of heavy metal ions, dyes, or micropollutants from water using nanoparticle-based adsorbents, performance is quantified through adsorption capacity (mg of pollutant per gram of adsorbent), rate constant, and selectivity in multi-component matrices. Zeta potential governs electrostatic attraction between adsorbent and adsorbate: iron oxide nanoparticles with a point of zero charge near pH 7 carry a net positive surface charge at typical wastewater pH values of 5–7, favouring adsorption of anionic contaminants such as arsenate and chromate [38]. FTIR identification of surface hydroxyl groups, carboxylate functionalities, or amine ligands predicts which adsorption mechanisms, surface complexation, ion exchange, or electrostatic interaction, will dominate, and guides the rational design of surface modifications to enhance capacity or selectivity. Magnetic characterization by VSM is particularly relevant for magnetically separable adsorbents: a saturation magnetization of at least 16.3 emu/g has been proposed as the practical minimum threshold for efficient recovery of particles from suspension using a hand-held permanent magnet, and adsorbents below this value require either high-gradient magnetic separation or unconventionally large external magnets [38].

Across all three application domains, a recurring theme is that no single characterization parameter is sufficient to explain or predict performance, and that the relationships between parameters are often non-linear and context-dependent. The field is increasingly moving toward quantitative structure–activity relationship (QSAR) modelling and machine-learning-assisted analysis of large characterization datasets, in which multiple physicochemical descriptors are combined to build predictive models of in vitro or in vivo performance [34]. These approaches, while still at an early stage of development for nanomaterials, represent a promising path toward

reducing the empirical burden of nanoparticle optimization and toward the eventual establishment of characterization-informed design rules, a goal that is only achievable if the underlying characterization data are collected with sufficient rigor, reproducibility, and transparency to serve as reliable training inputs for predictive models.

References

References

1. Fadeel B, Farcal L, Hardy B, et al (2018) Advanced tools for the safety assessment of nanomaterials. Nat Nanotechnol 13:537–543. https://doi.org/10.1038/s41565-018-0185-0
2. Mourdikoudis S, Pallares RM, Thanh NTK (2018) Characterization techniques for nanoparticles: Comparison and complementarity upon studying nanoparticle properties. Nanoscale 10:12871–12934. https://doi.org/10.1039/c8nr02278j
3. Hardy A, Benford D, Halldorsson T, et al (2018) Guidance on risk assessment of the application of nanoscience and nanotechnologies in the food and feed chain: Part 1, human and animal health. EFSA J 16:5327. https://doi.org/10.2903/j.efsa.2018.5327
4. Holder CF, Schaak RE (2019) Tutorial on Powder X-ray Diffraction for Characterizing Nanoscale Materials. ACS Nano 13:7359–7365. https://doi.org/10.1021/acsnano.9b05157
5. Ingham B (2015) X-ray scattering characterisation of nanoparticles. Crystallogr Rev 21:229–303. https://doi.org/10.1080/0889311X.2015.1024114
6. Rizzello L, Pompa PP (2014) Nanosilver-based antibacterial drugs and devices: Mechanisms, methodological drawbacks, and guidelines. Chem Soc Rev 43:1501–1518. https://doi.org/10.1039/c3cs60218d
7. Bellare JR, Davis HT, Scriven LE, Talmon Y (1988) Controlled environment vitrification system: An improved sample preparation technique. J Electron Microsc Tech 10:87–111. https://doi.org/10.1002/jemt.1060100111
8. Inkson BJ (2016) Scanning Electron Microscopy (SEM) and Transmission Electron Microscopy (TEM) for Materials Characterization. In: Materials Characterization Using Nondestructive Evaluation (NDE) Methods. Elsevier, pp 17–43
9. Lam CD, Park S (2025) Nanomechanical characterization of soft nanomaterial using atomic force microscopy. Mater Today Bio 31:. https://doi.org/10.1016/j.mtbio.2025.101506
10. Bhattacharjee S (2016) DLS and zeta potential - What they are and what they are not? J Control Release 235:337–351. https://doi.org/10.1016/j.jconrel.2016.06.017
11. Filipe V, Hawe A, Jiskoot W (2010) Critical evaluation of nanoparticle tracking analysis (NTA) by NanoSight for the measurement of nanoparticles and protein aggregates. Pharm Res 27:796–810. https://doi.org/10.1007/s11095-010-0073-2
12. Derjaguin D DLVO theory : General DLVO theory : General. As Rev Greg J

13. Dragovic RA, Gardiner C, Brooks AS, et al (2011) Sizing and phenotyping of cellular vesicles using Nanoparticle Tracking Analysis. Nanomedicine Nanotechnology, Biol Med 7:780–788. https://doi.org/10.1016/j.nano.2011.04.003
14. Tauc J (1968) Optical properties and electronic structure of amorphous Ge and Si. Mater Res Bull 3:37–46. https://doi.org/10.1016/0025-5408(68)90023-8
15. Haiss W, Thanh NTK, Aveyard J, Fernig DG (2007) Determination of Size and Concentration of Gold Nanoparticles from UV−Vis Spectra. Anal Chem 79:4215–4221. https://doi.org/10.1021/ac0702084
16. Semwal V, Jensen OR, Bang O, Janting J (2023) Investigation of Performance Parameters of Spherical Gold Nanoparticles in Localized Surface Plasmon Resonance Biosensing. Micromachines 14:1717. https://doi.org/10.3390/mi14091717
17. Bērziņš K Challenges and limitations of attenuated total reflection Fourier-transform infrared (ATR-FTIR) spectroscopy for colloidal nanoparticle characterization. Chem Commun 56:15267–15277. https://doi.org/10.1039/D0CC03613A
18. Ferrari AC, Basko DM (2013) Raman spectroscopy as a versatile tool for studying the properties of graphene. Nat Nanotechnol 8:235–246. https://doi.org/10.1038/nnano.2013.46
19. Xue R-S, Dai J-Y, Wang X-J, Chen M-Y (2025) Research Progress of Surface-Enhanced Raman Scattering (SERS) Technology in Food, Biomedical, and Environmental Monitoring. Photonics 12:809. https://doi.org/10.3390/photonics12080809
20. Efros AL, Brus LE (2021) Nanocrystal Quantum Dots: From Discovery to Modern Development. ACS Nano 15:6192–6210. https://doi.org/10.1021/acsnano.1c01399
21. Greczynski G, Hultman L (2022) A step-by-step guide to perform x-ray photoelectron spectroscopy. J Appl Phys 132:11101. https://doi.org/10.1063/5.0086359
22. Shard AG (2012) A straightforward method for interpreting XPS data from core-shell nanoparticles. J Phys Chem C 116:16806–16813. https://doi.org/10.1021/jp305267d
23. Ognjanović M, Bošković M, Kolev H, et al (2024) Synthesis, Surface Modification and Magnetic Properties Analysis of Heat-Generating Cobalt-Substituted Magnetite Nanoparticles. Nanomaterials 14:782. https://doi.org/10.3390/nano14090782
24. Zaluzec NJ (2009) Innovative Instrumentation for Analysis of Nanoparticles: The π Steradian Detector. Micros Today 17:56–59. https://doi.org/10.1017/S1551929509000224

25. Laborda F Inductively coupled plasma mass spectrometry for the analysis, characterization and speciation of organic nanoparticles. J Anal At Spectrom 36:229–242. https://doi.org/10.1039/D0JA00415D
26. Mansor M, Drabesch S, Bayer T, et al (2021) Application of Single-Particle ICP-MS to Determine the Mass Distribution and Number Concentrations of Environmental Nanoparticles and Colloids. Environ Sci Technol Lett 8:589–595. https://doi.org/10.1021/acs.estlett.1c00314
27. Marbella LE, Millstone JE (2015) NMR techniques for noble metal nanoparticles. Chem Mater 27:2721–2739. https://doi.org/10.1021/cm504809c
28. Sandler SE, Fellows B, Thompson Mefford O (2019) Best Practices for Characterization of Magnetic Nanoparticles for Biomedical Applications. Anal Chem 91:14159–14169. https://doi.org/10.1021/acs.analchem.9b03518
29. Reyes-ortega F, Delgado Á V., Iglesias GR (2021) Modulation of the magnetic hyperthermia response using different superparamagnetic iron oxide nanoparticle morphologies. Nanomaterials 11:1–14
30. Rosensweig RE (2002) Heating magnetic fluid with alternating magnetic field. J Magn Magn Mater 252:370–374. https://doi.org/10.1016/S0304-8853(02)00706-0
31. Mirri F, Ma AWK, Hsu TT, et al (2012) High-performance carbon nanotube transparent conductive films by scalable dip coating. ACS Nano 6:9737–9744. https://doi.org/10.1021/nn303201g
32. Oliver WC, Pharr GM (2004) Measurement of hardness and elastic modulus by instrumented indentation: Advances in understanding and refinements to methodology. J Mater Res 19:3–20. https://doi.org/10.1557/jmr.2004.19.1.3
33. Zeng Z, Tan JC (2017) AFM Nanoindentation to Quantify Mechanical Properties of Nano- and Micron-Sized Crystals of a Metal-Organic Framework Material. ACS Appl Mater Interfaces 9:39839–39854. https://doi.org/10.1021/acsami.7b13402
34. Mitchell MJ, Billingsley MM, Haley RM, et al (2021) Engineering precision nanoparticles for drug delivery. Nat Rev Drug Discov 20:101–124. https://doi.org/10.1038/s41573-020-0090-8
35. Anselmo AC, Mitragotri S (2016) Nanoparticles in the clinic. Bioeng Transl Med 1:10–29. https://doi.org/10.1002/btm2.10003

36. Leroueil PR, Berry SA, Duthie K, et al (2008) Wide varieties of cationic nanoparticles induce defects in supported lipid bilayers. Nano Lett 8:420–424. https://doi.org/10.1021/nl0722929
37. Jenny S, Masaya M, Masato T, et al (2014) Understanding TiO2 photocatalysis: mechanisms and materials. Chem Rev 114:9919–9986
38. Yusuf M, Elfghi FM, Zaidi SA, et al (2015) Applications of graphene and its derivatives as an adsorbent for heavy metal and dye removal: A systematic and comprehensive overview. RSC Adv 5:50392–50420. https://doi.org/10.1039/c5ra07223a

CHAPTER IV
Nanoparticles in Wastewater Remediation

IV.1. Overview of Wastewater Contaminants (Heavy Metals, Dyes, Pharmaceuticals, Emerging Pollutants)

IV.1.1. Heavy Metal Contaminants

Heavy metals, defined as high-density metallic elements such as lead (Pb), arsenic (As), chromium (Cr), cadmium (Cd), mercury (Hg), and nickel (Ni), represent a significant category of inorganic pollutants that are highly toxic even at trace concentrations [1]. These contaminants are primarily released into aquatic environments from diverse industrial operations, including mining, electroplating, battery manufacturing, and metallurgical processes [2]. Unlike organic pollutants, heavy metals are non-biodegradable and tend to bioaccumulate through the food chain, leading to chronic health issues in humans such as kidney failure, permanent neurological damage, and various forms of cancer [2, 3].

In recent years, the focus of wastewater remediation has shifted toward nanotechnology, specifically the utilization of Iron Oxide Magnetic Nanoparticles (IONPs). IONPs, particularly magnetite (Fe_3O_4), offer a high specific surface area which facilitates strong interactions with metal ions [1, 4]. Their most distinctive advantage is their magnetic character, allowing for efficient separation from treated water using external magnets [3]. Furthermore, the performance of these nanoparticles can be significantly enhanced through surface functionalization with ligands like dimercaptosuccinic acid (DMSA), which creates additional active sites to improve selectivity for specific ions like Pb^{2+} and Cu^{2+} [5]. As illustrated in **Figure (IV.1)**, functionalized magnetic nanoparticles utilize these surface interactions to sequester heavy-metal ions effectively from complex wastewater matrices.

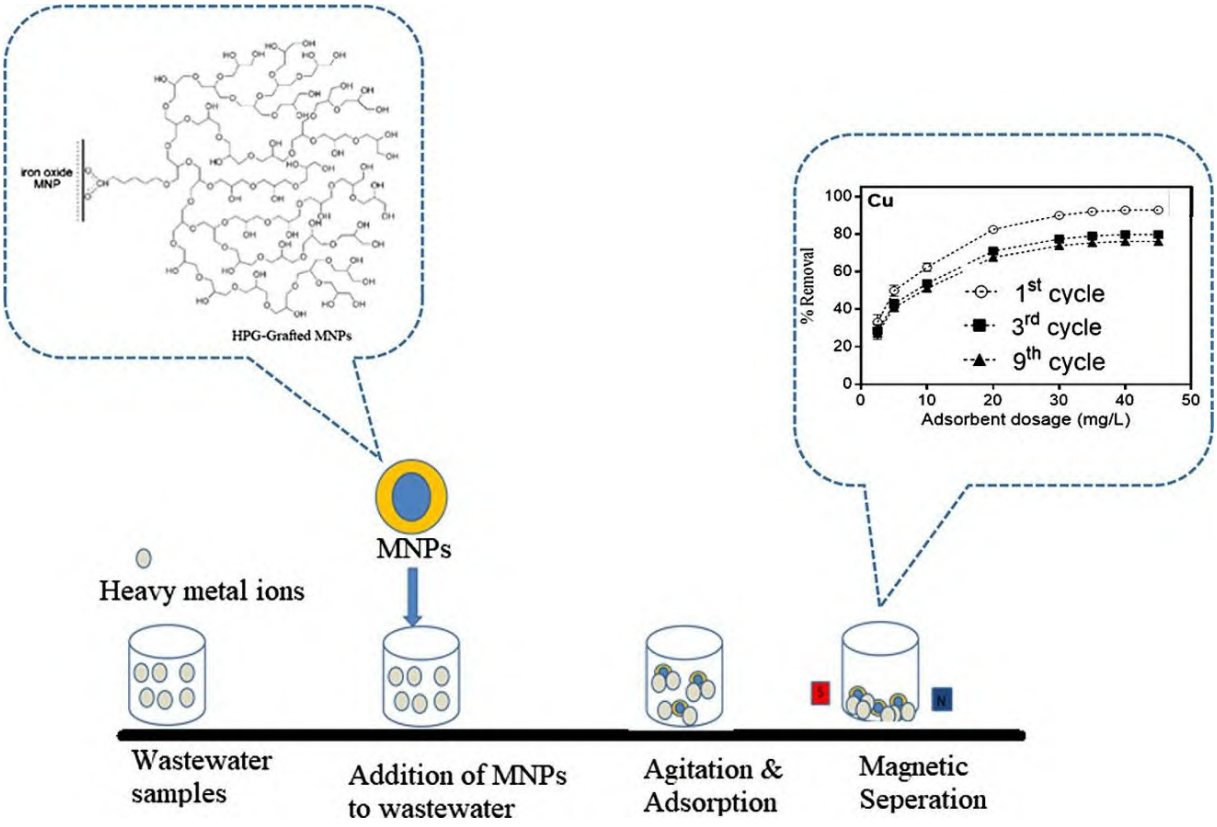

Figure (IV.1): Mechanism of removing heavy-metal ions using functionalized magnetic nanoparticles [6].

IV.1.2. Organic Dyes

The discharge of dye-laden effluents from the textile, paper, and printing industries is a major environmental concern due to the high visibility and complex chemical nature of these pollutants [3, 7]. Synthetic dyes are identified by chromophores (responsible for color) and auxochromes (which enhance solubility) [3]. Many of these dyes, including Methylene Blue and Reactive Black 5, are highly stable, mutagenic, and carcinogenic [7]. Their presence in water systems blocks light penetration, which inhibits photosynthesis in aquatic flora and disrupts the ecological balance [3].

Because most synthetic dyes are resistant to conventional aerobic biological degradation, advanced technologies such as Advanced Oxidation Processes (AOPs) are required. Among these, heterogeneous photocatalysis using semiconductor nanomaterials like TiO_2 and ZnO has proven highly efficient [8]. The process is initiated when the semiconductor absorbs light energy, generating electron-hole pairs that produce highly reactive species, specifically hydroxyl radicals

(*OH·*). These radicals attack the dye molecules, breaking down stable bonds and mineralizing them into harmless substances such as CO_2 and H_2O [7]. The general mechanism of this photocatalytic degradation is depicted in **Figure (IV.2)**.

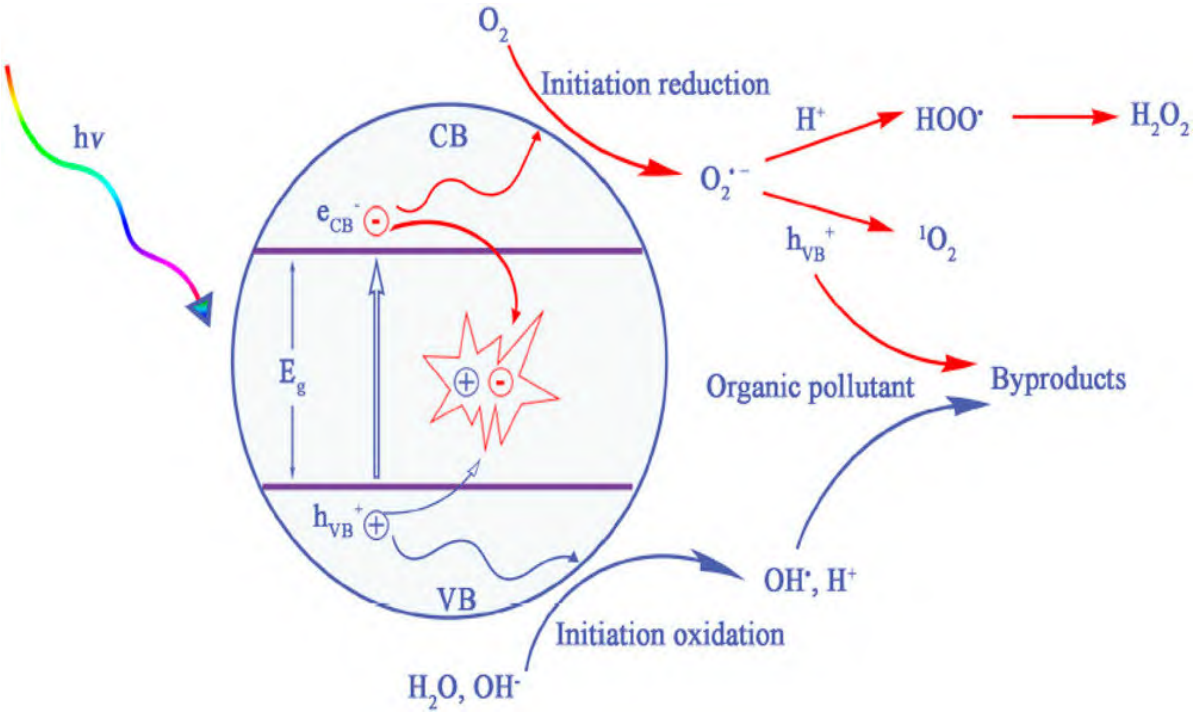

Figure (IV.2): General mechanism of photocatalysis for pollutant degradation [9].

IV.1.3. Pharmaceutical Pollutants

Pharmaceuticals are a critical class of emerging organic contaminants entering the water cycle through domestic wastewater and hospital effluents. This category includes antibiotics (e.g., amoxicillin), analgesics (e.g., ibuprofen), and psychiatric drugs. Traditional wastewater treatment plants (WWTPs) were not designed to eliminate these xenobiotic compounds, leading to their persistence in groundwater. Long-term exposure is linked to the development of drug-resistant bacteria and reproductive disruption in aquatic species [2, 10].

To address these limitations, advanced adsorbents such as magnetic nanocomposites have been developed. One innovative approach involves using biochar (BC) derived from agricultural waste impregnated with nanoscale zerovalent iron (nZVI) and chitosan. These hybrid materials exhibit high removal efficiencies through mechanisms such as hydrogen bonding, π–π interactions, and pore filling. For instance, drug molecules can diffuse into the pores of the biochar or interact with the composite surface via molecular stacking. These magnetic composites

can be recovered within seconds using an external magnetic field, making them a sustainable option for remediation [10]. **Figure (IV.3)** illustrates the interaction mechanisms between magnetic nanocomposites and drug molecules.

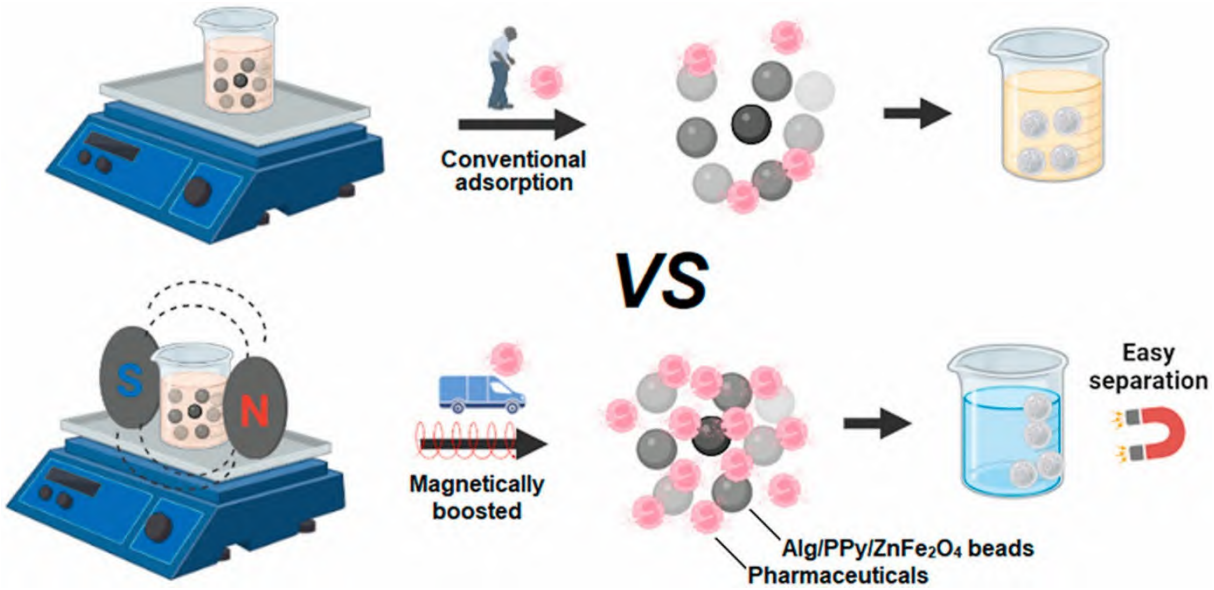

Figure (IV.3): Removal of pharmaceuticals from aqueous medium by alginate/polypyrrole/$ZnFe_2O_4$ beads via magnetic field enhanced adsorption [11].

IV.1.4. Emerging Pollutants (ECs)

Emerging pollutants, or micropollutants, encompass chemicals that are not yet commonly monitored but have the potential for significant ecological impact. According to the US EPA, these include Endocrine Disrupting Chemicals (EDCs) like Bisphenol A (BPA) and Personal Care Products (PCPs) such as triclosan and synthetic fragrances. Found in trace concentrations (*ng*/*L* to *μg*/*L*), they are dangerous because they act as hormonal mimics, causing damage to the human immune and reproductive systems [12].

Effective management requires nanotechnology-powered modular processes. Engineered nanomaterials possess unique features such as exceptional electrical properties and the ability to be easily modified with specific surface groups. These characteristics allow them to precisely manage functional features that traditional systems fail to capture. For example, nanomembranes can separate pollutants via size exclusion, while nanosorbents can be engineered to be highly selective toward specific EDCs [13]. As shown in **Figure (IV.4)**, the unique physical and

chemical features of various nanoparticles allow for a tailored approach to treating the diverse classes of emerging pollutants found in waste streams.

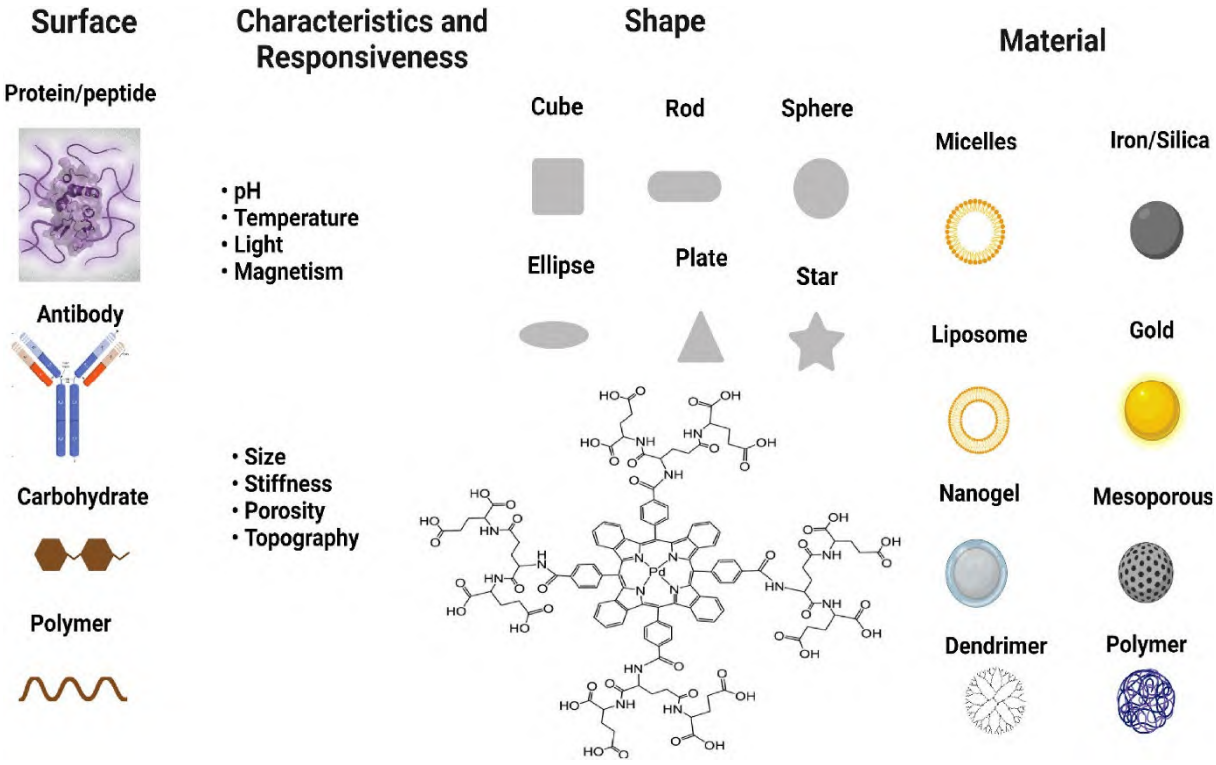

Figure (IV.4): Main features and classifications of nanoparticles used in advanced wastewater treatment.

IV.2. Nanoparticles as Adsorbents

The exponential growth of industrial activity worldwide has led to the widespread discharge of toxic contaminants, most notably heavy metals and recalcitrant organic pollutants, into aquatic and terrestrial environments. In response, adsorption has emerged as one of the most widely adopted physicochemical strategies for water treatment, owing to its operational simplicity, high efficiency, low energy demand, and remarkable versatility in terms of adsorbent design [14]. Conventional adsorbents such as activated carbon and zeolites, while effective, are increasingly being supplemented or replaced by engineered nanomaterials, which offer surface areas several orders of magnitude greater than their bulk counterparts along with tunable surface chemistry and high reactivity [15].

Nanoparticles are generally defined as discrete units with at least one dimension in the range of 1–100 nm. At this scale, quantum and surface effects dominate over bulk properties,

giving rise to extraordinary adsorption capacities, rapid kinetics, and the possibility of selective pollutant capture. The surface-area-to-volume ratio increases dramatically as particle size decreases, maximising the density of active sites available for pollutant binding. Furthermore, nanoparticle surfaces can be deliberately functionalised with organic ligands, polymers, or metal ions to engineer selectivity toward specific target contaminants [16].

This section examines the most extensively studied classes of nanoparticulate adsorbents, namely metal and metal oxide nanoparticles (Section IV.2.1) and carbon-based nanomaterials (Section IV.2.2), with particular emphasis on their structural characteristics, mechanistic behaviour, and demonstrated performance in the removal of heavy metal ions from contaminated water matrices.

IV.2.1. Metal and Metal Oxide Nanoparticles for Heavy Metal Removal

Among the diverse range of engineered nanomaterials investigated for heavy metal remediation, metal and metal oxide nanoparticles occupy a central position, combining high surface reactivity with the possibility of magnetic recovery and versatile surface functionalisation [17]. Iron oxide nanoparticles, particularly magnetite (Fe_3O_4) and maghemite (γ-Fe_2O_3), have attracted particular attention due to their superparamagnetic behaviour, which facilitates facile separation from treated water by applying an external magnetic field, thereby circumventing the costly filtration steps associated with conventional sorbents [18].

The adsorption of heavy metal cations onto iron oxide surfaces proceeds primarily through inner-sphere surface complexation, wherein metal ions displace coordinated water molecules and form direct bonds with surface hydroxyl (≡Fe–OH) groups. The density and protonation state of these hydroxyl groups are pH-dependent, rendering iron oxide nanoparticles highly sensitive to solution pH. Under circumneutral to mildly alkaline conditions, the surface acquires a net negative charge that electrostatically attracts divalent and trivalent cations such as Pb^{2+}, Cd^{2+}, Cu^{2+}, and Cr^{3+} [19]. Studies on Fe_3O_4, ZnO, and CuO nanoparticles reported by Mahdavi *et al.* demonstrated maximum uptake values (sum of four metals) in multiple-component solutions of 360.6, 114.5, and 73.0 mg g^{-1} for ZnO, CuO, and Fe_3O_4, respectively, with the preferential adsorption order $Cd^{2+} > Pb^{2+} > Cu^{2+} > Ni^{2+}$ for single-component solutions, as illustrated in ***Figure (IV.5)*** [19].

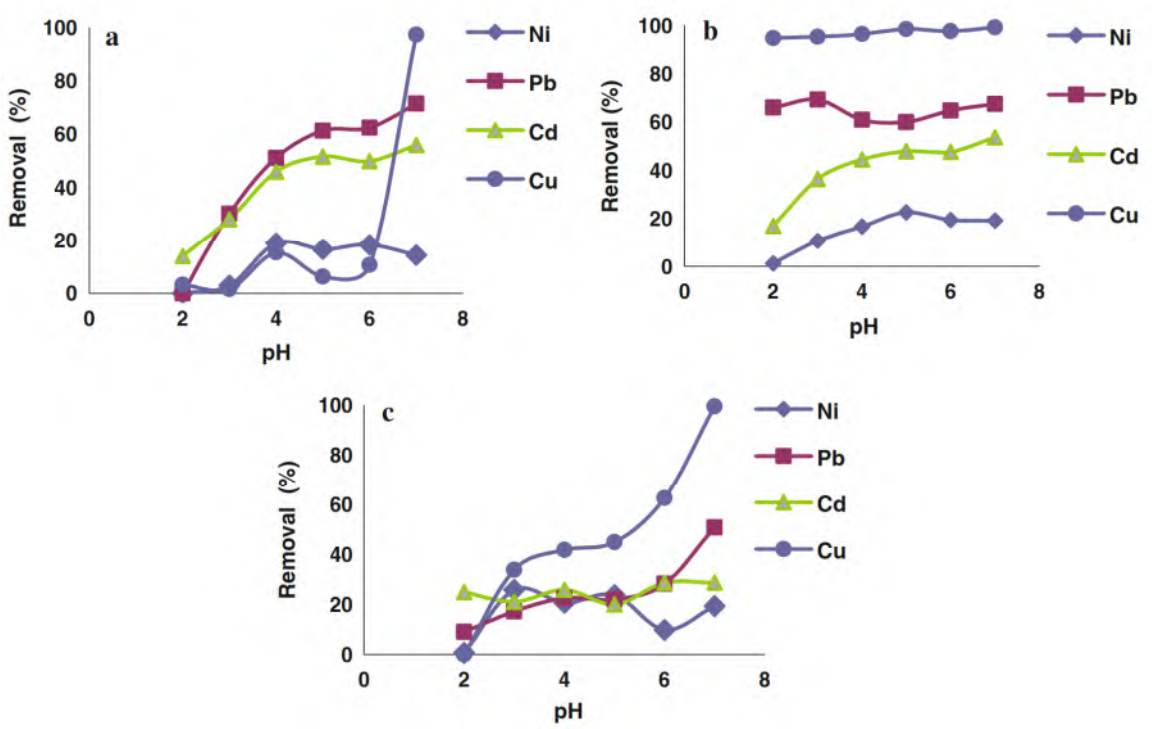

Figure (IV.5): Effect of pH on the adsorption efficiency of Fe_3O_4, ZnO, and CuO nanoparticles for Pb^{2+}, Cd^{2+}, Cu^{2+}, and Ni^{2+} ions from single- and multi-component aqueous solutions [19].

Functionalisation strategies substantially amplify the performance of bare iron oxide nanoparticles. Ge *et al.* synthesised Fe_3O_4 nanoparticles surface-modified with acrylic acid–crotonic acid copolymer (polymer content ≈ 36.7 wt%), achieving effective removal of Cd^{2+}, Zn^{2+}, Pb^{2+}, and Cu^{2+} with a selectivity order of Pb > Cu > Zn > Cd, attributable to differences in ionic radius, electronegativity, and stability constants of surface complexes [20]. Similarly, Lu *et al.* demonstrated that core–shell Fe_3O_4@SiO_2 architectures protect the magnetic core from oxidative dissolution while providing a silanol-rich outer surface amenable to further amine or thiol functionalisation, enabling sequential magnetic recovery and adsorbent regeneration [16].

Zinc oxide (ZnO) and titanium dioxide (TiO_2) nanoparticles represent another prominent class of metal oxide adsorbents. ZnO nanoparticles typically exhibit amphoteric surface hydroxyl groups with a point of zero charge (pH_0 ≈ 9), enabling them to adsorb both cationic (e.g., Pb^{2+}, Cd^{2+}) and anionic (e.g., arsenate, chromate) species depending on the prevailing pH. Sheela *et al.* reported maximum Langmuir adsorption capacities of 714 and 384 mg g^{-1} for Hg^{2+} and Cd^{2+}, respectively, on precipitated ZnO nanoparticles (BET surface area ≈ 31.2 m^2 g^{-1}) at pH 5.5 and 303 K, with pseudo-second-order kinetics confirming chemisorption as the rate-limiting step

[21]. TiO_2 nanoparticles in the anatase polymorph are also well-documented for arsenate (As(V)) adsorption via ligand-exchange mechanisms at surface Ti–OH sites, following Langmuir monolayer behaviour [22].

Zero-valent iron nanoparticles (nZVI) combine reductive and adsorptive mechanisms, making them particularly effective for hexavalent chromium (Cr(VI)) removal. The reductive transformation of Cr(VI) to the far less toxic Cr(III) proceeds at the nZVI surface concurrently with Fe^0 oxidation, and the resulting Cr(III) ions are subsequently co-precipitated as $Cr_xFe_{1-x}(OH)_3$. Crane and Scott reviewed the mechanistic pathways and engineering constraints of nZVI deployment, noting its outstanding reactivity but also its susceptibility to passivation and agglomeration in complex groundwater matrices [23].

Adsorption isotherms of metal oxide nanoparticles are frequently well-described by the Langmuir model, indicating monolayer adsorption on energetically homogeneous surface sites. Pseudo-second-order kinetics prevail in the majority of published studies, implying that chemisorption, rather than mass-transfer resistance, is the rate-controlling step [21]. Thermodynamic analyses consistently reveal spontaneous (negative $\Delta G°$) and endothermic (positive $\Delta H°$) adsorption processes, suggesting that elevated temperatures favour heavier metal uptake by increasing ion mobility and promoting ion exchange at the nanoparticle surface [21].

Despite their outstanding laboratory-scale performance, the practical deployment of metal oxide nanoparticles in water treatment systems faces challenges including agglomeration under high ionic strength and potential ecotoxicological effects of nanoparticle release. Immobilisation strategies, incorporating Fe_3O_4 in alginate beads, anchoring nanoparticles on magnetic substrates, or embedding them within polymeric membranes, are being actively explored to reconcile high adsorptive capacity with operational practicability [16].

IV.2.2. Carbon-Based Nanomaterials (CNTs, Graphene, Activated Carbon Nanocomposites)

Carbon-based nanomaterials constitute one of the most intensively studied classes of adsorbents in contemporary environmental remediation research. Their structural diversity, ranging from one-dimensional carbon nanotubes (CNTs) to two-dimensional graphene and graphene oxide (GO) sheets, and further to three-dimensional activated carbon nanocomposites,

translates into a correspondingly broad spectrum of adsorptive properties [24]. Fundamentally, the exceptional performance of these materials is rooted in the sp^2-hybridised carbon lattice, which confers high mechanical strength, chemical stability, and an extensive aromatic surface capable of engaging in π–π stacking, hydrophobic partitioning, and electrostatic attraction with pollutant molecules [24].

Carbon Nanotubes (CNTs). CNTs are seamless cylindrical structures formed by rolling graphene sheets into tubes of nanometre diameter. They are classified as single-walled (SWCNTs, diameter 0.4–2 nm) or multi-walled (MWCNTs, diameter 2–100 nm) depending on the number of concentric graphene layers. Pristine CNTs are largely hydrophobic and exhibit limited dispersibility in aqueous media; oxidative treatment with strong acid mixtures (HNO_3/H_2SO_4) introduces carboxyl, hydroxyl, and carbonyl functional groups at defect sites and tube ends, dramatically improving both hydrophilicity and heavy metal affinity [25]. Lu *et al.* demonstrated that oxidised MWCNTs achieved a Pb^{2+} adsorption capacity of 97.1 mg g^{-1}, significantly exceeding the performance of unmodified tubes. The mechanism involves simultaneous electrostatic attraction, surface complexation with oxygen-containing functional groups, and precipitation within nanotube cavities (***Figure (IV.6)***) [25].

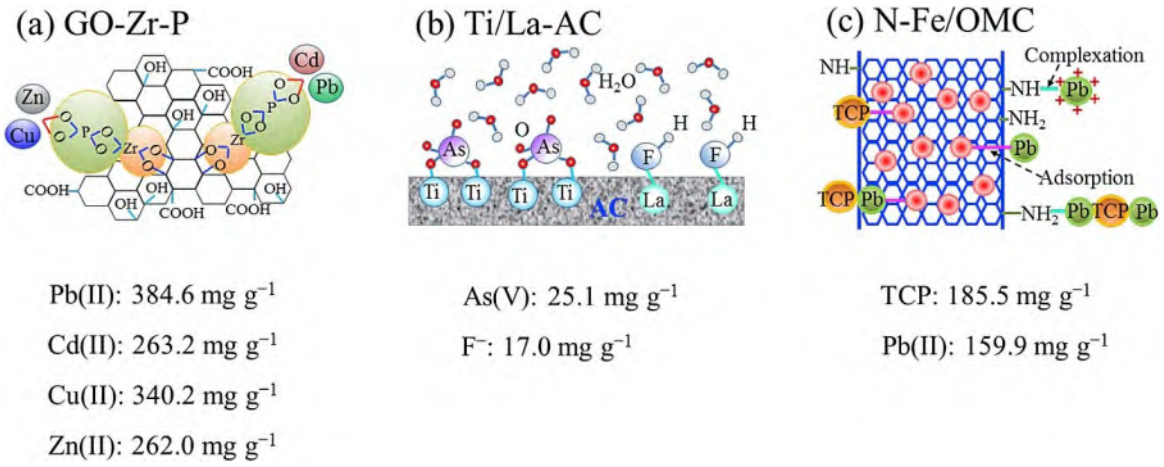

Figure (IV.6): Schematic representation of the adsorption mechanisms of heavy metal ions on functionalized carbon nanotube and graphene-based nanomaterials, highlighting the roles of surface functional groups (–COOH, –OH, $–NH_2$), electrostatic interactions, and surface complexation [24].

Ihsanullah *et al.* conducted a critical review of CNT-based adsorbents for heavy metal removal and identified surface oxidation, amine grafting, and magnetic functionalisation as the three most productive modification strategies, collectively yielding adsorption capacities that are typically 2–5 fold higher than those of bare CNTs across a range of target metals including Hg^{2+}, Pb^{2+}, Cd^{2+}, and Cr(VI) [26]. The authors also emphasised that competing ionic species (Ca^{2+}, Mg^{2+}, SO_4^{2-}) and natural organic matter substantially reduce uptake in real water matrices, underscoring the necessity of pilot-scale validation studies.

Graphene and Graphene Oxide. Graphene is a two-dimensional monolayer of carbon atoms arranged in a hexagonal lattice, possessing a theoretical specific surface area of ~2630 $m^2\ g^{-1}$, far exceeding that of conventional activated carbons and CNTs [27]. In practice, restacking of graphene sheets via van der Waals interactions substantially reduces the accessible surface area, prompting the use of GO as the adsorbent of choice. GO, synthesised by chemical oxidation of graphite (typically via the modified Hummers method), presents an abundant array of epoxide, hydroxyl, and carboxyl groups on its basal plane and edges, rendering it strongly hydrophilic and negatively charged in water [28].

These oxygen functionalities act as chelation sites for heavy metal cations. Sitko *et al.* systematically investigated the adsorptive properties of GO toward Cu(II), Zn(II), Cd(II), and Pb(II). Maximum adsorption capacities at pH = 5 were reported as 294, 345, 530, and 1119 mg g^{-1}, respectively, following the affinity order Pb(II) > Cd(II) > Zn(II) > Cu(II), consistent with differences in ionic radius and the stability of surface complexes [28]. The pH dependence of adsorption for each metal, with optimal ranges of 3–7 for Cu(II), 5–8 for Zn(II), 4–8 for Cd(II), and 3–7 for Pb(II), is depicted in ***Figure (IV.7)***, reproduced from that same study. Adsorption isotherms and kinetic analyses confirmed monolayer chemisorption as the dominant mechanism, well-described by the Langmuir model and pseudo-second-order kinetics [28].

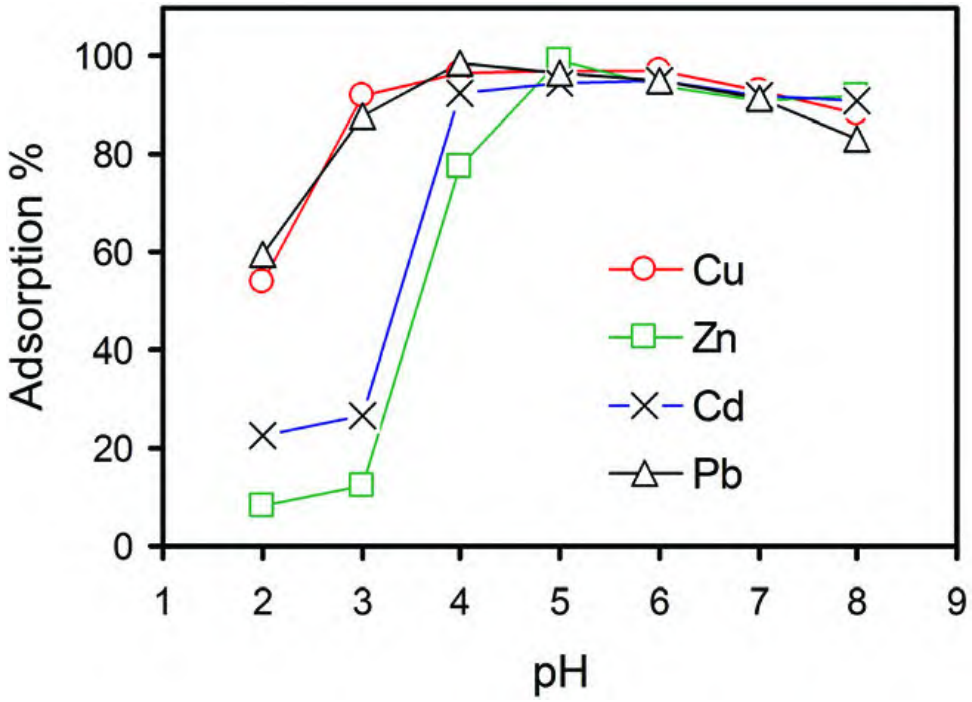

Figure (IV.7): Effect of pH on the adsorption of Cu(II), Zn(II), Cd(II), and Pb(II) ions onto graphene oxide (GO) nanosheets prepared by the modified Hummers method, demonstrating optimal pH ranges for each divalent metal ion [28].

Zhao *et al.* synthesised few-layered GO nanosheets by the modified Hummers method and demonstrated their superior performance as sorbents for Cd(II) and Co(II) in water, reporting maximum adsorption capacities of 106.3 and 68.2 mg g^{-1}, respectively, while confirming that adsorption was strongly influenced by pH and that the presence of humic acid suppressed metal uptake through competitive complexation [29]. Reduced graphene oxide (rGO)–Fe_3O_4 composites, synthesised by one-pot co-precipitation or hydrothermal routes, combine the large surface area and oxygen-rich chemistry of rGO with the magnetic recoverability of Fe_3O_4, yielding an adsorbent architecture that is both highly efficient and practically separable [30].

Activated Carbon Nanocomposites. Activated carbon (AC) has historically been the gold standard among adsorbents for water treatment, owing to its well-developed pore network (BET surface areas typically 500–2000 m^2 g^{-1}), chemical inertness, and low cost when derived from abundant precursors such as agricultural biomass [31]. The emergence of nanotechnology has given rise to a new generation of activated carbon nanocomposites (ACNCs) in which AC matrices are co-synthesised or impregnated with nanoparticles, including ZnO, TiO_2, Fe_3O_4, and

MnO_2, to combine the adsorptive capacity of the carbon matrix with the enhanced surface reactivity and specific functionalities of the embedded nanoparticles [32]. This synergistic design mitigates the tendency of nanoparticles to agglomerate by anchoring them within the porous AC scaffold, thereby preserving their high surface area and reactivity.

A critical consideration across all carbon-based nanomaterial adsorbents is the influence of competing ions in real wastewater matrices. The presence of alkaline earth metal cations (Ca^{2+}, Mg^{2+}), natural organic matter (NOM), and anions such as phosphate and sulfate can significantly reduce heavy metal uptake by competing for available binding sites or by forming complexes with target ions [26]. Functionalisation strategies and composite design must therefore account for the complexity of authentic water chemistry. Batch isotherm studies conducted in synthetic solutions frequently overestimate real-world performance, underlining the imperative for pilot-scale and field-validation studies [24].

IV.3. Nanocatalysts and Photocatalysts

Alongside adsorption, catalytic degradation processes represent a second major pillar of nanomaterial-based environmental remediation. Unlike adsorption, which merely transfers pollutants from the aqueous phase to a solid surface, catalytic and photocatalytic processes achieve the chemical transformation, and, in optimal cases, the complete mineralisation, of contaminants into benign end products such as CO_2, H_2O, and inorganic salts. This distinction is of profound practical importance: it eliminates the secondary waste disposal burden associated with spent adsorbents and permits the treatment of recalcitrant organic pollutants that resist biological degradation [33]. The convergence of nanotechnology and catalysis has yielded a new generation of nanocatalysts, materials in which the exceptionally high surface-area-to-volume ratio, quantum confinement effects, and tunable surface chemistry collectively deliver catalytic performance that far surpasses that of their bulk counterparts [34].

The field encompasses two broad mechanistic families. The first, semiconductor photocatalysis, exploits the absorption of photons to generate reactive charge carriers, electron–hole pairs, at the surface of metal oxide semiconductors such as TiO_2 and ZnO, which then drive oxidative and reductive reactions that decompose organic pollutants [34]. The second family, heterogeneous Fenton and Fenton-like catalysis, centres on the activation of hydrogen peroxide (H_2O_2) by solid iron-containing catalysts, most notably magnetite (Fe_3O_4) nanoparticles, to

produce hydroxyl radicals (•OH) in a controlled, recyclable process [35]. Section IV.3 reviews both families in detail, examining the fundamental principles, material design strategies, and documented performance of the principal nanocatalyst classes.

IV.3.1. TiO_2, ZnO, and Other Metal Oxide Photocatalysts

Semiconductor photocatalysis is one of the most extensively studied advanced oxidation processes (AOPs) for environmental remediation, with titanium dioxide (TiO_2) and zinc oxide (ZnO) occupying a pre-eminent position owing to their chemical stability, non-toxicity, low cost, and well-matched electronic structure for generating reactive oxygen species (ROS) under irradiation [34]. The fundamental mechanism of photocatalysis was articulated in a landmark review by Schneider *et al.*, who described a sequence initiated by the absorption of a photon (hν) with energy equal to or exceeding the semiconductor band gap (E_g), promoting an electron (e^-) from the valence band (VB) to the conduction band (CB) and simultaneously generating a positive hole (h^+) in the VB, as depicted in **Figure (IV.8)** [34]. These charge carriers migrate to the semiconductor surface where they initiate redox reactions: h^+ oxidises adsorbed water or hydroxyl groups to produce hydroxyl radicals (•OH), while e^- reduces dissolved oxygen to superoxide radical anions ($•O_2^-$), both of which are powerful oxidising agents capable of mineralising a broad spectrum of organic pollutants [34].

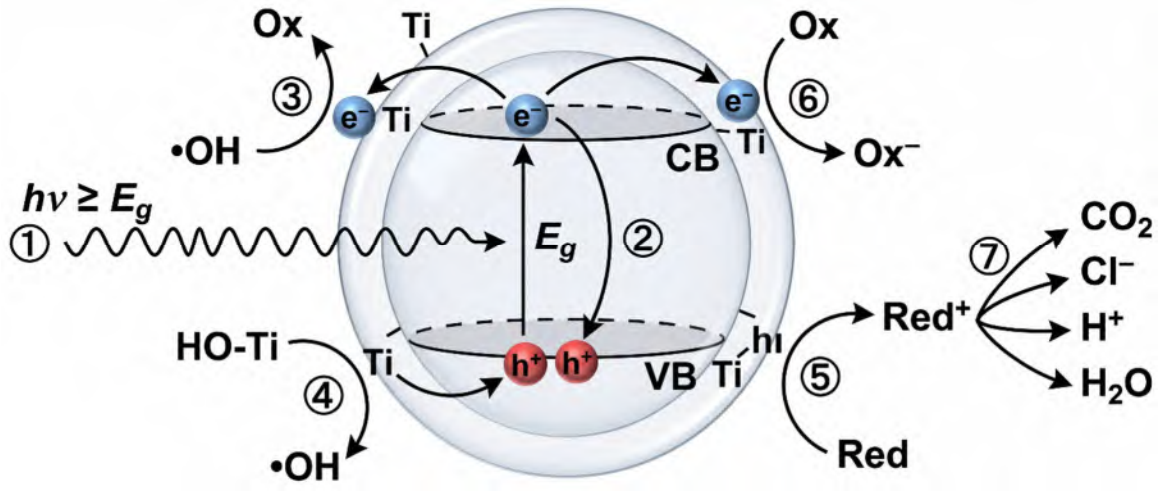

Figure (IV.8): Schematic representation of the fundamental mechanism of semiconductor photocatalysis, illustrating band-gap excitation, electron–hole pair generation, charge carrier migration to the particle surface, and the production of reactive oxygen species (•OH, $•O_2^-$) responsible for organic pollutant degradation [34].

TiO_2 in its anatase polymorph has a band gap of approximately 3.2 eV, corresponding to an absorption edge near 387 nm, within the UV region, which represents less than 5% of the incident solar spectrum. This spectral restriction constitutes the principal limitation of pristine TiO_2 photocatalysis and has stimulated extensive research into strategies for extending its light-harvesting capability toward the visible range [36]. The three most productive modification strategies identified in the literature are: (i) doping with non-metal anions (N, C, S), which introduces intra-gap localised states that extend the absorption edge toward 550 nm; (ii) metal ion implantation (Fe^{3+}, Cr^{3+}, V^{5+}), which can narrow the effective band gap through the formation of new electronic energy levels; and (iii) the construction of semiconductor–semiconductor heterojunctions (e.g., TiO_2/ZnO, TiO_2/g-C_3N_4), which promote charge carrier separation by creating an internal electric field at the heterointerface [36].

ZnO shares several key attributes with TiO_2, including a similar band gap (~3.37 eV), high electron mobility (115–155 $cm^2\ V^{-1}\ s^{-1}$), and an abundance of surface hydroxyl groups that facilitate •OH generation. Several studies have demonstrated that ZnO exhibits equal or superior photocatalytic efficiency relative to TiO_2 under UV irradiation for the degradation of organic dyes and pharmaceutical compounds, attributable to its higher rate of electron–hole pair generation per unit photon flux [37]. However, ZnO is susceptible to photocorrosion under prolonged UV exposure, with the release of Zn^{2+} ions into the treated solution limiting its reusability and raising ecotoxicological concerns [37].

The degradation kinetics of organic pollutants in photocatalytic systems are almost universally described by the Langmuir–Hinshelwood (L–H) model, in which the rate of surface reaction is first-order in the surface concentration of adsorbed pollutant and in the surface hydroxyl radical concentration. Under dilute pollutant conditions, this simplifies to a pseudo-first-order expression with an apparent rate constant k_{app} (min^{-1}) that is proportional to the photocatalyst loading, incident light intensity, and dissolved oxygen concentration [34]. Competing anions such as carbonate, phosphate, and chloride, as well as natural organic matter, can act as •OH scavengers and substantially suppress k_{app} in authentic wastewater matrices, a factor that must be accounted for in engineering design [33].

Beyond TiO_2 and ZnO, a diverse range of metal oxide photocatalysts has been investigated, including bismuth vanadate ($BiVO_4$, $E_g \approx 2.4$ eV), tungsten trioxide (WO_3, $E_g \approx 2.6$

eV), hematite (α-Fe_2O_3, $E_g \approx 2.2$ eV), and cerium dioxide (CeO_2, $E_g \approx 3.0$ eV), all of which absorb visible light due to their narrower band gaps [34]. These narrow-band-gap photocatalysts are of particular interest for solar-driven treatment applications, though their frequent challenges include poor charge carrier mobility, rapid recombination, and limited oxidative potential relative to •OH [34].

IV.3.2. Magnetic Nanoparticles for Catalytic and Fenton-Like Processes

The classical Fenton reaction, the homogeneous oxidation of organic pollutants by hydrogen peroxide catalysed by dissolved Fe^{2+} ions in acidic media, has been extensively documented since the seminal work of Fenton in 1894. Although highly effective, this process is constrained to a narrow pH window (pH 2–4), generates significant quantities of ferric hydroxide sludge that requires downstream treatment, and incurs the continuous expense of iron salt replenishment [35]. Heterogeneous Fenton-like catalysis, in which the iron catalyst is immobilised on a solid support, most prominently magnetite (Fe_3O_4) nanoparticles, circumvents many of these limitations, offering operational stability over a wider pH range, facile magnetic recovery and recyclability, and the elimination of secondary sludge disposal [38].

The catalytic activity of Fe_3O_4 in Fenton-like processes derives from the coexistence of Fe^{2+} and Fe^{3+} ions on adjacent octahedral sites within its inverse spinel crystal structure. The surface Fe^{2+} species react with H_2O_2 to generate •OH radicals ($\equiv Fe^{2+} + H_2O_2 \rightarrow \equiv Fe^{3+} + \bullet OH + OH^-$), while $\equiv Fe^{3+}$ is subsequently regenerated by reaction with H_2O_2 or, in photo-Fenton systems, by photoreduction. Nidheesh reviewed the mechanistic landscape of heterogeneous Fenton catalysts comprehensively, reporting that the surface-mediated •OH generation rate is strongly dependent on Fe^{2+}/Fe^{3+} site density, surface area, H_2O_2 concentration, and solution pH, with optimal activity generally observed between pH 3 and 7 for Fe_3O_4-based systems, a substantially broader window than the classical Fenton process (**Figure (IV.9)**)[35].

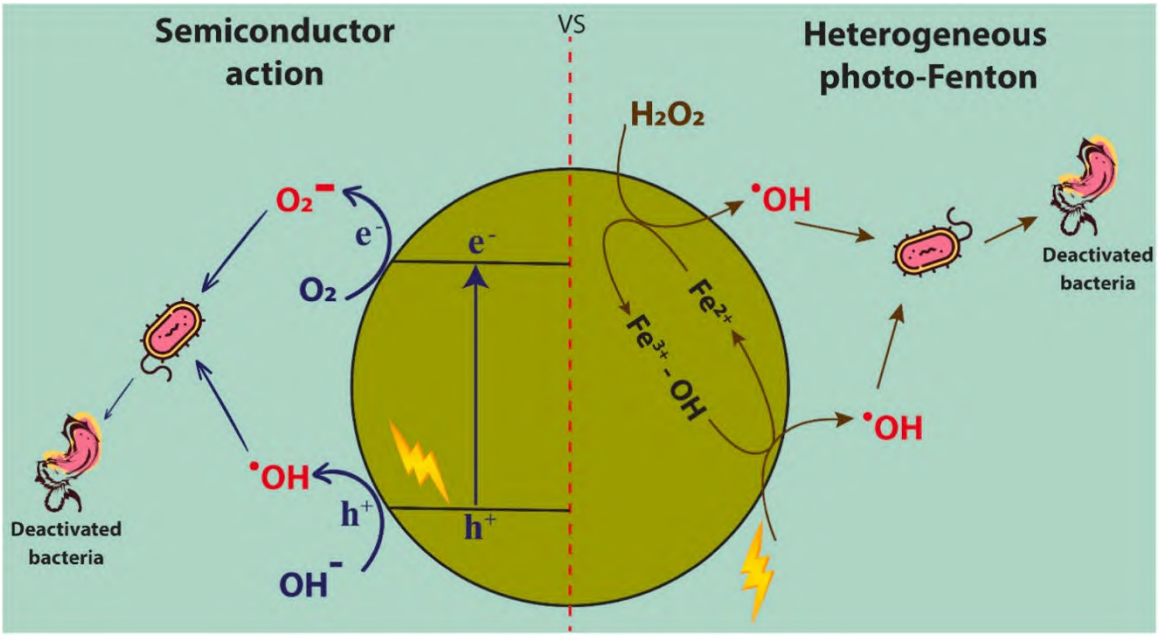

Figure (IV.9): Heterogeneous Fenton-like degradation mechanism using Fe_3O_4 nanoparticles with H_2O_2 [38].

The Fenton-like catalytic efficiency of Fe_3O_4 nanoparticles is markedly enhanced by composite design. Yang *et al.* demonstrated that Fe_3O_4@SiO_2 core–shell nanoparticles exhibit superior Fenton-like activity relative to bare Fe_3O_4 cores at neutral pH, attributing the improvement to the SiO_2 shell's role in preventing nanoparticle agglomeration and iron leaching while providing a hydrophilic surface that concentrates H_2O_2 near the catalytic iron sites [39]. Analogously, Fe_3O_4/reduced graphene oxide (rGO) composites achieve an amplified •OH yield because the high electrical conductivity of rGO accelerates the intramolecular $Fe^{3+} \rightarrow Fe^{2+}$ reduction, effectively shortening the catalytic cycle [30].

The photo-Fenton process, the coupling of UV or visible light irradiation with Fe^{2+}/H_2O_2 chemistry, substantially accelerates the rate of organic pollutant degradation relative to either photocatalysis or Fenton oxidation alone. Under irradiation, Fe^{3+} is photoreduced to Fe^{2+} with the concomitant generation of an additional •OH radical per photon absorbed ($Fe^{3+} + H_2O + h\nu \rightarrow Fe^{2+} + \bullet OH + H^+$), closing the catalytic cycle and eliminating the pH and iron-sludge limitations of classical Fenton chemistry. Thomas *et al.* reviewed recent advances in heterogeneous Fenton catalysts, noting that ferrite-based composites (MFe_2O_4, M = Cu, Mn, Zn, Co) offer enhanced visible-light photo-Fenton activity due to their narrower band gaps (1.3–2.0 eV) and superior charge carrier separation compared to pure Fe_3O_4 [38]. The superparamagnetic behaviour of

Fe_3O_4 and ferrite nanoparticles enables their rapid and complete recovery from treated water by application of an external magnet, with demonstrated recyclability over five or more consecutive treatment cycles without significant loss of catalytic activity [39].

IV.3.3. Heterogeneous Catalysis for Degradation of Organic Pollutants

The degradation of persistent organic pollutants (POPs), encompassing synthetic dyes, pharmaceuticals and personal care products (PPCPs), endocrine-disrupting compounds (EDCs), and pesticides, by heterogeneous nanocatalysts represents one of the most active frontiers in environmental chemistry. These compounds are characterised by their structural complexity, resistance to biodegradation, and tendency to accumulate in aquatic ecosystems, where even trace concentrations (ng L^{-1} to µg L^{-1}) can exert adverse ecological and human health effects [33]. The critical review by Miklos *et al.* evaluated the electrical energy per order (EE/O) of diverse AOPs for micropollutant removal, concluding that UV/H_2O_2, O_3/H_2O_2, and heterogeneous photocatalysis offer the most energy-efficient pathways for large-scale implementation, as represented in **Figure (IV.10)** [33].

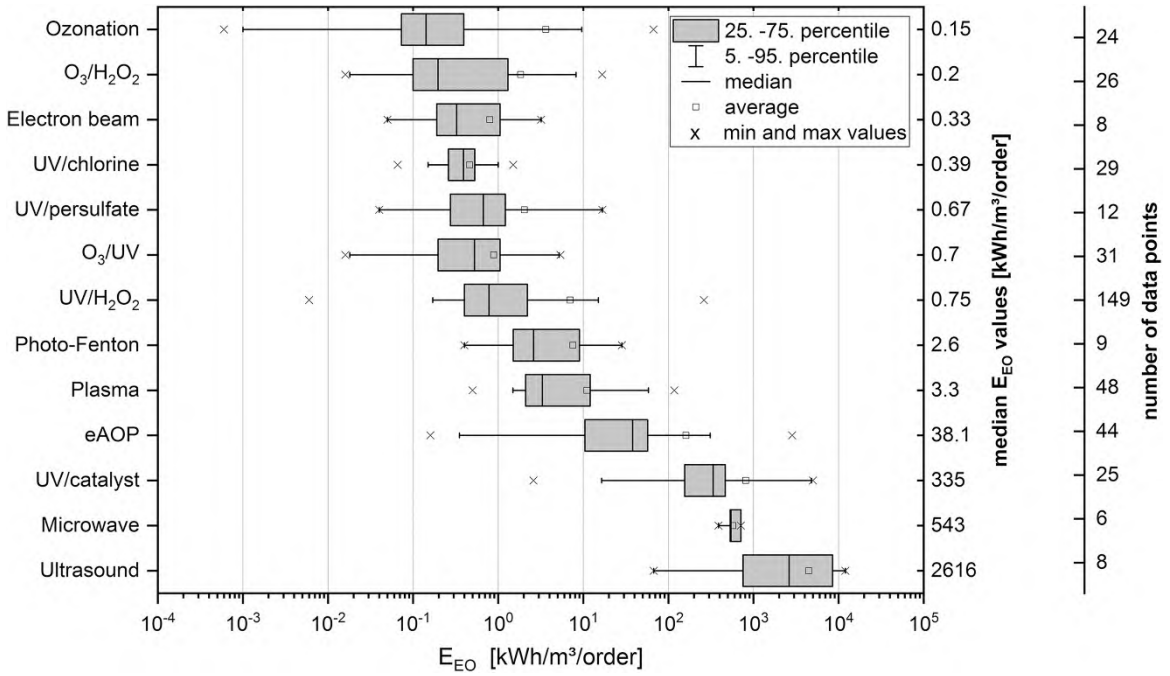

Figure (IV.10): Comparative electrical energy per order (EE/O) of advanced oxidation processes (AOPs) [33].

Synthetic azo dyes constitute one of the most widely studied model pollutant classes in heterogeneous catalysis research, owing to their chromophoric azo (–N=N–) linkage, which can be cleaved by •OH attack, and their commercial relevance to the textile industry. Methylene blue (MB), Rhodamine B (RhB), methyl orange (MO), and Congo red (CR) are particularly favoured as model substrates because of their strong UV–visible absorption, which permits simple spectrophotometric monitoring of degradation kinetics [40]. TiO_2-mediated photocatalytic degradation of MB follows L–H kinetics with k_{app} values typically in the range of 0.01–0.05 min^{-1} under UV irradiation (365 nm, irradiance 1 mW cm^{-2}), accelerating to 0.10–0.30 min^{-1} when noble metal co-catalysts (Pt, Au) are deposited on the TiO_2 surface to create Schottky junctions that suppress charge carrier recombination [34].

Pharmaceutical compounds and EDCs present a more stringent challenge than synthetic dyes owing to their structural heterogeneity and lower initial concentrations. The degradation of carbamazepine, diclofenac, bisphenol A (BPA), 17α-ethinylestradiol (EE2), and tetracycline by TiO_2-based photocatalysis has been extensively documented, with complete mineralisation (assessed by total organic carbon, TOC reduction) typically requiring irradiation times of 60–180 min under optimised conditions [33]. Importantly, photocatalytic treatment does not necessarily produce non-toxic effluents at intermediate stages: the formation of hydroxylated, nitrated, or oxidised transformation products that may themselves be bioactive or even more toxic than the parent compound has been identified as a critical concern, necessitating complementary toxicity assessment (e.g., Daphnia magna or Vibrio fischeri bioassays) alongside chemical analysis [33].

The integration of heterogeneous catalysis with other treatment processes has attracted considerable interest as a strategy for enhancing overall mineralisation efficiency and process economics. Sequential systems combining biological treatment with photocatalytic or Fenton-like polishing, so-called bio-AOP hybrid systems, exploit the biodegradability of photocatalytic transformation products as a carbon source for downstream biological reactors, thereby reducing the photon and oxidant dose required for complete mineralisation [33]. Immobilised photocatalyst systems, in which TiO_2 or Fe_3O_4 nanoparticles are deposited on glass beads, ceramic membranes, or polymer fibres, eliminate the need for post-treatment catalyst separation while maintaining reactive surface areas sufficient for acceptable degradation kinetics [41]. Pilot-scale and full-scale implementation of nanocatalytic water treatment systems remains, however,

limited by the challenges of photon delivery at scale, the cost of H_2O_2 dosing, and the regulatory frameworks governing the deliberate introduction of engineered nanomaterials into treated water supplies [33].

Looking forward, the coupling of magnetic Fe_3O_4 nanoparticles with visible-light-active semiconductor shells (Fe_3O_4@$BiVO_4$, Fe_3O_4@g-C_3N_4) represents a promising design paradigm for solar-driven Fenton-like catalysis with integrated magnetic recovery, an architecture that addresses, in a single material, the major practical challenges of photon utilisation efficiency, pH tolerance, catalyst recyclability, and scalability. The continued development of such multifunctional nanocatalysts, guided by mechanistic understanding and real wastewater validation, will be essential to translating the laboratory-scale achievements reviewed in this section into operational water treatment technologies [38].

IV.4. Green-Synthesized and Bio-Inspired Nanoparticles for Wastewater Treatment

The increasing global awareness of environmental sustainability has catalysed a significant shift in the way nanoparticles (NPs) are produced and applied in water remediation. Conventional physicochemical synthesis routes, while effective in generating well-defined nanomaterials, typically rely on hazardous reducing agents, organic solvents, and energy-intensive conditions. These limitations have prompted considerable scientific interest in green synthesis, a broad set of methodologies that exploit biological resources, such as plant extracts, microbial metabolites, and biopolymers, as both reducing and capping agents during NP formation [42]. The resulting bio-inspired nanomaterials not only offer a lower environmental footprint but frequently exhibit enhanced biocompatibility and surface functionalisation, making them particularly attractive for wastewater treatment applications.

In essence, the green synthesis route capitalises on the rich phytochemistry of plant biomass. Phenolic compounds, flavonoids, terpenes, alkaloids, and reducing sugars present in leaf, stem, fruit, and root extracts act simultaneously as electron donors and stabilising ligands during metal ion reduction [43]. The resultant NPs typically exhibit a narrow size distribution, good colloidal stability, and chemically active surfaces, attributes directly traceable to the organic corona retained from the synthesis medium. These surface-adsorbed biomolecules confer chelating functionality that is often directly exploitable for heavy metal uptake, obviating the need for post-synthesis chemical modification.

IV.4.1. Plant-Mediated Synthesis of Metal and Metal Oxide Nanoparticles

Plant-extract-mediated synthesis constitutes the most widely investigated green route, primarily because plant biomass is inexpensive, renewably available, and rich in phytochemicals, phenolics, flavonoids, tannins, terpenoids, and organic acids, that simultaneously perform the roles of metal-ion reductant and particle-capping agent. As illustrated in **Figure (IV.11)** [44], the process proceeds through a well-defined sequence: (i) preparation of the aqueous plant extract from *Mentha pulegium L.* leaves powder; (ii) admixture with metal precursor salts ($FeCl_3$, $CaCl_2$, $CuCl_2$, and $ZnCl_2$, 0.1 M); (iii) stirring (150 rpm, 1 h at 85 °C), centrifugation/washing (3000 rpm, 5 min, 3 times), oven drying (100 °C, 12 h), and calcination (500 °C, 3 h) to obtain the stabilized Ca/α-Fe_2O_3/ZnO/CuO nanocomposite; and (iv) application of the resulting nanocomposite for the adsorption of heavy metals from petroleum-contaminated sludge through external diffusion, internal diffusion, surface diffusion, and fixation at active adsorption sites [42, 45].

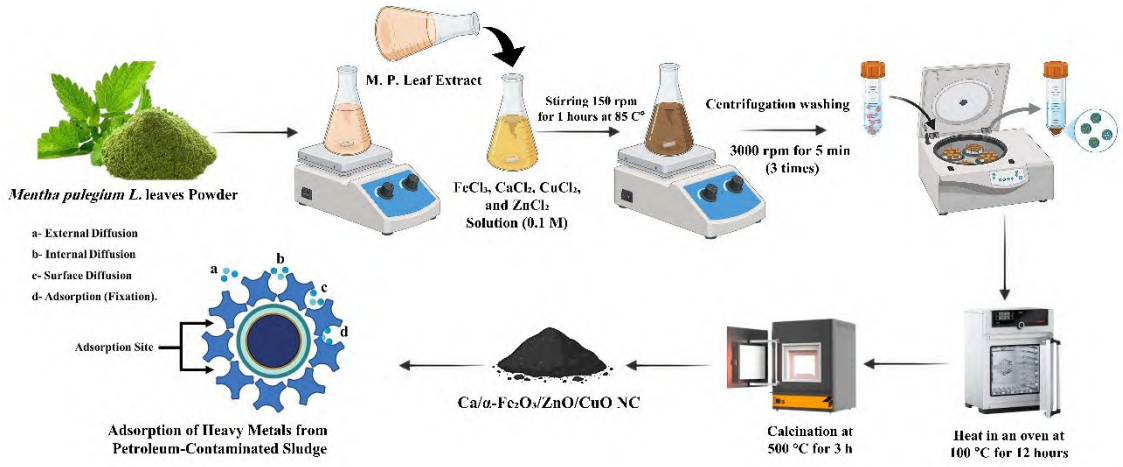

Figure (IV.11): Schematic representation of the plant-extract-mediated green synthesis of Ca/α-Fe_2O_3/ZnO/CuO nanocomposite using *Mentha pulegium* L. leaf extract and its subsequent application in the removal of heavy metals from petroleum-contaminated sludge [44].

Wang et al.[45] provided an early and compelling demonstration of this approach, preparing zerovalent iron nanoparticles (nZVI-G) from eucalyptus leaf extract and applying them to the remediation of eutrophic wastewater. The polyphenol-rich extract reduced Fe^{3+} ions at ambient temperature, yielding particles of 20–80 nm with a specific surface area of 35 $m^2\ g^{-1}$, sufficient to achieve near-complete removal of phosphate and nitrate within 30 minutes of contact. Complementing this work, Machado et al.[46] systematically screened eleven different tree-leaf

extracts as reducing media for nZVI synthesis and demonstrated a strong positive correlation between total polyphenol content and the resulting BET surface area of the particles, providing a rational basis for selecting optimal botanical feedstocks.

Iron oxide NPs merit particular emphasis because their inherent ferrimagnetic character permits rapid, low-energy post-treatment recovery by external magnetic field, a decisive practical advantage over non-magnetic nano-adsorbents. Gan et al.[47] reported that magnetically recoverable Fe_3O_4 NPs synthesised through a biogenic route achieved removal efficiencies exceeding 90 % for Pb^{2+}, Cd^{2+}, and Cr^{3+} from a synthetic multi-metal feed, with the adsorbent capacity maintained over five consecutive regeneration cycles. Khatami et al.[43] extended the plant-mediated approach to ZnO, using *Stevia rebaudiana* extract to produce unusual rectangular-morphology particles with a Langmuir maximum capacity of 142.8 mg g^{-1} for methylene blue, performance attributable to the high density of surface hydroxyl groups introduced by the biogenic process.

IV.4.2. Microbial and Fungal Biosynthesis

Beyond plant extracts, microorganisms, including bacteria, fungi, and algae, offer a fundamentally distinct biosynthesis paradigm in which living cells or their cell-free filtrates perform the reduction and assembly of nanostructures through enzymatic and metabolic pathways. Fungal biosynthesis is of particular industrial relevance because the high secretion of extracellular enzymes and secondary metabolites by species such as *Aspergillus niger*, *Fusarium oxysporum*, and *Trichoderma asperellum* enables scale-up in conventional bioreactors without the harvesting and pre-processing steps required for plant material. Khandel and Shahi [48] provided a comprehensive overview of mycogenic NP synthesis, highlighting how the surface of fungal-derived Ag and ZnO NPs retains an extracellular protein corona that imparts colloidal stability and selective affinity towards cationic heavy metals, a feature exploited in the treatment of mixed-metal effluents from the electroplating and mining sectors.

Bacterial synthesis routes, while offering precise metabolic controllability through genetic engineering, face inherent challenges related to culture maintenance and the potential presence of endotoxins in the product. Nevertheless, the biosynthesis of magnetite (Fe_3O_4) by dissimilatory iron-reducing bacteria such as *Geobacter metallireducens* under anaerobic conditions has

attracted attention as a route towards highly crystalline, superparamagnetic NPs for magnetically assisted separation in wastewater treatment. [49] The synthesis occurs at ambient temperature without chemical oxidising agents, aligning with green chemistry principles articulated by Anastas and Warner.

Algal-mediated synthesis represents a third biogenic route of growing interest, particularly because macroalgae are available in large biomass quantities and their exopolysaccharides provide effective NP capping. Silver NPs produced using brown algae extracts have demonstrated competitive adsorption capacities for Pb^{2+} and Hg^{2+} under circumneutral pH conditions, with the carboxylate and sulphonate groups of the algal polysaccharides acting as primary binding sites [49]. Irrespective of the biological platform employed, the mechanistic understanding of contaminant removal by bio-inspired NPs converges on the same physicochemical principles that govern conventional nano-adsorbents: electrostatic attraction, surface complexation, ion exchange, and co-precipitation, as depicted schematically in **Figure (IV.11)**. The advantage of the bio-inspired approach lies in the added value of the organic corona, which can amplify chelation and introduce selectivity for specific metal species.

IV.5. Fixed-Bed, Membrane, and Hybrid Systems Incorporating Nanoparticles

While batch-mode adsorption experiments provide essential thermodynamic and kinetic information, forming the basis of isotherm and rate constant determinations, they offer limited guidance for real-world implementation. Industrial wastewater treatment demands continuous operation, predictable throughput, and straightforward regeneration, requirements that are most naturally met by fixed-bed column systems, pressure-driven membrane processes, and, increasingly, hybrid configurations that couple both principles. [50] This section critically examines how nanoparticles are integrated into each of these operational configurations, with particular attention to the engineering parameters that govern performance at the pilot and industrial scale.

IV.5.1. Fixed-Bed Adsorption Columns

The fixed-bed column is the workhorse of adsorption-based water treatment. In this configuration, contaminated feed is passed continuously through a packed bed of adsorbent

material until the effluent concentration reaches a pre-defined breakthrough threshold, commonly taken as 5–10 % of the inlet concentration (C/C_0 = 0.05–0.10). The resulting breakthrough curve, a sigmoidal plot of C/C_0 against cumulative volume or time, encapsulates all the performance-critical parameters of the system: the length of the mass transfer zone, the usable bed capacity, the saturation time, and the pressure drop across the bed [50].

When nanoparticles are deployed as the adsorbent phase, two competing considerations arise immediately. On the one hand, the sub-micron particle size maximises accessible surface area and eliminates intraparticle diffusion limitations that plague granular activated carbon and zeolite beds. On the other hand, the same fine particle size generates prohibitive hydraulic resistance when packed directly into a column, frequently resulting in unacceptably high pressure drops and preferential channelling [51]. The engineering community has responded to this challenge through several strategies: (i) immobilising NPs onto granular supports such as sand, alumina, and silica foam; (ii) consolidating NPs into hierarchically porous monoliths or pellets using polymer binders; and (iii) growing NPs in situ on the surface of conventional adsorbent grains through controlled precipitation [50].

The breakthrough behaviour of nano-adsorbent columns is most commonly interpreted using the Thomas model and the Yoon–Nelson model, both of which yield the maximum volumetric adsorption capacity (q_0) and the rate constant (k_{Th}) from least-squares regression to the experimental breakthrough curve. The Thomas model, developed under the assumption of Langmuirian equilibrium and second-order reversible kinetics, is well-suited to systems in which axial dispersion is negligible and the driving force for mass transfer is predominantly film diffusion .

Column studies incorporating multi-metal binding biosorbent (MMBB) have demonstrated Thomas q_0 values of 38–108 mg g^{-1} for Cd^{2+}, Cu^{2+}, Pb^{2+} and Zn^{2+} at pH 5.5, with breakthrough occurring between 50–170 min and exhaustion at ~170–420 min under a flow rate of 10 mL min^{-1} [52]. As shown in **Figure (IV.12)**, these results compare favourably with those of conventional granular activated carbon operating under identical hydraulic conditions. Critically, the biosorbent can be regenerated by acid elution, with capacity retention exceeding 90 % over three successive cycles, a performance benchmark that supports economic viability at scale.

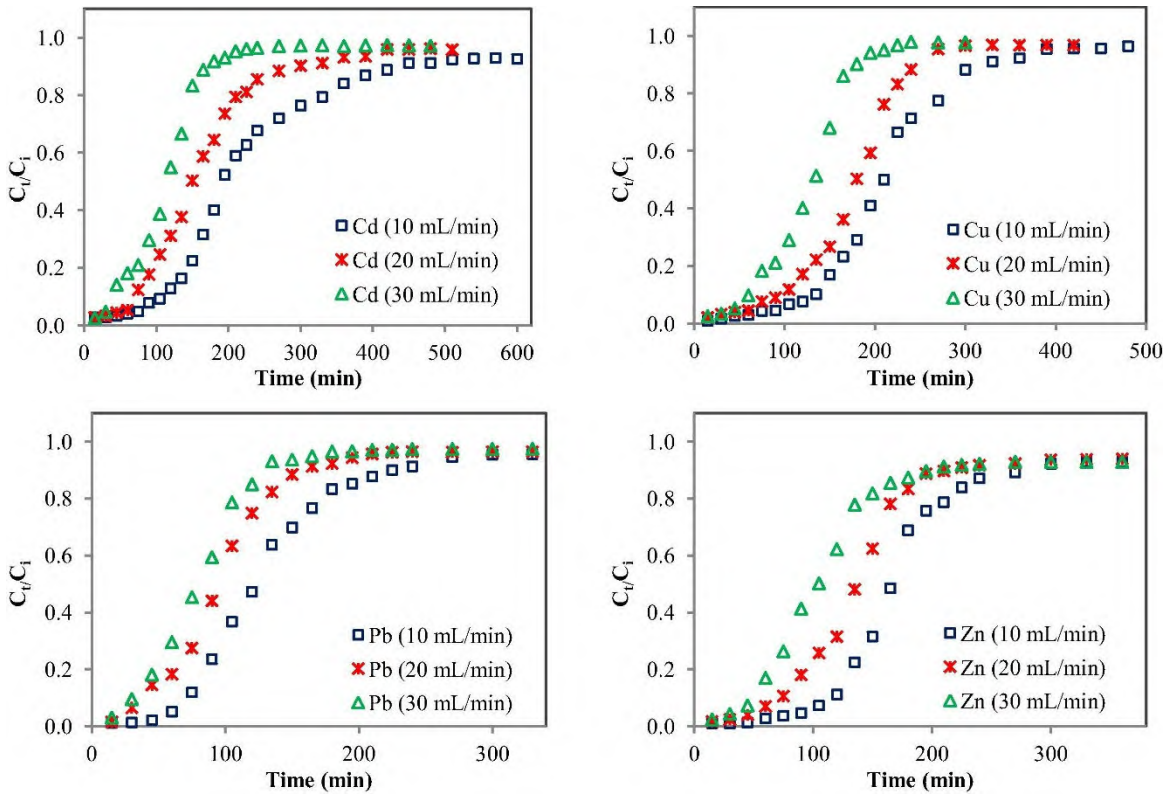

Figure (IV.12): Typical breakthrough curve (C/C_0 vs. time) for heavy metal removal in a nano-adsorbent fixed-bed column, with Thomas model fit (experimental data shown as symbols; model predictions as solid lines) [52].

IV.5.2. Nanoparticle-Enhanced Membranes

Pressure-driven membrane processes, microfiltration (MF), ultrafiltration (UF), nanofiltration (NF), and reverse osmosis (RO), represent a complementary and increasingly dominant technology for the removal of dissolved contaminants from wastewater. Their integration with engineered nanomaterials has given rise to a new class of mixed-matrix membranes (MMMs) and thin-film nanocomposite (TFN) membranes in which NPs are embedded within or grafted onto the membrane polymer matrix to improve flux, antifouling resistance, and ion rejection simultaneously [53].

Nanofiltration membranes are particularly relevant in the context of heavy metal removal because their pore size range (0.5–2 nm) and molecular weight cut-off (300–500 Da) allow them to reject divalent metal cations while maintaining substantial water flux at operating pressures of 5–20 bar [54]. The incorporation of TiO_2 NPs into polyethersulfone (PES) NF membranes has been shown

to increase pure water flux by 30–40 % relative to unmodified PES, attributable to the hydrophilicity imparted by the TiO_2 surface hydroxyl groups [54]. Concurrently, TiO_2 inclusion reduces biofouling under UV irradiation through photocatalytic generation of reactive oxygen species that inactivate attached microorganisms, a self-cleaning functionality absent in conventional polymeric membranes [55].

Graphene oxide (GO) nanosheets have emerged as a particularly versatile membrane filler. When incorporated as a coating layer on polyamide (PA) thin-film composite membranes, GO enhances rejection of Co^{2+} to 97 % while improving anti-fouling performance, as evidenced by a flux recovery ratio exceeding 92 % following bovine serum albumin fouling tests [53]. The mechanism is two-fold: the negative surface charge of GO under near-neutral pH conditions repels co-charged divalent anions and impedes the adsorption of charged foulant macromolecules, while the sub-nanometre interlayer spacing of stacked GO lamellae creates tortuous transport pathways that size-exclude hydrated metal cations. **As shown in Figure (IV.13)** [56].

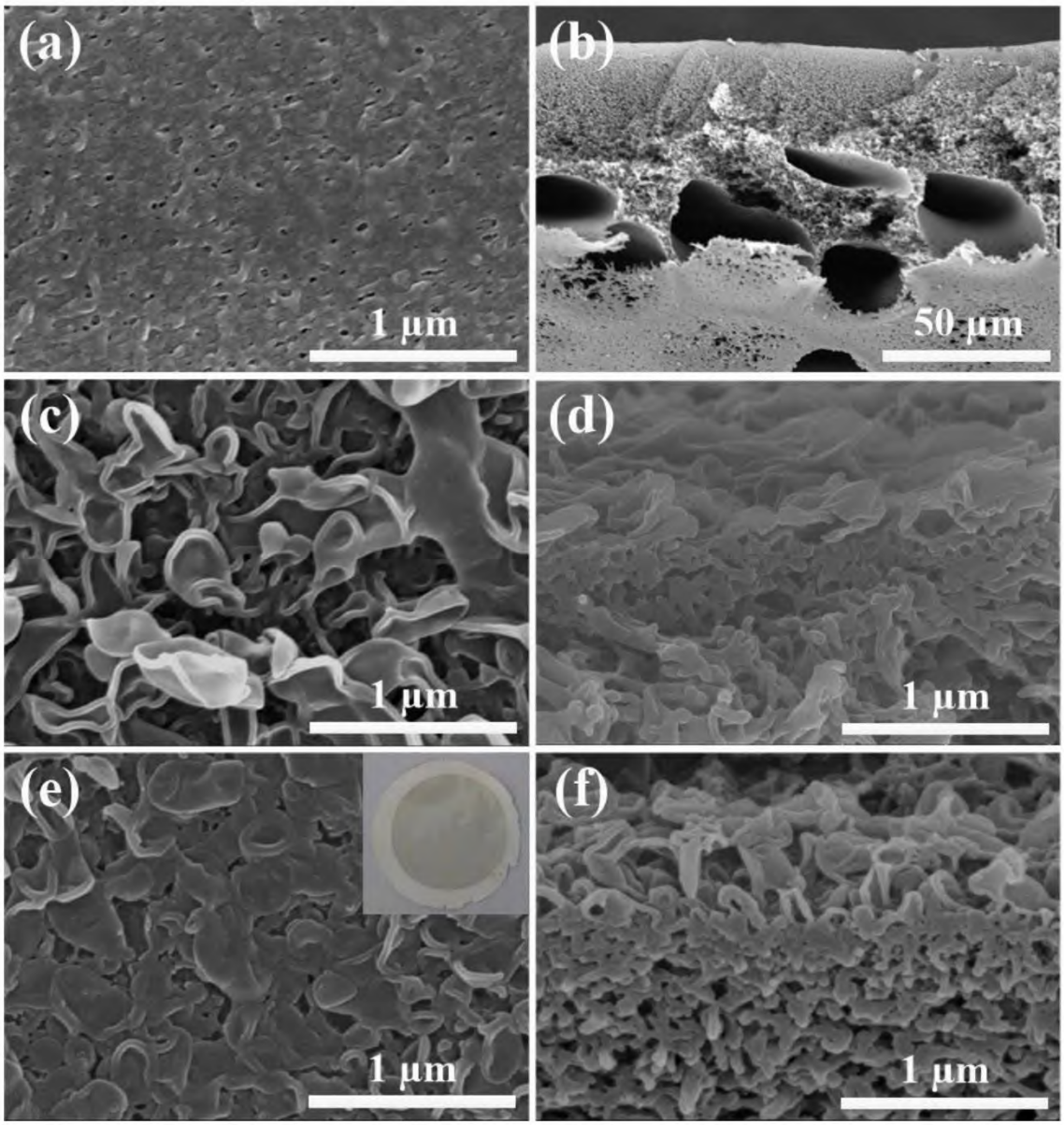

Figure (IV.13). Cross-sectional SEM and schematic of thin-film nanocomposite (TFN) membrane with embedded TiO_2 or GO nanoparticles, showing layered structure and ion rejection mechanism [56].

IV.5.3. Hybrid Adsorption–Membrane Systems

A particularly promising development in nano-enabled water treatment is the emergence of hybrid systems that sequentially or simultaneously combine adsorption and membrane separation. In a typical pre-adsorption/NF hybrid configuration, the contaminated feed first contacts a nano-

adsorbent slurry, often in a rapid-mix tank, before being passed through a UF or NF membrane that retains the NPs and the metals sorbed to them [57]. This two-stage design offers several synergistic advantages: the high surface area and rapid kinetics of NPs in suspension handle the initial contaminant loading, while the membrane provides a reliable separation barrier and the driving force for NP recovery.

Santhosh et al. [57] reviewed hybrid nano-adsorbent/membrane configurations and demonstrated that coupling magnetic Fe_3O_4–GO nanocomposites with a low-pressure UF membrane achieved simultaneous removal of Pb^{2+} (98.3 %), Cd^{2+} (97.1 %), and As^{3+} (95.6 %) from a synthetic multi-metal feed, with the adsorbent phase recoverable and regenerated magnetically for reuse, and the permeate complying with WHO drinking water guidelines. The economic feasibility of such systems remains an active area of inquiry: capital costs are dominated by the membrane module, while operating costs depend on regenerant chemical consumption and the longevity of the adsorbent phase over repeated cycles.

Another variant, the membrane adsorber, embeds nano-adsorbent material directly into the membrane structure, eliminating the need for a separate contact stage. Functionalised carbon nanotube (CNT) membranes, for example, achieve simultaneous filtration and adsorption of heavy metals via π–cation interactions and surface complexation with their carboxylated or aminated outer walls [58]. While membrane adsorbers offer compactness and operational simplicity, their adsorption capacity per unit volume is inherently limited by the available internal surface area of the membrane, which typically constrains their application to polishing steps operating at low influent concentrations rather than high-load primary treatment.

IV.6. Challenges: Fouling, Recovery, Toxicity, and Regulatory Considerations

Notwithstanding the remarkable performance data accumulated in laboratory and pilot studies, the translation of nano-enabled wastewater treatment technologies from controlled research settings to robust, commercially viable processes faces a cluster of interconnected challenges. These span the technical domains of membrane fouling and adsorbent deactivation, the practical difficulties of NP recovery and end-of-life management, and the broader societal dimensions of nanotoxicology and regulatory governance. A candid assessment of these barriers is essential for identifying the research directions and engineering innovations most likely to unlock the full promise of nanotechnology in environmental remediation.

IV.6.1. Fouling and Adsorbent Deactivation

Fouling, the progressive loss of permeability or adsorption capacity due to the accumulation of foulant species on active surfaces, is arguably the most operationally significant challenge facing both nano-adsorbent and nano-enhanced membrane systems [59]. In membrane processes, fouling manifests as a decline in transmembrane flux over time and takes four principal forms: (i) reversible cake/gel layer fouling caused by the accumulation of particulate matter and colloids on the membrane surface; (ii) pore blocking by species whose hydrodynamic diameter approximates the membrane pore size; (iii) biofouling, driven by the formation of microbial biofilms; and (iv) scaling, resulting from the precipitation of sparingly soluble mineral salts as the concentrate-side activity product exceeds the solubility product [59].

The incorporation of hydrophilic NPs such as TiO_2 and SiO_2 into membrane polymers reduces organic fouling by lowering the contact angle and thereby the adhesion energy of hydrophobic macromolecular foulants, a strategy that has demonstrated promising results in pilot trials with municipal secondary effluent [60]. However, the long-term photocatalytic activity of TiO_2 within a polymer matrix is constrained by UV penetration depth and by the gradual burial of surface-active sites as NPs aggregate within the polymer phase. Biofouling, which is particularly problematic in low-pressure membrane applications, is more durably mitigated by silver NP inclusion, which exerts continuous oligodynamic toxicity against bacteria; however, this also raises questions about the ecotoxicological implications of silver release into the permeate stream.

For nano-adsorbent systems, deactivation occurs through competing mechanisms: the progressive occupation of active binding sites by co-existing anions (e.g., sulphate, carbonate) and natural organic matter (NOM) that competes with target metal cations; the attrition and loss of nano-adsorbent mass during repeated regeneration cycles; and the sintering or Ostwald ripening of NPs under the mildly elevated temperatures or pH excursions encountered during acidic regeneration [59]. These mechanisms collectively reduce the effective adsorption capacity over successive operational cycles and represent a major obstacle to demonstrating the 'cyclability' required for a convincing techno-economic case.

IV.6.2. Nanoparticle Recovery and Post-Treatment Management

One of the most persistent criticisms of dispersed nano-adsorbent systems is the difficulty, and in some configurations the practical impossibility, of achieving complete recovery of nanomaterials after treatment. The sub-micron size of NPs renders conventional gravity sedimentation or sand filtration ineffective as recovery strategies, necessitating either high-pressure filtration, centrifugation, magnetic separation, or flocculation-assisted settling [60]. Each of these methods introduces additional energy and chemical costs that must be factored into lifecycle assessments.

Magnetic NPs, Fe_3O_4 and its surface-functionalised derivatives, offer a particularly elegant solution to this recovery challenge. The application of an external low-gradient magnetic field can achieve >99 % particle capture from dilute aqueous dispersions within seconds to minutes, without the addition of reagents or the generation of secondary waste streams [60]. However, repeated magnetic capture-and-redispersion cycles may promote irreversible aggregation as the steric or electrostatic stabilisation of the NP surface deteriorates, progressively reducing accessible surface area and increasing the susceptibility of residual free NPs to escape into the treated effluent. As shown in **Figure (IV.14)**.

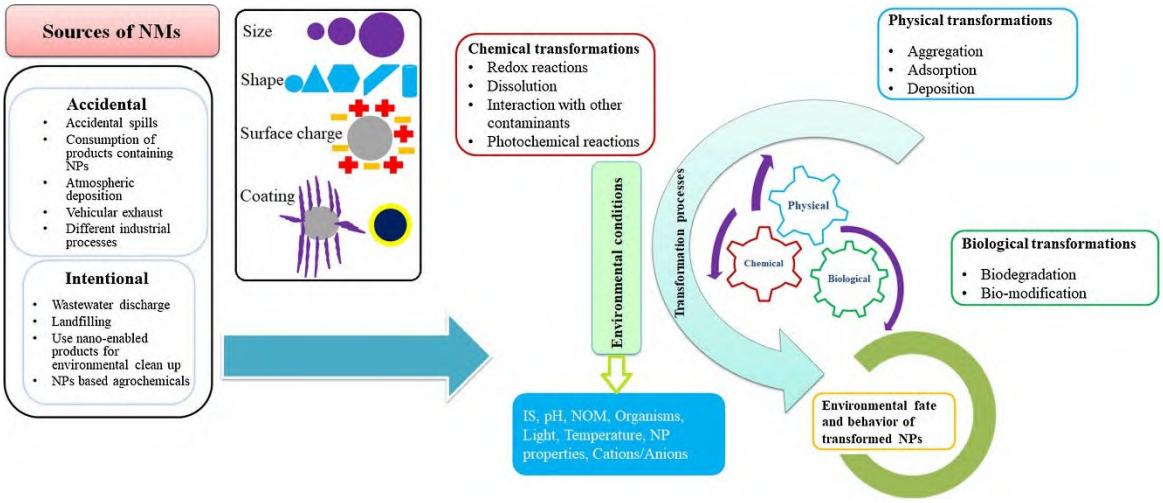

Figure (IV.14): Schematic representation of the full environmental life cycle of engineered nanoparticles, from production and application through various release pathways to environmental fate and transformations [61].

IV.6.3. Ecotoxicity and Health Concerns

The same physicochemical properties that endow engineered nanomaterials with exceptional reactivity, high surface-area-to-volume ratios, quantum confinement effects, and surface-mediated radical generation, are also responsible for potentially adverse interactions with biological systems. Oberdörster et al. [62] were among the first to systematically examine the toxicological implications of engineered NPs, establishing that particle size, specific surface area, and surface reactivity are more reliable predictors of biological effect than mass concentration, a finding with profound implications for regulatory risk assessment frameworks that historically relied on mass-based exposure metrics.

At the cellular level, the primary mechanism of NP toxicity is the generation of reactive oxygen species (ROS) that overwhelm endogenous antioxidant defences, triggering oxidative stress, lipid peroxidation, protein carbonylation, and ultimately apoptosis or necrosis. Nel et al. [63] demonstrated that the oxidative stress paradigm could organise a hierarchy of nanoparticle toxicity, with ZnO, CuO, and Ag NPs occupying the upper tier due to their propensity to release toxic dissolved cations in biological fluids, a process sometimes termed the *Trojan horse mechanism*. The magnitude and reversibility of these effects depend critically on the surface chemistry, dissolution kinetics, and aggregation state of the NPs in the specific medium, all of which can differ substantially between the controlled conditions of a toxicity assay and the physicochemically complex environment of a real wastewater matrix [63].

From an ecological perspective, Klaine et al. [59] provided an early and comprehensive assessment of the fate and effects of nanomaterials in the environment, identifying aquatic organisms as a primary concern due to the potential for NPs released from wastewater treatment plants to accumulate in receiving water bodies. Subsequent studies have confirmed that TiO_2 NPs at concentrations of 1–10 mg L^{-1} inhibit the photosynthesis of freshwater algae, disrupt the reproductive cycles of *Daphnia magna*, and impair the behaviour and gill function of teleost fish [59]. Bioaccumulation through dietary exposure adds a further dimension of ecological risk by introducing NPs into food webs at trophic levels distant from the point of initial exposure [64].

IV.6.4. Regulatory Frameworks and Knowledge Gaps

The regulatory governance of engineered nanomaterials lags considerably behind the pace of technological innovation, creating a situation in which products incorporating NPs reach commercial deployment before the long-term environmental and health implications are fully characterized [65]. The European Union's 2011 Recommendation on the definition of nanomaterial represented an important step towards regulatory coherence, establishing that a material should be considered nano if at least 50 % of its particle number size distribution falls within the 1–100 nm range. However, this dimensional definition has been criticised for its failure to account for the surface-area-dependent hazard profiles of different NP types and for the complexity of speciation transformations that occur in environmental matrices [65].

In the United States, the Environmental Protection Agency (EPA) regulates nanomaterials primarily through the Toxic Substances Control Act (TSCA), which requires pre-manufacture notification for new chemical substances, including new forms of existing materials at the nanoscale. However, the evidentiary standards applied in these reviews have been challenged as insufficient given the novelty of nanomaterial hazard profiles [66]. Wiesner et al. [66] argued that the regulatory gap stems not from a lack of legislative will but from genuine scientific uncertainty regarding the dose–response relationships, exposure routes, and transformation kinetics that govern nanomaterial risk, gaps that only coordinated, long-duration field studies and harmonised testing protocols can address.

A further dimension of regulatory complexity concerns the intentional release of nanomaterials into treatment systems. While nano-adsorbents and nano-catalysts may be deployed with full containment intentions, accidental losses through imperfect membrane systems or incomplete magnetic recovery inevitably result in some degree of discharge into receiving waters. Current discharge regulations do not include nano-specific effluent standards; instead, NPs would need to comply with conventional total suspended solids (TSS) or metal-specific limits, framings that are largely inapplicable to the dispersed, chemically active nanoscale phase [67].

In summary, the path to the responsible large-scale deployment of nanoparticles in wastewater treatment requires progress on multiple fronts: the development of validated, scalable NP recovery technologies; the establishment of standardised nanotoxicology testing protocols

that account for environmental transformations; the construction of robust long-term ecotoxicological datasets for key nanomaterials; and the creation of regulatory frameworks that are both scientifically grounded and proportionate to actual risk. Meeting these challenges is not merely an academic exercise, it is a prerequisite for earning the societal licence to operate that any genuinely transformative environmental technology must ultimately secure [67].

References

References

1. Mohammed MN, Abdullah OI Comprehensive Review on Wastewater Treatment using Nanoparticles: Synthesis of IONPs, Publication Trends, and Future Perspectives. ASEAN J Sci Eng 5:1–30
2. Zahmatkesh S, Hajiaghaei-Keshteli M, Bokhari A, et al (2023) Wastewater treatment with nanomaterials for the future: A state-of-the-art review. Environ Res 216:114652. https://doi.org/10.1016/j.envres.2022.114652
3. Deblonde T, Cossu-Leguille C, Hartemann P (2011) Emerging pollutants in wastewater: A review of the literature. Int J Hyg Environ Health 214:442–448. https://doi.org/10.1016/j.ijheh.2011.08.002
4. Mahmood T, Momin S, Ali R, et al (2022) Technologies for Removal of Emerging Contaminants from Wastewater. Wastewater Treat.
5. Arman NZ, Salmiati S, Aris A, et al (2021) A review on emerging pollutants in the water environment: Existences, health effects and treatment processes. Water (Switzerland) 13:3258. https://doi.org/10.3390/w13223258
6. Almomani F, Bhosale R, Khraisheh M, et al (2020) Heavy metal ions removal from industrial wastewater using magnetic nanoparticles (MNP). Appl Surf Sci 506:144924. https://doi.org/10.1016/j.apsusc.2019.144924
7. Mbarek W Ben, Escoda L, Saurina J, et al (2022) Nanomaterials as a Sustainable Choice for Treating Wastewater: A Review. Materials (Basel) 15:8576. https://doi.org/10.3390/ma15238576
8. Kumari P, Alam M, Siddiqi WA (2019) Usage of nanoparticles as adsorbents for waste water treatment: An emerging trend. Sustain Mater Technol 22:128. https://doi.org/10.1016/j.susmat.2019.e00128
9. Lu J, Zhang M, Zheng N, et al (2026) Application of optical properties and photocatalytic degradation behavior of N, P-CQDs in organic dyes degradation. Spectrochim Acta - Part A Mol Biomol Spectrosc 348:127223. https://doi.org/10.1016/j.saa.2025.127223
10. Lu H, Wang J, Stoller M, et al (2016) An Overview of Nanomaterials for Water and Wastewater Treatment. Adv Mater Sci Eng 2016:1–10. https://doi.org/10.1155/2016/4964828
11. Silva EC, Soares VR, Fajardo AR (2023) Removal of pharmaceuticals from aqueous medium by alginate/polypyrrole/ZnFe2O4 beads via magnetic field enhanced adsorption.

Chemosphere 316:137734. https://doi.org/10.1016/j.chemosphere.2022.137734

12. Lei T, Jiang X, Zhou Y, et al (2023) A multifunctional adsorbent based on 2,3-dimercaptosuccinic acid/dopamine-modified magnetic iron oxide nanoparticles for the removal of heavy-metal ions. J Colloid Interface Sci 636:153–166. https://doi.org/10.1016/j.jcis.2023.01.011
13. Siddiqui AJ, Kumari N, Adnan M, et al (2023) Impregnation of Modified Magnetic Nanoparticles on Low-Cost Agro-Waste-Derived Biochar for Enhanced Removal of Pharmaceutically Active Compounds: Performance Evaluation and Optimization Using Response Surface Methodology. Water (Switzerland) 15:. https://doi.org/10.3390/w15091688
14. Fu F, Wang Q (2011) Removal of heavy metal ions from wastewaters: A review. J Environ Manage 92:407–418. https://doi.org/10.1016/j.jenvman.2010.11.011
15. Ali I (2012) New generation adsorbents for water treatment. Chem Rev 112:5073–5091. https://doi.org/10.1021/cr300133d
16. Lu AH, Salabas EL, Schüth F (2007) Magnetic nanoparticles: Synthesis, protection, functionalization, and application. Angew Chemie - Int Ed 46:1222–1244. https://doi.org/10.1002/anie.200602866
17. Yean S, Cong L, Yavuz CT, et al (2005) Effect of magnetite particle size on adsorption and desorption of arsenite and arsenate. J Mater Res 20:3255–3264. https://doi.org/10.1557/jmr.2005.0403
18. Cornell RM, Schwertmann U (2004) The Iron Oxides: Structure, Properties, Reactions, Occurences and Uses. Iron Oxides Struct. Prop. React. Occur. Uses 1–664
19. Mahdavi S, Jalali M, Afkhami A (2012) Removal of heavy metals from aqueous solutions using Fe3O 4, ZnO, and CuO nanoparticles. J Nanoparticle Res 14:846. https://doi.org/10.1007/s11051-012-0846-0
20. Ge F, Li MM, Ye H, Zhao BX (2012) Effective removal of heavy metal ions Cd 2+, Zn 2+, Pb 2+, Cu 2+ from aqueous solution by polymer-modified magnetic nanoparticles. J Hazard Mater 211–212:366–372. https://doi.org/10.1016/j.jhazmat.2011.12.013
21. Sheela T, Nayaka YA, Viswanatha R, et al (2012) Kinetics and thermodynamics studies on the adsorption of Zn(II), Cd(II) and Hg(II) from aqueous solution using zinc oxide nanoparticles. Powder Technol 217:163–170. https://doi.org/10.1016/j.powtec.2011.10.023
22. Pena ME, Korfiatis GP, Patel M, et al (2005) Adsorption of As(V) and As(III) by

nanocrystalline titanium dioxide. Water Res 39:2327–2337. https://doi.org/10.1016/j.watres.2005.04.006

23. Crane RA, Scott TB (2012) Nanoscale zero-valent iron: Future prospects for an emerging water treatment technology. J Hazard Mater 211–212:112–125. https://doi.org/10.1016/j.jhazmat.2011.11.073
24. Xu J, Cao Z, Zhang Y, et al (2018) A review of functionalized carbon nanotubes and graphene for heavy metal adsorption from water: Preparation, application, and mechanism. Chemosphere 195:351–364. https://doi.org/10.1016/j.chemosphere.2017.12.061
25. Lu C, Chiu H, Liu C (2006) Removal of zinc(II) from aqueous solution by purified carbon nanotubes: Kinetics and equilibrium studies. Ind Eng Chem Res 45:2850–2855. https://doi.org/10.1021/ie051206h
26. Ihsanullah, Abbas A, Al-Amer AM, et al (2016) Heavy metal removal from aqueous solution by advanced carbon nanotubes: Critical review of adsorption applications. Sep Purif Technol 157:141–161. https://doi.org/10.1016/j.seppur.2015.11.039
27. Novoselov KS, Geim AK, Morozov S V., et al (2004) Electric field in atomically thin carbon films. Science (80-) 306:666–669. https://doi.org/10.1126/science.1102896
28. Sitko R, Turek E, Zawisza B, et al (2013) Adsorption of divalent metal ions from aqueous solutions using graphene oxide. J Chem Soc Dalt Trans 42:5682–5689. https://doi.org/10.1039/c3dt33097d
29. Zhao G, Li J, Ren X, et al (2011) Few-layered graphene oxide nanosheets as superior sorbents for heavy metal ion pollution management. Environ Sci Technol 45:10454–10462. https://doi.org/10.1021/es203439v
30. Chandra V, Park J, Chun Y, et al (2010) Water-dispersible magnetite-reduced graphene oxide composites for arsenic removal. ACS Nano 4:3979–3986. https://doi.org/10.1021/nn1008897
31. Bhatnagar A, Sillanpää M (2010) Utilization of agro-industrial and municipal waste materials as potential adsorbents for water treatment-A review. Chem Eng J 157:277–296. https://doi.org/10.1016/j.cej.2010.01.007
32. Mohan D, Pittman CU (2006) Activated carbons and low cost adsorbents for remediation of tri- and hexavalent chromium from water. J Hazard Mater 137:762–811. https://doi.org/10.1016/j.jhazmat.2006.06.060
33. Miklos DB, Remy C, Jekel M, et al (2018) Evaluation of advanced oxidation processes for water and wastewater treatment – A critical review. Water Res 139:118–131.

https://doi.org/10.1016/j.watres.2018.03.042

34. Schneider J, Matsuoka M, Takeuchi M, et al (2014) Understanding TiO 2 Photocatalysis: Mechanisms and Materials. Chem Rev 114:9919–9986. https://doi.org/10.1021/cr5001892
35. Nidheesh P V. (2015) Heterogeneous Fenton catalysts for the abatement of organic pollutants from aqueous solution: A review. RSC Adv 5:40552–40577. https://doi.org/10.1039/c5ra02023a
36. Etacheri V, Di Valentin C, Schneider J, et al (2015) Visible-light activation of TiO2 photocatalysts: Advances in theory and experiments. J Photochem Photobiol C Photochem Rev 25:1–29. https://doi.org/10.1016/j.jphotochemrev.2015.08.003
37. Ong CB, Ng LY, Mohammad AW (2018) A review of ZnO nanoparticles as solar photocatalysts: Synthesis, mechanisms and applications. Renew Sustain Energy Rev 81:536–551. https://doi.org/10.1016/j.rser.2017.08.020
38. Thomas N, Dionysiou DD, Pillai SC (2021) Heterogeneous Fenton catalysts: A review of recent advances. J Hazard Mater 404:. https://doi.org/10.1016/j.jhazmat.2020.124082
39. Yang ST, Zhang W, Xie J, et al (2015) Fe3O4@SiO2 nanoparticles as a high-performance Fenton-like catalyst in a neutral environment. RSC Adv 5:5458–5463. https://doi.org/10.1039/c4ra10207j
40. Yao Y, Li G, Ciston S, et al (2008) Photoreactive TiO2/carbon nanotube composites: Synthesis and reactivity. Environ Sci Technol 42:4952–4957. https://doi.org/10.1021/es800191n
41. Hoffmann MR, Martin ST, Choi W, Bahnemann DW (1995) Environmental Applications of Semiconductor Photocatalysis. Chem Rev 95:69–96. https://doi.org/10.1021/cr00033a004
42. Iravani S (2011) Green synthesis of metal nanoparticles using plants. Green Chem 13:2638–2650. https://doi.org/10.1039/c1gc15386b
43. Khatami M, Alijani HQ, Heli H, Sharifi I (2018) Rectangular shaped zinc oxide nanoparticles: Green synthesis by Stevia and its biomedical efficiency. Ceram Int 44:15596–15602. https://doi.org/10.1016/j.ceramint.2018.05.224
44. Khezzane A, Saoud A, Bouafia A, et al (2025) Eco-friendly Ca/α-Fe 2 O 3 / ZnO / CuO nanocomposite: Green synthesis, characterization, and high-efficiency heavy metal removal from contaminated sludge. Environ Prog Sustain Energy. https://doi.org/10.1002/ep.70207
45. Wang T, Jin X, Chen Z, et al (2014) Green synthesis of Fe nanoparticles using eucalyptus

leaf extracts for treatment of eutrophic wastewater. Sci Total Environ 466–467:210–213. https://doi.org/10.1016/j.scitotenv.2013.07.022

46. Machado S, Pinto SL, Grosso JP, et al (2013) Green production of zero-valent iron nanoparticles using tree leaf extracts. Sci Total Environ 445–446:1–8. https://doi.org/10.1016/j.scitotenv.2012.12.033
47. Gan L, Lu Z, Cao D, Chen Z (2018) Effects of cetyltrimethylammonium bromide on the morphology of green synthesized Fe3O4 nanoparticles used to remove phosphate. Mater Sci Eng C 82:41–45. https://doi.org/10.1016/j.msec.2017.08.073
48. Khandel P, Shahi SK (2018) Mycogenic nanoparticles and their bio-prospective applications: current status and future challenges. J Nanostructure Chem 8:369–391. https://doi.org/10.1007/s40097-018-0285-2
49. Ahmed S, Ahmad M, Swami BL, Ikram S (2016) A review on plants extract mediated synthesis of silver nanoparticles for antimicrobial applications: A green expertise. J Adv Res 7:17–28. https://doi.org/10.1016/j.jare.2015.02.007
50. Han R, Wang Y, Han P, et al (2006) Removal of methylene blue from aqueous solution by chaff in batch mode. J Hazard Mater 137:550–557. https://doi.org/10.1016/j.jhazmat.2006.02.029
51. Sharma YC, Srivastava V, Singh VK, et al (2009) Nano-adsorbents for the removal of metallic pollutants from water and wastewater. Environ Technol 30:583–609. https://doi.org/10.1080/09593330902838080
52. Abdolali A, Ngo HH, Guo W, et al (2017) Application of a breakthrough biosorbent for removing heavy metals from synthetic and real wastewaters in a lab-scale continuous fixed-bed column. Bioresour Technol 229:78–87. https://doi.org/10.1016/j.biortech.2017.01.016
53. Yin J, Deng B (2015) Polymer-matrix nanocomposite membranes for water treatment. J Memb Sci 479:256–275. https://doi.org/10.1016/j.memsci.2014.11.019
54. Ng LY, Mohammad AW, Leo CP, Hilal N (2013) Polymeric membranes incorporated with metal/metal oxide nanoparticles: A comprehensive review. Desalination 308:15–33. https://doi.org/10.1016/j.desal.2010.11.033
55. Lin YS (2001) Microporous and dense inorganic membranes: current status and prospective. Sep Purif Technol 25:39–55. https://doi.org/10.1016/S1383-5866(01)00089-2
56. Zhang X, Zheng J, Xu L, et al (2021) Novel Thin Film Nanocomposite Forward Osmosis Membranes Prepared by Organic Phase Controlled Interfacial Polymerization with

Functional Multi-Walled Carbon Nanotubes. Membranes (Basel) 11:476. https://doi.org/10.3390/membranes11070476

57. Santhosh C, Velmurugan V, Jacob G, et al (2016) Role of nanomaterials in water treatment applications: A review. Chem Eng J 306:1116–1137. https://doi.org/10.1016/j.cej.2016.08.053
58. Simate GS, Iyuke SE, Ndlovu S, et al (2012) Human health effects of residual carbon nanotubes and traditional water treatment chemicals in drinking water. Environ Int 39:38–49. https://doi.org/10.1016/j.envint.2011.09.006
59. Klaine SJ, Alvarez PJJ, Batley GE, et al (2008) Nanomaterials in the environment: Behavior, fate, bioavailability, and effects. Environ Toxicol Chem 27:1825–1851. https://doi.org/10.1897/08-090.1
60. Lowry G V., Gregory KB, Apte SC, Lead JR (2012) Transformations of nanomaterials in the environment. Environ Sci Technol 46:6893–6899. https://doi.org/10.1021/es300839e
61. Abbas Q, Yousaf B, Amina, et al (2020) Transformation pathways and fate of engineered nanoparticles (ENPs) in distinct interactive environmental compartments: A review. Environ Int 138:105646. https://doi.org/10.1016/j.envint.2020.105646
62. Oberdörster G, Oberdörster E, Oberdörster J (2005) Nanotoxicology: An emerging discipline evolving from studies of ultrafine particles. Environ Health Perspect 113:823–839. https://doi.org/10.1289/ehp.7339
63. Nel A, Xia T, Mädler L, Li N (2006) Toxic potential of materials at the nanolevel. Science (80-) 311:622–627. https://doi.org/10.1126/science.1114397
64. Lead JR, Wilkinson KJ (2006) Aquatic colloids and nanoparticles: Current knowledge and future trends. Environ Chem 3:159–171. https://doi.org/10.1071/EN06025
65. E.U._Executive (2011) Commission Recommendation of 18 October 2011 on the Definition of Nanomaterial. Off J Eur Union L 275:1. https://doi.org/10.3000/19770677.L_2011.275.eng
66. Wiesner MR, Lowry G V., Alvarez P, et al (2006) Assessing the risks of manufactured nanomaterials. Environ Sci Technol 40:4336–4345. https://doi.org/10.1021/es062726m
67. Aitken RJ, Chaudhry MQ, Boxall ABA, Hull M (2006) Manufacture and use of nanomaterials: Current status in the UK and global trends. Occup Med (Chic Ill) 56:300–306. https://doi.org/10.1093/occmed/kql051

CHAPTER V
Nanoparticles in Biomedical Applications

IV.1. Overview of Nanomedicine and Theranostics

The convergence of nanotechnology and medicine over the past three decades has given rise to the interdisciplinary field of nanomedicine, a discipline that exploits the distinctive physicochemical properties of materials engineered at the nanoscale (1–100 nm) to address longstanding limitations of conventional therapeutic and diagnostic strategies. At dimensions comparable to biological macromolecules and subcellular structures, nanoparticles (NPs) interact with living systems in fundamentally different ways than their bulk counterparts, exhibiting tunable surface chemistry, high surface-area-to-volume ratios, and size-dependent optical, magnetic, and electronic properties that can be precisely tailored for biomedical ends [1]. The first clinically approved nanomedicine, Doxil®, a liposomal formulation of doxorubicin, received FDA clearance in 1995 and remains a landmark demonstration of how nanocarriers can dramatically reshape the pharmacokinetic and toxicological profile of cytotoxic agents [2].

Among the most intellectually compelling developments within nanomedicine is the emergence of theranostics, a term coined to describe nanoplatforms designed to simultaneously perform therapeutic and diagnostic functions within a single, integrated construct [3]. Rather than relying on sequential, often disconnected steps of disease imaging and treatment, theranostic nanosystems allow clinicians to monitor biodistribution, assess target accumulation, and gauge therapeutic response in real-time. This integration of diagnostic capabilities is facilitated by various molecular imaging instruments, as illustrated in **Figure (V.1).**

A canonical theranostic nanoparticle typically integrates at least three functional elements: an inorganic or polymeric core endowed with intrinsically useful physical properties (e.g., superparamagnetism for MRI contrast, or plasmonic resonance for photoacoustic imaging); a biocompatible shell or coating that confers colloidal stability, prolongs blood circulation, and shields the construct from premature immune clearance; and a payload compartment capable of encapsulating or surface-conjugating therapeutic agents such as small-molecule drugs, siRNA, or radionuclides [4]. These architectural elements are not merely additive, the design of each layer must account for how it will interact with the others and with the biological microenvironment encountered upon systemic administration**.**

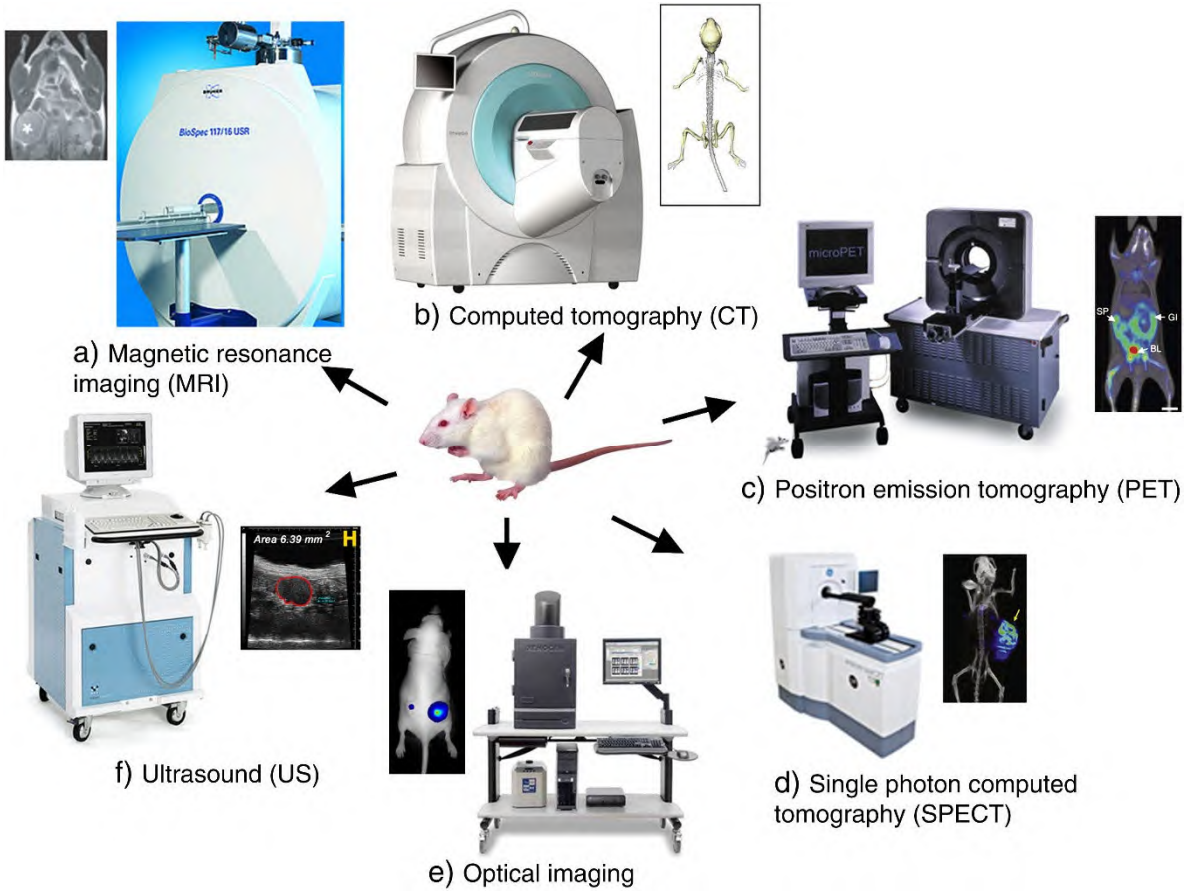

Figure (V.1): Major molecular imaging modalities used in nanomedicine and theranostics: MRI, CT, PET, SPECT, optical imaging, and ultrasound [4].

The enhanced permeability and retention (EPR) effect constitutes the principal biophysical rationale underpinning passive tumor targeting of nanoparticles. Solid tumors characteristically develop leaky vasculature with wide fenestrations (200–2000 nm) and a dysfunctional lymphatic drainage system, conditions that permit macromolecular constructs in the 10–200 nm size range to preferentially accumulate in the tumor interstitium and be retained there for extended periods [5]. However, recent meta-analyses of nanoparticle delivery efficiency have raised important caveats about the universality of the EPR effect, with some studies reporting that fewer than 1% of administered nanoparticles ultimately reach the tumor site, a sobering statistic that underscores the complexity of the tumor microenvironment and the need for more sophisticated active targeting strategies [6].

The clinical and translational trajectory of theranostic nanomedicine is, nonetheless, genuinely promising. Platforms coupling superparamagnetic iron oxide nanoparticles (SPIONs)

with chemotherapeutic agents, gold nanostructures enabling photoacoustic imaging and photothermal therapy, and liposomal constructs co-loaded with imaging dyes and cytotoxic drugs have all demonstrated compelling proof-of-concept efficacy in preclinical cancer models [3, 4]. The challenge now lies in bridging the bench-to-bedside gap: achieving reproducible large-scale synthesis, demonstrating long-term biocompatibility, navigating complex regulatory frameworks, and ultimately generating the robust clinical evidence needed to position theranostic nanomedicine as a standard-of-care modality in personalized oncology.

V.2. Nanoparticles for Drug Delivery

Drug delivery represents the most extensively investigated application of nanotechnology in biomedicine, with a global research output that has expanded exponentially over the past two decades. The fundamental premise is straightforward: by encapsulating a therapeutic agent within, or conjugating it to the surface of, a nanoscale carrier, one can radically improve that agent's solubility, protect it from enzymatic degradation during circulation, prolong its plasma half-life, and, most critically, direct it preferentially toward the pathological site while sparing healthy tissues from unnecessary exposure [7]. This multi-attribute enhancement of the pharmacokinetic-pharmacodynamic profile represents the primary reason why nanoparticulate drug delivery systems have attracted such sustained scientific and commercial attention.

The diversity of nanocarrier architectures available to researchers is remarkable, encompassing organic systems such as liposomes, polymeric nanoparticles, dendrimers, and solid lipid nanoparticles, alongside inorganic platforms including gold nanoparticles, iron oxide nanoparticles, and mesoporous silica nanoparticles [1, 8]. Each class of carrier brings a distinct set of advantages and trade-offs in terms of drug loading capacity, release kinetics, biocompatibility, scalability, and regulatory acceptability, and the selection of an appropriate platform must therefore be guided by the specific therapeutic context, the physicochemical properties of the drug of interest, and the biological barriers to be overcome at the target site.

V.2.1. Polymeric and Lipid-Based Nanocarriers

Polymeric nanoparticles, and particularly those fabricated from poly(lactic-co-glycolic acid) (PLGA) and its PEGylated derivatives, occupy a position of particular prominence in the nanomedicine landscape, a status attributable in large measure to their dual approval by the U.S. Food and Drug Administration (FDA) and the European Medicines Agency (EMA) for use in

biomedical applications [9]. PLGA undergoes hydrolytic biodegradation in physiological conditions, yielding lactic acid and glycolic acid as end products that are readily metabolized via the citric acid cycle, thus generating a negligible systemic toxic burden. This intrinsic biocompatibility, combined with the exceptional versatility of PLGA nanoparticles in encapsulating both hydrophobic and hydrophilic payloads, ranging from small-molecule chemotherapeutics such as paclitaxel and doxorubicin, to proteins, oligonucleotides, and even vaccines, has made PLGA arguably the most widely studied polymeric nanocarrier in preclinical oncology.

Passive tumor targeting of PLGA-based nanoparticles relies on the EPR effect, whereby constructs in the 100–300 nm size range extravasate through the leaky tumor vasculature and accumulate in the interstitium over time [10]. Surface PEGylation, the conjugation of polyethylene glycol chains to the nanoparticle exterior, further augments tumor accumulation by creating a hydrophilic, sterically stabilizing brush layer that inhibits opsonization and subsequent reticuloendothelial system (RES) clearance, thereby extending systemic circulation half-life from minutes to several hours or even days. In a representative study, Zhang et al. demonstrated that PEG-PLGA nanoparticles loaded with photosensitizer croconaine exhibited superior photoacoustic imaging contrast and significantly enhanced photothermal tumor ablation in vivo compared to the free drug, attributing this performance to the prolonged tumor retention mediated by PEGylation and EPR-driven passive targeting [11]. The mechanistic pathways of both passive and active targeting within the complex tumor microenvironment are schematically represented in **Figure (V.2)**.

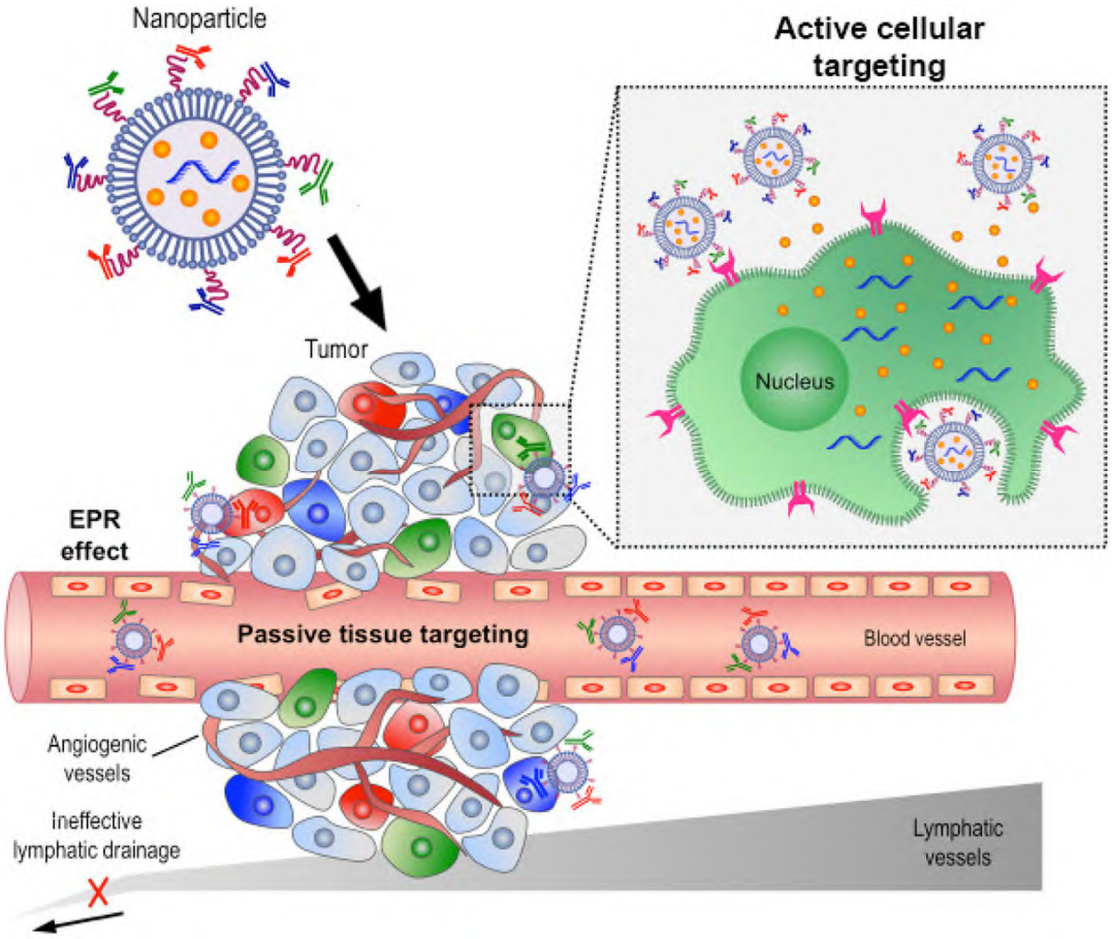

Figure (V.2): Schematic illustration of passive (EPR-mediated) and active targeting of polymeric nanoparticles within the tumor microenvironment [11].

Beyond passive targeting, the surface of PLGA nanoparticles can be functionalized with a wide variety of targeting ligands, including monoclonal antibodies, aptamers, peptides, and small-molecule receptor agonists, to achieve receptor-mediated active internalization by specific cancer cell populations. This approach has been deployed to target receptors characteristically overexpressed in tumor cells, such as the folate receptor, the transferrin receptor, and various integrin subtypes, thereby improving selectivity and intracellular drug delivery in vitro and in vivo [12].

Lipid-based nanocarriers, of which liposomes represent the most mature and clinically advanced subclass, offer a complementary set of properties to polymeric systems. Liposomes are self-assembled phospholipid bilayer vesicles that closely mimic the structural organization of the cell membrane, a resemblance that confers outstanding biocompatibility and facilitates membrane

fusion-mediated drug delivery [2]. The aqueous core of a liposome can accommodate hydrophilic drugs, while the lipid bilayer itself serves as a reservoir for lipophilic compounds, allowing co-encapsulation of agents with vastly different physicochemical characters within the same carrier, a feature particularly attractive for combination chemotherapy regimens designed to minimize drug resistance.

Solid lipid nanoparticles (SLNs) and nanostructured lipid carriers (NLCs) represent second-generation lipid-based systems developed to address the tendency of conventional liposomes toward drug leakage and limited stability during storage. By replacing the liquid lipid core with a solid matrix, SLNs provide improved physical stability and better-controlled drug release kinetics, making them well-suited for the delivery of lipophilic active substances that require sustained exposure over extended periods [3]. More recently, lipid nanoparticles (LNPs) have gained extraordinary clinical relevance as the delivery vehicle of choice for mRNA-based therapeutics, a modality thrust into global prominence by the COVID-19 pandemic, underscoring the versatility of lipid-based architectures beyond their traditional oncological applications.

V.2.2. Inorganic Nanoparticles (Gold, Iron Oxide, Silica) in Drug Delivery

Inorganic nanoparticles occupy a unique and increasingly important niche in the drug delivery landscape, primarily because their core physical properties, optical, magnetic, or structural, can be exploited not only to facilitate drug transport, but also to enable direct therapeutic actions or diagnostic imaging that are entirely unavailable from organic nanocarriers. Gold nanoparticles (AuNPs), iron oxide nanoparticles (IONPs), and mesoporous silica nanoparticles (MSNs) represent the three most extensively investigated inorganic platforms, each distinguished by a different primary functional attribute that can be harnessed in combination with appropriate drug payloads.

Gold nanoparticles are perhaps the most photophysically versatile of these platforms. Their strong and tunable localized surface plasmon resonance (LSPR), which can be shifted from the visible to the near-infrared (NIR) region by adjusting particle geometry (nanospheres, nanorods, nanoshells, or nanostars), makes them uniquely suitable as photothermal transduction agents [13]. When irradiated with NIR light, AuNPs convert photon energy into localized heat with high efficiency, enabling the thermal ablation of tumor tissue at temperatures above 42°C while sparing surrounding healthy cells. Critically, this photothermal effect can also be exploited

to trigger controlled drug release: thermolabile chemical bonds or temperature-responsive polymeric coatings wrapping the gold core can be engineered to release their drug cargo specifically upon NIR irradiation, providing spatiotemporal control over the delivery event [14].

Iron oxide nanoparticles, particularly superparamagnetic iron oxide nanoparticles (SPIONs) composed of magnetite (Fe_3O_4) or maghemite (γ-Fe_2O_3) in the 15–100 nm size range, have attracted enormous interest as dual-purpose theranostic agents capable of serving simultaneously as MRI T_2 contrast agents and drug delivery vehicles [15]. Their superparamagnetism means they exhibit strong magnetization in the presence of an applied magnetic field but retain no residual magnetism upon its removal, thereby preventing problematic magnetic aggregation in circulation. The surface of SPIONs can be functionalized with a broad variety of coatings, including PEG, dextran, chitosan, and silica, to modulate biocompatibility, circulation half-life, and drug loading capacity. Magnetically guided delivery, achieved by positioning an external permanent magnet at the tumor site following systemic administration, represents a particularly elegant strategy for concentrating SPION-drug conjugates at the pathological focus while substantially reducing off-target accumulation.

Mesoporous silica nanoparticles (MSNs) distinguish themselves from gold and iron oxide platforms through their extraordinary structural properties: a highly ordered, tunable pore architecture with pore diameters typically ranging from 2 to 10 nm and surface areas exceeding 1000 $m^2\ g^{-1}$, providing unparalleled drug loading capacity for small molecules that can be physically adsorbed within or covalently anchored to the pore walls [16]. The silica framework is inherently biocompatible and chemically inert, and the pore openings can be 'gated' with stimuli-responsive gatekeepers, including pH-sensitive polymers, redox-responsive disulfide bonds, or enzyme-cleavable substrates, that maintain the drug securely encapsulated during systemic circulation but trigger rapid release specifically within the acidic or oxidative tumor microenvironment.

A particularly compelling frontier in inorganic nanoparticle drug delivery involves the rational integration of two or more inorganic platforms within a single hybrid construct. Iron oxide@mesoporous silica core-shell nanoparticles, for example, combine the MRI contrast capability and magnetic guidance afforded by the IONP core with the high drug loading capacity and stimuli-responsive release provided by the silica shell, As schematically illustrated in **Figure**

(V.3), this hybrid architecture yields a multifunctional theranostic system capable of executing simultaneous imaging, hyperthermia, and controlled drug delivery, thereby outperforming either component in isolation [17]. Similarly, gold-coated iron oxide nanoparticles merge photothermal therapy and MRI imaging in a single nanoconstruct, as has been demonstrated in multiple preclinical studies involving doxorubicin-loaded platforms exhibiting synergistic chemo-photothermal antitumor efficacy [14]. These hybrid architectures epitomize the broader trajectory of the field: from simple, single-function nanocarriers toward sophisticated, stimulus-responsive, multi-modal platforms capable of executing complex therapeutic programs with a degree of precision that was inconceivable even a decade ago.

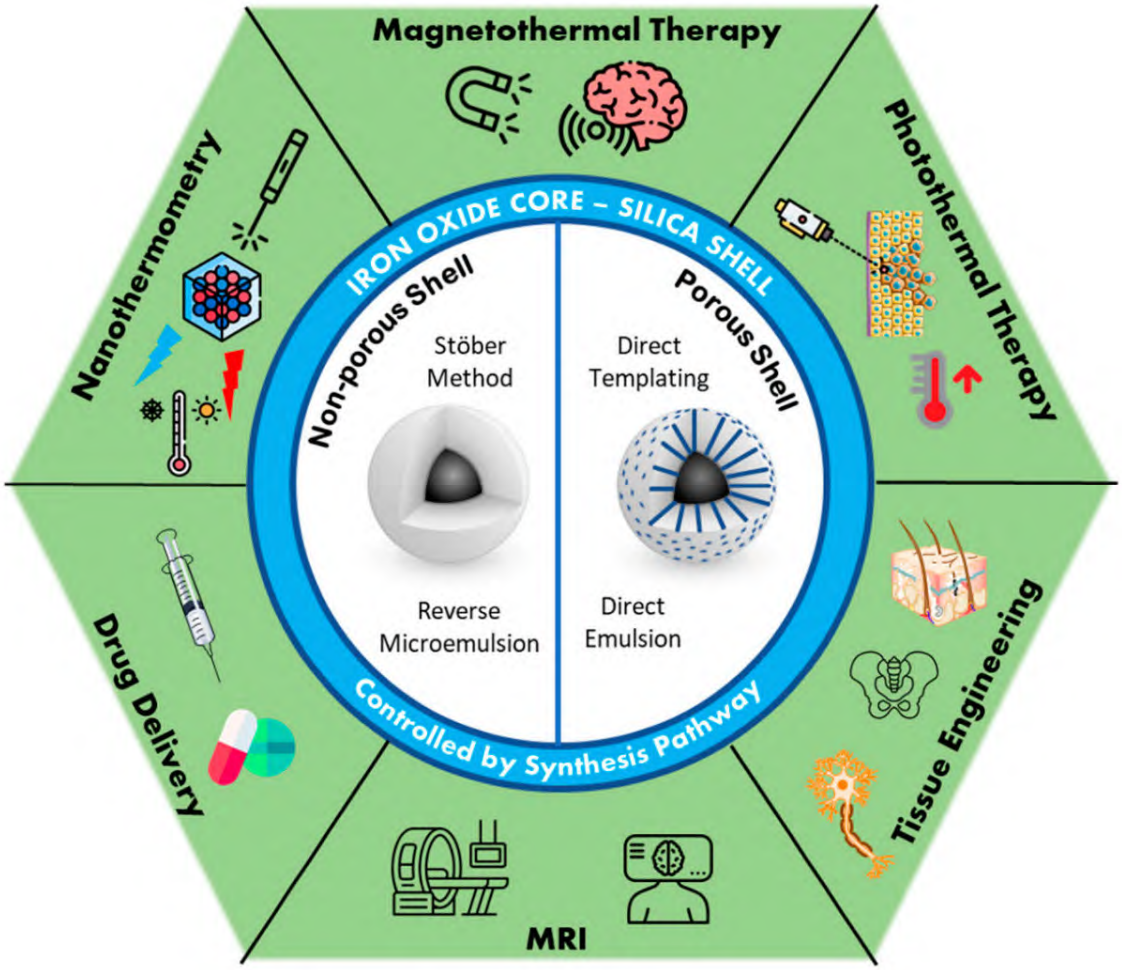

Figure (V.3): Iron oxide@mesoporous silica core–shell nanoparticles for multimodal theranostic applications [18].

V.3. Imaging and Diagnostic Applications

The capacity to visualize disease at the molecular and cellular level, long before anatomical changes become macroscopically detectable, represents one of the most transformative contributions that nanotechnology has made to clinical medicine. Conventional imaging contrast agents, including gadolinium chelates for magnetic resonance imaging (MRI) and iodinated compounds for computed tomography (CT), suffer from rapid renal clearance, poor tissue specificity, and, in some cases, significant toxicological concerns that limit their clinical utility [19]. Nanoparticle-based imaging probes have emerged as a compelling alternative class of contrast agents, offering prolonged circulation lifetimes, surface-tunable targeting functionalities, amplified signal-to-noise ratios, and, critically, the ability to integrate multiple contrast-generating mechanisms within a single nanoarchitecture, thereby enabling the simultaneous acquisition of complementary anatomical, functional, and molecular information.

The field of nanoparticle-enhanced imaging now encompasses an extraordinarily diverse array of platforms, from superparamagnetic iron oxide nanoparticles (SPIONs) and gadolinium-based T_1 agents for MRI, to semiconductor quantum dots (QDs), carbon nanodots, and organic fluorophore-loaded nanocarriers for optical and fluorescence imaging, to radiolabeled constructs enabling positron emission tomography (PET) and single-photon emission computed tomography (SPECT) [15]. Each of these platforms brings a distinct set of physicochemical properties that determine its sensitivity, spatial resolution, tissue penetration depth, and compatibility with clinical imaging hardware. Understanding the advantages and limitations of each modality, and the strategies available to overcome those limitations through multimodal integration, is essential for designing next-generation diagnostic agents that can meet the demanding requirements of precision oncology and personalized medicine.

V.3.1. MRI Contrast Agents (Superparamagnetic Iron Oxide Nanoparticles)

Magnetic resonance imaging remains the gold standard for soft-tissue visualization in clinical radiology, offering unparalleled spatial resolution and exceptional anatomical detail without exposing the patient to ionizing radiation. The intrinsic contrast of MRI, however, is often insufficient for the early detection of small lesions or the molecular characterization of pathological tissue, necessitating the use of exogenous contrast agents that modulate the longitudinal (T_1) or transverse (T_2) relaxation times of water protons in the vicinity of the agent [20]. Gadolinium-based contrast agents (GBCAs) have historically dominated clinical T_1-

weighted MRI, but their potential to dissociate and deposit gadolinium in tissues, particularly in patients with renal insufficiency, has raised serious safety concerns and prompted substantial research into gadolinium-free alternatives.

Superparamagnetic iron oxide nanoparticles (SPIONs) have emerged as the most extensively investigated gadolinium-free MRI contrast agents, a distinction attributable to their potent effect on T_2 relaxation, their favorable biocompatibility profile, and the well-established metabolic pathways through which iron is processed by the reticuloendothelial system (RES) after nanoparticle degradation [21]. The contrast-enhancing mechanism of SPIONs is fundamentally different from that of gadolinium chelates: rather than shortening T_1 relaxation times to produce positive (bright) contrast, SPIONs generate strong local magnetic field inhomogeneities that accelerate T_2 and T_2* relaxation, resulting in a characteristic darkening, or negative contrast, of tissues in which the particles accumulate. The efficiency of this contrast effect is quantified by the transverse relaxivity r_2 (expressed in $mM^{-1}\ s^{-1}$), with higher values indicating greater contrast-generating capacity at lower iron concentrations.

The relationship between SPION size and magnetic behavior is of fundamental importance in determining imaging performance. Particles larger than approximately 20 nm in diameter contain multiple magnetic domains and behave ferromagnetically, exhibiting residual magnetism even in the absence of an applied field, a property that promotes irreversible aggregation and is therefore undesirable in vivo. SPIONs in the 10–20 nm range (**Figure V.4**), by contrast, reside within the single-domain superparamagnetic regime: they display strong magnetization when exposed to an external magnetic field, but this magnetization collapses entirely upon field removal, ensuring colloidal stability and preventing thrombus formation [22]. Ultrasmall superparamagnetic iron oxide nanoparticles (USPIONs), with core diameters below 5 nm, exhibit a qualitatively different behavior: their surface-to-volume ratio is so large that surface iron atoms with irregular coordination environments dominate the magnetic response, conferring paramagnetic-like T_1 enhancement properties that make USPIONs attractive as positive MRI contrast agents, a feature particularly advantageous in applications where bright-contrast imaging is clinically preferred, such as vascular and lymph node imaging.

The surface chemistry of SPIONs exerts a profound influence on their in vivo behavior, governing colloidal stability, blood circulation half-life, protein corona formation, and

biodistribution. Bare iron oxide nanoparticles are rapidly opsonized and cleared by Kupffer cells in the liver and splenic macrophages within minutes of intravenous administration; this RES tropism, though limiting for tumor imaging, has been deliberately exploited for clinical liver imaging using agents such as Endorem® (ferumoxides) and Resovist® (ferucarbotran), which specifically accumulate in normal hepatic tissue and are absent from lesions lacking Kupffer cells, thereby providing lesion-to-background contrast [23]. PEGylation substantially extends the circulation half-life of SPIONs by creating a hydrophilic steric barrier that inhibits opsonin adsorption, enabling passive accumulation in tumors via the EPR effect and facilitating active targeting when combined with surface-conjugated ligands.

Recent developments have focused on engineering stimuli-responsive SPIONs capable of switching their contrast modality, from T_2 to T_1, or vice versa, in response to specific features of the tumor microenvironment, such as elevated reactive oxygen species (ROS), acidic pH, or enzymatic activity. Wang and colleagues demonstrated a pH-activatable T_1-T_2 dual-modal system (SPIO@SiO_2@MnO_2) in which MnO_2 decomposed under acidic conditions to release Mn^{2+}, simultaneously restoring T_1 enhancement while the SPION core maintained T_2 contrast, a conceptually elegant approach to creating environment-sensitive imaging agents that can provide metabolically meaningful information about the lesion they image [24]. Such stimuli-responsive platforms represent a paradigm shift from passive contrast enhancement toward active, chemically intelligent imaging probes that can report on the functional and molecular state of the tumor rather than merely its anatomical boundaries.

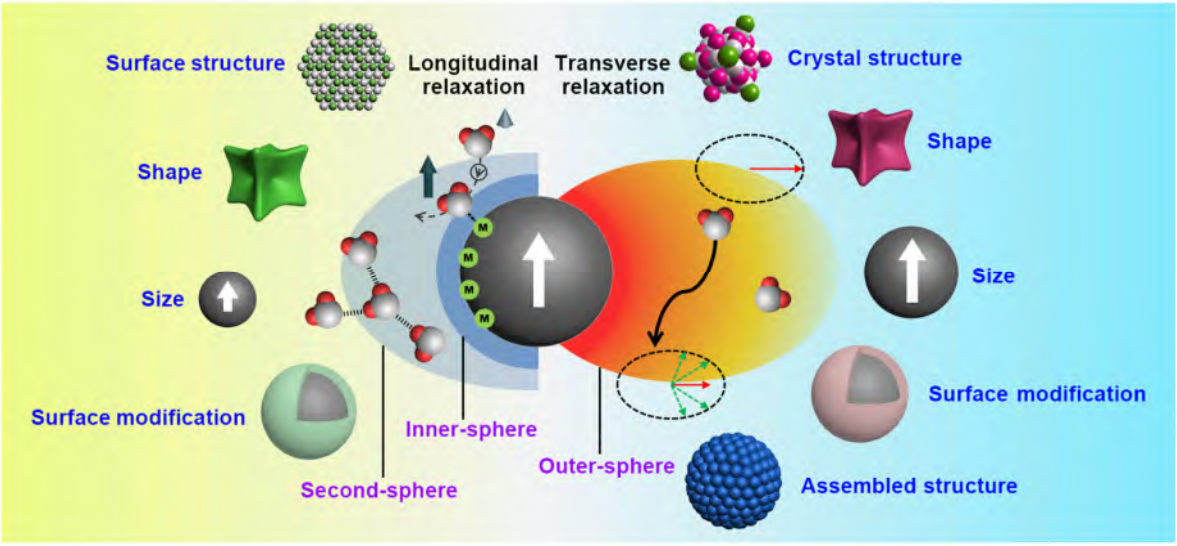

Figure (V.4): Size-dependent transition from paramagnetic to ferromagnetic behavior in iron oxide nanoparticles [22].

V.3.2. Optical and Fluorescent Nanoprobes

Optical imaging techniques, encompassing fluorescence microscopy, whole-animal fluorescence imaging, and photoacoustic imaging, occupy an increasingly important niche in the biomedical imaging landscape, particularly for applications in which real-time, high-resolution visualization at the cellular and subcellular level is required. The central challenge of optical imaging in biological systems is the severe attenuation and scattering of visible light by tissue chromophores, principally hemoglobin and melanin, which limits the penetration depth of conventional fluorescence techniques to approximately 1–2 cm at wavelengths below 700 nm [25]. This limitation has motivated a sustained research effort to develop nanoprobes with emission in the near-infrared (NIR) optical windows, the first NIR window (NIR-I, 700–900 nm) and, more recently, the second NIR window (NIR-II, 1000–1700 nm), where tissue absorption and scattering are substantially reduced and imaging depths of several centimeters become accessible.

Semiconductor quantum dots (QDs) represent arguably the most intensively studied class of inorganic fluorescent nanoprobes for biomedical imaging, distinguished from conventional organic fluorophores by a constellation of photophysical properties that render them uniquely suitable for demanding in vivo applications. QDs are semiconductor nanocrystals, most commonly composed of CdSe, CdTe, CdS, or InP cores passivated by wider-bandgap shell materials such as ZnS, with diameters in the 2–10 nm range [26]. The unique optical properties of QDs arise from the quantum confinement effect, where their emission wavelength can be precisely tuned by varying the nanocrystal size. As illustrated in **Figure (V.5)**, a single light source can simultaneously excite multiple sizes of QDs, producing a broad spectrum of non-overlapping colors, a feature essential for multiplexed biological imaging [26].

Their fluorescence emission wavelength is governed primarily by particle size through the quantum confinement effect: smaller QDs emit at shorter (bluer) wavelengths, while larger particles emit further in the red or NIR, enabling continuous wavelength tuning across the entire visible and near-infrared spectrum simply by controlling the synthetic conditions. This size-tunable emission, combined with exceptionally narrow emission linewidths, high quantum yields,

and, crucially, outstanding resistance to photobleaching that allows imaging over extended periods, makes QDs far superior to conventional organic dyes for applications requiring sustained, high-brightness fluorescent labeling.

The photostability of QDs under continuous illumination is particularly remarkable: whereas conventional organic dyes such as fluorescein or rhodamine bleach within seconds to minutes of intense excitation, QDs can withstand prolonged, high-intensity irradiation with minimal loss of emission intensity, enabling long-term tracking of dynamic biological processes, including intracellular trafficking, receptor internalization, and cell migration, that are wholly inaccessible with conventional fluorophores [27]. Furthermore, the broad, featureless excitation spectra of QDs allow multiple spectrally distinct QD populations to be simultaneously excited by a single light source and resolved by their narrow, non-overlapping emission peaks, a multiplexing capability that allows the simultaneous imaging of several molecular targets within the same biological sample, providing a systems-level view of complex signaling pathways that cannot be achieved with conventional single-color imaging.

Despite these compelling photophysical advantages, the clinical translation of cadmium-based QDs has been significantly hampered by concerns regarding the potential cytotoxicity of cadmium ions released upon nanoparticle degradation in biological environments. This has motivated intensive research into the development of cadmium-free alternatives, including indium phosphide (InP/ZnS), copper indium sulfide ($CuInS_2$/ZnS), and silicon QDs, which offer tunable emission with substantially more benign toxicological profiles [28]. Carbon-based nanodots, including graphene quantum dots (GQDs) and carbon quantum dots (CQDs), have emerged as particularly promising candidates in this regard, combining fluorescent properties reminiscent of semiconductor QDs with excellent aqueous solubility, facile surface functionalization, low cytotoxicity, and remarkably inexpensive and scalable synthesis from abundant, non-toxic carbon precursors. Their intrinsic fluorescence, arising from surface defect states and sp^2-hybridized aromatic domains rather than from quantum confinement per se, can be tuned by varying precursor composition, reaction conditions, and surface passivation strategies.

Beyond QDs, gold nanoclusters (AuNCs), discrete, atomically precise gold assemblies comprising typically fewer than 25 metal atoms protected by thiol or protein ligands, have attracted substantial attention as NIR-emitting fluorescent probes, combining the biocompatibility

well-established for larger gold nanoparticles with photoluminescent properties absent in larger plasmonic AuNPs. Protein-templated gold nanoclusters, synthesized using bovine serum albumin (BSA) or transferrin as stabilizing scaffolds, exhibit bright red-to-NIR emission, good biocompatibility, renal clearability, and facile conjugation with targeting ligands, making them well-suited for in vivo tumor imaging with a favorable safety profile [29].

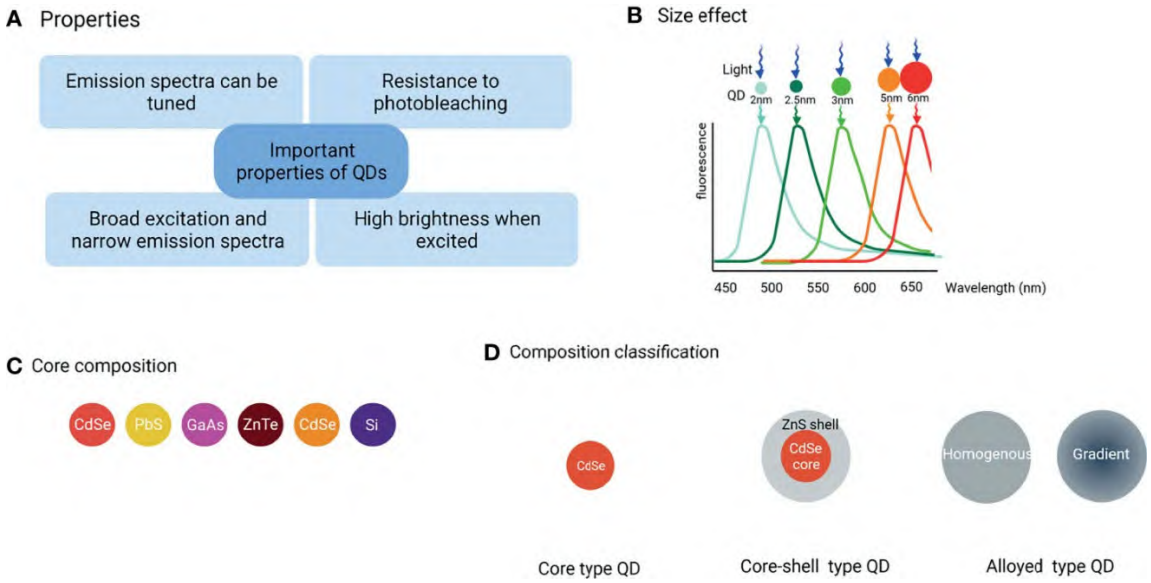

Figure (V.5): Size-tunable fluorescence emission of semiconductor quantum dots illustrating the quantum confinement effect [26].

V.3.3. Multimodal Imaging Agents

No single imaging modality provides a complete picture of disease biology. MRI offers exquisite soft-tissue contrast and anatomical detail but suffers from relatively low sensitivity (requiring micromolar contrast agent concentrations), long acquisition times, and an inability to provide functional metabolic information. PET provides extraordinarily high sensitivity, capable of detecting picomolar tracer concentrations, and quantitative physiological information, but is limited by poor spatial resolution and high ionizing radiation dose. Optical fluorescence imaging offers real-time, high-resolution cellular visualization but is severely depth-limited in tissue. Each modality, in isolation, therefore reveals only a partial view of the complex, multidimensional reality of tumor biology [30].

Multimodal nanoparticle imaging agents address this fundamental challenge by integrating two or more contrast-generating functions within a single nanoplatform, enabling the acquisition of complementary information within the same imaging session or the seamless transition between modalities without requiring separate contrast agent injections. The key advantage of such integrated constructs over the co-administration of separate contrast agents is pharmacokinetic colocalization: because all imaging modalities are carried by the same particle, they necessarily share identical biodistribution, tissue accumulation, and clearance kinetics, ensuring that anatomical, functional, and molecular information derived from different imaging channels is intrinsically spatiotemporally registered [31].

Iron oxide nanoparticles have served as the most versatile scaffold for multimodal probe construction, in large part because their inherent MRI contrast-generating capability can be straightforwardly augmented with additional imaging functionalities through surface modification. PET-MRI bimodal agents have been constructed by chelating positron-emitting radioisotopes, most commonly ^{64}Cu ($t_{1/2}$ = 12.7 h) or ^{89}Zr ($t_{1/2}$ = 78.4 h), to SPION surfaces via macrocyclic chelators such as DOTA or DFO, yielding particles that simultaneously serve as T_2 MRI contrast agents and PET tracers. The MRI component provides high-resolution anatomical localization, while PET adds quantitative physiological and metabolic information with unmatched sensitivity, a combination that is particularly powerful for tracking nanoparticle biodistribution and tumor accumulation in living subjects [32].

The integration of optical imaging functionalities into SPION-based multimodal systems extends the diagnostic versatility even further. SPION-fluorophore conjugates, in which near-infrared organic dyes such as Cy5.5 or NIR-664 are covalently attached to the nanoparticle surface alongside DOTA chelators for radiolabeling, enable PET-MRI-NIRF tri-modal imaging from a single nanoparticulate platform (**Figure V.6**). Such trimodal probes benefit from the unmatched sensitivity of PET for whole-body biodistribution mapping, the high spatial resolution of MRI for precise anatomical localization, and the real-time, high-resolution optical imaging capability for fluorescence-guided intraoperative resection, a combination of properties that no single modality could provide alone [33].

Nanoparticle platforms incorporating gold, particularly gold nanorods and gold nanostars, have been extensively explored as photoacoustic imaging agents, a modality that combines NIR

optical excitation with ultrasound detection to achieve centimeter-scale tissue penetration with optical-level contrast and resolution far superior to conventional ultrasound. The strong, geometry-dependent LSPR of gold nanostructures results in efficient light absorption in the NIR window, followed by rapid non-radiative relaxation that generates localized thermoelastic expansion and detectable acoustic waves; by tuning nanorod aspect ratio to shift the longitudinal LSPR into the NIR region, photoacoustic contrast can be generated in the tissue-transparent wavelength range while simultaneously enabling photothermal therapy, a theranostic combination of particular appeal in translational oncology [34].

Radiolabeled mesoporous silica nanoparticles (MSNs) have also attracted considerable attention as multimodal platforms, in part because the large, functionalizable internal surface area of MSNs can simultaneously accommodate radiolabeling agents, fluorescent dyes, and drug payloads within a single construct. The incorporation of ^{89}Zr-labeled CuS nanoparticles onto the surface of hollow MSN shells packed with porphyrin fluorophores yielded a tetramodal PET/fluorescence/chemiluminescence/CRET probe that demonstrated rapid and accurate tumor identification, underscoring the extraordinary versatility of silica-based architectures as scaffolds for constructing increasingly complex multimodal diagnostic systems [35].

Despite the remarkable preclinical achievements described above, the clinical translation of multimodal nanoparticle imaging agents remains a formidable challenge. The regulatory complexity of constructs containing multiple imaging agents, therapeutic payloads, and targeting ligands, each of which may be subject to independent toxicological scrutiny, substantially increases the burden of preclinical characterization and clinical development relative to simple single-agent contrast media. Issues of batch-to-batch reproducibility in nanoscale synthesis, the long-term fate of inorganic core materials that do not undergo complete biodegradation, and the potential for accelerated blood clearance upon repeated administration due to anti-PEG antibody formation are all significant hurdles that must be systematically addressed before multimodal nanoparticle probes can realize their clinical promise in personalized oncology [30, 31].

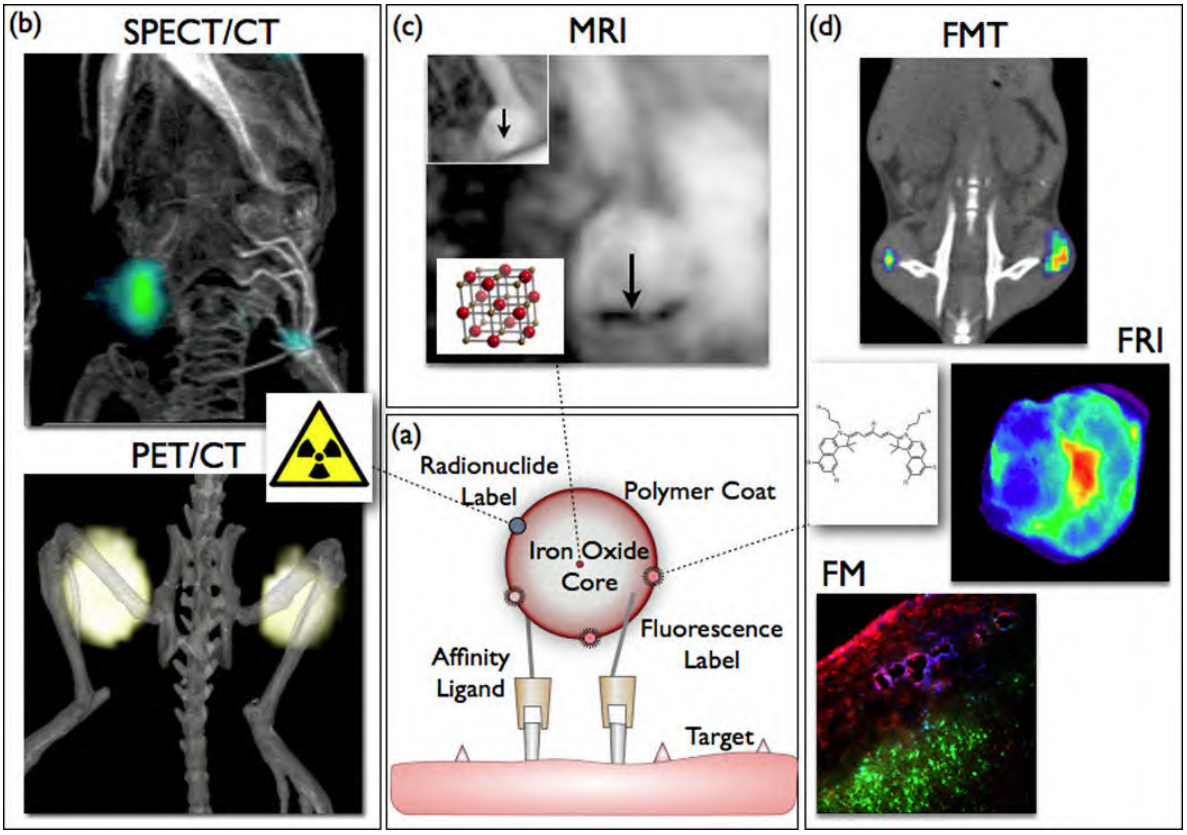

Figure (V.6): Multimodal iron oxide nanoparticle platform for targeted imaging and theranostic applications [54].

V.4. Antimicrobial and Antiviral Nanoparticles

The accelerating global crisis of antimicrobial resistance (AMR) represents one of the most consequential public health challenges of the twenty-first century. Infections caused by multidrug-resistant (MDR) bacterial pathogens, including methicillin-resistant *Staphylococcus aureus* (MRSA), carbapenem-resistant *Klebsiella pneumoniae*, and pan-resistant *Acinetobacter baumannii*, were associated with an estimated 4.95 million deaths globally in 2019 alone, a figure projected to escalate dramatically in the absence of effective countermeasures [36]. The classical pipeline of antibiotic discovery has largely stalled, with very few genuinely novel classes of antibacterial agents reaching clinical approval in the past four decades, while bacteria have demonstrated a remarkable, and deeply concerning, capacity to evolve resistance to each new antibiotic within years or even months of its introduction. This convergence of rising resistance and dwindling therapeutic options has created an urgent imperative to develop fundamentally

different classes of antimicrobial agents that operate through mechanisms sufficiently distinct from those of classical antibiotics to preclude cross-resistance.

Inorganic nanoparticles have emerged as among the most promising candidates for this role. Unlike antibiotics, which typically target a single molecular mechanism, the bacterial ribosome, cell wall biosynthesis, DNA replication, or folate metabolism, metal and metal oxide nanoparticles exert their antimicrobial effects through multiple, simultaneous mechanisms of action that attack several cellular targets concurrently, making the acquisition of resistance through any single genetic mutation substantially less likely [37]. Silver, copper, and a range of metal oxide nanoparticles, most notably zinc oxide (ZnO), titanium dioxide (TiO_2), and copper oxide (CuO), have been most intensively investigated in this context, each bringing a distinct mechanistic profile and a set of practical advantages that make them suitable for specific biomedical, environmental, and industrial applications. The antimicrobial utility of these nanomaterials extends beyond bacterial pathogens: mounting evidence indicates that several classes of inorganic nanoparticles also exhibit potent antiviral activity, a finding that has attracted heightened attention in the aftermath of the COVID-19 pandemic.

V.4.1. Silver, Copper, and Metal Oxide Nanoparticles for Microbial Control

Silver nanoparticles (AgNPs) occupy a position of undisputed primacy in the landscape of inorganic antimicrobial agents, a status reflecting both their extraordinarily broad spectrum of activity, encompassing Gram-positive and Gram-negative bacteria, fungi, viruses, and mycobacteria, and a long history of safe medicinal use of silver in various forms that predates the nanotechnology era by more than a century [38]. As early as 1881, Credé introduced 2% silver nitrate solutions for the prevention of neonatal ophthalmia, and silver-impregnated dressings have been employed in burn wound management for decades. What distinguishes AgNPs from earlier ionic silver preparations is the dramatic amplification of biological activity that accompanies the transition to the nanoscale: at diameters typically in the 1–100 nm range, AgNPs present an enormously expanded surface area relative to bulk silver, increasing the density of reactive surface sites and the rate of silver ion (Ag^+) release in aqueous and biological environments.

The antimicrobial mechanism of AgNPs is genuinely multifaceted, and its full complexity is still being elucidated. The primary bactericidal pathway involves the oxidative dissolution of AgNPs to release Ag^+ ions, which exhibit high affinity for sulfhydryl (–SH) groups in bacterial

membrane proteins and respiratory enzymes, forming Ag–S coordination bonds that irreversibly inhibit enzymatic activity, collapse the transmembrane proton gradient, and ultimately compromise the structural integrity of the cell envelope [39]. In parallel, AgNPs and Ag^{+} ions stimulate the intracellular generation of reactive oxygen species (ROS), including superoxide anions ($O_2^{\bullet -}$), hydrogen peroxide (H_2O_2), and hydroxyl radicals (•OH), at levels that overwhelm the bacterium's antioxidant defenses, causing peroxidative damage to membrane lipids, oxidative modification of cytoplasmic proteins, and strand breaks in genomic DNA. A third, size-dependent mechanism involves the direct physical interaction of AgNPs with the bacterial cell surface: nanoparticles in the 1–10 nm range are small enough to penetrate through porins and defects in the outer membrane of Gram-negative bacteria, accumulating in the periplasm and cytoplasm where they exert direct toxic effects on intracellular machinery.

Figure (V.7) provides a comparative overview highlighting how the multimodal antibacterial mechanisms of AgNPs can overcome common bacterial resistance strategies to conventional antibiotics.

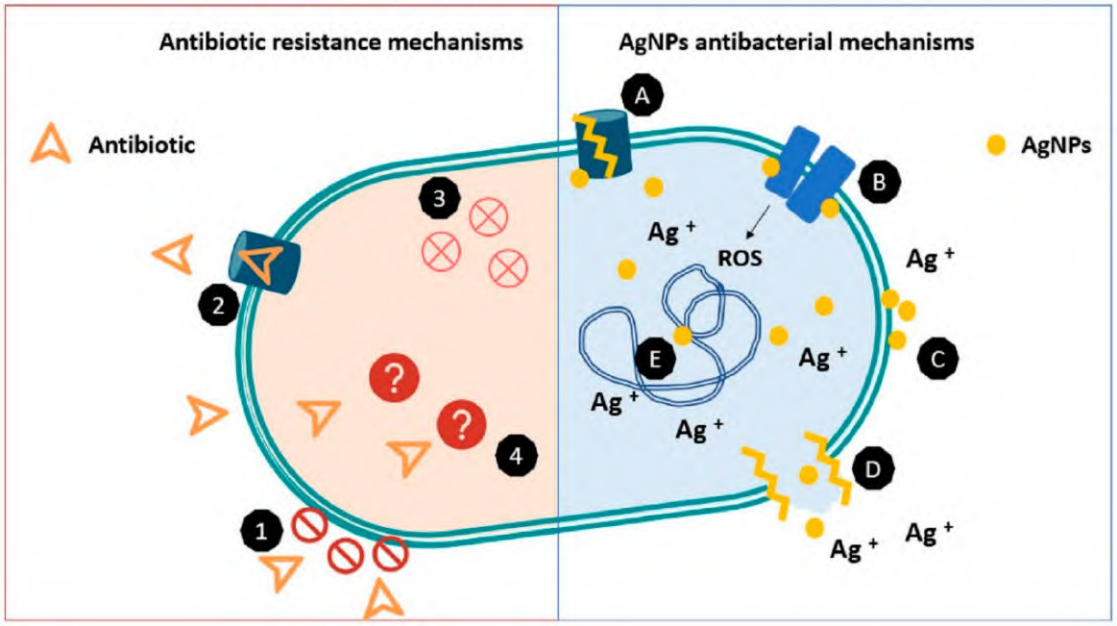

Figure (V.7): Comparison of bacterial resistance mechanisms and antibacterial mechanisms of Ag nanoparticles [38].

The physicochemical determinants of AgNP antimicrobial activity, particle size, shape, surface coating, and zeta potential, have been systematically investigated and found to

profoundly influence biological potency. Smaller AgNPs consistently demonstrate greater antibacterial efficacy than larger particles against both *S. aureus* and *E. coli*, an observation attributable to their higher surface-area-to-volume ratio and greater release of Ag^+ per unit mass. Morphologically, triangular and truncated triangular nanoplates exhibit more potent activity than nanospheres of equivalent silver content, likely because their high-index facets present a greater proportion of reactive crystal faces that dissolve more readily [40]. Surface functionalization with citrate, PVP, chitosan, or amphiphilic polymers modulates not only colloidal stability and Ag^+ release kinetics, but also the nature of the protein corona that forms upon contact with biological fluids, a factor that can either enhance or attenuate cellular interactions depending on the specific proteins recruited.

Copper nanoparticles (CuNPs) and copper oxide nanoparticles (CuO NPs) have attracted sustained interest as cost-effective alternatives or complements to AgNPs, with the significant practical advantage that copper is dramatically less expensive than silver and is inherently biocompatible at trace concentrations, as it is an essential micronutrient for mammalian cellular function. The antimicrobial mechanisms of copper nanoparticles share several features with those of AgNPs: Cu^{2+} ion release, ROS generation, and direct membrane disruption all contribute to bacterial killing [41]. However, copper exerts a distinctive additional bactericidal effect through the Fenton-like Haber–Weiss cycle, in which Cu^+/Cu^{2+} redox cycling catalyzes the conversion of H_2O_2 to highly reactive hydroxyl radicals, amplifying oxidative damage beyond what can be achieved by silver alone. This catalytic ROS amplification has been exploited in the development of CuO-coated medical device surfaces and copper-impregnated wound dressings that maintain durable antimicrobial activity without requiring sustained drug release, an important practical advantage over systems relying on exhaustible silver reservoirs.

Zinc oxide nanoparticles (ZnO NPs) represent the most thoroughly characterized metal oxide antimicrobial agent and the only nanomaterial in this class to receive GRAS (Generally Recognized as Safe) designation from the U.S. Food and Drug Administration for use in food contact materials, a distinction that has facilitated its widespread commercial adoption in food packaging, textile coatings, and personal care products [42]. The antibacterial activity of ZnO NPs is size-dependent and inversely proportional to particle diameter, reflecting the role of surface area in determining Zn^{2+} ion release kinetics and photocatalytic ROS generation. Under UV and even visible light illumination, ZnO undergoes photoexcitation to generate electron-hole

pairs that react with surface-adsorbed water and oxygen to produce •OH and $O_2^{\bullet -}$ radicals, a photocatalytic bactericidal mechanism that is particularly valuable in hospital settings and public environments where self-disinfecting surface coatings are desired. Critically, ZnO NPs demonstrate activity against a range of clinically relevant pathogens including MRSA and extended-spectrum beta-lactamase-producing *E. coli*, underscoring their relevance in the context of MDR infection control [43].

The antiviral properties of metal and metal oxide nanoparticles, thrust into global prominence by the SARS-CoV-2 pandemic, constitute an increasingly important dimension of their biomedical utility. AgNPs have been shown to inhibit multiple enveloped viruses, including influenza A, hepatitis B, respiratory syncytial virus (RSV), and herpes simplex virus (HSV), by binding to viral surface glycoproteins and preventing receptor-mediated cell entry. The mechanisms appear to involve both direct physical interference with virus-cell attachment and, for enveloped viruses, disruption of the lipid bilayer by silver ions [44]. ZnO NPs have demonstrated virucidal activity against SARS-CoV-2 in surface decontamination studies, where ROS-mediated oxidation of viral envelope lipids and spike protein inactivation were identified as the primary mechanisms of action [45]. Copper-based surfaces, including solid copper, copper alloys, and copper nanoparticle-impregnated coatings, have demonstrated rapid contact inactivation of SARS-CoV-2 within minutes, attributed to Cu^{2+}-mediated oxidation of viral proteins and nucleic acids, a mechanism that holds particular promise for the development of self-sanitizing hospital surfaces and personal protective equipment.

V.4.2. Biofilm Disruption and Surface Coatings

Bacterial biofilms, structured, surface-adherent communities of microorganisms encased within a self-produced extracellular polymeric substance (EPS) matrix, represent a profoundly challenging clinical problem that is qualitatively distinct from planktonic (free-floating) bacterial infection. Biofilm-associated pathogens can exhibit tolerance to antibiotics at concentrations 100 to 1000 times greater than those required to kill their planktonic counterparts. This tolerance arises from multiple concurrent mechanisms: limited antibiotic diffusion through the dense EPS matrix, reduced metabolic activity of cells in the biofilm interior creating a population of antibiotic-tolerant persister cells, and the activation of biofilm-specific stress response programs [46].

It has been estimated that biofilms are responsible for 65–80% of all nosocomial infections, including catheter-associated urinary tract infections (CAUTIs), central line-associated bloodstream infections (CLABSIs), ventilator-associated pneumonias (VAPs), and prosthetic joint infections, collectively representing an enormous burden of morbidity, mortality, and healthcare cost worldwide.

Nanoparticles offer a mechanistically distinct and genuinely promising approach to biofilm control, for reasons that are both physical and chemical in nature. Their nanoscale dimensions enable them to penetrate into the interior of mature biofilms to an extent that is inaccessible to most conventional antibiotics. Positively charged nanoparticles (achieved by coating with chitosan, polyethylenimine (PEI), or lysine-functionalized polymers) exhibit superior biofilm penetration due to electrostatic attraction to the anionic EPS matrix [47].

As illustrated in **Figure (V.8)**, the development of bacterial biofilms typically progresses through distinct stages: (I) reversible attachment of planktonic bacteria to the surface, (II) irreversible attachment accompanied by initial EPS production, (III) quorum sensing (QS)-regulated maturation with enhanced EPS matrix formation and cellular heterogeneity, and (IV) dispersal of cells or aggregates. Nanoparticle interventions can target these stages effectively, through surface coatings to prevent initial attachment, QS inhibition to disrupt maturation, nanoparticle penetration into the EPS matrix, and EPS degradation (e.g., via localized ROS generation) to promote dispersal and sensitize persister cells.

Once internalized, nanoparticles can disrupt biofilms through multiple pathways: direct bactericidal action, generation of localized ROS bursts that degrade EPS polysaccharides, interference with quorum sensing (QS) signaling, and enhancement of dispersal.

Quorum sensing (QS), the cell density-dependent chemical signaling system through which bacteria coordinate collective behaviors including biofilm formation, virulence factor production, and antibiotic tolerance, has emerged as a particularly attractive target for anti-biofilm nanoparticle strategies. By disrupting QS rather than directly killing bacteria, QS-inhibitory nanoparticles can suppress biofilm formation and attenuate pathogenicity without imposing the strong selective pressure for resistance that accompanies bactericidal approaches [48].

AgNPs have been shown to inhibit QS in *Pseudomonas aeruginosa* by downregulating the expression of *lasI* and *rhlI* synthase genes responsible for N-acyl homoserine lactone (AHL) signal molecule biosynthesis, thereby reducing pyocyanin production, biofilm biomass, and alginate secretion at sub-minimum inhibitory concentrations (sub-MIC) [49].

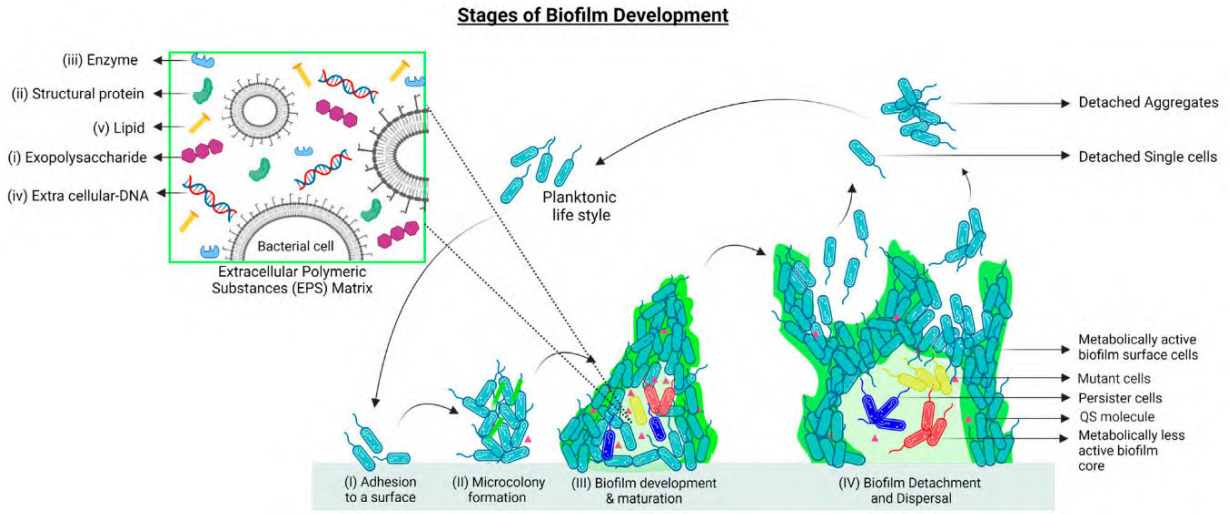

Figure (V.8): Biofilm formation stages and nanoparticle-based inhibition strategies [50].

The development of nanoparticle-functionalized surface coatings for medical devices constitutes one of the most clinically consequential applications of antimicrobial nanotechnology, directly targeting the primary substrate on which biofilm-associated nosocomial infections originate. Catheters, orthopedic implants, dental prostheses, wound dressings, and endotracheal tubes are among the biomedical devices most urgently requiring effective anti-biofilm surfaces, as each represents a foreign body that provides an ideal surface for bacterial colonization in the proximity of a compromised host tissue interface [51]. The design of antimicrobial surface coatings must balance two often competing objectives: achieving sufficient local antimicrobial activity to prevent colonization, while avoiding systemic toxicity from leached nanoparticles or metal ions and maintaining the mechanical and functional properties of the underlying device. Several strategies have been developed to meet this challenge, including incorporation of nanoparticles into polymer matrices for sustained controlled release, covalent tethering of nanoparticles to device surfaces to prevent leaching, and the creation of nanostructured surface topographies that physically prevent bacterial adhesion through contact angle and surface energy effects.

Silver nanoparticle-impregnated coatings on urinary catheters and central venous catheters have been the most extensively evaluated in clinical settings, with multiple studies demonstrating reductions in bacterial colonization rates and catheter-associated infection incidence compared to uncoated controls [38]. Copper nanoparticle coatings on high-touch hospital surfaces, door handles, bedrails, nurse call buttons, and IV poles, have demonstrated in situ antimicrobial efficacy against MRSA and *Clostridioides difficile* in clinical trial environments, with contact inactivation occurring within minutes of bacterial deposition. ZnO nanoparticle coatings have been explored for textile and wound dressing applications, where their photocatalytic antimicrobial activity under ambient light conditions provides sustained antibiofilm protection that does not depend on drug release and is therefore not subject to the exhaustion that limits the long-term utility of silver-releasing systems [43].

A conceptually advanced class of anti-biofilm coatings combines nanoparticles with enzymes capable of degrading the EPS matrix, a strategy termed enzymatic debridement at the nanoscale. Nanoparticle carriers loaded with dispersin B (a glycoside hydrolase that cleaves the poly-N-acetylglucosamine component of biofilm matrices), DNase I (which degrades extracellular DNA, a structural component of the EPS of many species), or proteinase K have been shown to significantly enhance the penetration of co-delivered antimicrobials into pre-formed biofilms by physically dismantling the diffusion barrier [52]. This combinatorial strategy, disrupting the structural integrity of the biofilm matrix while simultaneously delivering bactericidal nanoparticles or antibiotics directly to the now-exposed bacterial cells, represents a particularly rational approach to eradicating the recalcitrant, mature biofilms that are responsible for the most clinically intractable device-associated infections. The integration of stimuli-responsive elements, such as pH-sensitive polymer shells that open in the acidic microenvironment characteristic of mature biofilms, or ROS-responsive linkers that release enzyme cargo in response to oxidative stress, further enhances the precision of this approach and reduces the risk of off-target enzyme activity in healthy tissues.

Notwithstanding these compelling advances, the translation of nanoparticle-based antimicrobial and anti-biofilm strategies into routine clinical practice faces significant obstacles. Concerns regarding the long-term ecotoxicological impact of AgNPs and CuNPs discharged into wastewater streams from nanoparticle-coated consumer products are scientifically legitimate and have prompted regulatory scrutiny in multiple jurisdictions. The potential for nanoparticle-

mediated co-selection of antibiotic resistance, whereby sub-lethal exposure to metal nanoparticles selects for cross-resistance to clinically used antibiotics through shared resistance mechanisms such as efflux pumps and membrane permeability changes, represents a concern that requires careful evaluation in both laboratory and real-world settings [53]. The development of standardized, clinically relevant testing methodologies for assessing nanoparticle antimicrobial efficacy against biofilms, complementing the established minimum inhibitory concentration (MIC) assays that were designed for planktonic bacteria, remains an important methodological priority for the field. Addressing these challenges in a rigorous and transparent manner is essential for the responsible advancement of nanoparticle-based antimicrobial technologies toward the clinical applications they have long promised.

V.5. Biosensors and Lab-on-a-Chip Platforms

The emergence of nanoparticle-enhanced biosensors represents one of the most consequential intersections of nanotechnology and analytical chemistry. Conventional diagnostic methods, enzyme-linked immunosorbent assay (ELISA), polymerase chain reaction (PCR), and mass spectrometry, although analytically robust, are constrained by their reliance on centralized laboratory infrastructure, trained personnel, and turnaround times incompatible with time-sensitive clinical scenarios. Nanoparticle-integrated biosensors address these limitations by exploiting the unique physicochemical properties of nanomaterials: their extraordinary surface-to-volume ratios, tunable optical and electrical characteristics, and capacity for precise surface functionalization. The result is a class of analytical devices capable of achieving detection sensitivities that rival or exceed conventional platforms, often within compact and field-deployable formats.

A biosensor, in its canonical form, couples a biological recognition element, antibody, aptamer, enzyme, or nucleic acid sequence, with a physicochemical transducer that converts the biorecognition event into a measurable signal. Nanoparticle incorporation into both the recognition and transduction layers has dramatically expanded biosensor performance. As reviewed by Pingarrón et al.[55], nanoparticle functionalization enhances electrochemical biosensor sensitivity through amplified electron-transfer kinetics, increased loading capacity for biorecognition molecules, and catalytically active surfaces that lower reaction activation energy.

The cumulative effect is a category of devices capable of detecting analytes at femtomolar concentrations, levels previously accessible only through elaborate laboratory protocols.

The rapid expansion of this field is documented in bibliometric analysis: annual publication output on nanoparticle-based electrochemical biosensors increased more than tenfold between 2014 and 2024 according to Scopus database records [56]. Driving this momentum are concurrent advances in nanomaterial synthesis, surface chemistry, and microfabrication techniques that have collectively enabled increasingly sophisticated sensing architectures.

V.5.1. Electrochemical Nanobiosensors: Principles and Nanoparticle Contributions

Among transduction modalities exploited in nanoparticle-enhanced biosensors, electrochemical detection occupies a privileged position owing to its inherent compatibility with miniaturization, low power requirements, and capacity for quantitative real-time measurement in complex biological matrices. Electrochemical biosensors convert biorecognition events, antibody–antigen binding, enzyme–substrate catalysis, or nucleic acid hybridization, into detectable electrical signals, typically expressed as amperometric currents, potentiometric shifts, or impedance changes. The integration of nanoparticles into such architectures amplifies analytical signals and lowers detection thresholds far beyond what passive electrode materials can achieve.

Gold nanoparticles (AuNPs) occupy a central role in electrochemical biosensor design. Their high surface area and ease of thiol-based functionalization make them ideal scaffolds for immobilizing biorecognition molecules without compromising biological activity. When deposited on electrode surfaces, AuNPs increase the electroactive area, facilitate direct electron transfer from redox-active biomolecules such as enzymes and proteins, and act as molecular wires bridging the insulating gap between the biological recognition layer and the conductive substrate [57]. Iron oxide nanoparticles contribute complementary advantages: their superparamagnetic properties allow external magnetic fields to concentrate analytes at the sensor surface, effectively pre-enriching the sample and improving detection limits without additional amplification reagents [58].

Carbon-based nanomaterials, graphene, reduced graphene oxide (rGO), and carbon nanotubes (CNTs), further complement metal and metal oxide nanoparticles by providing

electrode substrates with outstanding electrical conductivity and surface areas exceeding 2,600 m^2/g for single-layer graphene. Graphene field-effect transistors (GFETs) functionalized with antibodies or aptamers enable label-free, real-time detection of biomarkers at clinically relevant concentrations. Recent work has demonstrated GFET-based detection of amyloid-beta oligomers associated with Alzheimer's disease at femtomolar concentrations, illustrating the transformative potential of nanomaterial-enabled sensors in early neurological diagnostics [59].

The performance of electrochemical nanobiosensors is further enhanced through the deployment of composite nanoarchitectures. Bimetallic nanostructures, MXene–AuNP hybrids, and metal–organic framework (MOF) composites offer superior electron-transfer kinetics and surface areas compared to single-component materials. An aptasensor built from a nickel–cobalt–porphyrin MOF decorated with rGO and AuNPs demonstrated a sevenfold increase in electroactive surface area relative to a bare gold electrode, achieving a detection limit of 48.6 fg/mL for amyloid-beta 42 using differential pulse voltammetry, a performance benchmark that underscores the synergistic amplification achievable through rational nanocomposite design [59]. **Figure (V.9)** illustrates the contribution of various nanomaterials to electrochemical biosensors.

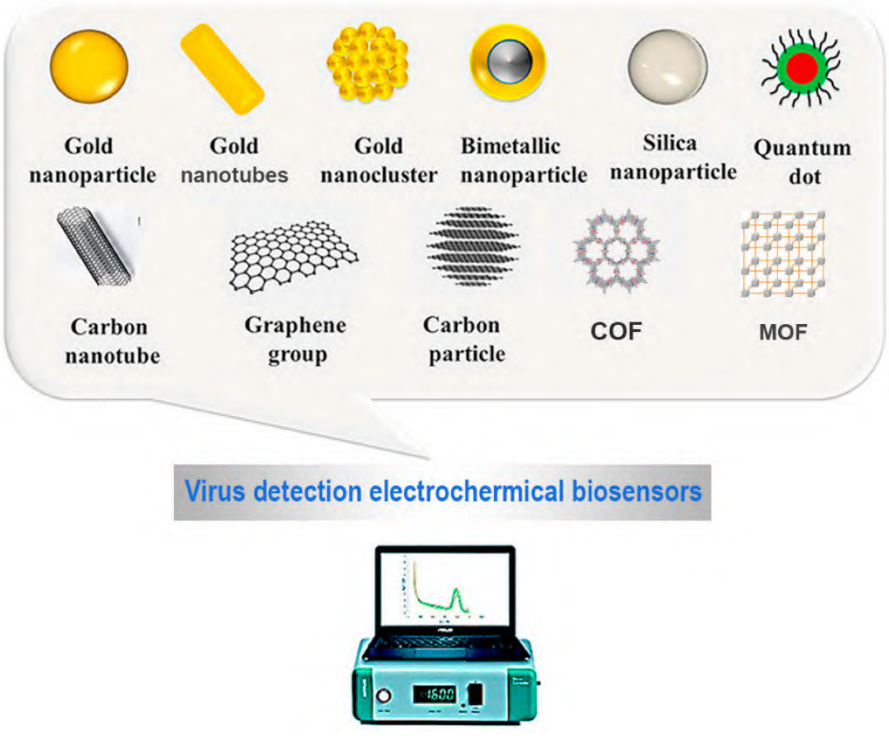

Figure (V.9): Schematic of nanomaterial-based electrochemical biosensors for viral detection [60].

V.5.2. Optical Biosensors: LSPR, SERS, and Colorimetric Detection

Optical transduction strategies exploit the interaction of light with nanomaterial structures to generate analytically useful signals. The most extensively developed optical biosensor platforms based on nanoparticles include those built on localized surface plasmon resonance (LSPR), surface-enhanced Raman spectroscopy (SERS), and colorimetric aggregation-based detection. Each modality derives its signal from distinct physical phenomena associated with nanoparticle optical behavior, and each has been successfully integrated into point-of-care and miniaturized diagnostic configurations.

LSPR biosensors exploit the highly localized, refractive-index-sensitive electromagnetic field arising when conduction electrons of gold or silver nanoparticles undergo collective resonant oscillation in response to incident light. The resonance wavelength shifts measurably upon binding of target molecules to the nanoparticle surface. Kim et al.[61] demonstrated an LSPR-based immunosensor for interleukin-10 (IL-10) using roll-to-roll nanoimprinted gold strips enhanced with colloidal AuNPs, achieving a 450% improvement in LSPR peak shift relative to unenhanced configurations, a striking illustration of how nanoparticle amplification extends the analytical range of plasmonic sensing platforms.

SERS biosensors operate through electromagnetic field enhancement generated by nanoparticle plasmons, which amplifies the Raman scattering cross-section of molecules adsorbed near the nanoparticle surface by factors as large as 10^{10}, enabling single-molecule detection in favorable conditions. A dual-mode SERS–fluorescence biosensor for aflatoxin B1 detection, employing aminated mesoporous silica nanoparticles loaded with Rhodamine 6G, achieved detection limits of 0.133 pg/mL by Raman and 0.214 pg/mL by fluorescence in real food matrices [62]. This multiplexed sensing capability, where a single nanostructured platform simultaneously delivers two orthogonal analytical signals, addresses a critical weakness of single-modality biosensors, namely susceptibility to false-positive responses from matrix components.

Colorimetric biosensors based on AuNP aggregation represent the most accessible optical detection format, requiring no instrumentation beyond the naked eye or a smartphone camera.

These sensors exploit the dramatic red-to-blue color transition accompanying AuNP aggregation triggered by analyte binding, reflecting a red-shift and broadening of the LSPR extinction band as interparticle plasmon coupling develops with decreasing particle separation. While sensitivity is generally lower than LSPR or SERS platforms, colorimetric sensors excel in resource-limited settings where simplicity and cost-effectiveness are paramount [63].

V.5.3. Lab-on-a-Chip Integration and Microfluidic Platforms

The clinical and public-health impact of nanoparticle-based biosensors can only be fully realized when integrated into miniaturized, autonomous platforms capable of executing complete analytical workflows, sample introduction, pre-concentration, reaction, detection, and readout, within a single compact device. Lab-on-a-chip (LOC) platforms, which integrate microfluidic channels, reaction chambers, and detection zones on a substrate typically no larger than a standard card, provide precisely this capability. The coupling of nanoparticle-enhanced sensing with microfluidic automation addresses the longstanding trade-off between analytical performance and operational simplicity.

Microfluidic integration confers multiple advantages relevant to nanoparticle-based detection. Reduced reagent volumes, often in the nanoliter range, lower cost per assay and minimize sample requirements. Laminar flow conditions within microchannels enable precise control over reaction kinetics and incubation times, improving assay reproducibility. Furthermore, the large surface-area-to-volume ratio of microchannels enhances mass transport of analytes to functionalized nanoparticle surfaces, accelerating the biorecognition event and reducing time-to-result [64].

A particularly promising direction is the integration of electrochemical genosensors with microfluidic sample to answer workflows. Recent advances have incorporated CRISPR Cas systems into electrochemical genosensor chips, exploiting the programmable sequence specificity of CRISPR guide RNAs to achieve attomolar detection limits for bacterial and viral pathogens, including Mycobacterium tuberculosis and SARS CoV 2, without requiring prior nucleic acid amplification [65]. The integration of anisotropic gold nanostructures and MXene composites into such chips further extends sensitivity by enhancing electron transfer kinetics and providing additional surface area for probe immobilization. Multiplexed LOC platforms capable of simultaneously detecting multiple analytes, each detection zone functionalized with nanoparticles

optimized for a specific target, represent the frontier of diagnostic nanotechnology, enabling comprehensive disease biomarker profiling from a single sample in minutes. **Figure (V.10)** illustrates an AuNPs-assisted electrochemical CRISPR-Cas12a biosensor for rapid and ultrasensitive pathogen detection.

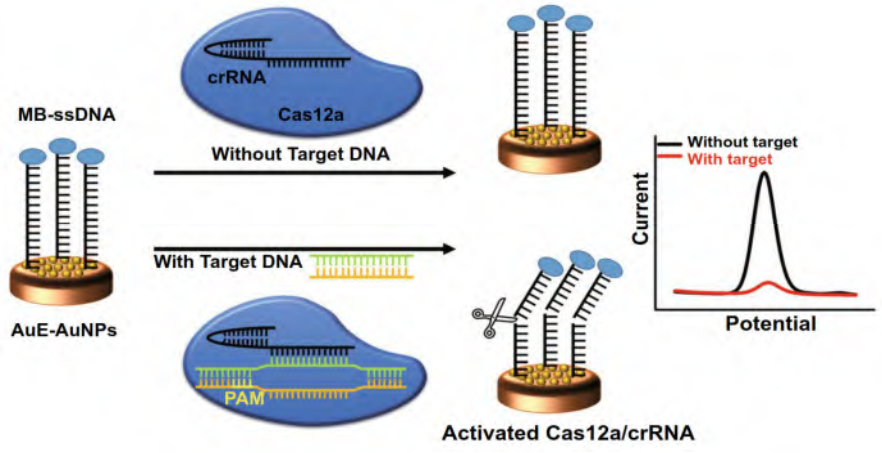

Figure (V.10): AuNP-assisted E-CRISPR electrochemical biosensor for SARS-CoV-2 detection [66].

V.6. Toxicity, Biocompatibility, and Regulatory Issues in Biomedical Use

The biomedical translation of nanoparticles is inseparable from a rigorous evaluation of their safety profiles. The same physicochemical properties that confer such compelling analytical and therapeutic advantages, nanoscale dimensions, high surface reactivity, and capacity for cellular internalization, also endow nanoparticles with the potential to interact with biological systems in harmful ways. Nanotoxicology, the discipline concerned with assessing these risks, has advanced considerably over the past two decades, yet significant knowledge gaps persist. The regulatory landscape governing nanomedicine products remains fragmented and, in many jurisdictions, inadequate to address the unique challenges that nanoparticles present to existing pharmaceutical frameworks. Understanding these dual imperatives, safety and clinical translation, is therefore fundamental to any meaningful discussion of nanoparticle-based biomedical applications.

V.6.1. Mechanisms of Nanotoxicity: Physicochemical Determinants

The toxicity of nanoparticles is not an intrinsic property of the material in isolation but rather an emergent consequence of the interplay between physicochemical characteristics and the biological environment they encounter. Parameters including particle size, shape, surface charge, chemical composition, and surface functionalization each modulate the nature and magnitude of toxic responses in ways that are poorly predicted by the bulk material's toxicological profile, a size-dependent divergence from bulk behavior often termed the 'nano-effect' [67].

Particle size governs biodistribution, cellular uptake pathways, and clearance kinetics. Nanoparticles below approximately 8 nm are rapidly cleared by renal filtration, while those in the 10–100 nm range are preferentially sequestered by the mononuclear phagocyte system in the liver and spleen. Critically, smaller particles exhibit greater mass-normalized surface reactivity and more readily penetrate subcellular compartments, including the nucleus, therapeutically advantageous for gene delivery but concerning for genotoxic risk [68].

Surface charge is a particularly important determinant of biological behavior. Cationic nanoparticles express strong affinity for the negatively charged phospholipid heads of plasma membranes, promoting endocytosis. Once internalized within the endolysosomal compartment, their positive charge can disrupt lysosomal membrane integrity via the proton-sponge effect, triggering lysosomal swelling and eventually cell death. Anionic nanoparticles, by contrast, exhibit greater skin penetration potential and may activate coagulation cascades at sufficient doses. Neutral or zwitterionic surface chemistries generally confer superior biocompatibility by minimizing non-specific protein adsorption and reducing immune activation [69].

The most widely documented molecular mechanism of nanoparticle-induced toxicity is oxidative stress mediated by reactive oxygen species (ROS). Surface-active nanoparticles, particularly metal oxides such as TiO_2, ZnO, and CuO, catalyze Fenton-type reactions or other redox cycling processes that generate superoxide anions, hydroxyl radicals, and hydrogen peroxide within the intracellular environment. When ROS generation exceeds cellular antioxidant defenses, oxidative stress causes lipid peroxidation, oxidative protein modification, and DNA strand breaks. Persistent oxidative damage activates NF-κB inflammatory cascades, promotes mitochondrial dysfunction, and, if unresolved, triggers apoptotic or necrotic cell death [70].

Beyond ROS-mediated cytotoxicity, nanoparticles can induce direct genotoxicity through physical interactions with the DNA double helix, interference with replication and repair

machinery, and epigenetic modifications. Immunotoxicity, the capacity to activate or inappropriately suppress immune responses, is a further documented concern, particularly relevant for intravenously administered formulations that encounter the complement system and innate immune pattern-recognition receptors. The formation of a protein corona, the layer of serum proteins adsorbing onto nanoparticle surfaces upon exposure to biological fluids, further modulates all these interactions by altering cellular uptake pathways, apparent surface properties, and immune recognition [71]. **Figure (V.11)** illustrates the central role of reactive oxygen species (ROS) accumulation in nanoparticle-induced toxicity.

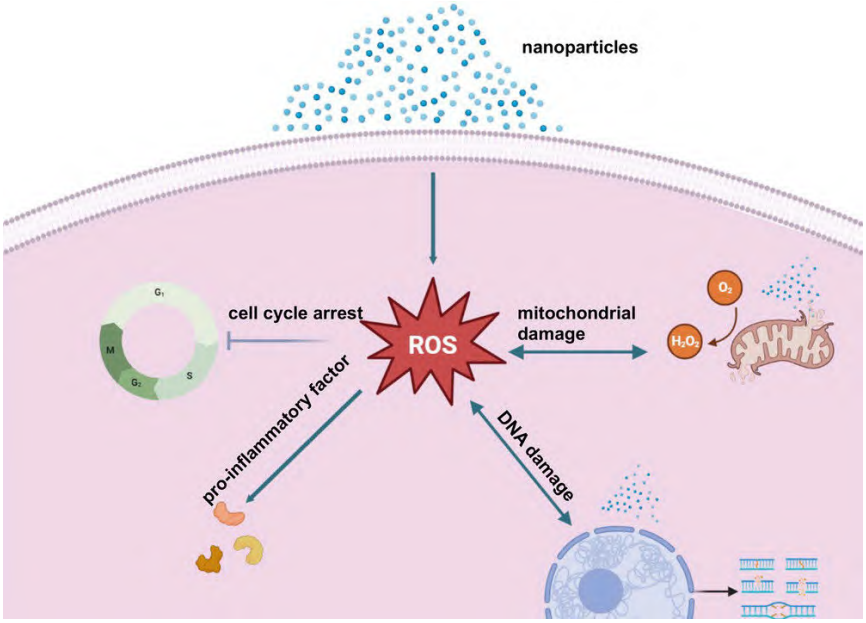

Figure (V.11): Nanoparticles are mainly related to the mechanism of toxicity induced by the accumulation of ROS [70].

V.6.2. Biocompatibility Assessment: From In Vitro to Emerging Models

Rigorous evaluation of nanoparticle biocompatibility requires a hierarchical testing strategy moving from reductionist in vitro cell-based assays through mechanistically informative in vivo animal studies toward clinically predictive models. No single assay or model suffices in isolation; the heterogeneity of nanoparticle interactions with biological systems demands a multi-endpoint, multi-model approach [72].

Standard cytotoxicity assays, MTT, MTS, and WST-1, remain widely employed but are fraught with methodological pitfalls in the context of nanoparticles. Many nanoparticles,

particularly carbon-based and metal oxide materials, absorb at the wavelengths used in these colorimetric formats, producing artifactually skewed signals that do not accurately reflect true cytotoxic activity. The lactate dehydrogenase (LDH) release assay is comparably susceptible to nanoparticle interference. These limitations necessitate parallel assays, propidium iodide exclusion by flow cytometry, annexin V staining for apoptosis assessment, or impedance-based real-time cell analysis, to generate reliable cytotoxicity profiles [73].

Emerging nanotoxicology approaches overcome the reductionism of conventional in vitro assays and the translational limitations of standard animal models through advanced biological systems. Organ-on-a-chip platforms, three-dimensional organoids, and co-culture systems incorporating multiple cell types recapitulate organ-level physiology with fidelity unachievable in monolayer cultures. Omics-based strategies, transcriptomics, proteomics, and metabolomics, offer mechanistic insight at the molecular level, enabling identification of pathway perturbations invisible to endpoint cytotoxicity assays [74]. The adverse outcome pathway (AOP) framework, which formalizes the causal chain from a molecular initiating event to an adverse outcome at organism level, provides a conceptual structure for integrating these diverse data streams into actionable risk assessments [72].

Biocompatibility design strategies center on surface engineering as the primary lever for toxicity mitigation. PEGylation, conjugation of polyethylene glycol chains to the nanoparticle surface, remains the most broadly implemented approach, reducing protein corona formation, diminishing immune recognition, and extending systemic circulation half-life. Zwitterionic coatings, lipid shells, and biodegradable polymer encapsulation represent complementary strategies. The choice of surface chemistry must, however, be integrated with active targeting considerations: surface modifications that improve biocompatibility may, if not carefully designed, attenuate targeting specificity [71].

V.6.3. Regulatory Landscape and Challenges in Clinical Translation

The pathway from laboratory innovation to clinically approved nanomedicine product is long, expensive, and navigated through a regulatory landscape not originally designed for nanotechnology. Major regulatory agencies, the United States Food and Drug Administration (FDA), the European Medicines Agency (EMA), and their counterparts, have, in principle, extended existing pharmaceutical and medical device frameworks to nanomedicine products. In

practice, however, the physicochemical complexity of nanoparticle formulations, the inadequacy of standard characterization methods to capture unique nanoscale properties, and the absence of validated in vitro–in vivo correlations specific to nanoparticle systems create regulatory uncertainty that substantially impedes efficient translation [75].

A fundamental regulatory challenge is the absence of a universally accepted definition of 'nanomaterial' across jurisdictions. The European Commission's 2011 recommendation specifies materials with at least one external dimension in the 1–100 nm range, but the FDA has historically avoided a bright-line definition, preferring case-by-case evaluation. This definitional divergence creates compliance complexity for manufacturers seeking simultaneous approval across multiple markets and impedes the harmonization of safety standards that would facilitate international evidence sharing [75].

The lack of consensus on validated characterization methods, covering particle size distribution, surface area, surface charge, and dissolution behavior in biologically relevant media, constitutes an equally significant impediment. Standard physicochemical protocols developed for bulk materials often fail to adequately characterize nanoparticle behavior in complex biological environments, where protein corona formation, agglomeration, and ionic dissolution dynamics profoundly alter apparent properties. Without validated methods, comparative safety assessments across formulations and laboratories are compromised, undermining the evidence base for regulatory decision-making [67].

The landmark approval of Doxil® (PEGylated liposomal doxorubicin) by the FDA in 1995 established nanomedicine as a clinically viable therapeutic modality, and more than 400 nanomedicine clinical trials are currently registered on ClinicalTrials.gov across oncology, infectious disease, autoimmune, and cardiovascular indications. Nevertheless, attrition from preclinical promise to clinical approval remains high. Contributing factors include the poor predictive validity of preclinical models for human pharmacokinetics and toxicology, manufacturing challenges in scaling up nanoparticle production while maintaining physicochemical consistency, and the immunogenic potential of certain nanoparticle materials that is not revealed in standard preclinical species [76].

The path forward demands coordinated effort across scientific, industrial, and regulatory communities. Priority areas include the development and international harmonization of validated

test methods specific to nanomaterials, the establishment of nanotoxicology reference databases supporting read-across risk assessment analogous to conventional chemical safety evaluation, the adoption of safe-by-design principles in nanomaterial development, and the integration of real-world post-market surveillance evidence into regulatory frameworks. Initiatives such as the FDA's Nanotechnology Regulatory Science Research Plan and the EMA's Reflection Paper on nanotechnology-based medicinal products represent meaningful steps toward these goals, but substantial work remains to close the gap between scientific knowledge and regulatory practice [75, 76].

References

References

1. Shi J, Kantoff PW, Wooster R, Farokhzad OC (2017) Cancer nanomedicine: Progress, challenges and opportunities. Nat Rev Cancer 17:20–37. https://doi.org/10.1038/nrc.2016.108
2. Immordino ML, Dosio F, Cattel L (2006) Stealth liposomes: Review of the basic science, rationale, and clinical applications, existing and potential. Int J Nanomedicine 1:297–315. https://doi.org/10.2147/nano.2006.1.3.297
3. Mura S, Couvreur P (2012) Nanotheranostics for personalized medicine. Adv Drug Deliv Rev 64:1394–1416. https://doi.org/10.1016/j.addr.2012.06.006
4. Janib SM, Moses AS, MacKay JA (2010) Imaging and drug delivery using theranostic nanoparticles. Adv Drug Deliv Rev 62:1052–1063. https://doi.org/10.1016/j.addr.2010.08.004
5. Maeda H, Wu J, Sawa T, et al (2000) Tumor vascular permeability and the EPR effect in macromolecular therapeutics: A review. J Control Release 65:271–284. https://doi.org/10.1016/S0168-3659(99)00248-5
6. Wilhelm S, Tavares AJ, Dai Q, et al (2016) Analysis of nanoparticle delivery to tumours. Nat Rev Mater 1:16014. https://doi.org/10.1038/natrevmats.2016.14
7. Mitchell MJ, Billingsley MM, Haley RM, et al (2021) Engineering precision nanoparticles for drug delivery. Nat Rev Drug Discov 20:101–124. https://doi.org/10.1038/s41573-020-0090-8
8. Beach MA, Nayanathara U, Gao Y, et al (2024) Polymeric Nanoparticles for Drug Delivery. Chem Rev 124:5505–5616. https://doi.org/10.1021/acs.chemrev.3c00705
9. Danhier F, Ansorena E, Silva JM, et al (2012) PLGA-based nanoparticles: An overview of biomedical applications. J Control Release 161:505–522. https://doi.org/10.1016/j.jconrel.2012.01.043
10. Danhier F (2016) To exploit the tumor microenvironment: Since the EPR effect fails in the clinic, what is the future of nanomedicine? J Control Release 244:108–121. https://doi.org/10.1016/j.jconrel.2016.11.015
11. Zhang D, Liu L, Wang J, et al (2022) Drug-loaded PEG-PLGA nanoparticles for cancer treatment. Front Pharmacol 13:990505. https://doi.org/10.3389/fphar.2022.990505
12. Rezvantalab S, Drude NI, Moraveji MK, et al (2018) PLGA-based nanoparticles in cancer

treatment. Front Pharmacol 9:. https://doi.org/10.3389/fphar.2018.01260

13. Kim HS, Lee DY (2018) Near-infrared-responsive cancer photothermal and photodynamic therapy using gold nanoparticles. Polymers (Basel) 10:961. https://doi.org/10.3390/polym10090961
14. Elbialy NS, Fathy MM, Khalil WM (2015) Doxorubicin loaded magnetic gold nanoparticles for in vivo targeted drug delivery. Int J Pharm 490:190–199. https://doi.org/10.1016/j.ijpharm.2015.05.032
15. Bobo D, Robinson KJ, Islam J, et al (2016) Nanoparticle-Based Medicines: A Review of FDA-Approved Materials and Clinical Trials to Date. Pharm Res 33:2373–2387. https://doi.org/10.1007/s11095-016-1958-5
16. Vallet-Regi M, Rámila A, Del Real RP, Pérez-Pariente J (2001) A new property of MCM-41: Drug delivery system. Chem Mater 13:308–311. https://doi.org/10.1021/cm0011559
17. Horue M, Silva JM, Berti IR, et al (2023) Bacterial Cellulose-Based Materials as Dressings for Wound Healing. Pharmaceutics 15:424. https://doi.org/10.3390/pharmaceutics15020424
18. Adam A, Mertz D (2023) Iron Oxide@Mesoporous Silica Core-Shell Nanoparticles as Multimodal Platforms for Magnetic Resonance Imaging, Magnetic Hyperthermia, Near-Infrared Light Photothermia, and Drug Delivery. Nanomaterials 13:1342. https://doi.org/10.3390/nano13081342
19. Wahsner J, Gale EM, Rodríguez-Rodríguez A, Caravan P (2019) Chemistry of MRI contrast agents: Current challenges and new frontiers. Chem Rev 119:957–1057. https://doi.org/10.1021/acs.chemrev.8b00363
20. Dadfar SM, Roemhild K, Drude NI, et al (2019) Iron oxide nanoparticles: Diagnostic, therapeutic and theranostic applications. Adv Drug Deliv Rev 138:302–325. https://doi.org/10.1016/j.addr.2019.01.005
21. Ali LMA, Marzola P, Nicolato E, et al (2019) Polymer-coated superparamagnetic iron oxide nanoparticles as T2 contrast agent for MRI and their uptake in liver. Futur Sci OA 5:235. https://doi.org/10.4155/fsoa-2017-0054
22. Zhou Z, Yang L, Gao J, Chen X (2019) Structure–Relaxivity Relationships of Magnetic Nanoparticles for Magnetic Resonance Imaging. Adv Mater 31:1804567. https://doi.org/10.1002/adma.201804567

23. Wang Y-XJ (2011) Superparamagnetic iron oxide based MRI contrast agents: Current status of clinical application. Quant Imaging Med Surg 1:35–40. https://doi.org/10.3978/j.issn.2223-4292.2011.08.03
24. Shen Z, Wu A, Chen X (2017) Iron Oxide Nanoparticle Based Contrast Agents for Magnetic Resonance Imaging. Mol Pharm 14:1352–1364. https://doi.org/10.1021/acs.molpharmaceut.6b00839
25. Key J, Leary JF (2014) Nanoparticles for multimodal in vivo imaging in nanomedicine. Int J Nanomedicine 9:711–726. https://doi.org/10.2147/IJN.S53717
26. Liang Z, Khawar MB, Liang J, Sun H (2021) Bio-Conjugated Quantum Dots for Cancer Research: Detection and Imaging. Front Oncol 11:749970. https://doi.org/10.3389/fonc.2021.749970
27. Hamidu A, Pitt WG, Husseini GA (2023) Recent Breakthroughs in Using Quantum Dots for Cancer Imaging and Drug Delivery Purposes. Nanomaterials 13:2566. https://doi.org/10.3390/nano13182566
28. Le N, Kim K (2023) Current Advances in the Biomedical Applications of Quantum Dots: Promises and Challenges. Int J Mol Sci 24:12682. https://doi.org/10.3390/ijms241612682
29. Xie J, Lee S, Chen X (2010) Nanoparticle-based theranostic agents. Adv Drug Deliv Rev 62:1064–1079. https://doi.org/10.1016/j.addr.2010.07.009
30. Rieffel J, Bhavane R, Kulkarni AA Trimodal nanoparticle imaging allows tracking of diverse biological processes. Angew Chemie Int Ed 54:5073–5078. https://doi.org/10.1002/anie.201410298
31. Chen H, Zhang W, Zhu G, et al (2017) Rethinking cancer nanotheranostics. Nat Rev Mater 2:17024. https://doi.org/10.1038/natrevmats.2017.24
32. Xie J, Chen K, Huang J, et al (2010) PET/NIRF/MRI triple functional iron oxide nanoparticles. Biomaterials 31:3016–3022. https://doi.org/10.1016/j.biomaterials.2010.01.010
33. Thomas G, Boudon J, Maurizi L, et al (2019) Innovative Magnetic Nanoparticles for PET/MRI Bimodal Imaging. ACS Omega 4:2637–2648. https://doi.org/10.1021/acsomega.8b03283
34. Fernandes DA (2023) Review on Metal-Based Theranostic Nanoparticles for Cancer Therapy and Imaging. Technol Cancer Res Treat 22:15330338231191492.

https://doi.org/10.1177/15330338231191493

35. Najdian A, Beiki D, Abbasi M, et al (2024) Exploring innovative strides in radiolabeled nanoparticle progress for multimodality cancer imaging and theranostic applications. Cancer Imaging 24:123. https://doi.org/10.1186/s40644-024-00762-z
36. Murray CJ, Ikuta KS, Sharara F, et al (2022) Global burden of bacterial antimicrobial resistance in 2019: a systematic analysis. Lancet 399:629–655. https://doi.org/10.1016/S0140-6736(21)02724-0
37. Baptista P V., McCusker MP, Carvalho A, et al (2018) Nano-strategies to fight multidrug resistant bacteria-"A Battle of the Titans". Front Microbiol 9:1441. https://doi.org/10.3389/fmicb.2018.01441
38. Bruna T, Maldonado-Bravo F, Jara P, Caro N (2021) Silver nanoparticles and their antibacterial applications. Int J Mol Sci 22:7202. https://doi.org/10.3390/ijms22137202
39. Dakal TC, Kumar A, Majumdar RS, Yadav V (2016) Mechanistic basis of antimicrobial actions of silver nanoparticles. Front Microbiol 7:. https://doi.org/10.3389/fmicb.2016.01831
40. Eckhardt S, Brunetto PS, Gagnon J, et al (2013) Nanobio silver: Its interactions with peptides and bacteria, and its uses in medicine. Chem Rev 113:4708–4754. https://doi.org/10.1021/cr300288v
41. Tamayo L, Azócar M, Kogan M, et al (2016) Copper-polymer nanocomposites: An excellent and cost-effective biocide for use on antibacterial surfaces. Mater Sci Eng C 69:1391–1409. https://doi.org/10.1016/j.msec.2016.08.041
42. Sirelkhatim A, Mahmud S, Seeni A, et al (2015) Review on zinc oxide nanoparticles: Antibacterial activity and toxicity mechanism. Nano-Micro Lett 7:219–242. https://doi.org/10.1007/s40820-015-0040-x
43. Izzi M, Sportelli MC, Torsi L, et al (2023) Synthesis and Antimicrobial Applications of ZnO Nanostructures: A Review. ACS Appl Nano Mater 6:10881–10902. https://doi.org/10.1021/acsanm.3c01432
44. Galdiero S, Falanga A, Vitiello M, et al (2011) Silver nanoparticles as potential antiviral agents. Molecules 16:8894–8918. https://doi.org/10.3390/molecules16108894
45. Wolfgruber S, Rieger J, Cardozo O, et al (2023) Antiviral Activity of Zinc Oxide Nanoparticles against SARS-CoV-2. Int J Mol Sci 24:8425.

https://doi.org/10.3390/ijms24098425

46. Flemming HC, Wingender J, Szewzyk U, et al (2016) Biofilms: An emergent form of bacterial life. Nat Rev Microbiol 14:563–575. https://doi.org/10.1038/nrmicro.2016.94
47. Gupta A, Mumtaz S, Li CH, et al (2019) Combatting antibiotic-resistant bacteria using nanomaterials. Chem Soc Rev 48:415–427. https://doi.org/10.1039/c7cs00748e
48. Ferreres G, Ivanova K, Ivanov I, Tzanov T (2023) Nanomaterials and Coatings for Managing Antibiotic-Resistant Biofilms. Antibiotics 12:310. https://doi.org/10.3390/antibiotics12020310
49. Ramasamy M, Lee J (2016) Recent nanotechnology approaches for prevention and treatment of biofilm-associated infections on medical devices. Biomed Res Int 2016:1851242. https://doi.org/10.1155/2016/1851242
50. Kauser A, Parisini E, Suarato G, Castagna R (2023) Light-Based Anti-Biofilm and Antibacterial Strategies. Pharmaceutics 15:2106. https://doi.org/10.3390/pharmaceutics15082106
51. Yang K, Shi J, Wang L, et al (2022) Bacterial anti-adhesion surface design: Surface patterning, roughness and wettability: A review. J Mater Sci Technol 99:82–100. https://doi.org/10.1016/j.jmst.2021.05.028
52. Thorn CR, Thomas N, Boyd BJ, Prestidge CA (2021) Nano-fats for bugs: the benefits of lipid nanoparticles for antimicrobial therapy. Drug Deliv Transl Res 11:1598–1624. https://doi.org/10.1007/s13346-021-00921-w
53. Seiler C, Berendonk TU (2012) Heavy metal driven co-selection of antibiotic resistance in soil and water bodies impacted by agriculture and aquaculture. Front Microbiol 3:399. https://doi.org/10.3389/fmicb.2012.00399
54. Heidt T, Nahrendorf M (2013) Multimodal iron oxide nanoparticles for hybrid biomedical imaging. NMR Biomed 26:756–765. https://doi.org/10.1002/nbm.2872
55. Pingarrón JM, Yáñez-Sedeño P, González-Cortés A (2008) Gold nanoparticle-based electrochemical biosensors. Electrochim Acta 53:5848–5866. https://doi.org/10.1016/j.electacta.2008.03.005
56. Hassan RYA Advances in nanoparticle-based electrochemical biosensors for bioanalytical applications
57. Saha K, Agasti SS, Kim C, et al (2012) Gold nanoparticles in chemical and biological

sensing. Chem Rev 112:2739–2779. https://doi.org/10.1021/cr2001178

58. Wang M, Jin L, Hang-Mei Leung P, et al (2024) Advancements in magnetic nanoparticle-based biosensors for point-of-care testing. Front Bioeng Biotechnol 12:1393789. https://doi.org/10.3389/fbioe.2024.1393789
59. Şak B, Sousa HBA, Prior JAV (2025) Carbon Nanomaterial-Based Electrochemical Biosensors for Alzheimer's Disease Biomarkers: Progress, Challenges, and Future Perspectives. Biosensors 15:684. https://doi.org/10.3390/bios15100684
60. Curulli A (2023) Functional Nanomaterials Enhancing Electrochemical Biosensors as Smart Tools for Detecting Infectious Viral Diseases. Molecules 28:3777. https://doi.org/10.3390/molecules28093777
61. Baek SH, Song HW, Lee S, et al (2020) Gold Nanoparticle-Enhanced and Roll-to-Roll Nanoimprinted LSPR Platform for Detecting Interleukin-10. Front Chem 8:285. https://doi.org/10.3389/fchem.2020.00285
62. Alvarez Cañarte E, Vergara Velez G, Intriago Flor FG, et al (2025) Cereals as sources of lysine in the reformulation of meat products. Evaluation using a biosensor. Biosens Bioelectron X 23:. https://doi.org/10.1016/j.biosx.2025.100592
63. Bobrinetskiy I, Radovic M, Rizzotto F, et al (2021) Advances in nanomaterials-based electrochemical biosensors for foodborne pathogen detection. Nanomaterials 11:2700. https://doi.org/10.3390/nano11102700
64. Abouhagger A, Celiešiūtė-Germanienė R, Bakute N, et al (2024) Electrochemical biosensors on microfluidic chips as promising tools to study microbial biofilms: a review. Front Cell Infect Microbiol 14:1419570. https://doi.org/10.3389/fcimb.2024.1419570
65. Dehghan A, Kiani MJ, Gholizadeh A, et al (2025) Electrochemical genosensors on-a-chip: Applications in early diagnosis of pathogens. Sensors and Actuators Reports 9:. https://doi.org/10.1016/j.snr.2025.100335
66. Wu C, Chen Z, Li C, et al (2022) CRISPR-Cas12a-Empowered Electrochemical Biosensor for Rapid and Ultrasensitive Detection of SARS-CoV-2 Delta Variant. Nano-Micro Lett 14:159. https://doi.org/10.1007/s40820-022-00888-4
67. Kumar R, Kumar A, Bhardwaj S, et al (2025) Nanotoxicity unveiled: Evaluating exposure risks and assessing the impact of nanoparticles on human health. J Trace Elem Miner 13:100252. https://doi.org/10.1016/j.jtemin.2025.100252

68. Nel A, Xia T, Mädler L, Li N (2006) Toxic potential of materials at the nanolevel. Science (80-) 311:622–627. https://doi.org/10.1126/science.1114397
69. Savage DT, Hilt JZ, Dziubla TD (2019) In vitro methods for assessing nanoparticle toxicity. Methods Mol Biol 1894:1–29. https://doi.org/10.1007/978-1-4939-8916-4_1
70. Xuan L, Ju Z, Skonieczna M, et al (2023) Nanoparticles-induced potential toxicity on human health: Applications, toxicity mechanisms, and evaluation models. MedComm 4:327. https://doi.org/10.1002/mco2.327
71. Sukhanova A, Bozrova S, Sokolov P, et al (2018) Dependence of Nanoparticle Toxicity on Their Physical and Chemical Properties. Nanoscale Res Lett 13:44. https://doi.org/10.1186/s11671-018-2457-x
72. Tirumala MG, Anchi P, Raja S, et al (2021) Novel Methods and Approaches for Safety Evaluation of Nanoparticle Formulations: A Focus Towards In Vitro Models and Adverse Outcome Pathways. Front Pharmacol 12:612659. https://doi.org/10.3389/fphar.2021.612659
73. Awashra M, Młynarz P (2023) The toxicity of nanoparticles and their interaction with cells: an in vitro metabolomic perspective. Nanoscale Adv 5:2674–2723. https://doi.org/10.1039/d2na00534d
74. Havelikar U, Ghorpade KB, Kumar A, et al (2024) Comprehensive insights into mechanism of nanotoxicity, assessment methods and regulatory challenges of nanomedicines. Discov Nano 19:148. https://doi.org/10.1186/s11671-024-04118-1
75. Mangla B Regulating nanomedicines: challenges, opportunities, and the path forward. Expert Opin Drug Deliv. https://doi.org/10.1080/17425247.2025.2527348
76. Boisseau P, Loubaton B (2011) Nanomedicine, nanotechnology in medicine. Comptes Rendus Phys 12:620–636. https://doi.org/10.1016/j.crhy.2011.06.001

GENERAL CONCLUSION

General Conclusion

The work presented in this thesis has traced the full arc of nanoparticle science and engineering — from the fundamental physicochemical principles that govern behavior at the nanoscale, through the diverse strategies by which nanoparticles are synthesized and characterized, to their deployment in two of the most socially and technically demanding application domains of our time: wastewater remediation and biomedical science. Rather than treating these topics in isolation, the thesis has consistently sought to establish the logical chain that connects synthesis decisions to structural outcomes, structural outcomes to characterization results, and characterization results to observed functional performance. It is this integrative perspective, more than any individual finding, that represents the central contribution of this work.

Conclusion and Outlook

The opening chapter made clear that nanoparticles are not simply small versions of bulk materials. The size-dependent emergence of quantum confinement effects, surface plasmon resonance, superparamagnetism, and dramatically elevated surface-to-volume ratios collectively confer on nanomaterials a set of properties that have no counterpart at the macroscale. Understanding the physical and chemical origins of these properties is not merely an academic exercise — it is the prerequisite for making rational, informed decisions at every subsequent stage of nanoparticle research and development.

Chapter II demonstrated that the synthesis route is perhaps the single most consequential decision in nanoparticle engineering, as it determines — often irreversibly — the size, morphology, crystallinity, surface chemistry, and colloidal behavior of the resulting material. Physical methods offer simplicity and scalability but sacrifice precise control over particle dimensions. Chemical routes, particularly co-precipitation, sol-gel, and hydrothermal synthesis, provide far greater tunability but often involve toxic reagents and generate hazardous by-products. Green and biogenic synthesis approaches have emerged as an attractive alternative, offering reduced environmental impact and inherent surface functionalization through biomolecules, though questions of batch-to-batch reproducibility and mechanistic understanding

remain open. Emerging technologies such as microfluidic and continuous-flow synthesis represent a promising path toward combining the precision of laboratory-scale chemistry with the throughput demanded by industrial application.

Chapter III established that characterization is not a formality to be completed after synthesis, but an integral part of the scientific process that validates what has been made and predicts how it will behave. No single technique is sufficient on its own. XRD identifies crystalline phase and estimates crystallite size but says nothing about particle morphology in solution. TEM reveals individual particle geometry with atomic resolution but risks introducing drying artifacts. DLS measures hydrodynamic diameter rapidly and non-invasively but is disproportionately sensitive to large aggregates. Zeta potential predicts colloidal stability but must be interpreted carefully for sterically stabilized systems. FTIR and XPS reveal surface chemistry with molecular and elemental specificity, respectively, but probe different depth regimes and require complementary interpretation. The overarching lesson is that a multi-modal characterization strategy — combining at minimum two independent sizing methods, a surface-sensitive spectroscopic technique, and a colloidal stability measurement — is the only reliable path to a complete and trustworthy picture of a nanoparticle system.

In the domain of wastewater remediation, Chapter IV showed that nanoparticles have demonstrated genuinely impressive performance as adsorbents, photocatalysts, and magnetically recoverable reagents for the removal of heavy metals, synthetic dyes, pharmaceutical contaminants, and other emerging pollutants. Iron oxide nanoparticles, TiO_2 and ZnO photocatalysts, and carbon-based nanomaterials have each carved out well-defined niches where their particular combination of surface area, surface chemistry, and functional properties gives them a decisive advantage over conventional treatment materials. Yet the chapter also made clear that laboratory-scale performance metrics — high adsorption capacities measured in idealized single-contaminant solutions — do not automatically translate into effective real-world treatment systems. Challenges of particle aggregation, post-treatment recovery, long-term stability in complex water matrices, potential ecotoxicity of released nanoparticles, and the absence of harmonized regulatory frameworks represent genuine and as-yet incompletely resolved obstacles to large-scale deployment.

Chapter V revealed an equally nuanced picture in the biomedical domain. Nanoparticles have opened genuinely new therapeutic and diagnostic possibilities — enabling targeted drug delivery to tumor tissue, generating MRI contrast with a sensitivity unachievable by molecular agents, providing optical imaging probes with tunable emission wavelengths, and offering antimicrobial activity against drug-resistant pathogens. At the same time, the chapter was frank about the gap that persists between preclinical promise and clinical reality. Protein corona formation reshapes the biological identity of nanoparticles within seconds of entering the bloodstream, often in ways that are difficult to predict from in vitro characterization alone. Size, surface charge, and surface chemistry each influence biodistribution, cellular uptake, and cytotoxicity in complex, sometimes non-linear ways. Regulatory pathways for nanomedicines remain less well-defined than those for conventional drugs, and the long-term fate of inorganic nanoparticles in the body is still incompletely understood for many systems.

Broader Reflections

Stepping back from the individual chapters, several themes emerge that cut across synthesis, characterization, and application alike.

The first is the theme of reproducibility. A recurring observation throughout this thesis is that nanoparticle research suffers from a reproducibility problem that is more acute than in many other areas of chemistry and engineering. Small, often unreported variations in synthesis conditions — precursor concentration, mixing order, temperature ramp rate, aging time — can produce materials with significantly different properties, and the characterization data needed to detect these differences are not always reported with sufficient completeness in the published literature. Addressing this problem requires both more rigorous reporting standards and greater investment in standardized reference materials and inter-laboratory validation studies.

The second theme is the indispensable role of characterization as a bridge between synthesis and application. Throughout this thesis, it has become evident that the most consequential advances in both wastewater remediation and nanomedicine have come not from the discovery of entirely new nanoparticle chemistries, but from a deeper mechanistic understanding of how well-characterized physicochemical properties connect to functional outcomes. The field is increasingly moving toward quantitative structure–activity relationship

modeling and machine-learning-assisted analysis of large characterization datasets — approaches that hold real promise for accelerating nanoparticle optimization, but that are only as reliable as the quality and completeness of the underlying characterization data on which they are trained.

The third theme is sustainability. Whether one is evaluating a synthesis route for its environmental footprint, assessing the ecotoxicological risk of nanoparticle release into treated effluent, or considering the long-term fate of inorganic nanoparticles administered as drug carriers, the question of sustainability — broadly conceived to include environmental, toxicological, and economic dimensions — runs through every aspect of applied nanotechnology. Green synthesis approaches, magnetically recoverable adsorbents, biodegradable nanocarriers, and life-cycle-aware process design are not peripheral concerns; they are increasingly central to the responsible practice of the discipline.

Perspectives and Future Directions

Looking ahead, several directions appear particularly promising and worthy of further investigation. In the area of synthesis, the continued development of continuous-flow and microfluidic platforms holds significant potential for achieving the kind of precise, reproducible, and scalable production that industrial and clinical applications demand. In characterization, the growing accessibility of cryo-electron microscopy, single-particle ICP-MS, and advanced NMR methods opens new possibilities for characterizing nanoparticles in conditions that closely approximate their functional environments, rather than in the idealized dried or diluted states that conventional techniques require. In wastewater remediation, the integration of nanoparticle-based treatment steps into hybrid systems combining adsorption, photocatalysis, and membrane filtration represents a more realistic path to practical deployment than relying on any single mechanism alone. In the biomedical domain, the rational engineering of nanoparticle surface chemistry to modulate protein corona composition — rather than simply minimizing it — is emerging as a sophisticated strategy for improving targeting specificity and reducing off-target toxicity.

Closing Remarks

This thesis was undertaken as a second-year Master's graduation project in Chemical Engineering, and it has been guided throughout by a conviction that a deep, integrated understanding of nanoparticle science — spanning synthesis, characterization, and application — is not only intellectually rewarding but practically necessary for any engineer who wishes to contribute meaningfully to this field. The challenges that remain are real and substantial. But so too is the potential of nanoparticle technologies to address some of the most urgent problems in environmental engineering and medicine. It is hoped that this work, in mapping the current state of knowledge and identifying where the most important gaps remain, will serve as a useful starting point for the research and development efforts that lie ahead.